UNIVERSITY OF Southampton
School of Physics and Astronomy

UNIVERSITY OF SOUTHAMPTON

FACULTY OF ENGINEERING, SCIENCE AND MATHEMATICS

School of Physics and Astronomy

Synthesis, surface modifications and biomedical applications of colloidal gold nanoparticles, towards controlled regulation of angiogenesis in conjunction with photo-thermal therapy.

by Dorota Bartczak

Thesis for the Degree of Doctor of Philosophy

January 2011

Abstract

The unique optical properties of colloidal gold nanoparticles: high extinction coefficient and adjustable plasmon band, as well as their excellent biocompatibility (low toxicity and a natural affinity towards thiols and amines) make them very attractive materials for biomedical research. In this project, two types of gold nanoparticles (NPs): spherical and anisotropic were utilised. Spherical NPs predominantly absorb in the visible range of the electromagnetic spectrum, while the plasmon band of anisotropic NPs, e.g. rod-like is shifted into the longer wavelengths. Such variety in the optical signatures of NPs enables their usage in a number of imaging and therapy techniques.

Biological activity of NPs is determined by the chemical composition of the organic corona, surrounding the gold core. Appropriate surface capping provides NPs with substantial stability against aggregation (and loss of their properties) in physiological media. Hence, crude colloids were stabilised with a variety of organic molecules, strongly interacting with the gold surface. A selection of functional peptides was incorporated into the organic corona of NPs, in order to achieve desired biological activity of colloids. Functionalised NPs interacted with a certain type of human cells in a selective manner. Such selectivity was obtained by precise recognition between peptides attached to NPs and cell receptors.

In this project, human umbilical vein endothelial cells (HUVECs) were studied. These cells build the interior layer of blood vessels in the entire circulatory system and participate in many important physiological processes, as well as pathological developments, e.g. blood vessels formation (angiogenesis). In angiogenesis, several cell receptors are involved. Two of them are: vascular endothelial growth factor receptor type 1 (VEGFR-1) and neuropilin receptor type 1 (NRP-1). Both, VEGFR-1 and NRP-1 were targeted with peptide functionalised NPs. Selectivity of the binding was investigated. Following the binding event, physiological changes in cell metabolism were triggered. The nature and efficiency of these changes were studied, by measuring the expression levels of several angiogenesis related genes, as well as the ability of cells to form capillaries using *in vitro* angiogenesis assays.

HUVECs targeted with anisotropic NPs were illuminated with near-infrared (NIR) laser light. Light at this frequency penetrates human tissue and is absorbed by associated with cells anisotropic NPs. NPs convert the absorbed light into heat, which causes an increase in the local temperature. Increased temperatures result in cell damage and/or stimulate cellular response. Physiological changes in HUVECs upon a moderate heat stimuli were assessed by measuring the expression levels of two genes (ELAM-1 and ELAM-1), which are responsive to the temperature changes. Elevated heat resulted in thermal damage of HUVECs, the degree of which was studied by cell viability assays.

In this project, a dual approach towards controlled regulation of HUVECs physiology was demonstrated. Not only regulation of cell metabolism, but the whole angiogenesis process was achieved with peptide functionalised NPs. Targeted with anisotropic NPs cells were illuminated with the NIR laser, which induced the heat shock response in the cell or at the extreme led to death. This work possesses a clear potential and relevance for therapy of various disorders related to insufficient or excessive angiogenesis of endothelial cells.

Table of contents:

Abstract

Table of contents.....I

Author's declaration.....V

Acknowledgements.....VIII

Abbreviations.....IX

1. Introduction..... 1

References.....6

2. Theoretical background..... 12

2.1. Synthesis of NPs.....12

2.1.1. Synthesis of spherical gold NPs.....13

2.1.2. Synthesis of gold nanorods.....14

2.1.3. Synthesis of silica/gold core/shell NPs..... 16

2.1.4. Synthesis of hollow gold NPs..... 18

2.2. NPs surface capping, further modifications and assembly.....20

2.2.1. Oligoethylene glycol based capping ligand.....22

2.2.1.1. Further modifications of NPs surface..... 23

2.2.2. Diacetylene based capping ligand.....25

2.2.3. CALNN peptide based capping ligand..... 26

2.2.3.1. Assembly of NPs on oligodeoxynucleotide templates..... 27

2.3. Physicochemical properties of capped gold NPs.....28

2.4. Interactions of NPs with mammalian cells.....32

2.5. HeLa cells.....33

2.6. Endothelial cells..... 34

2.6.1. Angiogenesis..... 35

2.6.1.1. Octa-peptide based angiogenic regulators.....37

2.6.1.2. NPs in angiogenesis..... 41

2.6.2. Physiology of HUVECs under heat shock..... 42

References.....44

3. Methods and Techniques.....53

3.1. Synthesis of NPs.....53

3.1.1. Synthesis of spherical gold NPs..... 53
3.1.2. Synthesis of gold nanorods.....54
3.1.3. Synthesis of silica/gold core/shell NPs..... 55
3.1.4. Synthesis of hollow gold NPs..... 57
3.2. NPs surface capping..... 57
3.2.1. NPs surface capping with OEG ligands..... 58
3.2.2. NPs surface capping with DA-PEG ligands.....59
3.2.3. NPs surface capping with CALNN based peptides and assembly on oligodeoxynucleotide templates.....59
3.2.4. Further modifications of NPs surface.....61
3.3. NPs characterisation techniques..... 62
3.3.1. Spectroscopy techniques..... 62
3.3.2. NPs surface coverage quantification..... 63
3.3.3. NPs size, shape and net charge measurements.....66
3.3.4. Stability tests of colloids..... 67
3.4. Cells isolation and culturing.....67
3.4.1. HUVECs isolation.....68
3.4.2. HUVECs culturing..... 68
3.4.3. HeLa cells culturing..... 69
3.5. Biological samples characterisation techniques and experimental methods.....69
3.5.1. Transmission electron microscopy of biological specimens incubated with NPs.....70
3.5.2. Flow cytometry.....71
3.5.3. Inductively coupled plasma mass spectrometry (ICP-MS)..72
3.5.4. Photo-thermal treatment (laser-hyperthermia)..... 73
3.5.5. Gene expression profiling..... 74
3.5.6. In vitro angiogenesis..... 75
References.....78
4. Synthesis, surface capping and assembly of NPs.....81
4.1. Synthesis of NPs.....81
4.1.1. Synthesis of spherical gold NPs..... 82

4.1.2. Synthesis of gold nanorods....86
4.1.3. Synthesis of silica/gold core/shell NPs.... 91
4.1.4. Synthesis of hollow gold NPs.... 97
4.2. Surface capping and assembly of NPs....101
4.2.1. NPs surface capping with CALNN based peptides and assembly on oligodeoxynucleotide templates....101
4.2.2. NPs surface capping with OEG ligand and further modifications....105
4.2.3. NPs surface capping with diacetylene based (DA-PEG) ligand....113
4.2.4. Stability tests of colloids.... 117
References....121
5. Cellular fate of OEG NPs..... 126
References....136
6. Cell targeting and regulation with pep-OEG NPs....139
6.1. Selective targeting of HUVECs....140
6.1.1. Cell receptors binding.... 140
6.1.2. Receptor mediated targeting....146
6.1.2.1. Anisotropic pep-OEG NPs in selective interactions with HUVECs....151
6.2. Regulation of basic biological functions of HUVEC....153
6.2.1. Overview at the molecular level: gene expression profiling....154
6.2.2. *In vitro* angiogenesis regulation.... 161
References....169
7. Laser-hyperthermia with OEG NPs and P1-OEG NPs....174
7.1. HUVECs survival rate....176
7.2. Metabolism changes in survived HUVECs....184
References....191
8. Summary and Outlook.... 194
8.1. Summary of results....195
8.1.1. Synthesis, surface capping and assembly of NPs....195
8.1.2. Cellular fate of OEG NPs....196

8.1.3. Cell targeting and regulation with pep-OEG NPs..... 197
8.1.4. Laser-hyperthermia with OEG-NPs and P1-OEG NPs..... 197
8.2. Outlook to future work..... 198
References..... 200

Appendix A – list of reagents suppliers..... i
Appendix B – supplementary information……..... iii
B1 – OEG and DA-PEG ligands quantification..... iii
B2 – octa-peptides quantification..... v
B3 – calculations of the number of gold atoms per nanoparticle..... vii
B4 – laser-hyperthermia with OEG NPs and P1-OEG NPs…….. ix

Author's declaration

I, **Dorota Bartczak**, declare that the thesis entitled:

Synthesis, surface modifications and biomedical applications of colloidal gold nanoparticles, towards controlled regulation of angiogenesis in conjunction with photo-thermal therapy

and the work presented in the thesis are both my own, and have been generated by me as the result of my own original research. I confirm that:

- this work was done wholly or mainly while in candidature for a research degree at this University;
- where any part of this thesis has previously been submitted for a degree or any other qualification at this University or any other institution, this has been clearly stated;
- where I have consulted the published work of others, this is always clearly attributed;
- where I have quoted from the work of others, the source is always given. With the exception of such quotations, this thesis is entirely my own work;
- I have acknowledged all main sources of help;
- where the thesis is based on work done by myself jointly with others, I have made clear exactly what was done by others and what I have contributed myself;
- parts of this work have been published as:

  Articles in Academic Press:

  1. "*A diacetylene-containing ligand as a new capping agent for the preparation of water-soluble colloidal nanoparticles of remarkable stability*"
     D. Bartczak and A.G. Kanaras; *Langmuir* **2010**, 26, 7072–7077.

  2. "*Controlling the three-dimensional morphology of nanocrystals*"
     H. A. Day, D. Bartczak, N. Fairbairn, E. Mcguire, M. Ardakani, A. E. Porter, A. G. Kanaras; *CrystEngComm*, **2010**, *12*, 4312-4316.

  3. "*Receptor-mediated interactions between colloidal gold nanoparticles and Human Umbilical Vein Endothelial Cells*"

D. Bartczak, T. Sanchez-Elsner, F. Louafi, T. M. Millar, A. G. Kanaras; *Small*, **ASAP**.

4. "*Programmed assembly of peptide-functionalized gold nanoparticles on DNA templates*"
   D. Coomber, D. Bartczak, S. R. Gerrard, S. Tyas, E. Stulz, A. G. Kanaras; *Langmuir*, **2010**, 26, 13760-13762.

5. "*Effects of non-destructive nanoparticle hyperthermia on endothelial cells*"
   D. Bartczak, O. L. Muskens, T. M. Millar, T. Sanchez-Elsner, A. G. Kanaras; *Nano Lett.*, submitted.

6. "*Regulation of angiogenesis using peptide coated NPs*"
   D. Bartczak, T. Sanchez-Elsner, T. M. Millar, A. G. Kanaras; in preparation.

7. "*Suspension of liquid crystal - gold nanoparticles as a photorefractive material*"
   O. Buchnev, D. Bartczak, A. G. Kanaras, N. Podoliak, V. Reshetnyak, Yu. Reznikov, M. Kaczmarek; in preparation.

8. "*Uptake of colloidal gold NPs by endothelial cells*"
   D. Bartczak, T. Sanchez-Elsner, T. M. Millar, A. G. Kanaras; in preparation.

Abstracts, Posters or Presentations at the following Conferences:

1. 238th ACS National Meeting (August 2009, Washington DC, USA)
2. NANAX3 (May 2008, Lecce, Italy)
3. NANAX4 (April 2010, Munich, Germany)
4. 13th Topical Meeting on the Optics of Liquid Crystal (September 2009, Erice Italy)
5. UK Nanoforum and Emerging Technologies 2009 (November 2009, London, UK)
6. 42nd IUPAC Congress (August 2009, Glasgow, UK)

Applications for the ‘PhD plus Fellowship’ and the ‘SET for Britain 2010’, which resulted in the following awards:

1. First prize (Mendel Medal) at the SET for Britain 2010 event in Biological and Biomedical Sciences.
2. EPSRC funded PhD Plus Fellowship for 2010/2011.

Signed:

Date: 31th January 2011

Acknowledgements

Firstly, I would like to thank Dr Antonios G. Kanaras for his supervision, financial support and for giving me the opportunity to represent our group at international conferences. I wish to express my gratitude to Dr Tilman Sanchez-Elsner for enlightening conversations, practical and technical advice, guidance and support, as well as for proof-reading my thesis. Thanks to Dr Timothy M. Millar for a continuous supply of the endothelial cells and to Dr Otto L. Muskens for assembling the laser-hyperthermia set-up. I would like to thank Dr Anton M. Page for his fruitful advice and discussions about TEM imaging and to Dr David A. Johnston for his assistance with light microscopy. Thanks to Dr Eugen Stulz and his group, especially Dr Simon R. Gerrard, for successful collaboration on the ODN templated assembly of NPs. I wish to thank our project and summer students: Daniele Coomber, Sarah Tyas, Hugo Day and Natasha Fairbairn for their hard work. Thanks to Dr Simone Nitti and by Dr J. Andy Milton for ICP-MS measurements. Special thanks to Mr Jonathan R. Burns for modelling of the RPL and LPPR motifs and for proof-reading of the whole thesis. Finally, I would like to thank my parents, Anna Bartczak and Władysław Bartczak for their continuous support, encouragement, unlimited number of thoughtful advice and for ensuring I would never lose motivation.

Abbreviations

A – adenosine

Å – Angstrom

Abs – absorbance

Ahex – aminohexanoic acid

APTMS – 3-(aminopropyl)trimethoxysilane

ASNPs – antisense oligonucleotide modified nanoparticles

BI – binding index

BN/GRP – bombesin/gastrin releasing receptor peptide

BPs – branching points

BrI – branching index

BSPP – bis(p-sulfonatophenyl)phenyl phosphine dehydrate dipotassium salt

c – concentration

CALNN – cysteine-alanine-leucine-asparagine-asparagine

CD31 – Cluster of Differentiation molecule number 31

c-DNA – complementary deoxyribonucleic acid

c-FQGII – CALNN-Ahex-FQGII

CL – capillaries length

cm – centimetre, equals to (10^{-2}) metre

C-MYC – myelocytomatosis oncogene

CO_2 – carbon dioxide

$CoCl_2$ – cobalt II chloride

COOH – carboxy group

CPP – cell penetrating peptide

CS – silica/gold core/shell nanoparticles

Ct – citrate

CTAB – hexadecyltrimethylammonium bromide

D – dilution

Da – Daltons

DA-PEG – 46-mercapto-22,43-dioxo-3,6,9,12,15,18-hexaoxa-21,44-diazahexatetraconta-31,33-diyn-1-oic acid

DDA – dipole approximation

DLS – dynamic light scattering

DNA – deoxyribonucleic acid

dNTPs – deoxynucleotide triphosphates

DTNB – Ellman's reagent; 5,5' – dithiobis(2-nitrobenzoic acid), DTNB

ε – extinction coefficient

ECs – endothelial cells

EDC – 1-(3-(dimethylamino)propyl)-3-ethyl-carbodiimidemethiodide

EDTA – ethylenediaminetetraacetic acid

EGFR – epidermal growth factor receptor

ELAM-1 – endothelial adhesion molecule type 1 (or Selectin E)

f – femto (10^{-15})

FBS – fetal bovine serum

FC-72 – tetradecafluorohexane

Fl – fluorescence

FQGII – phenyloalanine glutamine glycine isoleucine isoleucine penta-peptide

FSC – forward scattered light

g – gram

GAPDH – glyceraldehyde 3-phosphate dehydrogenase

h – hour

HBSS – Hank's balanced salt solution

He-Ne – helium-neon

HeLa – cervical cancer cells isolated from a patient named Henrietta Lacks

HF – hydrofluoric acid

HG – hollow gold nanoparticles

HIF1-α – hypoxia-inducible factor 1, α subunit

HiLyte – HiLyte Fluor 680 amine fluorescent dye

HiLyte-P1-OEG NPs – HiLyte conjugated to P1-OEG NPs

HSPs – heat shock proteins

HUVECs – human umbilical vein endothelial cells

ICAM-1 – inter-cellular adhesion molecule type 1

k – kilo (10^{3})

l – litre

Laser – Light amplification by stimulated emission of radiation

LL-RPE – Lightning-Link R-Phycoerythrin

LPD – laser power density

LPPR – leucine-proline-proline-arginine

n – nano (10^{-9})

nm – nanometre (10^{-9} metre)

NH_2 – amine group

NIR – near-infrared

NP – nanoparticle

NPs – nanoparticles

NR – rod-like nanoparticles

NRP-1 – neuropilin receptor type 1

NRP-2 – neuropilin receptor type 2

µ – micro (10^{-6})

µm – micrometre (10^{-6} metre)

m – milli (10^{-3})

M – molar (number of moles per 1000 ml)

max – maximum

method I – one-step seed mediated synthesis of gold nanorods

method II – three-step seed mediated synthesis of gold nanorods and nanowires

MHz – mega Hertz

Mn – Mean

min. – minutes

m-RNA – messenger RNA

MW – molecular weight

OD – optical density

ODN – oligodeoxynucleotide templates

ODN_{1+2} – pseudo-infinite sequence

ODN_3 – short palindromic sequence

OEG – monocarboxy (1-mercaptoundec-11-yl) hexaethylene glycol

OEG CS – core/shell nanoparticles capped with OEG

OEG HG – hollow gold nanoparticles capped with OEG

OEG NPs – nanoparticles capped with OEG

OEG NR – rod-like nanoparticles capped with OEG

OH – hydroxy group

p – pico (10^{-12})

P1 – KPQPRPLS octa-peptide (lysine-proline-glutamine-proline-arginine-proline-leucine-serine)

P1-LL-PRE – P1 peptide conjugated to LL-RPE

P1-OEG NPs – P1 peptide conjugated to OEG-capped nanoparticles

P2 – KATWLPPR octa-peptide (lysine-alanine-threonine-tryptophan-leucine-proline-proline-arginine)

P2-OEG NPs – P2 peptide conjugated to OEG-capped nanoparticles

P3 – KPRQPSLP octa-peptide (lysine-proline-arginine-glutanine-proline-serine-leucine-proline)

P3-OEG NPs – P3 peptide conjugated to OEG-capped nanoparticles

PBS – phosphate buffered saline

PEG – poly-ethylene glycol

pep-OEG NP – peptide-OEG nanoparticle conjugates

PET – polyethylene terephthalate

PIGF – placental growth factor

PIPES – piperazine-1,4-bis(2-ethanesulfonic acid)

ppm – parts per million

QDs – quantum dots

QNRs – quantum nanorods

Q-PCR – quantitative polymerase chain reaction

rec. – recovery

RI – regulation index

RME – receptor mediated endocytosis

RNA – ribonucleic acid

RNAsin – RNase inhibitor

ROS – reactive oxygen species

RPL – arginine-proline-leucine

rpm – rotation per minute

RT-PCR – reverse transcriptase polymerase chain reaction

s - seconds

SERS – surface enhanced Raman spectroscopy

SH – thiol group

s-NHS – N-hydroxysulfosuccinimide

SP – spherical nanoparticles

SPR – surface plasmon resonance

SSC – side scattered light

T– thymidine

TBE – Tris borate EDTA buffer

TEOS – tetraethyl orthosilicate

TEM – transmission electron microscopy

THPC – tetrakis(hydroxymetyl)phosphonium chloride

TNB – 5-thio-2-nitrobenzoic acid

TNF-α – tumour necrosis factor type α

UPD – under-potential deposition

UV – ultra-violet

V – volts

VEGF-A – vascular endothelial growth factor type A

VEGF A – vascular endothelial growth factor gene

VEGF-B – vascular endothelial growth factor type B

VEGFR-1 – vascular endothelial growth factor receptor type 1

VEGFR-2 – vascular endothelial growth factor receptor type 2

VEGFR-3 – vascular endothelial growth factor receptor type 3

vis – visible

vVWF – von Willebrand factor

W – watt

ξ – zeta

°C – degrees Celsius

1. Introduction.

Within the circulatory system in the human body, the interior layer of blood vessels is composed of endothelial cells (endothelium) [1]. These cells perform several important functions in the organism, e.g. responding to a pathogen and developing new blood vessels (angiogenesis) [1-3]. Angiogenesis is a physiological process occurring naturally (e.g. wound healing), but is also involved in pathological developments [2-5], e.g. excessive blood vessels growth is associated with cancer, while insufficient angiogenesis occurs in coronary artery disease and strokes [4,5]. Pathological angiogenesis in general derives from disruptions in a fragile balance (homeostasis) between stimulating and inhibiting factors [5]. To restore the homeostasis and gain control upon pathological angiogenesis, anti- or pro-angiogenic molecules can be introduced [3-16]. Consequently, some of the angiogenic therapies developed in recent years, are based on synthetic or natural angiogenesis regulating drugs [3,6,7,10-14] (**chapter 2**).

Pioneering work conducted by Ferrara and co-workers demonstrated that by inhibiting angiogenesis, the growth and progression of tumours can be suppressed *in vivo* [10]. Following this idea, nanoparticles (NPs) were employed in selective regulation of blood vessel growth towards the development of alternative cancer therapies. Specifically, this research project was focused on the design and synthesis of 'smart' nanocomposites, which can selectively target desired cell types (human umbilical vein endothelial cells, HUVECs) and regulate their primary cellular function (angiogenesis).

Recently, Mukhopadhyay and co-workers reported that inorganic NPs, e.g. europium III hydroxide nanorods promote proliferation and vascular sprouting of HUVECs in a dose dependent manner [17]. These pro-angiogenic properties were attributed to an increase in production of reactive oxygen species, induced by nanorods. Moreover, Murkhopadhyay's and Mukherjee's groups demonstrated that other types of inorganic NPs have anti-angiogenic properties [18-21]. Specifically, it was shown that gold NPs pre-incubated with vascular endothelial growth factor (VEGF, natural angiogenesis stimulator, **chapter 2**) could not induce angiogenesis in endothelial cells, because the VEGF activity was blocked by gold NPs [18,20]. All these attractive properties of nanomaterials were however based on non-selective (hence non-controllable) interactions of nanocomposites with complex biological systems.

To achieve selectivity and more efficient control upon the cellular fate of NPs, biomolecules such as peptides or oligonucleotides can be employed in NPs surface capping

[22-50]. Capped NPs show desired bioactivity and serve as, e.g. endothelium targeting vectors, for imaging and manipulation of angiogenesis.

Possible applications of engineered gold NPs, e.g. as *in vivo* drug delivery systems, therapeutics and high contrast imaging agents [22,35,41,43,47,49,51-87] are based on the interesting optoelectronic properties of gold (along with its high biocompatibility). Specifically, at the nanoscale (10^{-9} metre) gold exhibits unique optical (highly efficient resonant absorption and scattering of light) and thermal (light absorption and conversion into heat) properties, which are strongly correlated with the size and shape of NPs (and not seen in bulk) [51,76,88-98]. Spherical NPs highly absorb the light in the visible spectral range [99-104], while the maximum absorption of anisotropic NPs (e.g. rod-like, hollow and core/shell) is shifted into longer wavelengths [78,89-94,96-98,102,105-107] (near-infrared 'NIR' region, **chapter 2**). Gold NPs are generally considered to be biocompatible because of the relatively low toxicity (referred to other types of inorganic NPs, e.g. cadmium based quantum dots) [61,108-113] and high affinity towards amines and thiols [23, 29,114]. Thiol based molecules are commonly used to cap NPs surface [24,26,29,33,34,37,39,114-123]. Appropriate surface stabilisation ensures water solubility and enhances stability of NPs against aggregation in biological environments, thus preserving their properties [92,115,118,119,124]. It is absolutely necessary to retain the properties of NPs to prevent any intoxication deriving from, e.g. exposure of the inorganic core and/or non-specific adsorption of biomolecules on the gold surface. Except of the stabilising role, the composition of an organic corona (chemical structure, net charge and hydrodynamic diameter and the presence of biomolecules) determines the cellular fate of colloids [23,24,42,58,108,125-129] (see **chapter 5** and **6** for results).

Nanocomposites, capable of selective targeting of HUVECs, were developed during this research project (see **Scheme 1**). Gold NPs (spherical and anisotropic) were synthesised following well-established wet chemistry methods [36,89,91,100,101,104-106,130-150] (see **chapter 2** for theoretical background), which were optimised to match the project requirements (see **chapter 3** for detailed synthetic protocols). The NPs surface was capped with a selection of ligands (see **chapter 2** for theoretical background; **chapter 3** for chemical structures and experimental protocols), including oligoethylene glycol (OEG) based molecules [23,151] and its diacetylene (DA-PEG) [119] modified version, as well as CALNN based peptides [24,34,35,46]. The physicochemical properties of the resulting colloids were studied (see **chapter 4** for results).

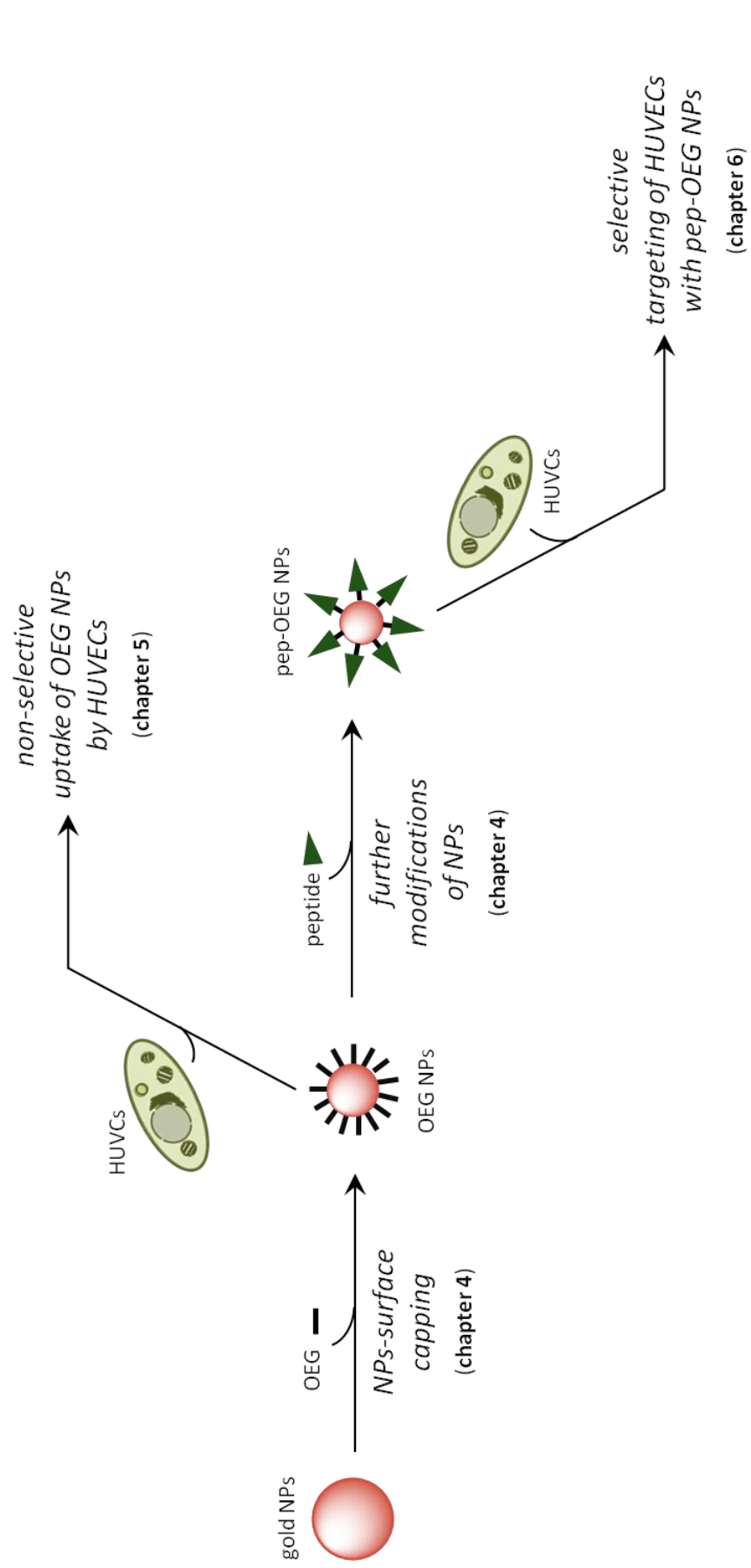

Scheme 1. Schematic illustration of: NPs surface capping and further modifications, non-selective uptake of OEG capped colloids by HUVECs versus selective cell targeting with pep-OEG NPs.

Basic mechanisms of interactions between OEG capped NPs and HUVECs were studied (see **chapter 5** for results). Internalisation of colloids by cells was attributed to the strong charge of the OEG capping layer. The overall uptake rate of NPs was predominantly size and shape dependent.

To obtain better selectivity and control upon the cellular fate of colloids, OEG NPs were modified with synthetic peptides. Peptides were designed (see **chapter 2** for details) to show versatile bioactivity, whilst exhibiting similar physicochemical properties. Each sequence was composed of the same overall number of amino acid residues, but different primary structure (amino acids arrangements, see **chapter 2** for sequences). The primary structure determined the biological activity of the peptides. All peptides, were conjugated to OEG NPs *via* standard coupling protocols [40,44,152] (see **chapter 2** for theoretical basis and **chapter 3** for experimental). Conjugated colloids (pep-OEG NPs) were used to target HUVECs. Targeting was achieved by a selective recognition between peptide sequences and appropriate receptors on HUVECs cellular membrane (see **chapter 2** for theoretical background and **chapter 6** for results). The receptor binding of pep-OEG NPs triggered a cellular response, resulting in selective regulation (activation or inhibition) of physiological processes in HUVECs.

HUVECs were also targeted with NIR absorbing, anisotropic pep-OEG NPs and exposed to NIR laser light (**Scheme 2**). The light at NIR frequency penetrated cells (see **chapter 2** for theoretical background) and was absorbed by NPs [84,98,153-155]. The absorbed light was converted to heat, resulting in a local temperature increase [76,84,98,156]. Elevated temperatures induced cellular response, or at the extreme lead to cell death [157-165] (see **chapter 2** for theoretical background). Detailed studies upon laser induced photo-thermal effects in HUVECs will be presented in **chapter 7**.

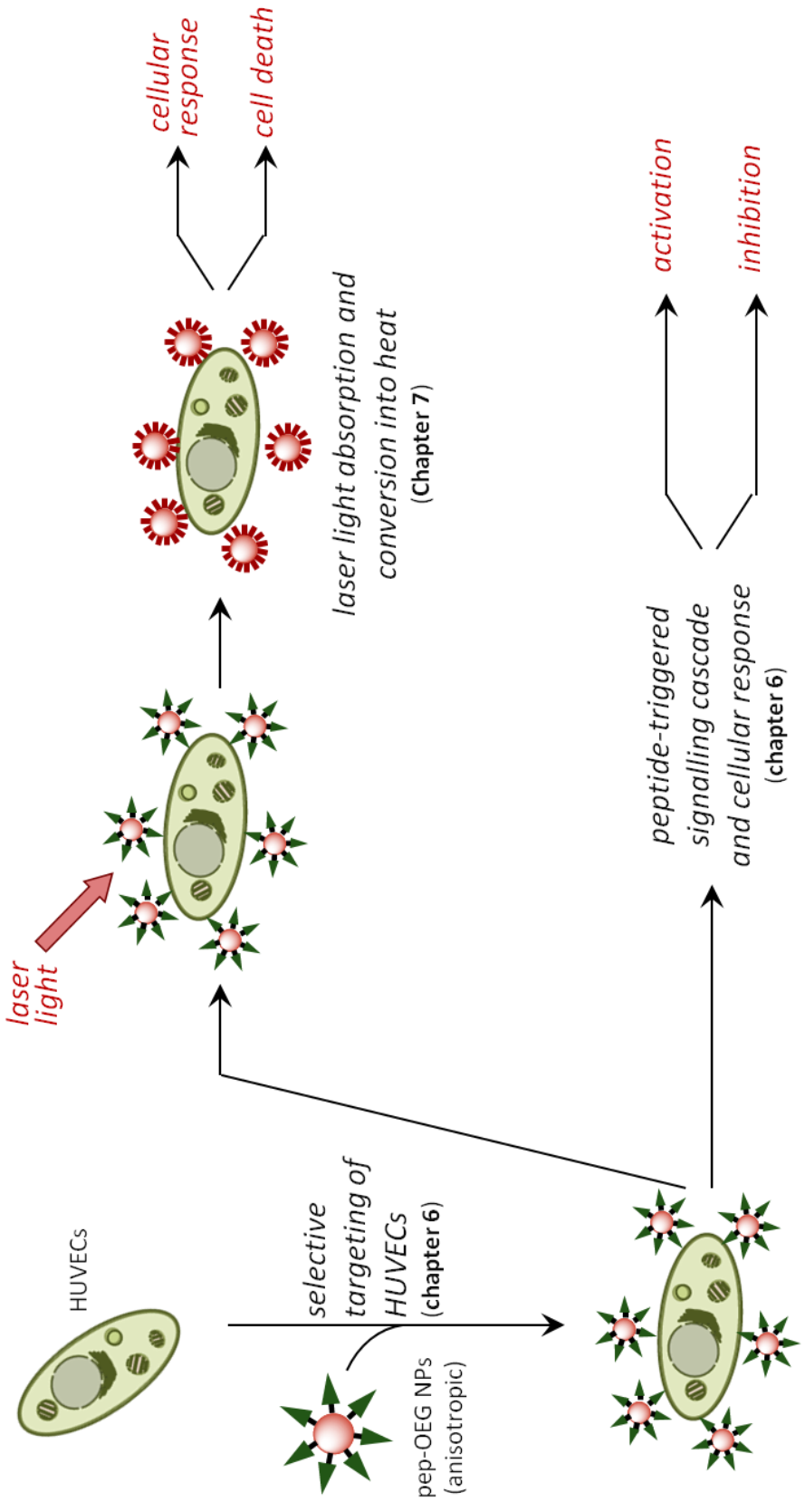

Scheme 2. Schematic illustration of biomedical applications of gold NPs: controlled regulation of angiogenesis in conjunction with photo-thermal therapy.

References:

[1] Michiels, C. *J Cell Physiol* **2003**, *196*, 430-443.

[2] Folkman, J. *Semin Cancer Biol* **2003**, *13*, 159-167.

[3] Goodwin, A. M. *Microvasc Res* **2007**, *74*, 172-183.

[4] Teicher, B. A. *Crit Rev Oncol/Hematol* **1995**, *20*, 9-39.

[5] Carmeliet, P.; Jain, R. K. *Nature* **2000**, *407*, 249-257.

[6] Shanafelt, T. D.; Kay, N. E. *Semin Oncol* **2006**, *33*, 174-185.

[7] Vincent, L.; Kermani, P.; Young, L. M.; Cheng, J.; Zhang, F.; Shido, K.; Lam, G.; Bompais-Vincent, H.; Zhu, Z.; Hicklin, D. J.; Bohlen, P.; Chaplin, D. J.; May, C.; Rafii, S. *J Clin Invest* **2005**, *115*, 2992-3006.

[8] Mustonen, T.; Alitalo, K. *J Cell Biol* **1995**, *129*, 895-898.

[9] Vastrik, I.; Kaipainen, A.; Penttila, T. L.; Lymboussakis, A.; Alitalo, R.; Parvinen, M.; Alitalo, K. *J Cell Biol* **1995**, *128*, 1197-1208.

[10] Kim, K. J.; Li, B.; Winer, J.; Armanini, M.; Gillett, N.; Phillips, H. S.; Ferrara, N. *Nature* **1993**, *362*, 841-844.

[11] D'Andrea, L. D.; Del Gatto, A.; Pedone, C.; Benedetti, E. *Chem Biol Drug Des* **2006**, *67*, 115-126.

[12] Starzec, A.; Ladam, P.; Vassy, R.; Badache, S.; Bouchemal, N.; Navaza, A.; du Penhoat, C. H.; Perret, G. Y. *Peptides* **2007**, *28*, 2397-2402.

[13] Mould, A. W.; Greco, S. A.; Cahill, M. M.; Tonks, I. D.; Bellomo, D.; Patterson, C.; Zournazi, A.; Nash, A.; Scotney, P.; Hayward, N. K.; Kay, G. F. *Circ Res* **2005**, *97*, e60-70.

[14] Olofsson, B.; Korpelainen, E.; Pepper, M. S.; Mandriota, S. J.; Aase, K.; Kumar, V.; Gunji, Y.; Jeltsch, M. M.; Shibuya, M.; Alitalo, K.; Eriksson, U. *Proc Natl Acad Sci USA* **1998**, *95*, 11709-11714.

[15] Li, Y.; Zhang, F.; Nagai, N.; Tang, Z.; Zhang, S.; Scotney, P.; Lennartsson, J.; Zhu, C.; Qu, Y.; Fang, C.; Hua, J.; Matsuo, O.; Fong, G.-H.; Ding, H.; Cao, Y.; Becker, K. G.; Nash, A.; Heldin, C.-H.; Li, X. *J Clin Invest* **2008**, *118*, 913-923.

[16] Zhang, F.; Tang, Z.; Hou, X.; Lennartsson, J.; Li, Y.; Koch, A. W.; Scotney, P.; Lee, C.; Arjunan, P.; Dong, L.; Kumar, A.; Rissanen, T. T.; Wang, B.; Nagai, N.; Fons, P.; Fariss, R.; Zhang, Y.; Wawrousek, E.; Tansey, G.; Raber, J.; Fong, G.-H.; Ding, H.; Greenberg, D. A.; Becker, K. G.; Herbert, J.-M.; Nash, A.; Yla-Herttuala, S.; Cao, Y.; Watts, R. J.; Li, X. *Proc Natl Acad Sci USA* **2009**, *106*, 6152-6157.

[17] Patra, C.; Bhattacharya, R.; Patra, S.; Vlahakis, N.; Gabashvili, A.; Koltypin, Y.; Gedanken, A.; Mukherjee, P.; Mukhopadhyay, D. *Advanced Materials* **2008**, *20*, 753-756.

[18] Mukherjee, P.; Bhattacharya, R.; Wang, P.; Wang, L.; Basu, S.; Nagy, J. A.; Atala, A.; Mukhopadhyay, D.; Soker, S. *Clin Cancer Res* **2005**, *11*, 3530-3534.

[19] Bhattacharya, R.; Mukherjee, P. *Adv Drug Deliv Rev* **2008**, *60*, 1289-1306.

[20] Bhattacharya, R.; Mukherjee, P.; Xiong, Z.; Atala, A.; Soker, S.; Mukhopadhyay, D. *Nano Lett* **2004**, *4*, 2479-2481.

[21] Mukherjee, P.; Bhattacharya, R.; Bone, N.; Lee, Y.; Patra, C.; Wang, S.; Lu, L.; Secreto, C.; Banerjee, P.; Yaszemski, M.; Kay, N.; Mukhopadhyay, D. *J Nanobiotechnology* **2007**, *5*, 4-17.

[22] Yu, D.-H.; Lu, Q.; Xie, J.; Fang, C.; Chen, H.-Z. *Biomaterials* **2010**, *31*, 2278-2292.

[23] You, C.-C.; Chompoosor, A.; Rotello, V. M. *Nano Today* **2007**, *2*, 34-43.

[24] Wang, Z.; Levy, R.; Fernig, D. G.; Brust, M. *Bioconjug Chem* **2005**, *16*, 497-500.

[25] Steven, V.; Ingram, A.; Graham, D. *Chem Commun* **2009**, 2872-2874.

[26] Schmid, G. *Chem Rev* **1992**, *92*, 1709-1727.

[27] Quarta, A.; Ragusa, A.; Deka, S.; Tortiglione, C.; Tino, A.; Cingolani, R.; Pellegrino, T. *Langmuir* **2009**, *25*, 12614-12622.

[28] Perrault, S. D.; Walkey, C.; Jennings, T.; Fischer, H. C.; Chan, W. C. W. *Nano Lett* **2009**, *9*, 1909-1915.

[29] Pengo, P.; Pasquato, L. In *The supramolecular chemistry of organic - inorganic hybrid materials*; Rurak, K., Martinez-Manez, R., Eds.; John Wiley & Sons, Inc. : Hoboken, New Jersey, **2010**, p 113-154.

[30] Oyelere, A. K.; Chen, P. C.; Huang, X.; El-Sayed, I. H.; El-Sayed, M. A. *Bioconjug Chem* **2007**, *18*, 1490-1497.

[31] Mandal, D.; Maran, A.; Yaszemski, M.; Bolander, M.; Sarkar, G. *J Mater Sci: Mater Med* **2009**, *20*, 347-350.

[32] Lynch, I.; Dawson, K. A. *Nano Today* **2008**, *3*, 40-47.

[33] Liu, Y.; Shipton, M. K.; Ryan, J.; Kaufman, E. D.; Franzen, S.; Feldheim, D. L. *Anal Chem* **2007**, *79*, 2221-2229.

[34] Levy, R.; Thanh, N. T. K.; Doty, R. C.; Hussain, I.; Nichols, R. J.; Schiffrin, D. J.; Brust, M.; Fernig, D. G. *J Am Chem Soc* **2004**, *126*, 10076-10084.

[35] Lévy, R. *ChemBioChem* **2006**, *7*, 1141-1145.

[36] Rayavarapu, R. G.; Ungureanu, C.; Krystek, P.; van Leeuwen, T. G.; Manohar, S. *Langmuir* **2010**, *26*, 5050-5055.

[37] Krpetic, Z.; Nativo, P.; Porta, F.; Brust, M. *Bioconjug Chem* **2009**, *20*, 619-624.

[38] Hosta-Rigau, L.; Olmedo, I.; Arbiol, J.; Cruz, L. J.; Kogan, M. J.; Albericio, F. *Bioconjug Chem* **2010**, *21*, 1070-1078.

[39] Hill, H. D.; Millstone, J. E.; Banholzer, M. J.; Mirkin, C. A. *ACS Nano* **2009**, *3*, 418-424.

[40] Hermanson, G. T. *Bioconjugate Techniques*; 2nd ed.; Elsevier Inc. , **2008**.

[41] Gu, F. X.; Karnik, R.; Wang, A. Z.; Alexis, F.; Levy-Nissenbaum, E.; Hong, S.; Langer, R. S.; Farokhzad, O. C. *Nano Today* **2007**, *2*, 14-21.

[42] Giljohann, D. A.; Seferos, D. S.; Patel, P. C.; Millstone, J. E.; Rosi, N. L.; Mirkin, C. A. *Nano Lett* **2007**, *7*, 3818-3821.

[43] Gil, P. R.; Parak, W. J. *ACS Nano* **2008**, *2*, 2200-2205.

[44] Eck, W.; Craig, G.; Sigdel, A.; Ritter, G.; Old, L. J.; Tang, L.; Brennan, M. F.; Allen, P. J.; Mason, M. D. *ACS Nano* **2008**, *2*, 2263-2272.

[45] de la Fuente, J. M.; Berry, C. C. *Bioconjug Chem* **2005**, *16*, 1176-1180.

[46] Coomber, D.; Bartczak, D.; Gerrard, S. R.; Tyas, S.; Kanaras, A. G.; Stulz, E. *Langmuir* **2010**, *26*, 13760-13762.

[47] Choi, M.-R.; Stanton-Maxey, K. J.; Stanley, J. K.; Levin, C. S.; Bardhan, R.; Akin, D.; Badve, S.; Sturgis, J.; Robinson, J. P.; Bashir, R.; Halas, N. J.; Clare, S. E. *Nano Lett* **2007**, *7*, 3759-3765.

[48] Chithrani, B. D.; Chan, W. C. W. *Nano Lett* **2007**, *7*, 1542-1550.

[49] Cheng, J.; Teply, B. A.; Sherifi, I.; Sung, J.; Luther, G.; Gu, F. X.; Levy-Nissenbaum, E.; Radovic-Moreno, A. F.; Langer, R.; Farokhzad, O. C. *Biomaterials* **2007**, *28*, 869-876.

[50] Love, J. C.; Estroff, L. A.; Kriebel, J. K.; Nuzzo, R. G.; Whitesides, G. M. *Chem Rev* **2005**, *105*, 1103-1170.

[51] Hu, M.; Chen, J.; Li, Z.-Y.; Au, L.; Hartland, G. V.; Li, X.; Marquez, M.; Xia, Y. *Chem Soc Rev* **2006**, *35*, 1084-1094.

[52] Gao, J.; Xu, B. *Nano Today* **2009**, *4*, 37-51.

[53] Salata, O. V. *J Nanobiotechnology* **2004**, *2*, 3-9.

[54] Jain, P. K.; El-Sayed, I. H.; El-Sayed, M. A. *Nano Today* **2007**, *2*, 18-29.

[55] Sperling, R. A.; Rivera Gil, P.; Zhang, F.; Zanella, M.; Parak, W. J. *Chem Soc Rev* **2008**, *37*, 1896-1908.

[56] Chen, C. S. *Nat Nano* **2008**, *3*, 13-14.

[57] Hirak, K. P.; Shuvojit, B.; Utpal, C.; Prabir, L.; Anjan Kr, D. *Nanomedicine* **2007**, *3*, 111-119.

[58] Ghosh, P. S.; Kim, C.-K.; Han, G.; Forbes, N. S.; Rotello, V. M. *ACS Nano* **2008**, *2*, 2213-2218.

[59] Green, J. J.; Chiu, E.; Leshchiner, E. S.; Shi, J.; Langer, R.; Anderson, D. G. *Nano Lett* **2007**, *7*, 874-879.

[60] Chen, J.; Wiley, B.; Li, Z. Y.; Campbell, D.; Saeki, F.; Cang, H.; Au, L.; Lee, J.; Li, X.; Xia, Y. *Adv Mater* **2005**, *17*, 2255-2261.

[61] Murphy, C. J.; Gole, A. M.; Stone, J. W.; Sisco, P. N.; Alkilany, A. M.; Goldsmith, E. C.; Baxter, S. C. *Acc Chem Res* **2008**, *41*, 1721-1730.

[62] Scheffer, A.; Engelhard, C.; Sperling, M.; Buscher, W. *Anal Bioanal Chem* **2008**, *390*, 249-252.

[63] Farokhzad, O. C.; Langer, R. *ACS Nano* **2009**, *3*, 16-20.

[64] Peer, D.; Karp, J. M.; Hong, S.; Farokhzad, O. C.; Margalit, R.; Langer, R. *Nat Nano* **2007**, *2*, 751-760.

[65] Cheng, H.; Kastrup, C. J.; Ramanathan, R.; Siegwart, D. J.; Ma, M.; Bogatyrev, S. R.; Xu, Q.; Whitehead, K. A.; Langer, R.; Anderson, D. G. *ACS Nano* **2010**, *4*, 625-631.

[66] Rosi, N. L.; Mirkin, C. A. *Chem Rev* **2005**, *105*, 1547-1562.

[67] Kobayashi, H.; Lin, P. C. *Nanomedicine* **2006**, *1*, 17-22.

[68] Lee, S.; Xie, J.; Chen, X. *Biochemistry* **2010**, *49*, 1364-1376.

[69] Sokolov, K.; Follen, M.; Aaron, J.; Pavlova, I.; Malpica, A.; Lotan, R.; Richards-Kortum, R. *Cancer Res* **2003**, *63*, 1999-2004.

[70] Sapsford, K. E.; Bradburne, C.; Delehanty, J. B.; Medintz, I. L. *Nano Today* **2008**, *11*, 38-49.

[71] El-Sayed, I. H.; Huang, X.; El-Sayed, M. A. *Nano Lett* **2005**, *5*, 829-834.

[72] Kim, G. J.; Nie, S. *Mater Today* **2005**, *8*, 28-33.

[73] Hu, M.; Chen, J.; Li, Z.-Y.; Au, L.; Hartland, G. V.; Li, X.; Marquez, M.; Xia, Y. *Chem Soc Rev* **2006**, *35*, 1084 - 1094.

[74] Huang, X.; El-Sayed, I. H.; Qian, W.; El-Sayed, M. A. *J Am Chem Soc* **2006**, *128*, 2115-2120.

[75] Hauck, T. S.; Jennings, T. L.; Yatsenko, T.; Kumaradas, J. C.; Chan, W. C. W. *Adv Mater* **2008**, *20*, 3832-3838.

[76] Govorov, A. O.; Richardson, H. H. *Nano Today* **2007**, *2*, 30-38.

[77] Huang, X.; Neretina, S.; El-Sayed, M. A. *Adv Mater* **2009**, *21*, 4880-4910.

[78] Chen, J.; Wang, D.; Xi, J.; Au, L.; Siekkinen, A.; Warsen, A.; Li, Z.-Y.; Zhang, H.; Xia, Y.; Li, X. *Nano Lett* **2007**, *7*, 1318-1322.

[79] Lowery, A. R.; Gobin, A. M.; Day, E. S.; Halas, N. J.; West, J. L. *Int J Nanomedicine* **2006**, *1*, 149-154.

[80] Loo, C.; Lowery, A.; Halas, N.; West, J.; Drezek, R. *Nano Lett* **2005**, *5*, 709-711.

[81] Lal, S.; Clare, S. E.; Halas, N. J. *Acc Chem Res* **2008**, *41*, 1842-1851.

[82] Cole, J. R.; Mirin, N. A.; Knight, M. W.; Goodrich, G. P.; Halas, N. J. *J Phys Chem C* **2009**, *113*, 12090-12094.

[83] O'Neal, D. P.; Hirsch, L. R.; Halas, N. J.; Payne, J. D.; West, J. L. *Cancer Lett* **2004**, *209*, 171-176.

[84] Huang, X.; Jain, P.; El-Sayed, I.; El-Sayed, M. *Lasers Med Sci* **2008**, *23*, 217-228.

[85] Huang, H.-C.; Barua, S.; Kay, D. B.; Rege, K. *ACS Nano* **2010**, *4*, 1769-1770.

[86] Li, J. L.; Day, D.; Gu, M. *Adv Mater* **2008**, *20*, 3866-3871.

[87] Chen, J.; Saeki, F.; Wiley, B. J.; Cang, H.; Cobb, M. J.; Li, Z.-Y.; Au, L.; Zhang, H.; Kimmey, M. B.; Li; Xia, Y. *Nano Lett* **2005**, *5*, 473-477.

[88] Hvolbćk, B.; Janssens, T. V. W.; Clausen, B. S.; Falsig, H.; Christensen, C. H.; Nřrskov, J. K. *Nano Today* **2007**, *2*, 14-18.

[89] Murphy, C. J.; Sau, T. K.; Gole, A. M.; Orendorff, C. J.; Gao, J.; Gou, L.; Hunyadi, S. E.; Li, T. *J Phys Chem B* **2005**, *109*, 13857-13870.

[90] Haiss, W.; Thanh, N. T. K.; Aveyard, J.; Fernig, D. G. *Anal Chem* **2007**, *79*, 4215-4221.

[91] Oldenburg, S. J.; Averitt, R. D.; Westcott, S. L.; Halas, N. J. *Chem Phys Lett* **1998**, *288*, 243-247.

[92] Kelly, K. L.; Coronado, E.; Zhao, L. L.; Schatz, G. C. *J Phys Chem B* **2002**, *107*, 668-677.

[93] Hao, E.; Li, S.; Bailey, R. C.; Zou, S.; Schatz, G. C.; Hupp, J. T. *J Phys Chem B* **2004**, *108*, 1224-1229.

[94] Halas, N. *Opt Photon News* **2002**, *13*, 26-30.

[95] Wang, H.; Brandl, D. W.; Nordlander, P.; Halas, N. J. *Acc Chem Res* **2006**, *40*, 53-62.

[96] Kooij, E. S.; Poelsema, B. *Phys Chem Chem Phys* **2006**, *8*, 3349-3357.

[97] Orendorff, C.; Sau, T.; Murphy, C. *Small* **2006**, *2*, 636-639.

[98] Link, S.; El-Sayed, M. A. *Int Rev Phys Chem* **2000**, *19*, 409-453.

[99] Frens, G. *Nature-Phys Sci* **1973**, *241*, 20-22.

[100] Turkevich, J.; Stevenson, P. C.; Hillier, J. *J Phys Chem* **1953**, *57*, 670-673.

[101] Kumar, S.; Gandhi, K. S.; Kumar, R. *Ind Eng Chem Res* **2006**, *46*, 3128-3136.

[102] Mie, G. *Ann Phys* **1908**, *330*, 377-445.

[103] Kreibig, U.; Vollmer, M. *Optical Properties of Metal Clusters*; Springer: Berlin, **1995**; Vol. 25.

[104] Ji, X.; Song, X.; Li, J.; Bai, Y.; Yang, W.; Peng, X. *J Am Chem Soc* **2007**, *129*, 13939-13948.

[105] Pérez-Juste, J.; Pastoriza-Santos, I.; Liz-Marzán, L. M.; Mulvaney, P. *Coord Chem Rev* **2005**, *249*, 1870-1901.

[106] Liz-Marzán, L. M. *Mater Today* **2004**, *7*, 26-31.

[107] Skrabalak, S. E.; Chen, J.; Sun, Y.; Lu, X.; Au, L.; Cobley, C. M.; Xia, Y. *Acc Chem Res* **2008**, *41*, 1587-1595.

[108] Hauck, T.; Ghazani, A.; Chan, W. *Small* **2008**, *4*, 153-159.

[109] Alkilany, A. M.; Nagaria, P. K.; Hexel, C. R.; Shaw, T. J.; Murphy, C. J.; Wyatt, M. D. *Small* **2009**, *5*, 701-708.

[110] Arnida; Malugin, A.; Ghandehari, H. *J Appl Toxicol* **2010**, *30*, 212-217.

[111] Connor, E.; Mwamuka, J.; Gole, A.; Murphy, C.; Wyatt, M. *Small* **2005**, *1*, 325-327.

[112] Maynard, A. D. *Nano Today* **2006**, *1*, 22-33.

[113] Derfus, A. M.; Chan, W. C. W.; Bhatia, S. N. *Nano Lett* **2003**, *4*, 11-18.

[114] Cortie, M. B.; McDonagh, A. In *Gold Chemistry: Applications and future directions in life sciences*; Mohr, F., Ed.; WILLEY-VCH Verlag GmbH & Co. KGaA Weinheim, **2009**, p 321-343.

[115] Rouhana, L. L.; Jaber, J. A.; Schlenoff, J. B. *Langmuir* **2007**, *23*, 12799-12801.

[116] Kanaras, A. G.; Kamounah, F. S.; Schaumburg, K.; Kiely, C. J.; Brust, M. *Chem Commun* **2002**, 2294-2295.

[117] Gentilini, C.; Evangelista, F.; Rudolf, P.; Franchi, P.; Lucarini, M.; Pasquato, L. *J Am Chem Soc* **2008**, *130*, 15678-15682.

[118] Duchesne, L.; Gentili, D.; Comes-Franchini, M.; Fernig, D. G. *Langmuir* **2008**, *24*, 13572-13580.

[119] Bartczak, D.; Kanaras, A. G. *Langmuir* **2010**, *26*, 7072-7077.

[120] Alloisio, M.; Demartini, A.; Cuniberti, C.; Dellepiane, G.; Muniz-Miranda, M.; Giorgetti, E. *Vib Spectrosc* **2008**, *48*, 53-57.

[121] Zheng, J.; Constantinou, P. E.; Micheel, C.; Alivisatos, A. P.; Kiehl, R. A.; Seeman, N. C. *Nano Lett* **2006**, *6*, 1502-1504.

[122] Wuelfing, W. P.; Gross, S. M.; Miles, D. T.; Murray, R. W. *J Am Chem Soc* **1998**, *120*, 12696-12697.

[123] Brust, M.; Fink, J.; Bethell, D.; Schiffrin, D. J.; Kiely, C. *J Chem Soc, Chem Commun* **1995**, 1655-1656.

[124] Burns, C.; Spendel, W. U.; Puckett, S.; Pacey, G. E. *Talanta* **2006**, *69*, 873-876.

[125] Ehrenberg, M. S.; Friedman, A. E.; Finkelstein, J. N.; Oberdörster, G.; McGrath, J. L. *Biomaterials* **2009**, *30*, 603-610.

[126] Liu, R.; Kay, B. K.; Jiang, S.; Chen, S. *MRS Bulletin* **2009**, *34*, 432-440.

[127] Decuzzi, P.; Ferrari, M. *Biomaterials* **2007**, *28*, 2915-2922.

[128] Verma, A.; Uzun, O.; Hu, Y.; Hu, Y.; Han, H.-S.; Watson, N.; Chen, S.; Irvine, D. J.; Stellacci, F. *Nat Mater* **2008**, *7*, 588-595.

[129] Nativo, P.; Prior, I. A.; Brust, M. *ACS Nano* **2008**, *2*, 1639-1644.

[130] Day, H. A.; Bartczak, D.; Fairbairn, N.; McGuire, E.; Ardakani, M.; Porter, A. E.; Kanaras, A. G. *CrystEngComm* **2010**, *12*, 4312-4316.

[131] Westcott, S. L.; Oldenburg, S. J.; Lee, T. R.; Halas, N. J. *Langmuir* **1998**, *14*, 5396-5401.

[132] Smith, D. K.; Korgel, B. A. *Langmuir* **2008**, *24*, 644-649.

[133] Busbee, B.; Obare, S.; Murphy, C. *Adv Mater* **2003**, *15*, 414-416.

[134] Smith, D. K.; Miller, N. R.; Korgel, B. A. *Langmuir* **2009**, *25*, 9518-9524.

[135] Lu, X.; Tuan, H.-Y.; Chen, J.; Li, Z.-Y.; Korgel, B. A.; Xia, Y. *J Am Chem Soc* **2007**, *129*, 1733-1742.

[136] Van Blaaderen, A.; Van Geest, J.; Vrij, A. *J Colloid Interface Sci* **1992**, *154*, 481-501.

[137] Duff, D. G.; Baiker, A.; Edwards, P. P. *Langmuir* **1993**, *9*, 2301-2309.

[138] Duff, D. G.; Baiker, A.; Gameson, I.; Edwards, P. P. *Langmuir* **1993**, *9*, 2310-2317.

[139] Nikoobakht, B.; El-Sayed, M. A. *Chem Mater* **2003**, *15*, 1957-1962.
[140] Lee, G.-J.; Shin, S.-I.; Kim, Y.-C.; Oh, S.-G. *Mater Chem Phys* **2004**, *84*, 197-204.
[141] Sau, T. K.; Murphy, C. J. *Philos Mag* **2007**, *87*, 2143-2158.
[142] Gole, A.; Murphy, C. J. *Chem Mater* **2004**, *16*, 3633-3640.
[143] Xia, Y.; Xiong, Y.; Lim, B.; Skrabalak, S. *Angew Chem, Int Ed* **2009**, *48*, 60-103.
[144] Cobley, C.; Skrabalak, S.; Campbell, D.; Xia, Y. *Plasmonics* **2009**, *4*, 171-179.
[145] Turkevich, J.; Stevenson, P. C.; Hillier, J. *Disc Faraday Soc* **1951**, *11*, 55-75.
[146] Yong, K.-T.; Sahoo, Y.; Swihart, M. T.; Prasad, P. N. *Colloids Surf, A* **2006**, *290*, 89-105.
[147] Phonthammachai, N.; Kah, J. C. Y.; Jun, G.; Sheppard, C. J. R.; Olivo, M. C.; Mhaisalkar, S. G.; White, T. J. *Langmuir* **2008**, *24*, 5109-5112.
[148] Arkhireeva, A.; Hay, J. N. *J Mater Chem* **2003**, *13*, 3122-3127.
[149] Jana, N. R.; Gearheart, L.; Murphy, C. J. *J Phys Chem B* **2001**, *105*, 4065-4067.
[150] Pillai, Z. S.; Kamat, P. V. *J Phys Chem B* **2003**, *108*, 945-951.
[151] Kanaras, A. G.; Kamounah, F. S.; Schaumburg, K.; Kiely, C. J.; Brust, M. *Chem Commun* **2002**, 20, 2294-2295.
[152] Chan, W. C. W.; Nie, S. *Science* **1998**, *281*, 2016-2018.
[153] Hale, G. M.; Querry, M. R. *Appl Opt* **1973**, *12*, 555-563.
[154] Prahl, S.; Oregon Medical Laser Center Oregon **1999**; Vol. 2010.
[155] Kim, J. G.; Mengna, X.; Hanli, L. *IEEE Eng Med Biol* **2005**, *24*, 118-121.
[156] Lukianova-Hleb, E. Y.; Anderson, L. J. E.; Lee, S.; Hafner, J. H.; Lapotko, D. O. *Phys Chem Chem Phys* **2010**, *12*, 12237-12244.
[157] Flanders, K. C.; Winokur, T. S.; Holder, M. G.; Sporn, M. B. *J Clin Invest* **1993**, *92*, 404-410.
[158] Brand, K.; Lubbe, A. S.; Justus, D. J. *Int J Hyperthermia* **1996**, *12*, 527-538.
[159] Lindquist, S. *Annu Rev Biochem* **1986**, *55*, 1151-1191.
[160] Creagh, E. M.; Sheehan, D.; Cotter, T. G. *Leukemia* **2000**, *14*, 1161-1173.
[161] Kühl, N. M.; Rensing, L. *Cell Mol Life Sci* **2000**, *57*, 450-463.
[162] Dinh, H.-K. B.; Zhao, B.; Schuschereba, S. T.; Merrill, G.; Bowman, P. D. *Physiol Genomics* **2001**, *7*, 3-13.
[163] Overgaard, J. *Cancer* **1977**, *39*, 2637-2646.
[164] Sawaji, Y.; Sato, T.; Takeuchi, A.; Hirata, M.; Ito, A. *Br J Cancer* **2002**, *86*, 1597-1603.
[165] Paidas, C. N.; Mooney, M. L.; Theodorakis, N. G.; De Maio, A. *Am J Physiol Regul Integr Comp Physiol* **2002**, *282*, 1374-1381.

2. Theoretical background.

Gold NPs were applied in selective regulation of an important physiological process – blood vessels growth, called angiogenesis [1]. Since angiogenesis is conducted by endothelial cells [1,2] (e.g. human umbilical vein endothelial cells: HUVECs), the research efforts were focused on studying the interactions between HUVECs and NPs. Selective interactions resulted in controlled stimulation or suppression of angiogenesis related cellular functions in HUVECs and effectively the whole angiogenesis process. The theoretical basis of this multidisciplinary project, covering the synthesis of bioactive NPs (**sections 2.1. and 2.2.**), as well as the biology of HUVECs (**section 2.6.**), will be discussed in this chapter.

Firstly, the basic principles of NPs preparation, including synthetic routes (**section 2.1.**) and capping techniques (**section 2.2.**), will be discussed. This will be then followed by a general overview on the physicochemical properties of resulting nanomaterials (**section 2.3.**). Advanced therapy technique based on the optoelectronic properties of NPs (heat generation upon laser exposure), which has evolved in recent years [3-16], will be introduced (**section 2.4.**). Biochemical basis of the resulting physiological changes in heat treated cells will also be discussed (**section 2.6.2.**).

The reader's attention will be drawn to the primary area of the research project – HUVECs and angiogenesis. Regulatory mechanisms of this process in HUVECs and the fundamental role of natural and pathological angiogenesis in the human body will be explained (**section 2.6.**). Therapy techniques based on angiogenesis regulating molecules [17-26] will then be introduced. Such therapeutics have inspired the design of pro- and anti-angiogenic peptides and their conjugation to NPs, as well as studying their interactions with HUVECs.

2.1. Synthesis of NPs.

Wet chemistry methods were employed in the synthesis of several types of colloidal gold NPs, including spherical (**section 2.1.1.**), rod-like (**section 2.1.2.**), core/shell (**section 2.1.3.**) and hollow (**section 2.1.4.**). Basic principles of synthetic routes, including reaction mechanisms will be given in the following sub-sections.

2.1.1. Synthesis of spherical gold NPs.

Gold colloids are one of the oldest known nanomaterials, dating back to ancient times, when they were used in glass staining techniques [27,28]. In modern science, the synthesis of spherical gold NPs was first reported by Faraday in 1851 [29]. Further development was conducted by Turkevich [30,31] and Frens [32] in 1951 and 1970s, respectively.

The citrate reduction method was utilised in the preparation of spherical gold NPs [30-34]. This method involves aqueous solutions of only two starting materials: chloroauric acid (gold precursor) and sodium citrate (see **chapter 3** for chemical structures and a protocol). Mixing their boiling solutions at certain molar ratios leads to the formation of NPs.

The mechanism of NPs formation was intensely investigated over the past years by several research groups [30-34]. Only recently Kumar and co-workers proposed that three simultaneous reactions (**Scheme 3**) are involved in this synthesis [33,34]. At first, citrate anions are oxidised (by oxygen from air, accompanied by heat) to dicarboxy acetone (**Scheme 3A**). At the same time, the gold precursor (Au^{3+} cations) is reduced to aurous salt (Au^{+} cations, **Scheme 3B**). Au^{+} cations form complexes with dicarboxy acetone, which according to Turkevich and co-workers, serves as 'an organiser' of this complexation [30,31]. Exactly three Au^{+} can be tethered to at least two dicarboxy acetone moieties, as demonstrated by Kumar's group [33,34]. Finally, aurous species are disproportionated to gold atoms (Au^{0}) (**Scheme 3C**).

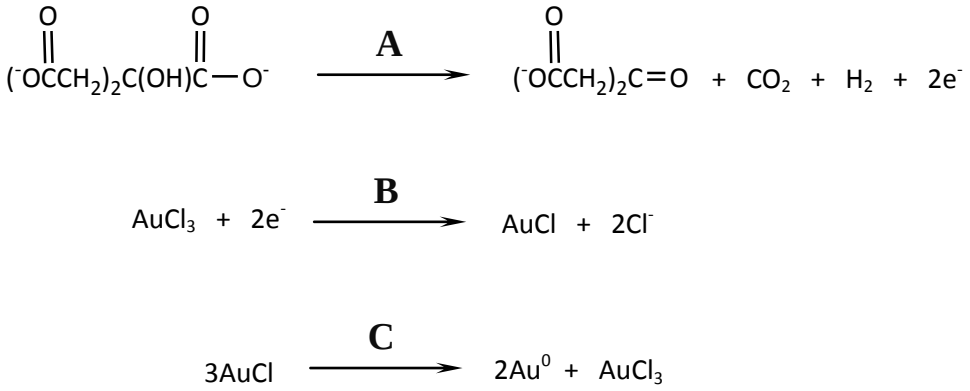

Scheme 3. Citrate oxidation (**A**), reduction of auric salt (**B**) and disproportionation of aurous species (**C**); taken from [34].

Au^0 produced during the disproportionation reaction, adsorbs Au^+ from the solution and forms large aggregates (by the complexation with dicarboxy acetone). When aggregates reach the critical size value (e.g. 2 nm was proposed by Kumar's group [34]), a nucleus of gold atoms is formed. More Au^0 are released during the disproportionation and absorbed by the nucleus, resulting in nanoparticle growth. Growing NPs are stabilised by the remaining sodium citrate (Na_3Ct) in the solution. Therefore, the Na_3Ct moiety serves as both, a reducing agent (gold precursor) and surface stabiliser (gold NPs).

However, according to Peng and co-workers there is a third role of Na_3Ct in NPs synthesis: a solution pH modulator [33]. It was demonstrated that depending on the solution pH, the reaction can undergo one of two possible pathways. Specifically, at low pH (3.7 ÷ 6.5) the rapid nucleation step (below 10 s) is followed by fast random attachment, resulting in elongated structures. Within these structures, an intra-particle ripening process effectively leads to the formation of spherical NPs. On the contrary, at pH above 6.5 (up to 7.7), nucleation is rather slow (60 s) and is followed by slow growth of NPs to spherical structures.

These two pH dependent pathways were attributed to dominant species of gold and citrate, which co-exist in the reaction mixture at the certain pH (**Scheme 4**). Specifically, at low pH, very reactive $[AuCl_3(OH)]^-$ can be found, which initiate fast nucleation. At higher pH values, these species are converted to the less reactive $[AuCl_2(OH)]_2^-$ and $[AuCl(OH)]_3^-$, resulting in slow nucleation and growth.

pH 3.7 ÷ 6.5 $[AuCl_3(OH)]^- + H_2Ct^- / HCt^{2-}$

pH 6.5 ÷ 7.7 $[AuCl_2(OH)]_2^- / [AuCl(OH)]_3^- + HCt^{2-} / Ct^{3-}$

Scheme 4. Schematic illustration of gold and citrate species found at low (top row) or high (bottom row) pH; taken from [33].

2.1.2. Synthesis of gold nanorods.

Murphy's group developed a seed mediated surfactant guided method for preparation of anisotropic gold NPs, e.g. nanorods [35-41]. The anisotropic growth into elongated structures is controlled by surfactant molecules (e.g. hexadecyltrimethylammonium bromide – CTAB, see **chapter 3** for chemical structure) and/or additive ions, like Ag^+ [35-

[40,42-48]. Rod-like NPs are grown from the gold precursor (chloroauric acid), which is reduced by ascorbic acid (in the presence of CTAB) on small NPs called seeds (see **chapter 3** for experimental protocol).

As demonstrated by Murphy and co-workers, the type of seeds (size and surface capping) strongly affects the length-to-width aspect ratio of the produced NPs, which increases with lowering the seed size [36]. According to El-Sayed and co-workers, good reaction yields can be achieved with CTAB-capped seeds, prepared by the reduction of the gold precursor with a strong reducing agent (e.g. sodium borohydride, see **Scheme 5**) in the presence of CTAB [42].

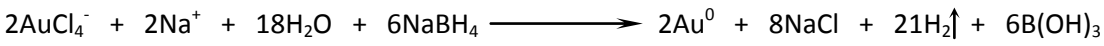

Scheme 5. Reduction of gold precursor with sodium borohydride.

As already mentioned, nanorod growth is guided by CTAB, which because of its amphiphilic character, forms micelles in aqueous solutions (see **Scheme 6**) [49]. The micelle shape depends on the concentration of surfactant and is spherical at low (below 0.1 M) or high (above 0.4 M) concentrations and rod-like in between [49].

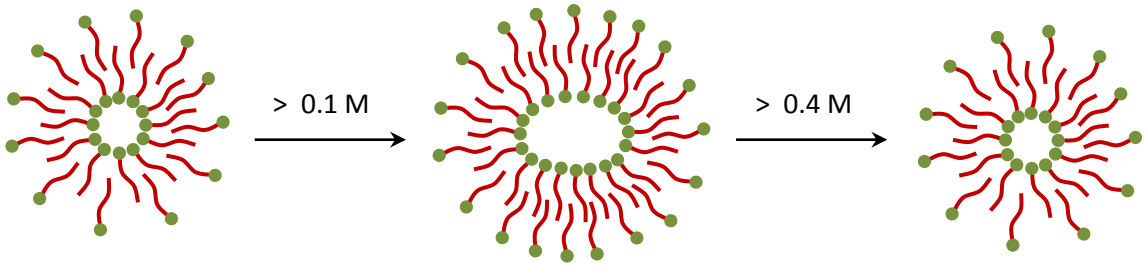

Scheme 6. Schematic illustration of the shape of CTAB micelle, formed in water with varying surfactant concentration [49]. Green circles represent ammonium head, while red zigzags carbon tails.

However, the shape of CTAB micelles is not the only aspect of the nanorod synthesis controlled by the surfactant moiety. According to the mechanism proposed by Mulvaney's group [48], CTAB molecules bind the gold precursor: $AuCl_4^-$ (Au^{3+}), which is then reduced to $AuCl_2^-$ (Au^+). As a consequence, stable $AuCl_2^-$-CTAB micelles are formed. These micelles collide with gold seeds, entrapped within. The frequency of collisions determines

the rate of nanorod formation. The collision rate is the fastest at the nanorod tips. As a consequence, growth along the longitudinal axis of nanorods is promoted.

Growth into elongated structures is promoted by another factor, also involving CTAB (in a combination with a reducing agent – ascorbic acid). Several research groups reported that in the presence of CTAB, ascorbate mono-anion (not ascorbic acid) is the favoured form [35,38,50]. Therefore, the ascorbate species act as a dominating reductant of the gold precursor. Murphy's group proposed that ascorbate along with its intermediate complexes (with CTAB and Au^{+}) preferably adsorb on the nanorod tips, thereby promoting the formation of longer nanorods [38].

As already mentioned, additive ions (e.g. Ag^{+}) also play an important role in controlling the nanorod growth direction. This can be explained by the under potential deposition (UPD) of silver (reduction of Ag^{+} to Ag^{0} on a metal substrate), reported by Guyot-Sionnest [51]. The UPD is favourable on the nanorod sides, followed by a strong CTAB binding, effectively leading to the inhibition of the side growth and elongation along the longitudinal axis (**Scheme 7**). The length-to-width aspect ratio of the resulting nanorods, depends on the initial concentration of Ag^{+} and increases with the amount of silver cations present (see **chapter 4** for experimental detail).

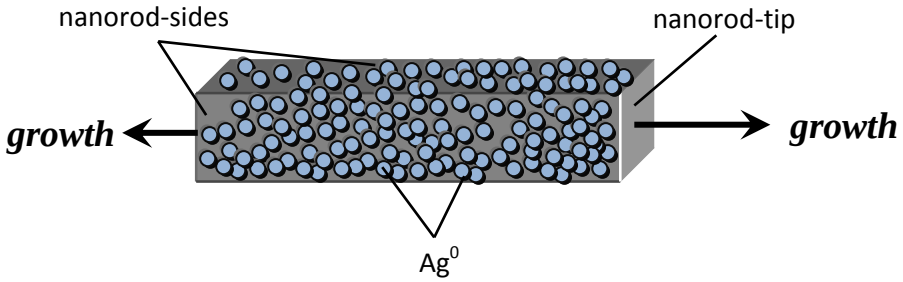

Scheme 7. Schematic illustration of nanorod-growth along longitudinal axis, promoted by under potential deposition of silver (Ag^{0}) [51].

2.1.3. Synthesis of silica/gold core/shell NPs.

Anisotropic NPs consisting of two components: gold and silica were developed by Halas and co-workers [52-55]. The synthesis of silica/gold hetero-structures (silica core and gold shell) is based on a template strategy (see **Scheme 8**). This involves separate preparation of large silica NPs (templates) and small gold NPs (seeds). Silica templates are decorated with seeds, from which the gold shell is grown around the silica core.

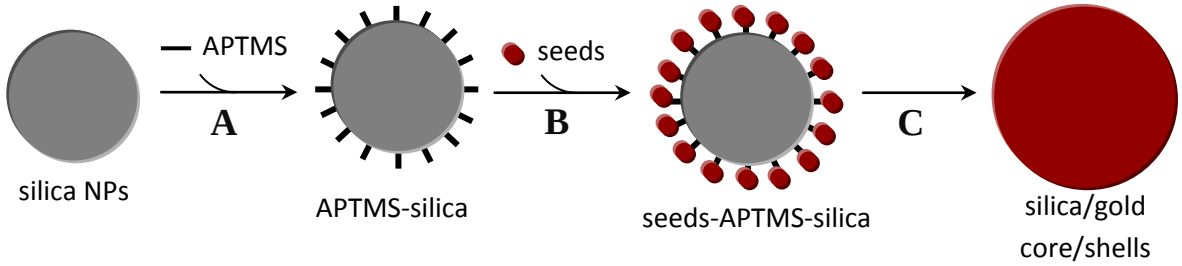

Scheme 8. Schematic illustration of: silica NPs grafted with APTMS (A), seeds-attachment (B) and gold shell growth (C).

Silica NPs can by prepared by a popular method [52,56-61], called Stöber or the sol-gel method, first reported in 1968 [62]. In this method, silica NPs are grown from tetraalkoxysilane precursor (specifically, tetraethyl orthosilicate – TEOS; see **chapter 3** for chemical structure and protocol) in alcoholic solution, containing water and ammonia. Water is required for hydrolysis (see **Scheme 9A**) of the alkyl silicates, while ammonia plays a role of a morphological catalyst. Subsequent, water (see **Scheme 9B**) and alcohol (see **Scheme 9C**) condensation reactions of silicic acid result in the formation of NPs. Vrij and co-workers reported that the nucleation process is realised by the aggregation of siloxane sub-structures, while the overall rate of NPs growth is limited by the hydrolysis of the alkoxide substrate [58]. Next, the surface of silica NPs is grafted with amine containing molecule ((3-aminopropyl)trimethoxysilane, see **chapter 3** for protocol), to allow further attachment of gold seeds (*via* amine groups) [52].

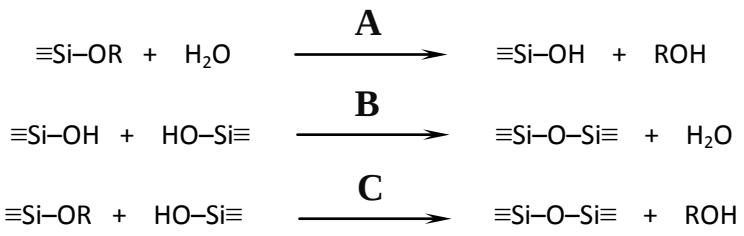

Scheme 9. Sol-gel synthesis of silica NPs. A – hydrolysis, B – water condensation, C – alcohol condensation; taken from [62].

The preparation of gold seeds (e.g. *via* Duff method) involves aqueous reduction of the gold precursor (chloroauric acid) with, e.g. alkaline tetrakis(hydroxymethyl)phosphonium chloride [63,64] (THPC, see **chapter 3** for chemical

structure and protocol). Duff and Baiker proposed that formaldehyde, released throughout the alkaline elimination of THPC (see **Scheme 10A**), acts as an active reducing agent of the Au^{3+} precursor [63,64]. The remaining tris(hydroxymethyl)phosphine can either undergo water hydrolysis (see **Scheme 10B**) and/or act as a NPs surface stabiliser (*via* phosphorous; see **section 2.2.** for BSPP).

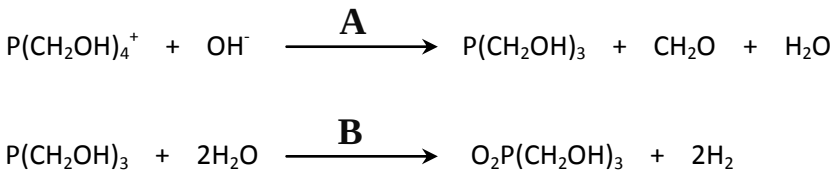

Scheme 10. Alkaline elimination (A) and hydrolysis (B) reactions of THPC; taken from [63, 64].

As already mentioned, gold seeds were attached to APTMS-grafted silica NPs (see **chapter 3** for experimental protocol) *via* amine groups. In the final step of the core/shell synthesis, the gold shell is grown from the gold precursor (chloroauric acid mixed with potassium carbonate; gold is transformed to $KAuO_2$ under the action of excess carbonate [65]; see **chapter 3** for protocol), assisted with formaldehyde [53].

2.1.4. Synthesis of hollow gold NPs.

Gold shells with hollow interiors can be prepared by dissolving (calcination or wet chemical etching) the core of core/shell hetero-structures [66], e.g. silica cores can be degraded by an etching with hydrofluoric acid (HF) [67]. This method however, involves very toxic HF reagent [68]. As an alternative, Xia's group developed a fairly simple, template based method for the preparation of gold NPs with hollow interiors [66,69-74]. This method is based on the galvanic replacement reaction (reflux at high temperatures) between solid silver NPs and an aqueous solution of the gold precursor (chloroauric acid).

Silver templates (NPs) determine the final size and shape of hollow gold NPs. According to the stoichiometry of the reaction (see **Scheme 11)**, silver templates are converted into soluble species, while the gold precursor is reduced to Au^0. One gold atom replaces three silver atoms at a time, leading to the formation of hollow nanostructures.

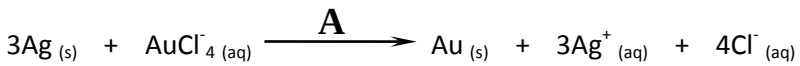

B

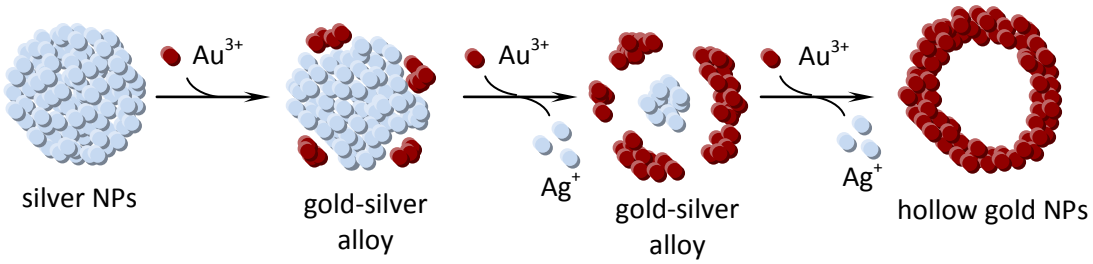

Scheme 11. Galvanic replacement reaction between Au^{3+} and Ag^{0} (A), taken from [66] and a schematic illustration of the formation of hollow gold NPs (B).

It is widely accepted that the replacement reaction begins from the highest surface energy sites on silver NPs (e.g. defects or stacking faults) [66,69,71,72,75,76]. At these sites, Au^{0} species are generated, while released Ag^{+} cations will diffuse away from the template. Within the template, remaining Ag atoms will migrate towards its surface. As a result, more Au^{3+} precursor will be converted to Au^{0} species and deposited on the template surface, until the critical concentration of Au^{0} is reached and nuclei are formed. Nuclei will grow into clusters, leading to the formation of a partial shell-like gold structure around the silver template. Alloying and de-alloying processes will continue until the complete shell is formed (or gold precursor is consumed). According to Xia and co-workers, at the final stage of the synthesis, the shell-wall will undergo an Ostwald ripening process (at high temperatures – reflux) resulting in a crystalline structure [66,69,71,72,76]. As already mentioned, the final morphology of hollow gold NPs is pre-determined by the silver template, e.g. shell-wall thickness of hollow gold will reach approximately 10 % of the template radius [66,69,71,72,76].

A variety of shapes and sizes of silver NPs can be synthesised by simple wet chemistry methods [66,69,71-73,76-79], e.g. Xia's group developed a polyol method, utilising ethylene glycol (a solvent and Ag^{+} reductant) [69,72,73,76,80,81]. At high temperatures (e.g. 160 ºC), ethylene glycol is oxidised to glycoaldehyde, which then serves as an active reducing agent of Ag^{+} to Ag^{0}. The reduction rate and the final shape of silver NPs can be controlled by adjusting the reaction temperature, which can lead to the formation of:

nanospheres, nanocubes, nanobars, nanobeams, nanorice, nanoplates, cuboctahedra or bipyramids.

As an alternative to the polyol route involving high temperatures, Oh and co-workers developed a seed mediated method for the preparation of silver nanorods and nanospheres, grown from small silver NPs (seeds) in the presence of a surfactant (CTAB) [78].

Seeds are prepared by the reduction of the silver precursor ($AgNO_3$, see **Scheme 12A**) with a strong reducing agent ($NaBH_4$) and stabilised with sodium citrate [78].

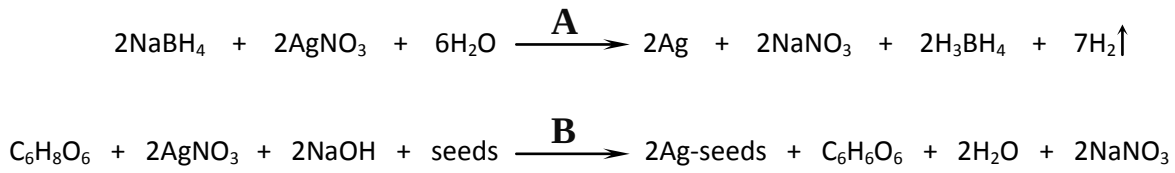

Scheme 12. Reduction of the silver precursor with a strong (A) and a weak (B) reducing agent, taken from [78].

From seeds, in an alkaline (NaOH) mixture of CTAB with the silver precursor and a weak reducing agent (ascorbic acid), silver NPs are grown (see **Scheme 12B**) [78]. Spherical NPs were also prepared by this method, according to the protocol described in **chapter 3**.

2.2. NPs surface capping, further modifications and assembly.

The surface of newly synthesised NPs (obtained with methods presented in the previous section) was stabilised by weakly bound protective agents (e.g. citrate anions, **Scheme 13A**) or ionic surfactants (e.g. CTAB) *via* electrostatic or Van der Waals interactions [82-84]. A physical barrier created by these molecules (steric hindrance) prevented direct contact between gold surfaces of neighbouring NPs [84].

Such NPs are soluble in water, but sensitive to pH and ionic strength changes in solution [84-86]. Specifically, NPs are subjected to aggregation in media containing high concentrations (e.g. 0.1 M) of sodium chloride (NaCl) or other salts [87]. To prevent instability in aqueous solutions, the surface of NPs can be capped with carefully chosen organic ligands (e.g. dithiols, thiols, amines and phosphines) [82-84,86-110]. These molecules, unlike CTAB or citrate, are chemisorbed on the gold surface, thus providing better

stability, e.g. Schultz's group demonstrated that *bis*(*p*-sulfonatophenyl)phenyl phosphine dehydrate dipotassium salt (BSPP, see **Scheme 13B** and **chapter 3** for protocol) capped 5 nm gold NPs are stable in 0.3 M NaCl and 1 mM magnesium chloride [87]. The precipitation of larger (10 nm) NPs with 0.15 M NaCl was a reversible process, since NPs could be easily redispersed in fresh water.

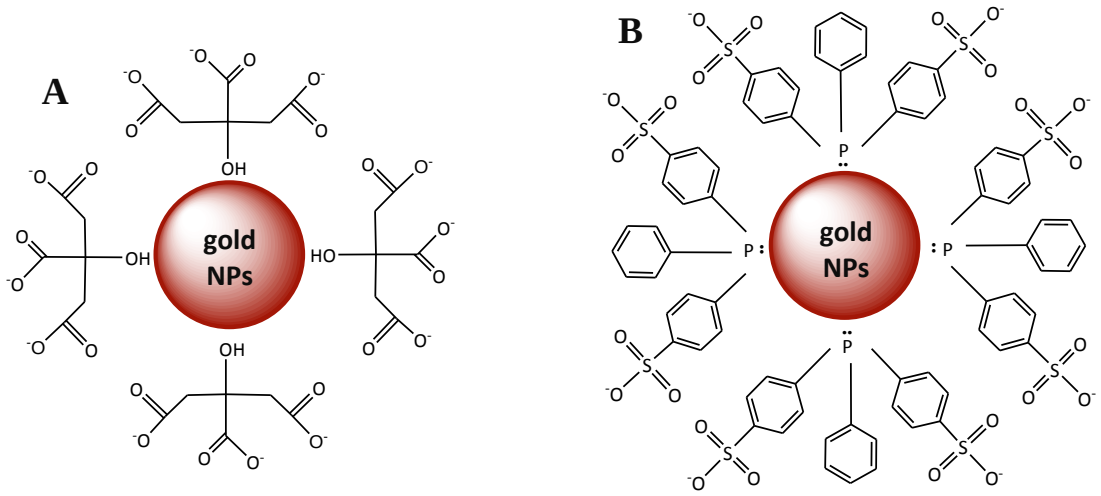

Scheme 13. Citrate (A) and BSPP (B) stabilised gold NPs [82].

However, in the presence of thiols (e.g. glutathione), NPs stabilised with weak ligands (e.g. BSPP or amines) or protective agents can undergo displacement reactions and lose their original functionality [82-84,89]. Complete ligand substitution is possible because of much stronger interactions between thiol anchoring groups and the gold surface than, e.g. amines and gold [83,84]. Displacement reactions were successfully adopted and are now commonly used to functionalise gold NPs larger than 5 nm with thiol based ligands, since larger NPs cannot be easily obtained by direct synthesis in the presence of thiols [83,84,111].

A number of thiol based capping ligands have been reported in recent years, including: oligonucleotides [87,103-106,112], peptides [90,92,95,113,114], lipids [115], polyethylene glycols [91,98,107,116-118], alkylthiols and mercaptoacids [88,97,100,111,119,120], as well as newly developed polydiacetylene based ligand (DA-PEG) [89]. Some have been employed in the NPs surface capping over the course of this research project, and will be discussed further in the following sub-sections.

2.2.1. Oligoethylene glycol based capping ligand.

An amphiphilic ligand based on oligoethylene glycol (OEG) was first employed to cap the surface of gold NPs by Brust and co-workers [99]. In the original version of the ligand proposed by Brust, the OEG unit contained four steps of ethylene glycol and was terminated with a hydroxy group [99]. The modified version employed here, was terminated with a carboxy group and consisted of six ethylene glycol steps (see **Scheme 14**).

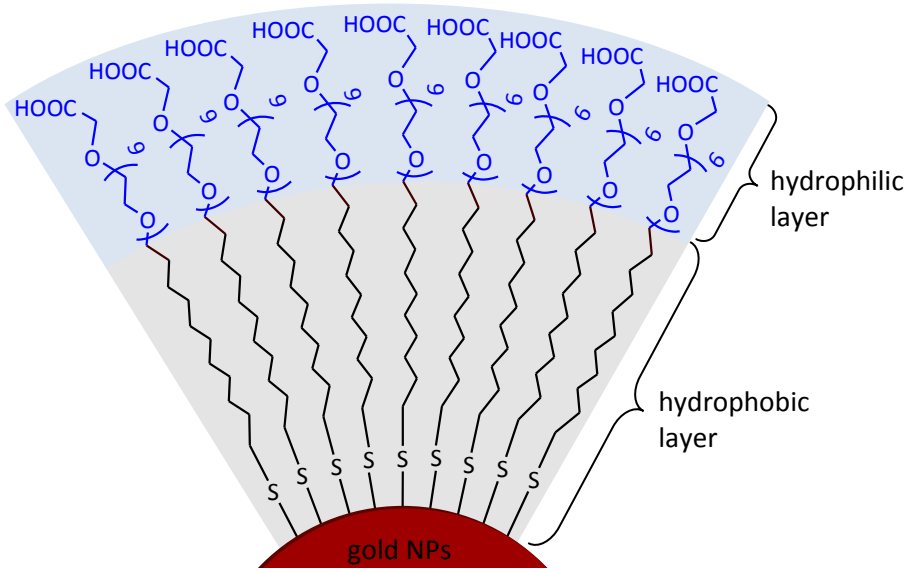

Scheme 14. Schematic representation of OEG capping layer on gold NPs.

In general, the hydrophilic unit [-$(CH_2CH_2O)_6$-OCH_2-COOH] ensured NPs solubility in aqueous media [82,99] and allowed further modifications with, e.g. amine containing molecules (*via* the formation of an amide bond) using standard catalysts, e.g. 1-ethyl-3-(3-dimethylaminopropyl)carbodiimide [117,121-123] (see **section 2.2.1.1.**). Except the OEG unit, the ligand also contained an alkyl chain, terminated with a thiol anchoring group, which chemisorbed directly on the surface of gold NPs [83,84,99]. The alkylthiol unit of OEG provided a uniform hydrophobic layer with carbon chains of neighbouring ligands closely packed *via* Van der Waals interactions [82,99].

As demonstrated in **chapter 4**, it was possible to stabilise with OEG, a number of different types of gold NPs, including spherical, rod-like, hollow and core/shell (see **chapter 3** for capping protocols). OEG capped NPs showed good stability against

aggregations in a wide pH range and in a presence of salts (see **chapter 4** for stability tests).

2.2.1.1. Further modifications of NPs surface.

As previously stated, OEG capped NPs can be further modified with amine containing molecules *via* simple coupling chemistry methods, e.g. using 1-ethyl-3-(3-dimethylaminopropyl)carbodiimide (EDC) as a catalyst [121].

EDC is a commonly used zero-length crosslinker, which couples carboxyl groups with primary amines [121]. Initially, EDC reacts with a carboxylic group to form an amine reactive intermediate (O-acylisourea, see **Scheme 15**). O-acylisourea can either react with the amine or undergo hydrolysis and regeneration to the carboxyl. To avoid hydrolysis, N-hydroxysulfosuccinimide (s-NHS) is often used to increase the efficiency of the reaction. S-NHS is known to stabilise O-acylisourea, by converting it into amine reactive s-NHS ester.

EDC/s-NHS method was reported before in conjugation of various biomolecules to NPs, e.g. Nie and co-workers coupled proteins to mercaptoacetic acid capped quantum dots using EDC [123], while Mason's group conjugated antibodies to polyethylene glycol (PEG) coated gold NPs with EDC/s-NHS [117]. It will be demonstrated in **chapter 4** that using EDC/s-NHS (see **chapter 3** for protocol) also small peptides can be conjugated to OEG stabilised gold NPs (spherical, rod-like, hollow and core/shell).

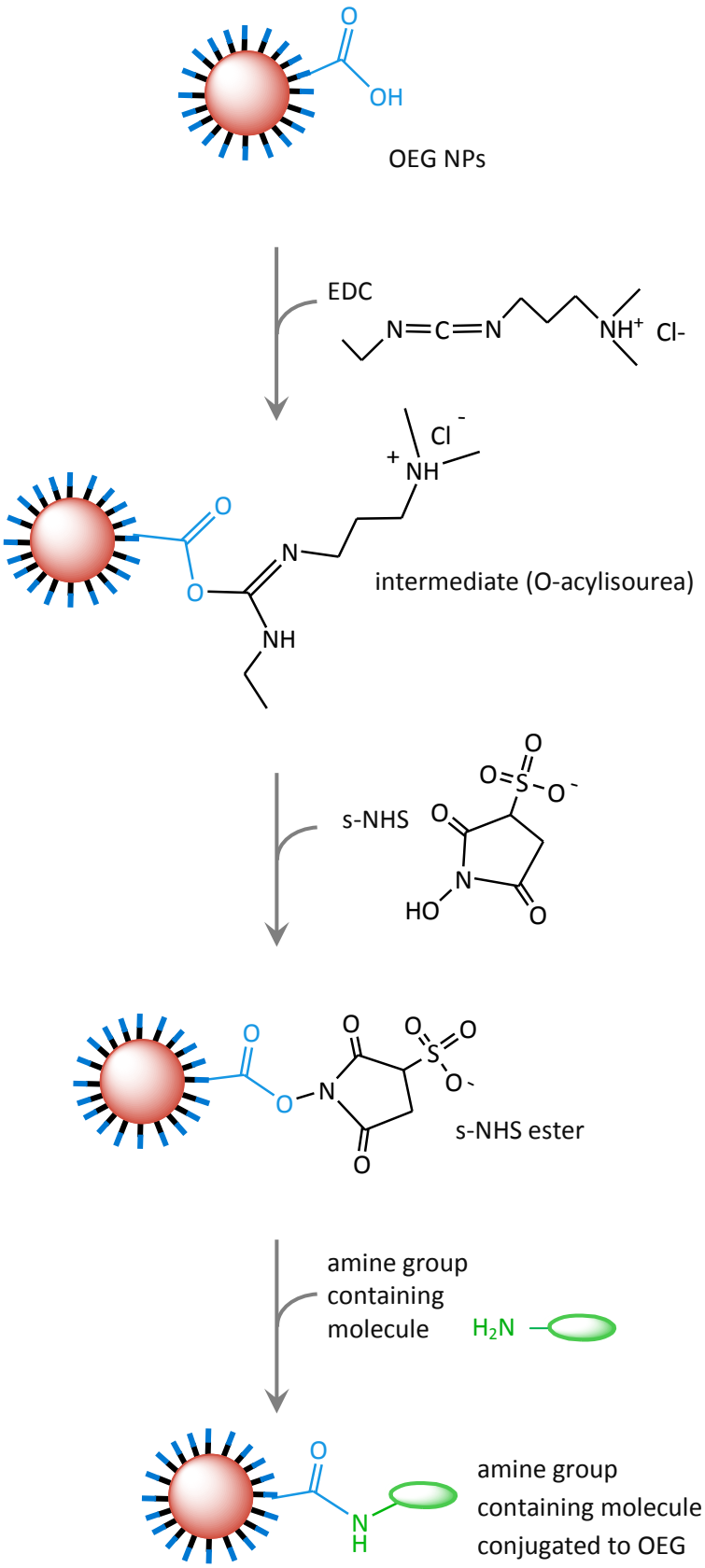

Scheme 15. Schematic illustration of EDC/s-NHS coupling reaction between OEG capped gold NPs and amine group containing molecule.

2.2.2. Diacetylene based capping ligand.

A new type of capping ligand, namely 46-mercapto-22,43-dioxo-3,6,9,12,15,18-hexaoxa-21,44-diazahexatetraconta-31,33-diyn-1-oic acid (DA-PEG) was developed during this research project [89]. The key feature of this design was a diacetylene group, which can be polymerised by ultra violet (UV) light induced 1,4-topochemical polymerisation, resulting in poly(enyne) structures [89,119,124-129] (**Scheme 16**).

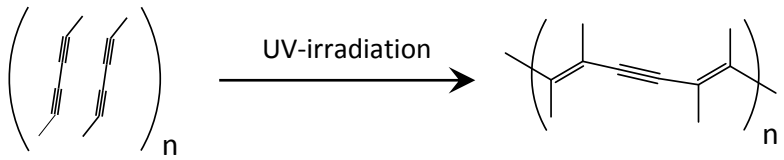

Scheme 16. Schematic representation of diacetylene groups photo-crosslinking [89, 118, 123-128].

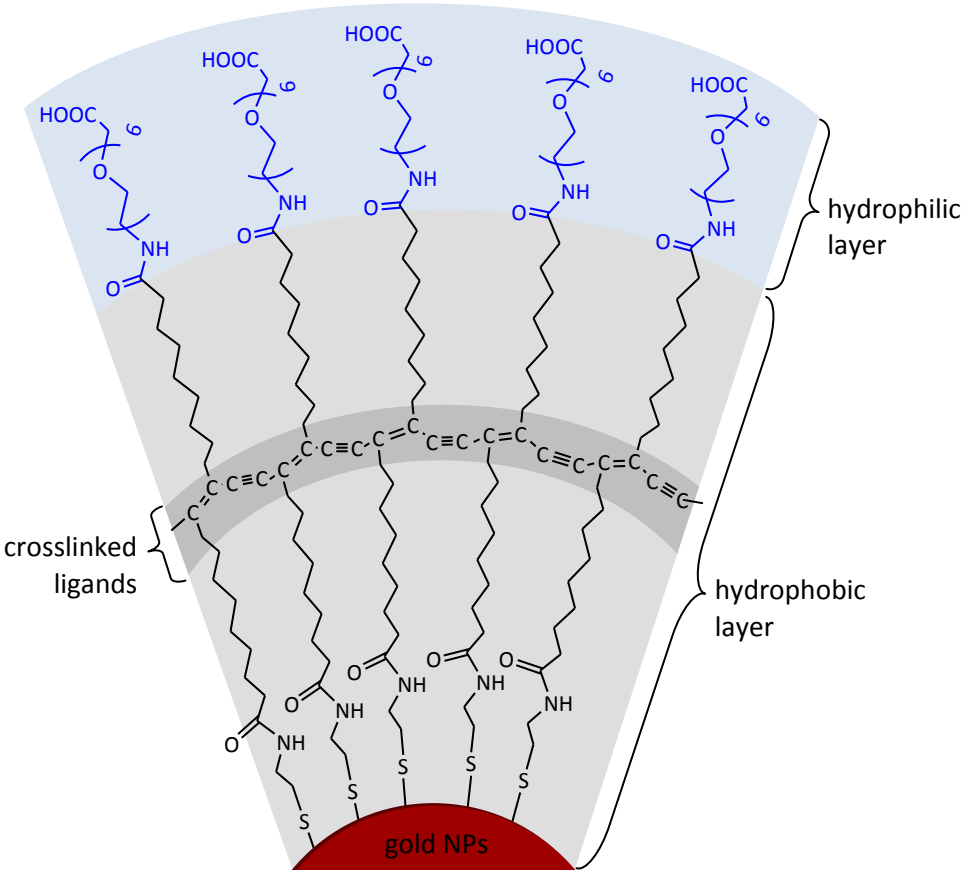

Scheme 17. Schematic representation of photo-crosslinked DA-PEG capping layer on gold NPs.

DA-PEG ligand consists of hydrophobic and hydrophilic units. The hydrophobic part contains an alkyl chain with a diacetylene group and is terminated with a thiol anchoring group. The hydrophilic component is based on a carboxyl terminated hexa-ethylene

glycol, providing water solubility and the possibility of further modifications (e.g. EDC/s-NHS coupling, see the previous section).

As demonstrated in **chapter 4**, photo-crosslinked DA-PEG capped NPs (see **Scheme 17**) display enhanced stability against aggregation in buffered environments at a broad range of pH. These NPs are also resistant to temperature variations, ligand exchange reactions and high ionic strength solutions. Their stability derives from a crosslinked shell, which is created by photo-polymerisation of DA-PEG monomers already attached to the surface of NPs.

2.2.3. CALNN peptide based capping ligand.

Levy and co-workers designed a penta-peptide (CALNN), which can serve as a capping ligand for gold NPs [92,95,113]. N-terminus cysteine (C) provides the peptide with a thiol anchoring group. Hydrophobic side chains of alanine (A) and leucine (L) residues promote self-assembly of peptides on the gold surface. The side chain of the first asparagine (N) is hydrophilic but uncharged, while the C-terminus asparagine (N) is negatively charged. CALNN-capped NPs are stable in buffered environments, up to 1 M NaCl, as well as basic, neutral and slightly acidic pH.

Brust and co-workers demonstrated that *bi*-functional CALNN based gold NPs can be prepared, simply by using mixed peptide monolayers composed of CALNN, CALNNGKbiotinG or CALNN-DNA conjugates [92]. Following this idea, oligodeoxynucleotide (ODN) binding NPs were developed during this research project, in a close collaboration with Stulz's group (School of Chemistry, University of Southampton, Southampton, UK) [114]. A key part of this design was a penta-peptide sequence (FQGII), which as shown by Sasaki and co-workers, can selectively bind to an AT-rich (A – adenosine, T – thymidine) region of a short deoxyribonucleic acid (DNA) duplex with a high binding constant [130,131]. Consequently, a *bi*-functional capping ligand composed of CALNN and FQGII sequences linked by aminohexanoic acid (Ahex) was derived. CALNN-Ahex-FQGII (c-FQGII) ligand was mixed with CALNN peptide and employed in the preparation of ODN binding gold NPs (see **Scheme 18** and **chapter 3** for experimental details).

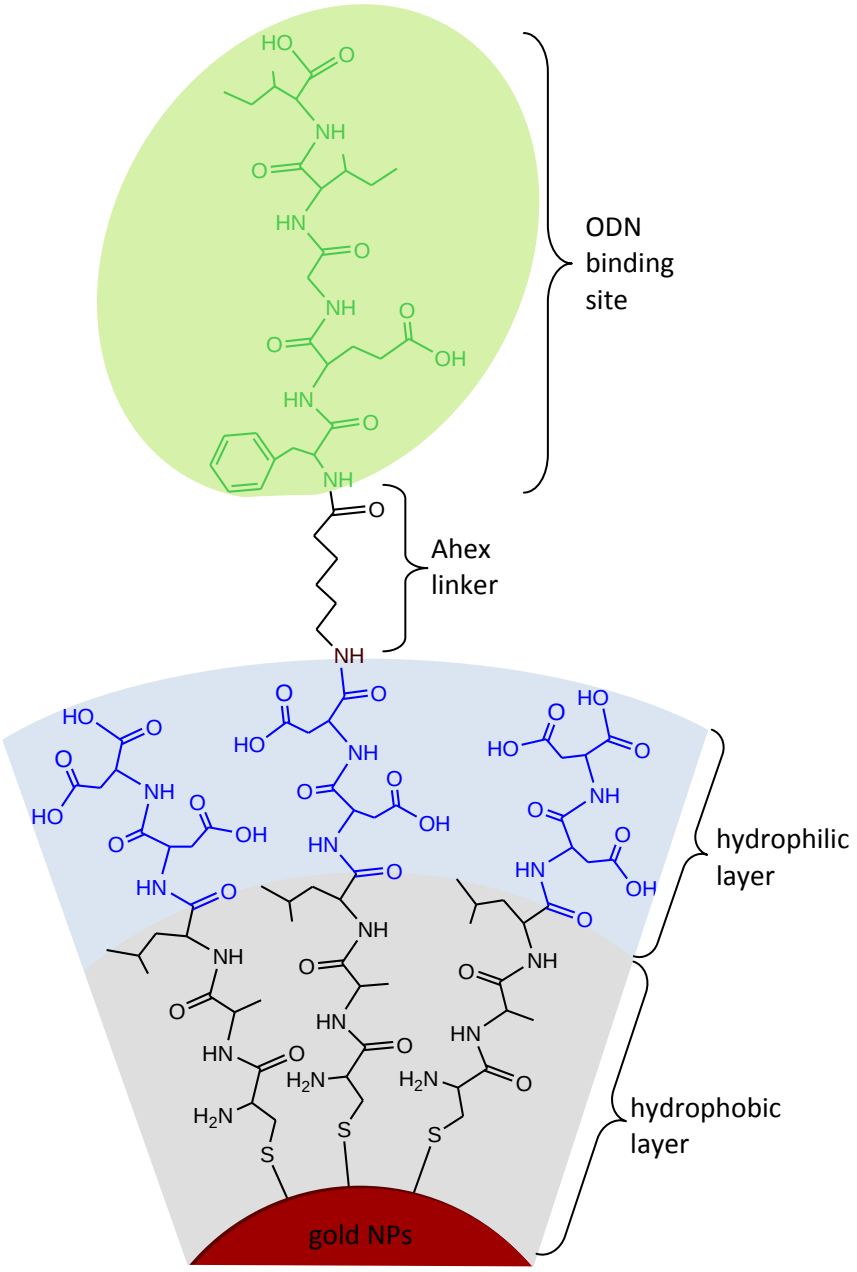

Scheme 18. Schematic representation of CALNN/c-FQGII capping layer.

2.2.3.1. Assembly of NPs on oligodeoxynucleotide templates.

Gold NPs capped with a mixed layer of CALNN/c-FQGII were employed in the formation of NPs assemblies on ODN templates [114]. Two ODN based systems were designed. Specifically, long DNA duplexes, which were formed from two different, staggered ODNs (**Scheme 19A**) and a short self-complementary building block (**Scheme 19B**). The self-complementary construct contained two AT-steps (see **chapter 3** for detailed sequence), while the staggered duplex had AT-regions at regular intervals along the duplex length.

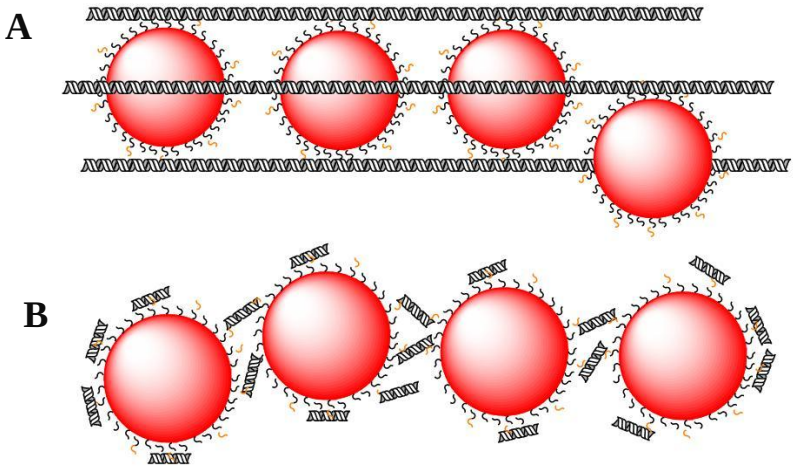

Scheme 19. Schematic representation of the ODN-NPs arrays formed along pseudo-infinite duplexes (A) or short self-complimentary building blocks (B) [114].

According to **Scheme 19**, it was anticipated that the long ODN based construct would form extended chains of NPs, while the short building blocks would rather bind around the NP with little or no control of NPs organisation. The resulting assemblies of NPs will be presented and discussed in **chapter 4**.

2.3. Physicochemical properties of capped gold NPs.

At the nanoscale, materials exhibit properties not seen in bulk [7,15,16,27-30,39,53-55,65,70,73,82,102,132-146], e.g. gold NPs smaller than the light wavelength, are subjected to an optical phenomenon, called surface plasmon resonance (SPR) [135,142,143,147]. SPR derives from free conductive electrons, which collectively oscillate in a resonant frequency with the electromagnetic wave, resulting in enhanced absorption and scattering (extinction) properties of NPs (see **Scheme 20**) [135,142,143,147].

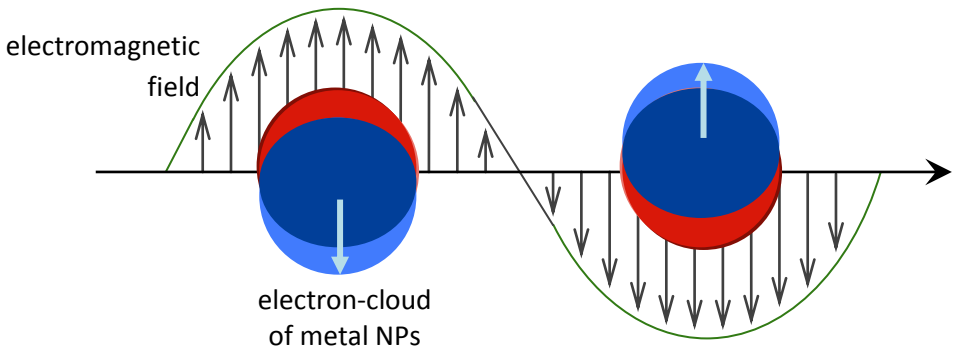

Scheme 20. Schematic representation of interactions between metal NPs and the electromagnetic radiation of wavelength, taken from [135].

As predicted by Mie's theory, SPR of NPs is controlled by the shape and size of NPs, as well as electric properties of the embedding material (**Fig. 1A**) [27,135,142,143,147]. If the dielectric constant of the surrounding medium is represented as ε_m, while $\varepsilon'(\lambda) + i\varepsilon''(\lambda)$ is the dielectric function of the nanoparticle, the maximum extinction of spherical NPs occurs as a single plasmon band at λ wavelength, where $\varepsilon' = -2\varepsilon_m$. According to equation **A**, the SPR position of spherical colloids, suspended in different solvents would vary slightly. Also self-assembly or aggregation of NPs would lead to a shift (into longer wavelengths, see **section 4.2.1.** for NPs assemblies spectra) of the SPR peak, based on the plasmonic coupling between NPs.

In general, spherical NPs absorb in the visible region of the electromagnetic spectrum. The SPR position of non-spherical NPs (e.g. rods) depends on the orientation of the electromagnetic field [27,142,148,149]. Consequently, in elongated nanostructures, two oscillation peaks are possible; along the longitudinal and the transverse axis. The longitudinal peak is usually shifted into the infra-red spectral region and its exact position depends on the nanoparticle width-to-length aspect ratio. To calculate the SPR of rod-like nanostructures, the orientation of NPs to the oscillating electric field must be accounted, as proposed by Gans (**Fig. 1B**) [149]. In this equation, depolarisation factors for the nanorod axes are represented by P_j. Following this idea, El-Sayed and co-workers calculated (**Fig. 1C**) how the nanorod aspect ratio (a/b) and the wavelength at which the maximum longitudinal SPR occurs (λ_{max}) are correlated [148].

A $$C_{ext} = \frac{24\pi^2 R^3 \varepsilon_m^{3/2}}{\lambda} \frac{\varepsilon''}{(\varepsilon' + 2\varepsilon_m)^2 + \varepsilon''^2}$$

B $$C_{ext} = \frac{8\pi^2 R^3 \varepsilon_m^{3/2}}{3\lambda} \sum_j \frac{(\frac{1}{P_j^2})\varepsilon''}{(\varepsilon' + \frac{1-P_j}{P_j}\varepsilon_m)^2 + \varepsilon''^2}$$

C $$\lambda_{max} = 33.34\varepsilon_m \frac{b}{a} - 46.31\varepsilon_m + 472.31$$

Figure 1. Mie's theory for spherical NPs (A) [142], extinction cross-section of elongated NPs by Gans (B) [149] and empirically calculated by El-Sayed the longitudinal SPR (C) [148].

The SPR of other types of NPs, like hollow gold or core/shell nanostructures can be calculated by other numerical approaches, e.g. the discrete dipole approximation (DDA) of Mie's theory [70,134,150-155]. In the DDA, the nanoparticle is considered as a group of N

identical elements. Each element is approximated by the polarisable dipole point, located at the certain position in the local electromagnetic field. The dipole moment is affected by other dipoles in the nanoparticle. Following this idea, it was calculated that the SPR of hollow gold NPs, strongly depends on the shell thickness and the nanoparticle radius, while the plasmon band of silica/gold core/shells is determined by core-to-shell size ratio [70,134,150,152,154].

As already mentioned the extinction of NPs is comprised of both, absorption and scattering. As demonstrated by El-Sayed and co-workers, small gold NPs (20 nm in diameter) mostly absorb the light, whilst scattering effects are negligible [154]. Whereas, increasing the size of NPs results in a more significant contribution of the scattering component to the overall excitation spectra. Absorption and scattering cross-section characteristics determine possible (based on the optical properties) applications of NPs, e.g. as high contrast agents in new imaging techniques [11,41,70,134,144,147,154,156-162]. Predominantly scattering NPs can be used in optical coherence tomography and reflectance confocal microscopy. Predominantly absorbing NPs can be employed in micro-absorption spectroscopy techniques, which are based on detecting shifts in the SPR caused by changes in the refractive index of the surrounding medium.

Gold NPs can generate heat after the SPR absorption of light, e.g. the laser light [5,7,15,16]. Specifically, the laser electric field induces carriers' vibrations inside the nanoparticle. These movements release energy, which is then converted into heat. Generated heat diffuses away from the nanoparticle and increases the local temperature of the surrounding medium. In general, the temperature increase is proportional to the second power of the nanoparticle radius and depends on the energy coming from the laser light and the heat transfer from the NPs surface. As an example, Richardson and co-workers calculated that a single gold nanoparticle, around 60 nm in diameter, can generate 5 μW of heat if SPR-illuminated with 2 mW laser light [16]. Moreover, the heating intensity can be enhanced by collective effects of several NPs, based on Coulomb interactions and accumulative effects; more NPs lead to a stronger temperature increase [16].

The ability to convert absorbed light into localised heat by gold NPs was applied in photo-thermal therapy of cancer [3,4,6-14,156,161,163-166] and bacterial infections [156,167] using near-infrared (NIR) absorbing NPs. Such requirements are necessary, because of the absorption properties of the tissue components, e.g. haemoglobin (red blood cells) or water (major component of all tissue types) [168-170]. As demonstrated in **Fig. 2**, haemoglobin strongly absorbs in the visible spectral range, while water becomes absorbing over the NIR

region. In the region between 650 and 900 nm both, water and haemoglobin are transparent, resulting in the highest transitivity of the tissue (biological NIR window). Consequently, tissue can be penetrated by the laser light at the frequency falling within the biological NIR window.

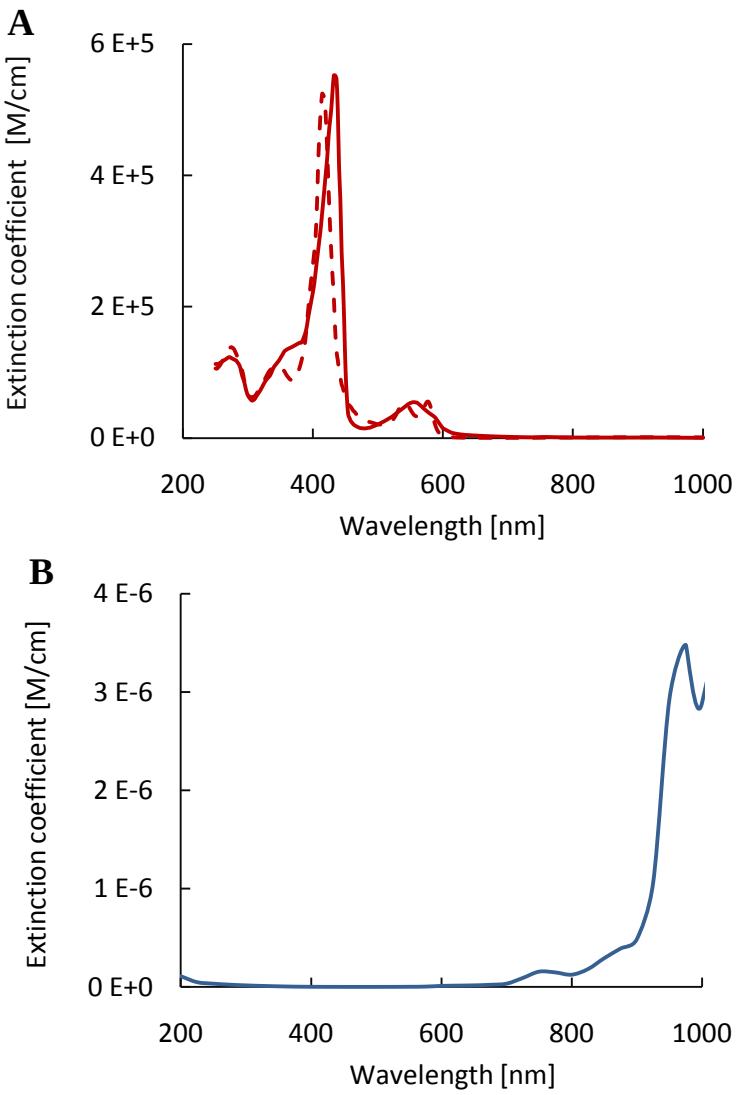

Figure 2. Extinction coefficients of haemoglobin (A, full line), haemoglobin-oxygen complex (A, dashed line) and water (B); taken from [168-170].

The main idea of the laser induced NPs mediated cancer treatment, is that the NIR laser light will pass through the healthy tissue (without causing any damage) and will be absorbed by NPs placed inside the tumour [3-15,47,134,144,147,156,161,163-166,168-175]. The light will be then converted into localised heat, resulting in the increase of the local temperature around the tumour site. A few degrees increase of the local temperature (depending on the laser power and heating properties of NPs) will cause damage to cancerous cells and

destroy the tumour [3,4,6-16,161,163,176-183]. The mechanism of heat damage in cells will be discussed in the **section 2.6.2.** (see also **chapter 7**).

Sufficient tumour damage can be obtained only when NPs optical signatures, thus the ability to generate heat, are retained within the cellular matrix. This can be achieved by capping of the NPs surface with appropriate ligands, which was already discussed in the previous section. The functionality of NPs also determines their chemical properties (e.g. hydrophilicity or charge, see **chapter 4**). When biomolecules (e.g. peptides or antibodies) are incorporated in the capping layer, NPs can be employed in selective targeting of desired tissue or cell types, e.g. tumours [116,117,122,147,157-159,164-166,175,184-197]. Possible mechanisms of interactions between cells and NPs will be discussed in the following section.

2.4. Interactions of NPs with mammalian cells.

As mentioned previously, the mechanism of interactions between NPs and cells depends on the NPs functionality [19,98,116,117,122,147,157-159,164-166,175,184-186,188-191,193-222]. 'Bare' NPs (meaning: without any specific functionality) would interact with cells in a non-selective manner, controlled by the size, shape and charge of NPs [186,190,206,213,214,221] (see also **chapter 5**). As demonstrated by several research groups, 'bare' NPs can be internalised by mammalian cells by engulfing with cellular membrane (endocytosis, **Scheme 21**) [186,206,214,221]. Uptaken NPs are confined within cellular vesicles (e.g. endosomes), which can be either secreted out of the cell (exocytosis) or fused with other organelles, like lysosomes.

Chan and co-workers reported that spherical and rod-like NPs are both endocytosed by cancerous cells (HeLa, see **section 2.5.**), however spherical NPs are taken-up more efficiently than rod-like NPs [206,214]. It was demonstrated that, the uptake rate of 50 nm NPs was higher than 14 or 74 nm, while 14 nm NPs were exocytosed the fastest. In general, neutral or positively charged NPs interact stronger with the cellular membrane than negatively charged NPs, which are repelled from it [206,213].

To achieve better control upon interactions between cells and colloids, biomolecules can be incorporated in their organic corona [84,92,98,116,117,121,122,147,157-159,164-166,173,184-190,193-198,201,202,204,205,207,210,217,223,224] (see also **chapter 6**). NPs conjugated to biomolecules can interact with cells in a selective manner, driven by precise recognition between biomolecules and their receptors allocated on the cellular membrane (**Scheme 21**). The

binding event triggers a cellular response, which can lead to NPs internalisation or a signal transduction within the cell (while the receptor-biomolecule-NPs complex stays outside the cell). The efficiency of selective targeting of mammalian cells, depends on the type of biomolecules attached to NPs and on the cell type [117,195,197,198,210,217,223]. This is because, on the cellular membrane of each cell type a different family of receptors is dominating, thus the use of cell type specific biomolecules and nanocomposites is required; e.g. Andres and co-workers demonstrated that folic acid functionalised gold NPs were selectively taken-up by foliate receptor positive cancer cells, while their uptake was minimal in cells that do not over-express these receptors [195].

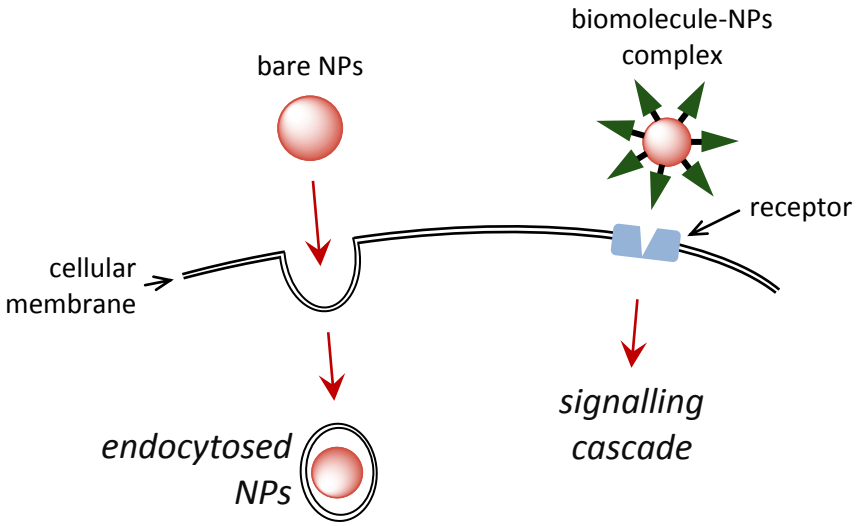

Scheme 21. Schematic illustration of selective (left) and non-selective (right) interactions between NPs and cells.

Since the cellular fate of NPs strongly depends on the cell type, two kinds of mammalian cells (cancerous and healthy human cells) employed in this research, will be introduced and discussed in the following sections.

2.5. HeLa cells.

HeLa is an immortal cell line, derived from human cancerous cells and one of the most commonly used in scientific research [225-229]. It was isolated from cervical cancer cells of Henrietta Lacks (Note: HeLa were named after the patient – two first characters of her

name and surname), who died of cancer in 1951 [225,226]. HeLa was propagated by George Otto Gey without donor's permission and later commercialised [225,229].

As long as sufficient amount of nutrients, oxygen and growth space are provided in the cell culture, HeLa can divide an unlimited number of times [225-228,230] (Note: healthy human cells normally split only several times, then undergo apoptosis – programmed cell death, while cancerous cells do not commit suicide [228,231]). HeLa evolved in many strains after being cultured in separate laboratories [227,232]. Some of them might over-express types of receptors, which are deficient in other HeLa strains. HeLa employed in this project, do not over-express growth factor receptors (see the next section), thus served as a negative control (see **chapter 6**).

2.6. Endothelial cells.

Endothelial cells are healthy human cells, which build the internal layer of blood vessels (endothelium) [2,233,234]. In the endothelium, cells are linked by cell-to-cell junctions or adhesive structures to form a continues monolayer [233,235,236]. Endothelial monolayers serve as selective barriers between blood and tissues, participating in important physiological processes [2,233,237]. Endothelial cells are involved in response of the organism to a pathogen (inflammation), in a modulation of blood flow and blood vessel tone, as well as the formation of blood vessels (angiogenesis) [1,2,26,233,238].

The angiogenesis process is controlled by a complex signalling between cells, involving binding of secreted biomolecules to appropriate cell surface receptors [1,2,17,18,20,21,24-26,233,237-251]. Three major types of signalling molecules have been reported: a) angiopoietins – important for further vessel remodelling, b) ephrins – participating in primary vessel remodelling and c) growth factors – acting as angiogenesis initiators. A growth factors family, called vascular endothelial growth factors (VEGF) is considered as a major regulator of angiogenesis [1,21,240,243,245,247-249,251]. There are six members of the VEGF family (types A, B, C, D, E and a placental growth factor – PIGF) [240,243,245,252-254]. Each type consists of several isoforms. Every isoform is composed of a different number of amino acids, resulting in molecular weight variations, e.g. there are two isoforms of VEGF-B with molecular masses of 167 and 186 kDa.

Each isoform binds to a specific receptor (or receptors) over-expressed by endothelial cells, including four types of vascular endothelial growth factor receptors (VEGFR type 1, 2 and 3, as well as a soluble form of VEGFR-1) and two neuropilin receptors (NRP types 1

and 2) [240,243-245,247,252-254]. NRP-1 and VEGFR-1 can both be targeted with VEGF-B_{167} isoform, while VEGF-A_{165} shows binding affinity towards VEGFR-2, NRP-1, NRP-2 and a soluble form of VEGFR-1. It is important to highlight that types of receptors over-expressed by different types of endothelial cells significantly vary, thus particular types of endothelial cells generate specific responses to the same stimuli [1,233,234,244,253,254]. For instance, lymphatic endothelial cells mainly express VEGFR-3, while VEGFR-1 and 2 are expressed by vascular endothelial cells.

A sub-type of vascular cells, specifically human umbilical vein endothelial cells (HUVECs) was employed in this project. These cells were isolated from umbilical cords by Dr Timothy M. Millar (School of Medicine, University of Southampton, Southampton, UK) according to a protocol described in **chapter 3**. Since cells isolated from individual donors, even from the same cord, can vary their response to the stimuli, each experiment (see **chapter 6** and **7**) was performed in at least three repeats, using separate cords of HUVECs. Research efforts were focused on targeting two receptors over-expressed by these cells; specifically VEGFR-1 and NRP-1 (see **chapters 6** and **7**).

VEGFR-1 is a trans-membrane tyrosine kinase receptor [240,244,247,249,250,252-254]. Meaning, receptor binding and formation of receptor-ligand complexes is followed by the phosphorylation and activation of the intracellular signalling pathways, while receptor-ligand complexes stay outside the cell. NRP-1 serves as a co-receptor, regulating the formation of VEGFR-1-ligand complexes [18,241,243,248,249,254]. NRP-1, upon ligand binding, undergoes trafficking on the cell surface followed by endocytosis of receptor-ligand complexes. Both, NRP-1 and VEGFR-1 actively participate in the regulation of angiogenesis process [1,18,21,26,233,238,240,243,244,247,248,252-254]. The mechanisms of blood vessels formation will be discussed in more details in the following sub-section.

2.6.1. Angiogenesis.

Physiological angiogenesis, in an adult healthy organism, occurs only during a cycling ovary, pregnancy and wound healing [1,2,26,233,234,238]. New capillaries are formed either by sprouting or by vessels splitting [1,2,233,255]. Sprouting angiogenesis starts from proteolitic digestion of the extracellular matrix. This is followed by migration and proliferation of endothelial cells, lumen formation and maturation of endothelium. In non-sprouting angiogenesis, vessels split by trans-capillary pillars or posts of extracellular matrix. Mature vessels undergo remodelling, until fully functional endothelium is formed [1,233,255].

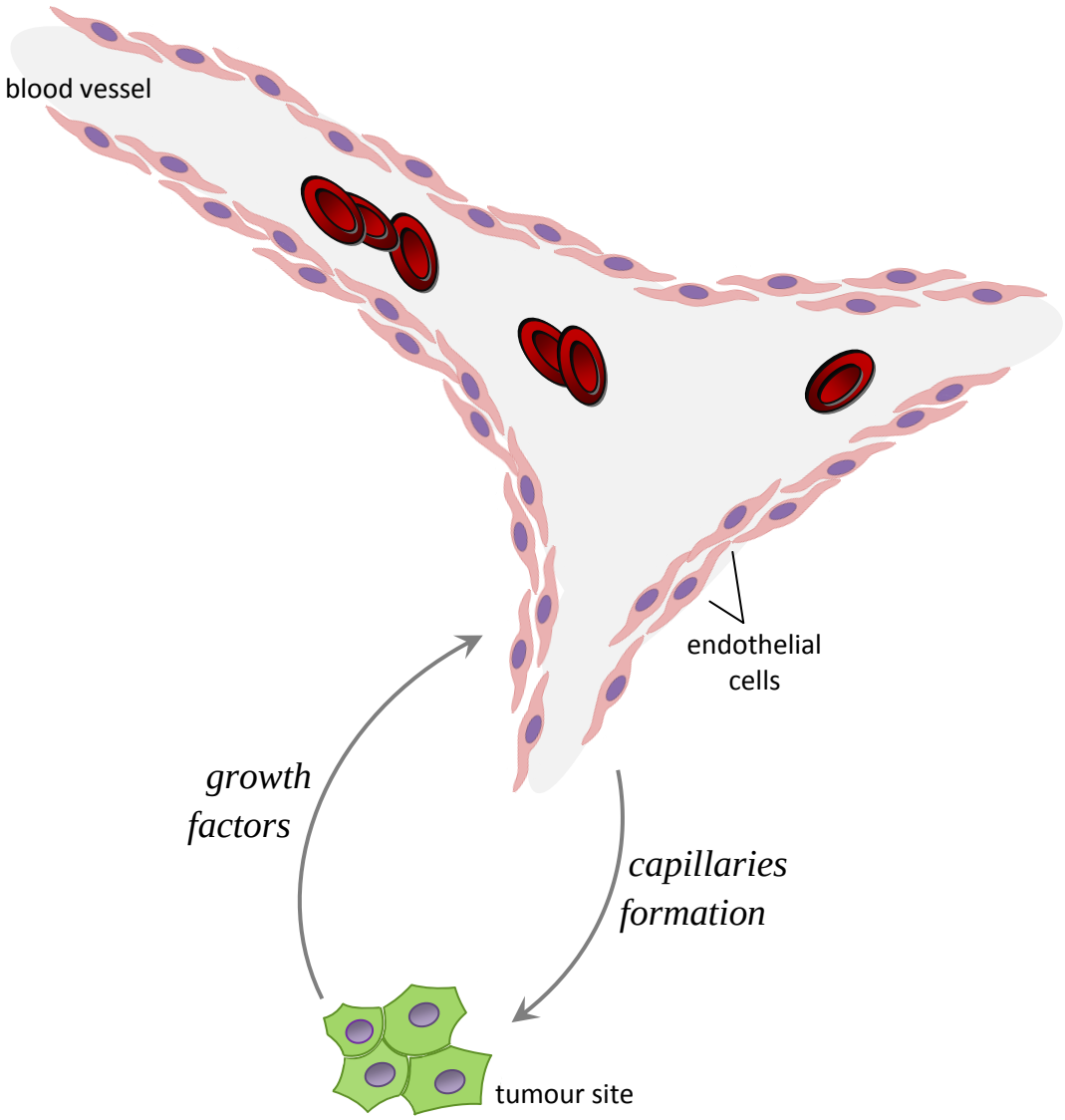

Scheme 22. Schematic illustration of tumour angiogenesis.

The formation of endothelium is regulated by a fragile balance (angiogenic switch) between angiogenesis stimulators (e.g. growth factors) and inhibitors [1,2,233,253,255]. Disruptions in this homeostasis lead to a pathological angiogenesis and many disorders [1,20,25,26,233,238,242,253,255]. Insufficient angiogenesis occurs in coronary artery disease and strokes, while excessive neo-vascularisation takes place in rheumatoid arthritis and cancer. As illustrated in **Scheme 22**, tumour angiogenesis is initiated by cancerous cells, which secrete various stimuli (e.g. VEGF-A) [1,25,233,238,253,255]. Upon stimulation, endothelial cells migrate into the tumour site and new blood vessels are being formed. Newly developed

blood vessels supply cancerous cells with essential nutrients and oxygen, resulting in tumour growth, progression and metastasis.

Since tumours require continues nutrient supply to expand, their prolonged cut off can lead to cancer regression [21,25,26,238]. This can be achieved by inhibiting tumour angiogenesis with e.g. angiogenesis inhibitors [20,21,24-26,238,242]. Consequently, a number of cancer therapies developed in recent years, are based on anti-angiogenic molecules [1,20-25,192,193,239,242,255,256]. These molecules are prone to target endothelial cells, rather than cancerous cells. This is a clear advantage, because endothelial cells, unlike cancerous cells, are genomically stable and remain sensitive to angiogenesis inhibiting drugs [1,2,20-26,192,193,228,230-234,239,242,255-257]. In general, anti-angiogenic therapies, baring minimum level of side effects, are considerably safer than e.g. tumour chemotherapy [1,2,20-23,25,26,192,234,238,239,255,256]. Also therapies against other disorders, e.g. coronary artery disease, are being developed [1,2,17,19,20,22,233,234,238,249,250,255]. These are based on pro-angiogenic drugs, stimulating insufficient angiogenesis.

Several natural (e.g. growth factors antibodies or interleukin) and synthetic (e.g. peptides) pro- and anti-angiogenic compounds are currently under clinical trials [20,238], but there is still a demand for new angiogenesis regulators. Especially peptide based molecules seem to be promising candidates. Following this idea pro- and anti-angiogenic octa-peptides were developed during this project (see the following sub-section for details).

2.6.1.1. Octa-peptide based angiogenic regulators.

In general, peptide based drugs can be prepared by undemanding, well-known and relatively cheap chemical protocols (e.g. solid state synthesis) [20,158,258]. It is possible to adjust the physicochemical properties of peptides (e.g. hydrophilicity) by simply replacing (mutating) the amino acid residues [259-261]. Shuffling the amino acid order leads to changes in the primary structure and conformation (secondary structure) and more importantly in the overall bioactivity of peptides [261-263]. Peptides, unlike large proteins or antibodies, possess only one epitope (biological recognition element) and are considered as structurally more stable [20,158]. Reduced molecular complexity makes them ideal candidates to study molecular pathways of dissect biological response and to visualise specific receptor targets (e.g. peptides labelled with fluorescent tags or NPs), as proposed by Benedetti and co-workers [20]. Any side effects and immunogenicity deriving from multiple epitopes is likely to be reduced, when employing peptides as drugs.

Several peptides showing pro- or anti-angiogenic activities have been reported so far [18,20,193,241,246,264]. Perret and co-workers reported anti-angiogenic ATWLPPR peptide, which inhibits VEGF-A_{165} binding to NRP-1 *via* LPPR motif [18]. Pedone and co-workers on the other hand, proposed a VEGF-A mimicking peptide (Ac-KLTWQELYQLKYKGI-amide), which can bind and activate VEGFR's, thus exhibits pro-angiogenic activity [264]. Also based on the VEGF-A structure was a cyclic peptide (CPQPRPLC), reported by Arap and co-workers [246]. The RPL tri-peptide within this sequence, displayed the affinity towards VEGFR-1 and NRP-1.

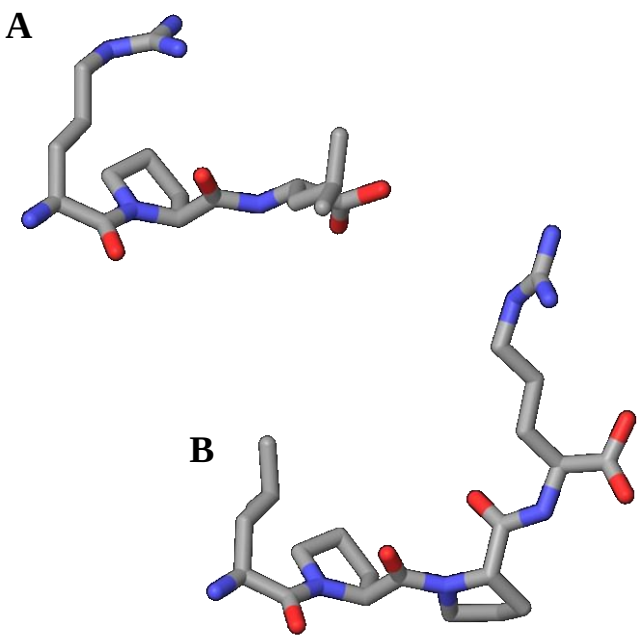

Scheme 23. Schematic illustration of RPL (A) and LPPR (B) motifs; prepared by Mr Jonathan R. Burns (Stulz's group, School of Chemistry, University of Southampton, Southampton, UK).

Following the idea of angiogenesis regulating peptides, it was intended to design a new family of peptides composed of the same number of amino acid residues and showing similar physicochemical properties (e.g. hydrophilicity), but different angiogenic activity. Consequently, three different sequences were deliberated, out of which one was designed to serve as an angiogenesis inhibitor, second as an activator and third to show no activity. The design of pro-angiogenic sequence was based on RPL motif (**Scheme 23A**), proposed by Arap and co-workers [246], while anti-angiogenic – on LPPR motif (**Scheme 23B**),

introduced by Perret's group [18]. Except of an appropriate activity, peptides had to contain a functional group, allowing conjugation with fluorescent tags or NPs (e.g. OEG NPs). One popular conjugation method is EDC/s-NHS coupling [121] (already discussed in **section 2.2.1.1.**). This technique requires a primary amine group, involved in the formation of an amide bond between conjugated molecules. Consequently, N-terminus lysine (K) containing two primary amines (N-terminus and side chain) was fixed in position one of all three deliberated sequences.

In one of proposed sequences, first amino acid residue (K) was extended by ATWLPPR fragment, which according to Perret and co-workers, shows anti-angiogenic activity [18]. By this way KATWLPPR octa-peptide was selected (**Scheme 24**, **P3**) to act as an inhibitor. Two remaining sequences should therefore also be eight amino acids long.

In the design of the pro-angiogenic octa-peptide, CPQPRPLC sequence served as a starting point [246]. Since this cyclic peptide already contains eight amino acids, at least one of them had to be replaced to introduce N-terminus K, which is necessary for the future conjugation. When conjugating to OEG NPs (see **section 2.2.**), two cysteine (C) residues (in positions one and eight) of the cyclic sequence should be considered as problematic, since side chain of cysteine contains a thiol group [83,84,89] (Note: thiols can bind to NPs surface, see **section 2.2.**). Consequently, both cysteines were removed from the sequence. First was replaced with K residue, while the other one with serine (S), which shows similar side chain structure as C, with a hydroxyl instead of a thiol group [260,261]. This resulted in KPQPRPLS sequence (**Scheme 24**, **P1**). Within this sequence, simply by scrambling the amino acid arrangement, randomly mutated version: KPRQPSLP was created. The mutated sequence (**Scheme 24**, **P2**) was expected to lose its binding affinity towards growth factor receptors and show no angiogenic activity.

All three sequences are positively charged, with a calculated [260] net charge value 2 (at pH 7). The isoelectric points are 11.5. There are only slight variations in peptides hydrophilicity. P3 consist of 25 % hydrophilic residues and its calculated [260] average hydrophilicity is 0, while P1 and its mutated version (P2) contain 50 % of hydrophilic amino acids, showing 0.6 average hydrophilicity. Detailed studies upon binding affinity towards growth factor receptors (VEGFR-1 and NRP-1) and the resulting bioactivity of these newly developed octa-peptides and peptide-OEG NPs (pep-OEG NPs) conjugates will be demonstrated in **chapter 6**.

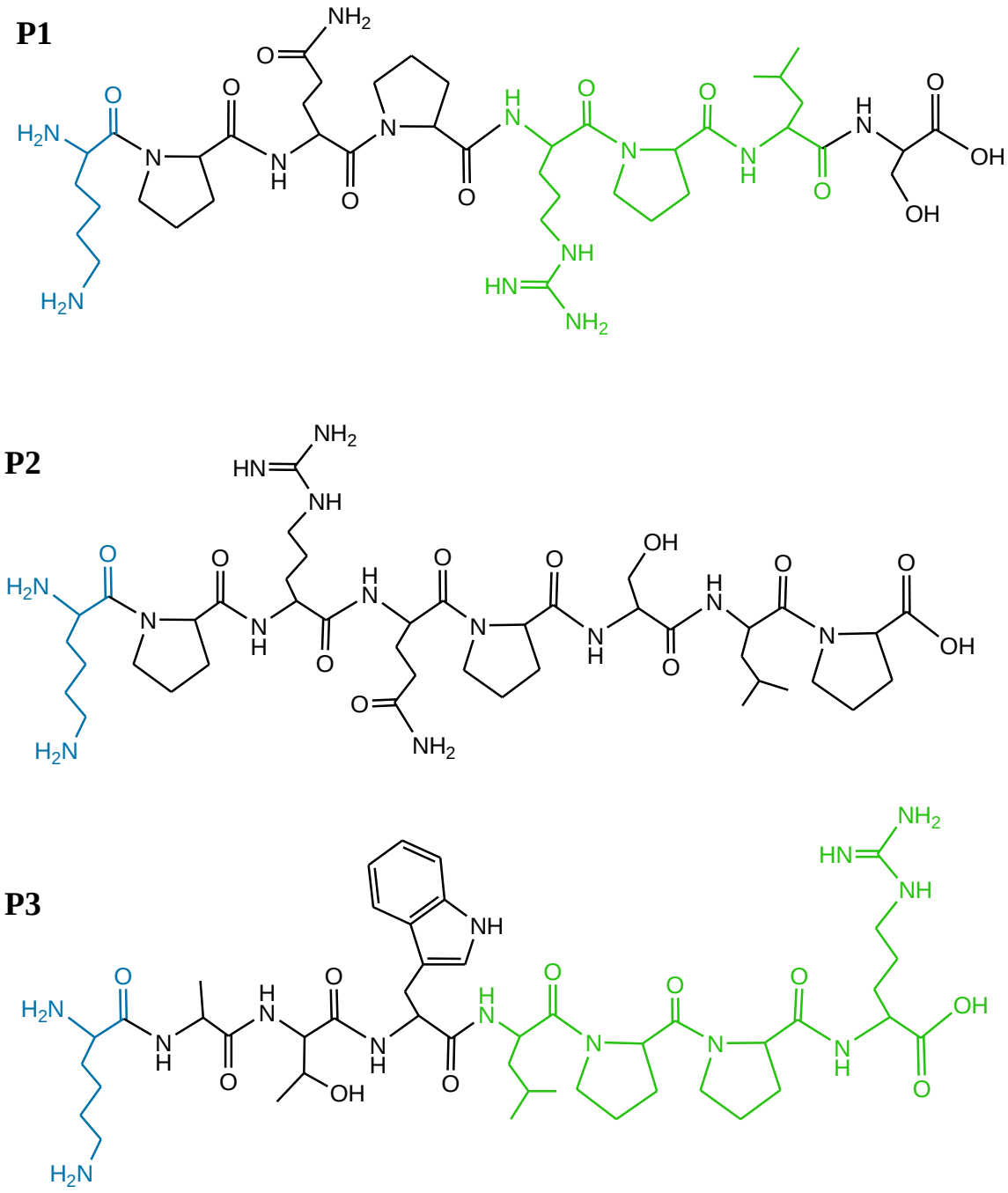

Scheme 24. Chemical structures of octa-peptides. N-terminus lysine (K) residue is marked in blue; binding motifs in green.

2.6.1.2. NPs in angiogenesis

NPs have been used before as angiogenesis regulators, e.g. Mukhopadhyay and co-workers demonstrated pro-angiogenic activity of europium (III) hydroxide nanorods, promoting the proliferation and vascular sprouting of HUVECs in a dose dependent manner [19]. Angiogenesis induction was attributed to an increase in the production of the reactive oxygen species (ROS), deriving from uptaken nanorods. Mukhopadhyay's group also reported anti-angiogenic activity of gold NPs, which were pre-incubated with VEGF-A_{165}, then employed in treatment of endothelial cells [23,200,256]. Angiogenesis was not induced with VEGF-A_{165}-NPs complexes, because VEGF-A_{165} binds to the gold surface through cysteine residue. Since, cysteine is located in the active site of the protein, VEGF-A_{165} activity is blocked upon NPs binding. These attractive properties of nanomaterials however, are purely based on non-selective interactions between 'bare' NPs and biostructures [19,23,200,256], which do not provide sufficient control over their cellular fate.

To overcome this issue, various molecules, including selective receptor targeting agents and/or pro- or anti-angiogenic drugs, can be attached to NPs [20,121,122,147,158,159,162,165,184,186,190,192-195,197,215,223] (see **sections 2.2.** and **2.4.**). Cheresh and co-workers reported cationic vesicles conjugated to a molecule, which selectively targets αvβ3 integrin (Note: αvβ3 integrin is a receptor involved in cell adhesion to the extracellular matrix and over-expressed by endothelial cells during neo-vascularisation) [265]. Except of the integrin, NPs were carrying a mutated gene, which blocks endothelial signalling and angiogenesis. *In vivo* treatment with these NPs resulted in endothelium apoptosis, leading to tumour regression.

A selective approach based on octa-peptides (see the previous section) conjugated to gold NPs (pep-OEG NPs) was adapted in this research project. Pep-OEG NPs have a uniform organic layer composed of OEG capping ligands and octa-peptides. The octa-peptide serves as both, selective targeting agent and angiogenesis regulator (see **chapter 6**). One clear advantage of using pep-OEG NPs is their diverse bioactivities, as determined by the peptide sequence (P1 is an activator, while P2 an inhibitor). Another benefit from adapting pep-OEG NPs comes from the metallic core of NPs, e.g. NIR absorbing gold NPs can be applied in laser induced thermal treatment of cells (see **section 2.3.**). Consequently, endothelium targeted with pep-OEG NPs and exposed to NIR laser light would either be destroyed or certain cellular response would be induced (see **chapter 7** for results and the following section for the theoretical background).

2.6.2. Physiology of HUVECs under heat shock.

It is widely accepted that all types of cells are affected by the exposure to elevated temperatures (hyperthermia) [3,4,6,8-14,161,163,176-183,239,266-269]. Heat acts as stress stimuli, leading to a cellular heat shock response [176-182,239,266-269]. This involves the expression of certain types of proteins, called heat shock proteins (HSPs) and is followed by cell recovery [178,181,266-269]. More severe heating eventually activates apoptotic program (programmed death; suicide), while extreme heat leads to cellular necrosis (premature death; external factors) [3,4,8,12,14,176,180,181].

Hence, it can be distinguished between death causing primary effects of heat and an active cellular response to the heat stressor (e.g. expression of HSPs) [176-183,239,266-269]. In general, direct heat leads to physicochemical and molecular changes, which include: inhibition of replication, transcription and translation of several genes, arrest in a certain cell cycle phase, degradation (e.g. denaturation) of proteins and cytoskeleton and disruption in cellular membrane permeability. These changes effectively lead to hyperthermia induced cell death and can be considered as its biochemical mechanisms. On the contrary, in a response to nonlethal heat stress, cells undergo complex biochemical adaptation processes. These include distortions in expression levels of several genes and activities of expressed proteins.

In HUVECs, hyperthermic treatment inhibits, e.g. biosynthesis of adhesion proteins, like endothelial adhesion molecule (ELAM-1) and inter-cellular adhesion molecule (ICAM-1), as reported by Justus and co-workers [267]. ELAM-1 is not constitutively expressed by HUVECs, but can be induced upon stimulation with various factors (e.g. tumour necrosis factor), while ICAM-1 is over-expressed by non-stimulated cells [267,270,271]. ELAM-1 serves as a mediator of neutrophil granulocytes (type of white blood cells) migration and adhesion to the endothelial layer, as well as adhesion of circulating cancerous cells (tumour metastasis) [270,272-274]. ICAM-1 participates in adhesion of T-cells (lymphocytes, a type of white blood cells), as well as neutrophil and eosinophil granulocytes (type of white blood cells) [271,275-278]. Heat mediated inhibition of adhesion molecules expression in HUVECs can therefore lead to the suppression of tumour metastasis, while tumour growth can be inhibited by the destruction of endothelium [21,24-26,192,239,265,279] (see **section 2.6.1.**). According to Bouchier-Hayes and co-workers, endothelial cell apoptosis can be induced when moderate heat treatment is combined with ROS treatment, resulting in enhanced heat shock by simultaneous oxidative stress response

[279]. However, as demonstrated in **chapter 7**, NPs mediated (laser induced) hyperthermia alone (without additional ROS stressors) can also lead to cell death.

It is also worth highlighting that healthy mammalian cells (e.g. HUVECs) are generally less sensitive to moderate heat (within the range of 41 ÷ 43 ºC) than malignant cells (e.g. HeLa) [14,176-182,267-269,279]. Selective destruction of malignant cells without noticeable damage to healthy cells (like endothelial cells) was reported by several research groups [3,4,8,12-14,176,180]. Enhanced sensitivity of cancerous cells was attributed to the differences in cell metabolism (e.g. respiration and lysosomal activity) and cell environment (increased acidity in the tumour site). Nonetheless, as demonstrated in **chapter 7**, thermal inactivation of healthy endothelial cells (HUVECs) was achieved with NPs mediated laser hyperthermia.

References:

[1] Clauss, M.; Breier, G. *Mechanisms of angiogenesis*; Brikhauser Verlag, Basel-Boston-Berlin, **2005**.

[2] Michiels, C. *J Cell Physiol* **2003**, *196*, 430-443.

[3] Li, J. L.; Day, D.; Gu, M. *Adv Mater* **2008**, *20*, 3866-3871.

[4] Huang, H.-C.; Rege, K.; Heys, J. J. *ACS Nano* **2010**, *4*, 2892-2900.

[5] Link, S.; El-Sayed, M. A. *Int Rev Phys Chem* **2000**, *19*, 409-453.

[6] Au, L.; Zheng, D.; Zhou, F.; Li, Z.-Y.; Li, X.; Xia, Y. *ACS Nano* **2008**, *2*, 1645-1652.

[7] Huang, X.; Jain, P.; El-Sayed, I.; El-Sayed, M. *Lasers Med Sci* **2008**, *23*, 217-228.

[8] O'Neal, D. P.; Hirsch, L. R.; Halas, N. J.; Payne, J. D.; West, J. L. *Cancer Lett* **2004**, *209*, 171-176.

[9] Cole, J. R.; Mirin, N. A.; Knight, M. W.; Goodrich, G. P.; Halas, N. J. *J Phys Chem C* **2009**, *113*, 12090-12094.

[10] Lal, S.; Clare, S. E.; Halas, N. J. *Acc Chem Res* **2008**, *41*, 1842-1851.

[11] Loo, C.; Lowery, A.; Halas, N.; West, J.; Drezek, R. *Nano Lett* **2005**, *5*, 709-711.

[12] Lowery, A. R.; Gobin, A. M.; Day, E. S.; Halas, N. J.; West, J. L. *Int J Nanomedicine* **2006**, *1*, 149-154.

[13] Chen, J.; Wang, D.; Xi, J.; Au, L.; Siekkinen, A.; Warsen, A.; Li, Z.-Y.; Zhang, H.; Xia, Y.; Li, X. *Nano Lett* **2007**, *7*, 1318-1322.

[14] Huff, T. B.; Tong, L.; Zhao, Y.; Hansen, M. N.; Cheng, J.-X.; Wei, A. *Nanomedicine* **2007**, *2*, 125-132.

[15] Lukianova-Hleb, E. Y.; Anderson, L. J. E.; Lee, S.; Hafner, J. H.; Lapotko, D. O. *Phys Chem Chem Phys* **2010**, *12*, 12237-12244.

[16] Govorov, A. O.; Richardson, H. H. *Nano Today* **2007**, *2*, 30-38.

[17] Mould, A. W.; Greco, S. A.; Cahill, M. M.; Tonks, I. D.; Bellomo, D.; Patterson, C.; Zournazi, A.; Nash, A.; Scotney, P.; Hayward, N. K.; Kay, G. F. *Circ Res* **2005**, *97*, 60-70.

[18] Starzec, A.; Ladam, P.; Vassy, R.; Badache, S.; Bouchemal, N.; Navaza, A.; du Penhoat, C. H.; Perret, G. Y. *Peptides* **2007**, *28*, 2397-2402.

[19] Patra, C.; Bhattacharya, R.; Patra, S.; Vlahakis, N.; Gabashvili, A.; Koltypin, Y.; Gedanken, A.; Mukherjee, P.; Mukhopadhyay, D. *Adv Mater* **2008**, *20*, 753-756.

[20] D'Andrea, L. D.; Del Gatto, A.; Pedone, C.; Benedetti, E. *Chem Biol Drug Des* **2006**, *67*, 115-126.

[21] Kim, K. J.; Li, B.; Winer, J.; Armanini, M.; Gillett, N.; Phillips, H. S.; Ferrara, N. *Nature* **1993**, *362*, 841-844.

[22] Goodwin, A. M. *Microvasc Res* **2007**, *74*, 172-183.

[23] Bhattacharya, R.; Mukherjee, P.; Xiong, Z.; Atala, A.; Soker, S.; Mukhopadhyay, D. *Nano Lett* **2004**, *4*, 2479-2481.

[24] Vincent, L.; Kermani, P.; Young, L. M.; Cheng, J.; Zhang, F.; Shido, K.; Lam, G.; Bompais-Vincent, H.; Zhu, Z.; Hicklin, D. J.; Bohlen, P.; Chaplin, D. J.; May, C.; Rafii, S. *J Clin Invest* **2005**, *115*, 2992-3006.

[25] Teicher, B. A. *Crit Rev Oncol/Hematol* **1995**, *20*, 9-39.

[26] Folkman, J. *Semin Cancer Biol* **2003**, *13*, 159-167.

[27] Liz-Marzán, L. M. *Mater Today* **2004**, *7*, 26-31.

[28] Mulvaney, P.; The University of Melbourne, UniNews Vol. 12, No. 13 Melbourne, **2003**.

[29] Faraday, M. *Philos Trans R Soc London* **1857**, *147*, 145-181.

[30] Turkevich, J.; Stevenson, P. C.; Hillier, J. *Disc Faraday Soc* **1951**, *11*, 55-75.

[31] Turkevich, J.; Stevenson, P. C.; Hillier, J. *J Phys Chem* **1953**, *57*, 670-673.

[32] Frens, G. *Nature-Phys Sci* **1973**, *241*, 20-22.

[33] Ji, X.; Song, X.; Li, J.; Bai, Y.; Yang, W.; Peng, X. *J Am Chem Soc* **2007**, *129*, 13939-13948.

[34] Kumar, S.; Gandhi, K. S.; Kumar, R. *Ind Eng Chem Res* **2006**, *46*, 3128-3136.
[35] Jana, N. R.; Gearheart, L.; Murphy, C. J. *J Phys Chem B* **2001**, *105*, 4065-4067.
[36] Gole, A.; Murphy, C. J. *Chem Mater* **2004**, *16*, 3633-3640.
[37] Sau, T. K.; Murphy, C. J. *Philos Mag* **2007**, *87*, 2143-2158.
[38] Busbee, B.; Obare, S.; Murphy, C. *Adv Mater* **2003**, *15*, 414-416.
[39] Murphy, C. J.; Sau, T. K.; Gole, A. M.; Orendorff, C. J.; Gao, J.; Gou, L.; Hunyadi, S. E.; Li, T. *J Phys Chem B* **2005**, *109*, 13857-13870.
[40] Orendorff, C. J.; Murphy, C. J. *J Phys Chem B* **2006**, *110*, 3990-3994.
[41] Murphy, C. J.; Gole, A. M.; Hunyadi, S. E.; Stone, J. W.; Sisco, P. N.; Alkilany, A.; Kinard, B. E.; Hankins, P. *Chem Commun* **2008**, 5, 544-557.
[42] Nikoobakht, B.; El-Sayed, M. A. *Chem Mater* **2003**, *15*, 1957-1962.
[43] Smith, D. K.; Miller, N. R.; Korgel, B. A. *Langmuir* **2009**, *25*, 9518-9524.
[44] Rayavarapu, R. G.; Ungureanu, C.; Krystek, P.; van Leeuwen, T. G.; Manohar, S. *Langmuir* **2010**, *26*, 5050-5055.
[45] Smith, D. K.; Korgel, B. A. *Langmuir* **2008**, *24*, 644-649.
[46] Pérez-Juste, J.; Pastoriza-Santos, I.; Liz-Marzán, L. M.; Mulvaney, P. *Coord Chem Rev* **2005**, *249*, 1870-1901.
[47] Huang, X.; Neretina, S.; El-Sayed, M. A. *Adv Mater* **2009**, *21*, 4880-4910.
[48] Pérez-Juste, J.; Liz-Marzán, L.; Carnie, S.; Chan, D.; Mulvaney, P. *Adv Func Mater* **2004**, *14*, 571-579.
[49] Tornblom, M.; Henriksson, U. *J Phys Chem B* **1997**, *101*, 6028-6035.
[50] Pal, T.; De; Jana, N. R.; Pradhan, N.; Mandal, R.; Pal, A.; Beezer, A. E.; Mitchell, J. C. *Langmuir* **1998**, *14*, 4724-4730.
[51] Liu, M.; Guyot-Sionnest, P. *J Phys Chem B* **2005**, *109*, 22192-22200.
[52] Westcott, S. L.; Oldenburg, S. J.; Lee, T. R.; Halas, N. J. *Langmuir* **1998**, *14*, 5396-5401.
[53] Oldenburg, S. J.; Averitt, R. D.; Westcott, S. L.; Halas, N. J. *Chem Phys Lett* **1998**, *288*, 243-247.
[54] Halas, N. *Opt Photon News* **2002**, *13*, 26-30.
[55] Wang, H.; Brandl, D. W.; Nordlander, P.; Halas, N. J. *Acc Chem Res* **2006**, *40*, 53-62.
[56] Raff, J.; Soltmann, U.; Matys, S.; Selenska-Pobell, S.; Bottcher, H.; Pompe, W. *Chem Mater* **2003**, *15*, 240-244.
[57] Wu, Y.; Chen, C.; Liu, S. *Anal Chem* **2009**, *81*, 1600-1607.
[58] Van Blaaderen, A.; Van Geest, J.; Vrij, A. *J Colloid Interface Sci* **1992**, *154*, 481-501.
[59] Yong, K.-T.; Sahoo, Y.; Swihart, M. T.; Prasad, P. N. *Colloids Surf, A* **2006**, *290*, 89-105.
[60] Phonthammachai, N.; Kah, J. C. Y.; Jun, G.; Sheppard, C. J. R.; Olivo, M. C.; Mhaisalkar, S. G.; White, T. J. *Langmuir* **2008**, *24*, 5109-5112.
[61] Arkhireeva, A.; Hay, J. N. *J Mater Chem* **2003**, *13*, 3122-3127.
[62] Stöber, W.; Fink, A.; Bohn, E. *J Colloid Interface Sci* **1968**, *26*, 62-69.
[63] Duff, D. G.; Baiker, A.; Edwards, P. P. *Langmuir* **1993**, *9*, 2301-2309.
[64] Duff, D. G.; Baiker, A.; Gameson, I.; Edwards, P. P. *Langmuir* **1993**, *9*, 2310-2317.
[65] Vaskelis, A.; Tarozaite, R.; Jagminiene, A.; Tamasiunaite, L. T.; Juskenas, R.; Kurtinaitiene, M. *Electrochim Acta* **2007**, *53*, 407-416.
[66] Sun, Y.; Xia, Y. *J Am Chem Soc* **2004**, *126*, 3892-3901.
[67] Kim, S.-W.; Kim, M.; Lee, W. Y.; Hyeon, T. *J Am Chem Soc* **2002**, *124*, 7642-7643.
[68] Clayton, G. D.; Clayton, F. E. *Patty's Industrial Hygiene and Toxicology*; 4th ed.; John Wiley & Sons: New York, **1994**; Vol. 2F.
[69] Sun, Y.; Xia, Y. *Science* **2002**, *298*, 2176-2179.
[70] Chen, J.; Saeki, F.; Wiley, B. J.; Cang, H.; Cobb, M. J.; Li, Z.-Y.; Au, L.; Zhang, H.; Kimmey, M. B.; Li; Xia, Y. *Nano Lett* **2005**, *5*, 473-477.
[71] Au, L.; Lu, X.; Xia, Y. *Adv Mater* **2008**, *20*, 2517-2522.

[72] Lu, X.; Tuan, H.-Y.; Chen, J.; Li, Z.-Y.; Korgel, B. A.; Xia, Y. *J Am Chem Soc* **2007**, *129*, 1733-1742.
[73] Cobley, C.; Skrabalak, S.; Campbell, D.; Xia, Y. *Plasmonics* **2009**, *4*, 171-179.
[74] Hu, M.; Chen, J.; Li, Z.-Y.; Au, L.; Hartland, G. V.; Li, X.; Marquez, M.; Xia, Y. *Chem Soc Rev* **2006**, *35*, 1084-1094.
[75] Wang, Z. L.; Ahmad, T. S.; El-Sayed, M. A. *Surf Sci* **1997**, *380*, 302-310.
[76] Xia, Y.; Xiong, Y.; Lim, B.; Skrabalak, S. *Angew Chem, Int Ed* **2009**, *48*, 60-103.
[77] Wang, H.; Qiao, X.; Chen, J.; Wang, X.; Ding, S. *Mater Chem Phys* **2005**, *94*, 449-453.
[78] Lee, G.-J.; Shin, S.-I.; Kim, Y.-C.; Oh, S.-G. *Mater Chem Phys* **2004**, *84*, 197-204.
[79] Pillai, Z. S.; Kamat, P. V. *J Phys Chem B* **2003**, *108*, 945-951.
[80] Skrabalak, S. E.; Au, L.; Li, X.; Xia, Y. *Nat Protocols* **2007**, *2*, 2182-2190.
[81] Siekkinen, A. R.; McLellan, J. M.; Chen, J.; Xia, Y. *Chem Phys Lett* **2006**, *432*, 491-496.
[82] You, C.-C.; Chompoosor, A.; Rotello, V. M. *Nano Today* **2007**, *2*, 34-43.
[83] Cortie, M. B.; McDonagh, A. In *Gold Chemistry: Applications and future directions in life sciences*; Mohr, F., Ed.; WILLEY-VCH Verlag GmbH & Co. KGaA Weinheim, **2009**, p 321-343.
[84] Pengo, P.; Pasquato, L. In *The supramolecular chemistry of organic - inorganic hybrid materials*; Rurak, K., Martinez-Manez, R., Eds.; John Wiley & Sons, Inc. : Hoboken, New Jersey, **2010**, p 113-154.
[85] Burns, C.; Spendel, W. U.; Puckett, S.; Pacey, G. E. *Talanta* **2006**, *69*, 873-876.
[86] Yang, J.; Lee, J. Y.; Too, H.-P. *Anal Chim Acta* **2005**, *546*, 133-138.
[87] Loweth, C. J.; Caldwell, W. B.; Peng, X.; Alivisatos, A. P.; Schultz, P. G. *Angew Chem, Int Ed* **1999**, *38*, 1808-1812.
[88] Rouhana, L. L.; Jaber, J. A.; Schlenoff, J. B. *Langmuir* **2007**, *23*, 12799-12801.
[89] Bartczak, D.; Kanaras, A. G. *Langmuir* **2010**, *26*, 7072-7077.
[90] Krpetic, Z.; Nativo, P.; Porta, F.; Brust, M. *Bioconjug Chem* **2009**, *20*, 619-624.
[91] Wuelfing, W. P.; Gross, S. M.; Miles, D. T.; Murray, R. W. *J Am Chem Soc* **1998**, *120*, 12696-12697.
[92] Wang, Z.; Levy, R.; Fernig, D. G.; Brust, M. *Bioconjug Chem* **2005**, *16*, 497-500.
[93] Malynych, S.; Luzinov, I.; Chumanov, G. *J Phys Chem B* **2002**, *106*, 1280-1285.
[94] Hussain, I.; Brust, M.; Papworth, A. J.; Cooper, A. I. *Langmuir* **2003**, *19*, 4831-4835.
[95] Levy, R.; Thanh, N. T. K.; Doty, R. C.; Hussain, I.; Nichols, R. J.; Schiffrin, D. J.; Brust, M.; Fernig, D. G. *J Am Chem Soc* **2004**, *126*, 10076-10084.
[96] Duchesne, L.; Gentili, D.; Comes-Franchini, M.; Fernig, D. G. *Langmuir* **2008**, *24*, 13572-13580.
[97] Love, J. C.; Estroff, L. A.; Kriebel, J. K.; Nuzzo, R. G.; Whitesides, G. M. *Chem Rev* **2005**, *105*, 1103-1170.
[98] Liu, Y.; Shipton, M. K.; Ryan, J.; Kaufman, E. D.; Franzen, S.; Feldheim, D. L. *Anal Chem* **2007**, *79*, 2221-2229.
[99] Kanaras, A. G.; Kamounah, F. S.; Schaumburg, K.; Kiely, C. J.; Brust, M. *Chem Commun* **2002**, 20, 2294-2295.
[100] Gentilini, C.; Evangelista, F.; Rudolf, P.; Franchi, P.; Lucarini, M.; Pasquato, L. *J Am Chem Soc* **2008**, *130*, 15678-15682.
[101] Hussain, I.; Graham, S.; Wang, Z.; Tan, B.; Sherrington, D. C.; Rannard, S. P.; Cooper, A. I.; Brust, M. *J Am Chem Soc* **2005**, *127*, 16398-16399.
[102] Schmid, G. *Chem Rev* **1992**, *92*, 1709-1727.
[103] Sharma, J.; Chhabra, R.; Cheng, A.; Brownell, J.; Liu, Y.; Yan, H. *Science* **2009**, *323*, 112-116.
[104] Park, S. Y.; Lytton-Jean, A. K. R.; Lee, B.; Weigand, S.; Schatz, G. C.; Mirkin, C. A. *Nature* **2008**, *451*, 553-556.

[105] Demers, L. M.; Mirkin, C. A.; Mucic, R. C.; Reynolds, R. A.; Letsinger, R. L.; Elghanian, R.; Viswanadham, G. *Anal Chem* **2000**, *72*, 5535-5541.
[106] Seeman, N. C. *Nano Lett* **2010**, *10*, 1971-1978.
[107] Kanaras, A. G.; Kamounah, F. S.; Schaumburg, K.; Kiely, C. J.; Brust, M. *Chem Commun* **2002**, 2294-2295.
[108] Di Corato, R.; Quarta, A.; Piacenza, P.; Ragusa, A.; Figuerola, A.; Buonsanti, R.; Cingolani, R.; Manna, L.; Pellegrino, T. *J Mater Chem* **2008**, *18*, 1991-1996.
[109] Leff, D. V.; Brandt, L.; Heath, J. R. *Langmuir* **1996**, *12*, 4723-4730.
[110] Pastoriza-Santos, I.; Liz-Marzan, L. M. *Langmuir* **2002**, *18*, 2888-2894.
[111] Brust, M.; Fink, J.; Bethell, D.; Schiffrin, D. J.; Kiely, C. *J Chem Soc, Chem Commun* **1995**, 1655-1656.
[112] Hill, H. D.; Millstone, J. E.; Banholzer, M. J.; Mirkin, C. A. *ACS Nano* **2009**, *3*, 418-424.
[113] Lévy, R. *ChemBioChem* **2006**, *7*, 1141-1145.
[114] Coomber, D.; Bartczak, D.; Gerrard, S. R.; Tyas, S.; Kanaras, A. G.; Stulz, E. *Langmuir* **2010**, *26*, 13760-13762.
[115] Dubertret, B.; Skourides, P.; Norris, D. J.; Noireaux, V.; Brivanlou, A. H.; Libchaber, A. *Science* **2002**, *298*, 1759-1762.
[116] Cheng, J.; Teply, B. A.; Sherifi, I.; Sung, J.; Luther, G.; Gu, F. X.; Levy-Nissenbaum, E.; Radovic-Moreno, A. F.; Langer, R.; Farokhzad, O. C. *Biomaterials* **2007**, *28*, 869-876.
[117] Eck, W.; Craig, G.; Sigdel, A.; Ritter, G.; Old, L. J.; Tang, L.; Brennan, M. F.; Allen, P. J.; Mason, M. D. *ACS Nano* **2008**, *2*, 2263-2272.
[118] Maus, L.; Spatz, J. P.; Fiammengo, R. *Langmuir* **2009**, *25*, 7910-7917.
[119] Alloisio, M.; Demartini, A.; Cuniberti, C.; Muniz-Miranda, M.; Giorgetti, E.; Giusti, A.; Dellepiane, G. *Phys Chem Chem Phys* **2008**, *10*, 2214-2220.
[120] Alloisio, M.; Demartini, A.; Cuniberti, C.; Dellepiane, G.; Muniz-Miranda, M.; Giorgetti, E. *Vib Spectrosc* **2008**, *48*, 53-57.
[121] Hermanson, G. T. *Bioconjugate Techniques*; 2nd ed.; Elsevier Inc. , **2008**.
[122] Hosta-Rigau, L.; Olmedo, I.; Arbiol, J.; Cruz, L. J.; Kogan, M. J.; Albericio, F. *Bioconjug Chem* **2010**, *21*, 1070-1078.
[123] Chan, W. C. W.; Nie, S. *Science* **1998**, *281*, 2016-2018.
[124] Kricheldorf, H. R.; Schwarz, G.; Marcel Dekker Inc.: New York, **1992**.
[125] Stanish, I.; Santos, J. P.; Singh, A. *J Am Chem Soc* **2001**, *123*, 1008-1009.
[126] Demartini, A.; Alloisio, M.; Cuniberti, C.; Dellepiane, G.; Jadhav, S. A.; Thea, S.; Giorgetti, E.; Gellini, C.; Muniz-Miranda, M. *J Phys Chem C* **2009**, *113*, 19475-19481.
[127] Alloisio, M.; Demartini, A.; Cuniberti, C.; Petrillo, G.; Thea, S.; Giorgetti, E.; Giusti, A.; Dellepiane, G. *J Phys Chem C* **2006**, *111*, 345-353.
[128] Alloisio, M.; Demartini, A.; Cuniberti, C.; Dellepiane, G.; Muniz-Miranda, M.; Giorgetti, E. *Vib Spectrosc* **2008**, *48*, 53-57.
[129] Jung, Y. K.; Kim, T. W.; Kim, J.; Kim, J. M.; Park, H. G. *Adv Funct Mater* **2008**, *18*, 701-708.
[130] Alam, M. R.; Maeda, M.; Sasaki, S. *Nucleic Acids Symp Ser (Oxf)* **1999**, *42*, 173-174.
[131] Alam, M. R.; Maeda, M.; Sasaki, S. *Bioorg Med Chem* **2000**, *8*, 465-473.
[132] Hvolbćk, B.; Janssens, T. V. W.; Clausen, B. S.; Falsig, H.; Christensen, C. H.; Nřrskov, J. K. *Nano Today* **2007**, *2*, 14-18.
[133] Haiss, W.; Thanh, N. T. K.; Aveyard, J.; Fernig, D. G. *Anal Chem* **2007**, *79*, 4215-4221.
[134] Hu, M.; Chen, J.; Li, Z.-Y.; Au, L.; Hartland, G. V.; Li, X.; Marquez, M.; Xia, Y. *Chem Soc Rev* **2006**, *35*, 1084-1094.
[135] Kelly, K. L.; Coronado, E.; Zhao, L. L.; Schatz, G. C. *J Phys Chem B* **2002**, *107*, 668-677.
[136] Hao, E.; Li, S.; Bailey, R. C.; Zou, S.; Schatz, G. C.; Hupp, J. T. *J Phys Chem B* **2004**, *108*, 1224-1229.
[137] Kooij, E. S.; Poelsema, B. *Phys Chem Chem Phys* **2006**, *8*, 3349-3357.

[138] Orendorff, C.; Sau, T.; Murphy, C. *Small* **2006**, *2*, 636-639.
[139] Lukianova-Hleb, E. Y.; Anderson, L. J. E.; Lee, S.; Hafner, J. H.; Lapotko, D. O. *Phys Chem Chem Phys* **ASAP**.
[140] Walther, A.; Muller, A. H. E. *Soft Matter* **2008**, *4*, 663-668.
[141] Lynch, I.; Dawson, K. A. *Nano Today* **2008**, *3*, 40-47.
[142] Mie, G. *Ann Phys* **1908**, *330*, 377-445.
[143] Kreibig, U.; Vollmer, M. *Optical Properties of Metal Clusters*; Springer: Berlin, **1995**; Vol. 25.
[144] Gao, J.; Xu, B. *Nano Today* **2009**, *4*, 37-51.
[145] McCarthy, J. R.; Weissleder, R. *Adv Drug Deliv Rev* **2008**, *60*, 1241-1251.
[146] Alivisatos, A. P.; Gu, W.; Larabell, C. *Annu Rev Biomed Eng* **2005**, *7*, 55-76.
[147] Jain, P. K.; El-Sayed, I. H.; El-Sayed, M. A. *Nano Today* **2007**, *2*, 18-29.
[148] Link, S.; El-Sayed, M. A. *J Phys Chem B* **1999**, *103*, 8410-8426.
[149] Gans, R. *Ann Phys* **1915**, *352*, 270-284.
[150] Chen, J.; McLellan, J. M.; Siekkinen, A.; Xiong, Y.; Li, Z.-Y.; Xia, Y. *J Am Chem Soc* **2006**, *128*, 14776-14777.
[151] Purcell, E. M.; Pennypacker, C. R. *Astrophys J* **1973**, *186*, 705-714.
[152] Yurkin, M. A.; Hoekstra, A. G. *J Quant Spectrosc Radiat Transf* **2007**, *106*, 558-589.
[153] Jin, R.; Cao, Y.; Mirkin, C. A.; Kelly, K. L.; Schatz, G. C.; Zheng, J. G. *Science* **2001**, *294*, 1901-1903.
[154] Jain, P. K.; Lee, K. S.; El-Sayed, I. H.; El-Sayed, M. A. *J Phys Chem B* **2006**, *110*, 7238-7248.
[155] Draine, B. T.; Flatau, P. J. *J Opt Soc Am A* **1994**, *11*, 1491-1499.
[156] Jain, P. K.; Huang, X.; El-Sayed, I. H.; El-Sayed, M. A. *Acc Chem Res* **2008**, *41*, 1578-1586.
[157] El-Sayed, I. H.; Huang, X.; El-Sayed, M. A. *Nano Lett* **2005**, *5*, 829-834.
[158] Lee, S.; Xie, J.; Chen, X. *Biochemistry* **2010**, *49*, 1364-1376.
[159] Sokolov, K.; Follen, M.; Aaron, J.; Pavlova, I.; Malpica, A.; Lotan, R.; Richards-Kortum, R. *Cancer Res* **2003**, *63*, 1999-2004.
[160] Tubbs, M. R. *J Sci Instrum* **1966**, *43*, 698-702.
[161] Huang, X.; El-Sayed, I. H.; Qian, W.; El-Sayed, M. A. *J Am Chem Soc* **2006**, *128*, 2115-2120.
[162] El-Sayed, I. H.; Huang, X.; El-Sayed, M. A. *Nano Lett* **2005**, *5*, 829-834.
[163] Hauck, T. S.; Jennings, T. L.; Yatsenko, T.; Kumaradas, J. C.; Chan, W. C. W. *Adv Mater* **2008**, *20*, 3832-3838.
[164] Gil, P. R.; Parak, W. J. *ACS Nano* **2008**, *2*, 2200-2205.
[165] Kim, G. J.; Nie, S. *Mater Today* **2005**, *8*, 28-33.
[166] Gu, F. X.; Karnik, R.; Wang, A. Z.; Alexis, F.; Levy-Nissenbaum, E.; Hong, S.; Langer, R. S.; Farokhzad, O. C. *Nano Today* **2007**, *2*, 14-21.
[167] Zharov, V. P.; Mercer, K. E.; Galitovskaya, E. N.; Smeltzer, M. S. *Biophys J* **2006**, *90*, 619-627.
[168] Prahl, S.; Oregon Medical Laser Center Oregon **1999**; Vol. 2010.
[169] Hale, G. M.; Querry, M. R. *Appl Opt* **1973**, *12*, 555-563.
[170] Kim, J. G.; Mengna, X.; Hanli, L. *IEEE Eng Med Biol* **2005**, *24*, 118-121.
[171] Skrabalak, S. E.; Chen, J.; Sun, Y.; Lu, X.; Au, L.; Cobley, C. M.; Xia, Y. *Acc Chem Res* **2008**, *41*, 1587-1595.
[172] Prevo, B. G.; Esakoff, S. A.; Mikhailovsky, A.; Zasadzinski, J. A. *Small* **2008**, *4*, 1183-1195.
[173] Salata, O. V. *J Nanobiotechnology* **2004**, *2*, 3-9.

[174] Sperling, R. A.; Rivera Gil, P.; Zhang, F.; Zanella, M.; Parak, W. J. *Chem Soc Rev* **2008**, *37*, 1896-1908.
[175] Perrault, S. D.; Walkey, C.; Jennings, T.; Fischer, H. C.; Chan, W. C. W. *Nano Lett* **2009**, *9*, 1909-1915.
[176] Overgaard, J. *Cancer* **1977**, *39*, 2637-2646.
[177] Tsuboi, A. *Int J Hyperthermia* **1988**, *4*, 655-664.
[178] Dinh, H.-K. B.; Zhao, B.; Schuschereba, S. T.; Merrill, G.; Bowman, P. D. *Physiol Genomics* **2001**, *7*, 3-13.
[179] Kühl, N. M.; Rensing, L. *Cell Mol Life Sci* **2000**, *57*, 450-463.
[180] Creagh, E. M.; Sheehan, D.; Cotter, T. G. *Leukemia* **2000**, *14*, 1161-1173.
[181] Lindquist, S. *Annu Rev Biochem* **1986**, *55*, 1151-1191.
[182] Flanders, K. C.; Winokur, T. S.; Holder, M. G.; Sporn, M. B. *J Clin Invest* **1993**, *92*, 404-410.
[183] Srinivasan, J. M.; Fajardo, L. F.; Hahn, G. M. *J Natl Cancer Inst* **1990**, *82*, 1904-1910.
[184] Choi, M.-R.; Stanton-Maxey, K. J.; Stanley, J. K.; Levin, C. S.; Bardhan, R.; Akin, D.; Badve, S.; Sturgis, J.; Robinson, J. P.; Bashir, R.; Halas, N. J.; Clare, S. E. *Nano Lett* **2007**, *7*, 3759-3765.
[185] Chen, J.; Wiley, B.; Li, Z. Y.; Campbell, D.; Saeki, F.; Cang, H.; Au, L.; Lee, J.; Li, X.; Xia, Y. *Adv Mater* **2005**, *17*, 2255-2261.
[186] Levy, R.; Shaheen, U.; Cesbron, Y.; See, V. *Nano Rev* **2010**, *1*, 4889-4907.
[187] Farokhzad, O. C.; Langer, R. *ACS Nano* **2009**, *3*, 16-20.
[188] Gao, X.; Cui, Y.; Levenson, R. M.; Chung, L. W. K.; Nie, S. *Nat Biotech* **2004**, *22*, 969-976.
[189] von Maltzahn, G.; Ren, Y.; Park, J.-H.; Min, D.-H.; Kotamraju, V. R.; Jayakumar, J.; Fogal, V.; Sailor, M. J.; Ruoslahti, E.; Bhatia, S. N. *Bioconjug Chem* **2008**, *19*, 1570-1578.
[190] Liu, R.; Kay, B. K.; Jiang, S.; Chen, S. *MRS Bulletin* **2009**, *34*, 432-440.
[191] Huang, Y.-F.; Liu, H.; Xiong, X.; Chen, Y.; Tan, W. *J Am Chem Soc* **2009**, *131*, 17328-17334.
[192] Kobayashi, H.; Lin, P. C. *Nanomedicine* **2006**, *1*, 17-22.
[193] Yu, D.-H.; Lu, Q.; Xie, J.; Fang, C.; Chen, H.-Z. *Biomaterials* **2010**, *31*, 2278-2292.
[194] Oyelere, A. K.; Chen, P. C.; Huang, X.; El-Sayed, I. H.; El-Sayed, M. A. *Bioconjug Chem* **2007**, *18*, 1490-1497.
[195] Dixit, V.; Van den Bossche, J.; Sherman, D. M.; Thompson, D. H.; Andres, R. P. *Bioconjug Chem* **2006**, *17*, 603-609.
[196] de la Fuente, J. M.; Berry, C. C. *Bioconjug Chem* **2005**, *16*, 1176-1180.
[197] Nativo, P.; Prior, I. A.; Brust, M. *ACS Nano* **2008**, *2*, 1639-1644.
[198] Hauck, T.; Ghazani, A.; Chan, W. *Small* **2008**, *4*, 153-159.
[199] Semmler-Behnke, M.; Kreyling, W. G.; Lipka, J.; Fertsch, S.; Wenk, A.; Takenaka, S.; Schmid, G.; Brandau, W. *Small* **2008**, *4*, 2108-2111.
[200] Bhattacharya, R.; Mukherjee, P. *Adv Drug Deliv Rev* **2008**, *60*, 1289-1306.
[201] Chen, C. S. *Nat Nano* **2008**, *3*, 13-14.
[202] Hirak, K. P.; Shuvojit, B.; Utpal, C.; Prabir, L.; Anjan Kr, D. *Nanomedicine* **2007**, *3*, 111-119.
[203] Alkilany, A. M.; Nagaria, P. K.; Hexel, C. R.; Shaw, T. J.; Murphy, C. J.; Wyatt, M. D. *Small* **2009**, *5*, 701-708.
[204] Mandal, D.; Maran, A.; Yaszemski, M.; Bolander, M.; Sarkar, G. *J Mater Sci: Mater Med* **2009**, *20*, 347-350.
[205] Huff, T. B.; Hansen, M. N.; Zhao, Y.; Cheng, J.-X.; Wei, A. *Langmuir* **2007**, *23*, 1596-1599.
[206] Chithrani, B. D.; Ghazani, A. A.; Chan, W. C. W. *Nano Lett* **2006**, *6*, 662-668.

[207] Ghosh, P. S.; Kim, C.-K.; Han, G.; Forbes, N. S.; Rotello, V. M. *ACS Nano* **2008**, *2*, 2213-2218.
[208] Green, J. J.; Chiu, E.; Leshchiner, E. S.; Shi, J.; Langer, R.; Anderson, D. G. *Nano Lett* **2007**, *7*, 874-879.
[209] Chithrani, B. D.; Chan, W. C. W. *Nano Lett* **2007**, *7*, 1542-1550.
[210] Bastus, N. G.; Sanchez-Tillo, E.; Pujals, S.; Farrera, C.; Lopez, C.; Giralt, E.; Celada, A.; Lloberas, J.; Puntes, V. *ACS Nano* **2009**, *3*, 1335-1344.
[211] Ehrenberg, M. S.; Friedman, A. E.; Finkelstein, J. N.; Oberdörster, G.; McGrath, J. L. *Biomaterials* **2009**, *30*, 603-610.
[212] Buranda, T.; Jones, G. M.; Nolan, J. P.; Keij, J.; Lopez, G. P.; Sklar, L. A. *J Phys Chem B* **1999**, *103*, 3399-3410.
[213] Minchin, R. *Nat Nano* **2008**, *3*, 12-13.
[214] Jiang, W.; Kim, B. Y. S.; Rutka, J. T.; Chan, W. C. W. *Nat Nano* **2008**, *3*, 145-150.
[215] Cheng, H.; Kastrup, C. J.; Ramanathan, R.; Siegwart, D. J.; Ma, M.; Bogatyrev, S. R.; Xu, Q.; Whitehead, K. A.; Langer, R.; Anderson, D. G. *ACS Nano* **2010**, *4*, 625-631.
[216] Nishikawa, T.; Iwakiri, N.; Kaneko, Y.; Taguchi, A.; Fukushima, K.; Mori, H.; Morone, N.; Kadokawa, J.-i. *Biomacromolecules* **2009**, *10*, 2074-2085.
[217] Giljohann, D. A.; Seferos, D. S.; Patel, P. C.; Millstone, J. E.; Rosi, N. L.; Mirkin, C. A. *Nano Lett* **2007**, *7*, 3818-3821.
[218] Free, P.; Shaw, C. P.; Levy, R. *Chem Commun* **2009**, 33, 5009-5011.
[219] Mukherjee, P.; Bhattacharya, R.; Bone, N.; Lee, Y.; Patra, C.; Wang, S.; Lu, L.; Secreto, C.; Banerjee, P.; Yaszemski, M.; Kay, N.; Mukhopadhyay, D. *J Nanobiotechnology* **2007**, *5*, 4-17.
[220] Decuzzi, P.; Ferrari, M. *Biomaterials* **2007**, *28*, 2915-2922.
[221] Zhang, S.; Li, J.; Lykotrafitis, G.; Bao, G.; Suresh, S. *Adv Mater* **2009**, *21*, 419-424.
[222] Verma, A.; Uzun, O.; Hu, Y.; Hu, Y.; Han, H.-S.; Watson, N.; Chen, S.; Irvine, D. J.; Stellacci, F. *Nat Mater* **2008**, *7*, 588-595.
[223] Quarta, A.; Ragusa, A.; Deka, S.; Tortiglione, C.; Tino, A.; Cingolani, R.; Pellegrino, T. *Langmuir* **2009**, *25*, 12614-12622.
[224] Steven, V.; Ingram, A.; Graham, D. *Chem Commun* **2009**, 2872-2874.
[225] Jones, H. W.; McKusick, V. A.; Harper, P. S.; Wuu, K. D. *Obstet Gynecol* **1971**, *38*, 945-949.
[226] Masters, J. R. *Nat Rev Cancer* **2002**, *2*, 315-319.
[227] Nelson-Rees, W. A.; Flandermeyer, R. R. *Science* **1976**, *191*, 96-98.
[228] Lewis, W. H. *Harvey Lect* **1936**, *31*, 214-234.
[229] Brown, R. W.; Henderson, J. H. M. *J Hist Med Allied Sci* **1983**, *38*, 415-431.
[230] Masters, J. R. W. *Nature Rev Mol Cell Biol* **2000**, *1*, 233-236.
[231] Srivastava, R. *Apoptosis, Cell Signaling, and Human Diseases*; Humana Press Inc.: New Jersey, **2007**.
[232] Henle, G.; Deinhardt, F. J. *J Immunol* **1957**, *79*, 54-59.
[233] Cliff, W. J. *Blood vessels (Biological structure and function; 6)*; Cambridge University Press: Cambridge, **1976**.
[234] Sumpio, B. E.; Timothy Riley, J.; Dardik, A. *Int J Biochem Cell Biol* **2002**, *34*, 1508-1512.
[235] Dejana, E.; Corada, M.; Lampugnani, M. G. *FASEB J* **1995**, *9*, 910-918.
[236] Schnittler, H. J. *Basic Res Cardiol* **1998**, *93*, 30-39.
[237] Dejana, E. *J Clin Invest* **1996**, *98*, 1949-1953.
[238] Carmeliet, P.; Jain, R. K. *Nature* **2000**, *407*, 249-257.
[239] Sawaji, Y.; Sato, T.; Takeuchi, A.; Hirata, M.; Ito, A. *Br J Cancer* **2002**, *86*, 1597-1603.
[240] Ferrara, N.; Davis-Smyth, T. *Endocr Rev* **1997**, *18*, 4-25.

[241] Jia, H.; Bagherzadeh, A.; Hartzoulakis, B.; Jarvis, A.; Lohr, M.; Shaikh, S.; Aqil, R.; Cheng, L.; Tickner, M.; Esposito, D.; Harris, R.; Driscoll, P. C.; Selwood, D. L.; Zachary, I. C. *J Biol Chem* **2006**, *281*, 13493-13502.
[242] Shanafelt, T. D.; Kay, N. E. *Semin Oncol* **2006**, *33*, 174-185.
[243] Makinen, T.; Olofsson, B.; Karpanen, T.; Hellman, U.; Soker, S.; Klagsbrun, M.; Eriksson, U.; Alitalo, K. *J Biol Chem* **1999**, *274*, 21217-21222.
[244] Mustonen, T.; Alitalo, K. *J Cell Biol* **1995**, *129*, 895-898.
[245] Li, X.; Eriksson, U. *Int J Biochem Cell Biol* **2001**, *33*, 421-426.
[246] Giordano, R. J.; Anobom, C. D.; Cardó-Vila, M.; Kalil, J.; Valente, A. P.; Pasqualini, R.; Almeida, F. C. L.; Arap, W. *Chem Biol* **2005**, *12*, 1075-1083.
[247] Shibuya, M. *Int J Biochem Cell Biol* **2001**, *33*, 409-420.
[248] Salikhova, A.; Wang, L.; Lanahan, A. A.; Liu, M.; Simons, M.; Leenders, W. P. J.; Mukhopadhyay, D.; Horowitz, A. *Circ Res* **2008**, *103*, 71-79.
[249] Olofsson, B.; Korpelainen, E.; Pepper, M. S.; Mandriota, S. J.; Aase, K.; Kumar, V.; Gunji, Y.; Jeltsch, M. M.; Shibuya, M.; Alitalo, K.; Eriksson, U. *Proc Natl Acad Sci USA* **1998**, *95*, 11709-11714.
[250] Li, Y.; Zhang, F.; Nagai, N.; Tang, Z.; Zhang, S.; Scotney, P.; Lennartsson, J.; Zhu, C.; Qu, Y.; Fang, C.; Hua, J.; Matsuo, O.; Fong, G.-H.; Ding, H.; Cao, Y.; Becker, K. G.; Nash, A.; Heldin, C.-H.; Li, X. *J Clin Invest* **2008**, *118*, 913-923.
[251] Zhang, F.; Tang, Z.; Hou, X.; Lennartsson, J.; Li, Y.; Koch, A. W.; Scotney, P.; Lee, C.; Arjunan, P.; Dong, L.; Kumar, A.; Rissanen, T. T.; Wang, B.; Nagai, N.; Fons, P.; Fariss, R.; Zhang, Y.; Wawrousek, E.; Tansey, G.; Raber, J.; Fong, G.-H.; Ding, H.; Greenberg, D. A.; Becker, K. G.; Herbert, J.-M.; Nash, A.; Yla-Herttuala, S.; Cao, Y.; Watts, R. J.; Li, X. *Proc Natl Acad Sci USA* **2009**, *106*, 6152-6157.
[252] Neufeld, G.; Cohen, T.; Gengrinovitch, S.; Poltorak, Z. *FASEB J* **1999**, *13*, 9-22.
[253] Veikkola, T.; Alitalo, K. *Semin Cancer Biol* **1999**, *9*, 211-220.
[254] Michael, K.; Patricia, A. D. A. *Cytokine Growth Factor Rev* **1996**, *7*, 259-270.
[255] Risau, W. *Nature* **1997**, *386*, 671-674.
[256] Mukherjee, P.; Bhattacharya, R.; Wang, P.; Wang, L.; Basu, S.; Nagy, J. A.; Atala, A.; Mukhopadhyay, D.; Soker, S. *Clin Cancer Res* **2005**, *11*, 3530-3534.
[257] Masters, J. R. W.; Palsson, B. O. *Human Cell Culture*, **1999**.
[258] Pennington, M. W.; Dunn, B. M. *Peptide synthesis protocols*; Humana Press Inc.: New Jersey, **1994**.
[259] Roseman, M. A. *J Mol Biol* **1988**, *200*, 513-522.
[260] INNOVAGEN **2010**.
[261] Barrett, G. C.; Elmore, D. T. *Amino Acids and Peptides*; Cambridge University Press: Cambridge, **1998**.
[262] Zhu, W.; Williams, R. S.; Kodadek, T. *J Biol Chem* **2000**, *275*, 32098-32105.
[263] Rhee, M.; Davis, P. *J Biol Chem* **2006**, *281*, 1233-1240.
[264] D'Andrea, L. D.; Iaccarino, G.; Fattorusso, R.; Sorriento, D.; Carannante, C.; Capasso, D.; Trimarco, B.; Pedone, C. *Proc Natl Acad Sci USA* **2005**, *102*, 14215-14220.
[265] Hood, J. D.; Bednarski, M.; Frausto, R.; Guccione, S.; Reisfeld, R. A.; Xiang, R.; Cheresh, D. A. *Science* **2002**, *296*, 2404-2407.
[266] Paidas, C. N.; Mooney, M. L.; Theodorakis, N. G.; De Maio, A. *Am J Physiol Regul Integr Comp Physiol* **2002**, *282*, 1374-1381.
[267] Brand, K.; Lubbe, A. S.; Justus, D. J. *Int J Hyperthermia* **1996**, *12*, 527-538.
[268] Fujio, N.; Hatayama, T.; Kinoshtta, H.; Yukioka, M. *J Biochem* **1987**, *101*, 181-187.
[269] Sonna, L. A.; Fujita, J.; Gaffin, S. L.; Lilly, C. M. *J Appl Physiol* **2002**, *92*, 1725-1742.
[270] Bevilacqua, M. P.; Stengelin, S.; Gimbrone, M. A., Jr.; Seed, B. *Science* **1989**, *243*, 1160-1165.

[271] Dustin, M. L.; Rothlein, R.; Bhan, A. K.; Dinarello, C. A.; Springer, T. A. *J Immunol* **1986**, *137*, 245-254.
[272] Phillips, M. L.; Nudelman, E.; Gaeta, F. C.; Perez, M.; Singhal, A. K.; Hakomori, S.; Paulson, J. C. *Science* **1990**, *250*, 1130-1132.
[273] Hession, C.; Osborn, L.; Goff, D.; Chi-Rosso, G.; Vassallo, C.; Pasek, M.; Pittack, C.; Tizard, R.; Goelz, S.; McCarthy, K. *Proc Natl Acad Sci USA* **1990**, *87*, 1673-1677.
[274] Lauri, D.; Needham, L.; Martin-Padura, I.; Dejana, E. *J Natl Cancer Inst* **1991**, *83*, 1321-1324.
[275] Gearing, A. J. H.; Newman, W. *Immunol Today* **1993**, *14*, 506-512.
[276] Williams, A. F.; Barclay, A. N. *Annu Rev Immunol* **1988**, *6*, 381-405.
[277] Smith, C. W.; Rothlein, R.; Hughes, B. J.; Mariscalco, M. M.; Rudloff, H. E.; Schmalstieg, F. C.; Anderson, D. C. *J Clin Invest* **1988**, *82*, 1746-1756.
[278] Wegner, C. D.; Gundel, R. H.; Reilly, P.; Haynes, N.; Letts, L. G.; Rothlein, R. *Science* **1990**, *247*, 456-459.
[279] Wang, J. H.; Redmond, H. P.; Watson, R. W.; Bouchier-Hayes, D. *Am J Physiol Cell Physiol* **1997**, *272*, 1543-1551.

3. Methods and techniques.

Experimental methods and techniques applied in the presented research, are considered a significant part of the development, therefore shown as an independent chapter in this thesis. Synthetic methods and protocols will be introduced in **sections 3.1.** and **3.2.**, while characterisation techniques in **sections 3.3.** and **3.5.**

3.1. Synthesis of NPs.

NPs, both spherical and anisotropic (rod-like, hollow and core/shell) were synthesised by relatively simple and cost effective wet chemistry methods, following conventional routes. Specifically, spherical gold NPs were synthesised *via* a citrate reduction method [1-6] (**section 3.1.1.**). Gold nanorods were prepared by seed mediated protocols [7-18] (**section 3.1.2.**). Silica/gold core/shell nanostructures were produced using a seed mediated method, utilising silica NPs as templates [19-29] (**section 3.1.3.**), while hollow gold NPs were synthesised by a galvanic replacement reaction [30-38] (**section 3.1.4.**). Standard protocols were slightly modified and optimised according to own requirements, which will be detailed in the following sub-sections.

3.1.1. Synthesis of spherical gold NPs.

Sodium citrate (**Scheme 25A**) stabilised spherical gold NPs were prepared by a citrate reduction method, developed by Turkevich [1-6] (see **chapter 2** for reaction mechanism). Citrate-NPs were capped with *bis*(*p*-sulfonatophenyl)phenyl phosphine dehydrate dipotassium salt – a phosphine derivative (BSPP, **Scheme 25B**, see **chapter 2** for theoretical background) *via* the ligand exchange reaction [39-43].

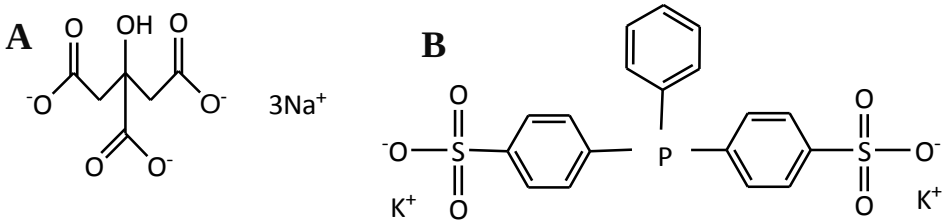

Scheme 25. Chemical structures of: trisodium citrate (A) and BSPP (B).

A solution of trisodium citrate (2.5 ml, 19.5 mM in Milli-Q water) was brought to boil and poured quickly into a vigorously stirred, boiling solution of sodium tetrachloroaurate (III) dihydrate (0.5 mM, 25 ml). The molar ratio between Ct^{3-} and Au^{3+} was 1 : 3.9 (Note: the ratio of Ct^{3-} to Au^{3+} can be decreased to 1 : 1.95 and further to 1 : 0.39 to prepare larger

NPs, see **chapter 4** for results). Colour change from pale yellow through colourless to deep red indicated the formation of NPs [1-6,44]. The reaction mixture was boiled and stirred for an additional 15 min., cooled to room temperature and purified by filtration (0.45 μm filter, Millipore). NPs were then capped with BSPP.

BSPP (10 mg; Molecular Weight, MW = 498.6) was added to citrate stabilised gold NPs (27.5 ml) and stirred overnight at room temperature. BSPP-coated nanocrystals were precipitated with sodium chloride (50 mg, MW = 58.5) and purified by centrifugation/decantation (5000 rpm, 5 min). Precipitated NPs were redispersed by sonication in 2 ml of Milli-Q water, characterised (see **chapter 4** for physicochemical characterisation) and kept at 4 °C prior to further surface modifications (see **section 3.2.** for experimental details).

3.1.2. Synthesis of gold nanorods.

Gold nanorods were prepared by the one-step seed mediated growth method (method I), reported by El-Sayed [14], while more elongated nanorods – gold nanowires were synthesised *via* a three-step protocol (method II), developed by Murphy [7,11,15-18]. Original versions of both methods were slightly modified.

In method I, the growth solution was prepared by mixing in the following order aqueous solutions of: CTAB (0.2 M, 7.12 ml, **Scheme 26**), sodium tetrachloroaurate (III) dihydrate (5 mM, 2 ml), silver nitrate (5 mM, 0.15 ÷ 0.4 ml) and freshly prepared L-ascorbic acid (0.0788 M, 0.16 ml). Gold seeds were prepared separately by the reduction of sodium tetrachloroaurate (III) dihydrate (5 mM, 1 ml) and CTAB (0.2 M, 1 ml) mixture, with an ice cold solution of sodium borohydride (0.01 M, 0.5 ml), added dropwise. Colour change from orange through colourless to deep brown indicated the formation of small gold NPs [44,45] (see **chapter 4** for physicochemical characterisation). Fresh solution of seeds (16 μl) was added to the growth solution, shaken gently and the reaction mixture was left overnight at 35 °C. The formation of gold nanorods was indicated by the solution colour change from colourless to blue [14,46] (when 0.17 ml of silver nitrate was added, see **chapter 4** for more details). Nanorods were purified from an excess of reagents by two steps of centrifugation/decantation (10'000 rpm, 10 min.), redispersed in 5 ml of Milli-Q water, characterised (see **chapter 4**) and kept at 4 °C prior to surface capping (see **section 3.2.**).

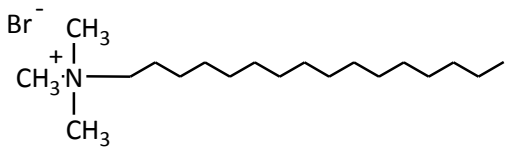

Scheme 26. Chemical structure of CTAB surfactant.

Nanowires were synthesised by method II. The growth solution containing CTAB (0.1 M) and sodium tetrachloroaurate (III) dihydrate (0.25 mM) was prepared and poured into three flasks (9 ml into flask 'A', 9 ml into 'B' and 45 ml into 'C'). Freshly prepared L-ascorbic acid (0.1 M) was then added to each flask (50 µl to 'A' and 'B', 250 µl ml to 'C') and shaken. To flask 'A' the seeds solution (0.4 ml, see method A) was added and mixed. After 15 s, solution 'A' (1 ml) was added to flask 'B', 30 s later solution 'B' (5 ml) was added to flask 'C' and the reaction mixture was left overnight at 35 °C. The formation of gold nanowires was indicated by the solution colour change from colourless to red [18]. Nanowires were purified by two steps of centrifugation/decantation (10'000 rpm, 10 min.), redispersed in 5 ml of Milli-Q water, characterised (see **chapter 4**) and kept at 4 °C.

3.1.3. Synthesis of silica/gold core/shell NPs.

Silica/gold core/shell NPs were prepared by Halas method [21,23,26,47] (see **chapter 2** for reaction mechanism), involving four steps: a) synthesis of silica NPs (by Stöber method [19,20,22,28]); b) functionalisation with 3-(aminopropyl)trimethoxysilane (APTMS, **Scheme 27A**); c) attachment of gold seeds (stabilised with tetrakis(hydroxymetyl)phosphonium chloride – THPC, **Scheme 27B**; prepared by Duff method [24,25]) and d) growth of the gold shell.

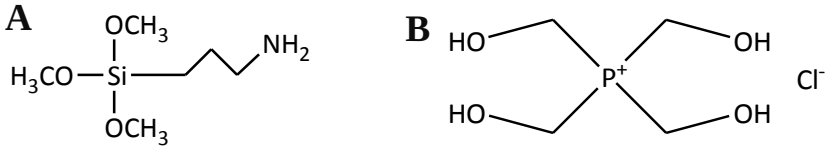

Scheme 27. Chemical structures of: APTMS (A) and THPC (B).

Silica NPs were prepared by mixing ammonia solution (30 %, 3 ml) with absolute ethanol (50 ml), to which tetraethyl orthosilicate (TEOS, 6.7 mmol, 1.5 ml, see **Scheme 28**) was added dropwise. Smaller silica NPs were prepared by a modified protocol, as reported by Liu and co-workers [20]. Specifically, absolute ethanol (50 ml) was mixed

with Milli-Q water (3.03 ml) and ammonia solution (30 %, 2.25 ml). Under vigorous stirring, TEOS (8.7 mmol, 1.94 ml) mixed with absolute ethanol (5 ml) was added quickly.

Both, sol-gel mixtures were stirred for 30 min. and purified by two steps of centrifugation/decantation (10'000 rpm, 10 min.). Silica NPs were redispersed by sonication in ethanol (50 ml). To vigorously stirred silica NPs, APTMS (2.8 mmol, 0.5 ml) was added and the reaction mixture was allowed to react for 2 h. APTMS-silica NPs were purified by two steps of centrifugation/decantation (10'000 rpm, 10 min.) and redispersed by sonication in 100 ml of Milli-Q water.

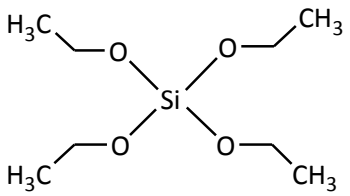

Scheme 28. Chemical structure of TEOS.

Meanwhile, gold seeds were prepared by mixing sodium hydroxide solution (1 M, 0.5 ml) with THPC (0.067 mmol, 1 ml) and Milli-Q water (45 ml), followed by the injection of sodium tetrachloroaurate (III) dihydrate solution (1 %, 0.75 ml). Colour change from colourless to yellowish/light brown indicated the formation of small gold NPs (seeds) [44,45] (see **chapter 4** for physicochemical characterisation). Gold seeds were purified by overnight dialysis against Milli-Q water (1'000 ml; 12 ÷ 14 k cellulose membrane, CelluSep). Fresh solution of seeds (5 ml) was added to APTMS-capped silica NPs (0.5 ml) and the reaction mixture was allowed to sit for 2 h at room temperature. Seeds-APTMS-silica NPs were purified by two steps of centrifugation/decantation (1'000 rpm, 10 min.) and redispersed in Milli-Q water (5 ml) prior to shell growth.

In a separate flask, potassium carbonate (25 mg, MW = 138.2) was dissolved in Milli-Q water (100 ml) by 5 min. stirring at room temperature. Next, sodium tetrachloroaurate (III) dihydrate solution (1 %, 1.5 ml) was added and the mixture was stirred for 30 min. then cooled down to 4 °C. To the cold growth solution (4 ml), seeds-APTMS-silica NPs (200 µl) were added. While stirring, formaldehyde (0.36 mmol, 10 µl) was injected and the mixture was allowed to react for 5 min. until colour change from colourless to blue. The growth was terminated by the addition of thiol containing molecule (100 µl, 5 mg/ml, MW = 526.7, see **section 3.2.1.** for the chemical structure and **chapter 2** for reaction mechanism), which binds to the gold surface and prevents further growth of NPs [39,40,48-51].

Silica/gold core/shell NPs were purified by three steps of centrifugation/decantation (10'000 rpm, 10 min.), redispersed in sodium borate buffer (0.01 M, pH 9, 1 ml), characterised (see **chapter 4**) and kept at 4 °C prior to further surface modifications (**section 3.2.**).

3.1.4. Synthesis of hollow gold NPs.

Hollow gold NPs were prepared by a protocol involving two steps. First, spherical silver NPs were grown by the seed mediated method, developed by Oh [35]. Silver NPs were then utilised as templates in the galvanic replacement reaction between silver (Ag^0 atoms) and gold (Au^{3+} ions) [30,31,33,34,52-54]. This method introduced by Xia, resulted in the formation of gold NPs with hollow interiors (see **chapter 2** for reaction mechanism).

The growth solution was prepared by mixing in the following order: CTAB (0.2 M, 80 ml), silver nitrate (0.05 M, 400 µl) and freshly prepared L-ascorbic acid (0.1 M, 2 ml). Silver seeds were prepared separately by the reduction of silver nitrate (2.5 mM, 1 ml), mixed with trisodium citrate (2.5 mM, 1 ml) and Milli-Q water (8 ml), with an ice cold solution of sodium borohydride (0.001 M, 25 µl). Colour change from colourless to pale yellow indicated the formation of small silver NPs [35,44,45,55] (seeds, see **chapter 4** for physicochemical characterisation). A fresh solution of seeds (400 µl) was added to the growth solution, followed by the injection of sodium hydroxide solution (1 M, 2 ml). Colour change from colourless to deep yellow indicated the formation of silver NPs [35,44,45]. The reaction mixture was left overnight at 35 °C, then purified by centrifugation/decantation (1'000 rpm, 10 min.).

Silver NPs were redispersed in Milli-Q water (40 ml), characterised (see **chapter 4**) and used as templates in the galvanic replacement reaction. The solution of silver NPs (10 ml) was brought to boil and refluxed for 10 min. While stirring, sodium tetrachloroaurate (III) dihydrate aqueous solution was added dropwise (1 mM, 0.25 ml). Colour change from yellow to blue indicated the formation of hollow NPs [33,34,52-54,56,57]. The reaction mixture was refluxed for an additional 20 min. then cooled to room temperature. NPs were characterised (see **chapter 4**) and kept at 4 °C prior to surface capping (**section 3.2.**).

3.2. NPs surface capping.

Gold NPs were capped with several types of ligands, including OEG ligand [50] (**section 3.2.1.**), DA-PEG ligand [48] (**section 3.2.2.**) and CALNN peptide [58-61] (**section 3.2.3.**). All

listed molecules were chemisorbed on the surface of gold NPs *via* thiol anchoring groups [39,40,62,63] (see **chapter 2** for theoretical background). OEG-capped NPs were further modified with octa-peptides (**section 3.2.4.**) by the EDC/s-NHS coupling chemistry method [64-66].

3.2.1. NPs surface capping with OEG ligands.

Freshly prepared OEG (monocarboxy (1-mercaptoundec-11-yl) hexaethylene glycol, **Scheme 29**) aqueous solution (5 mg/ml, 200 µl, MW = 526.7) was added to a solution of gold nanospheres (10 ml, 5 nM), while stirring. The mixture was incubated for 2 h at room temperature, then overnight at 4 °C. Capped NPs were purified by three steps of centrifugation/decantation (16'400 rpm, 15 min) and redispersed by sonication in sodium borate buffer (10 ml, 0.01 M, pH 9) prior to physicochemical characterisation (see **chapter 4**) or growth media (1 ml) prior to experiments with cells (see **chapter 5**). NPs were stored at 4 °C.

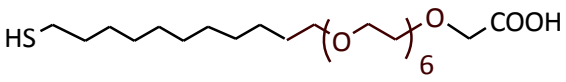

Scheme 29. Chemical structure of OEG.

Anisotropic (rod-like, hollow or core/shell) gold NPs were capped with OEG ligands according to a slightly modified procedure. A fresh solution of OEG (5 mg/ml, 200 µl, MW = 526.7) was injected into an aqueous solution of gold NPs (5 ml; optical density, OD = 0.5), whilst sonicating at 4 ºC, this was immediately followed by the addition of sodium borate buffer (5 ml, 0.02 M, pH 9). Gradually over an 1 h, the temperature was increased to room temperature, then held at room temperature for 2 h with stirring. This was followed by 30 min. of sonication at room temperature and overnight incubation at 4 °C. Capped NPs were purified by three steps of centrifugation/decantation and redispersed by sonication in sodium borate buffer (10 ml, 0.01 M, pH 9) prior to characterisation (see **chapter 4**) or growth media (1 ml) prior to experiments with cells (see **chapter 5**; Note: supernatants left at each step of purification were combined and stored at 4 ºC prior to quantification of the thiol content, as described in **section 3.3.2.**). NPs were stored at 4 °C.

3.2.2. NPs surface capping with DA-PEG ligands.

Freshly prepared DA-PEG (46-mercapto-22,43-dioxo-3,6,9,12,15,18-hexaoxa-21,44-diazahexatetraconta-31,33-diyn-1-oic acid, **Scheme 30**) solution in methanol (5 mg/ml, 100 µl, MW = 729.0) was added to an aqueous solution of gold NPs (5 ml, 5 nM), whilst stirring in the dark at room temperature. After 10 min., sodium phosphate buffer (5 ml, 0.2 M; 0.3 M sodium chloride; pH 8) was introduced and the reaction mixture was left overnight at 4 °C in the dark. NPs were purified from the excess of DA-PEG ligand by triple centrifugation (16'400 rpm, 15 min.), followed by decantation (Note: supernatants, from each step of purification were combined prior to the thiol quantification; see **section 3.3.2.**). NPs were redispersed in sodium phosphate buffer (10 ml,0.1 M, pH 8) and UV-irradiated for 15 min. (254 nm light wavelength, 35 W lamp power, 10 cm from the UV-lamp) to photo-crosslink DA-PEG monomers [48]. The colloidal solution was purified from small aggregates by centrifugation (5'000 rpm, 5 min.). The supernatant containing dispersed NPs was placed in a clean vial prior to the second step of capping.

A fresh portion of DA-PEG solution (5 mg/ml, 10 µl, MW = 729.0, in methanol) was introduced and the reaction mixture was incubated overnight at 4 °C in the dark. NPs were purified by triple centrifugation/decantation (16'400 rpm, 15 min.), redispersed in sodium phosphate buffer (10 ml, 0.1 M, pH 8) and UV-crosslinked using the same irradiation conditions. After purification (centrifugation 5'000 rpm, 5 min.), the supernatant containing dispersed photo-polymerised NPs was characterised (see **chapter 4**) and stored at 4 °C.

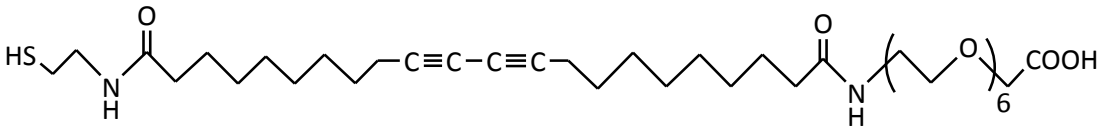

Scheme 30. Chemical structure of DA-PEG.

3.2.3. NPs surface capping with CALNN based peptides and assembly on oligodeoxynucleotide templates.

The surface of spherical gold NPs was functionalised with CALNN and CALNN-Ahex-FQGII (c-FQGII, **Fig. 3A**; Ahex is aminohexanoic acid) peptides through the thiol

anchoring group [39,40,58,61] (see **chapter 2** for chemical structures and theoretical background). CALNN/c-FQGII capped NPs were assembled on two types of oligodeoxynucleotide templates (ODN) [60]. From which, one was composed of a short palindromic sequence (ODN_3, **Fig. 3B**), while second formed pseudo-infinite duplexes (ODN_{1+2}, **Fig. 3C**). As stated in **chapter 2**, NPs bound to ODN templates *via* the interaction between AT-rich regions of ODN and FQGII sequence in the outer shell on NPs [60,67,68].

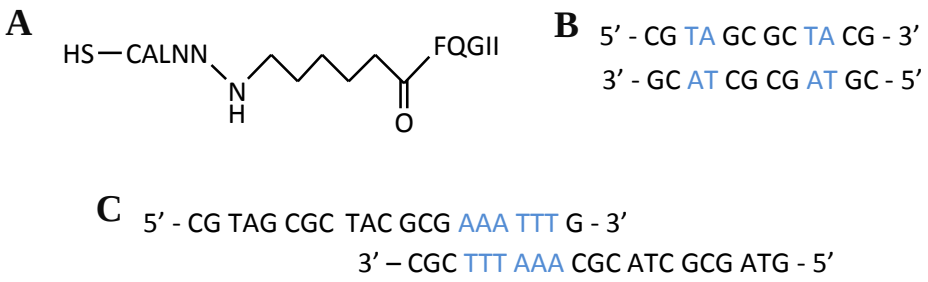

Figure 3. The structure of c-FQGII (A), short ODN_3 self-complimentary sequence (B) and pseudo-infinite ODN_{1+2} sequence (C).

A mixture of CALNN and c-FQGII (5 ÷ 25 % of c-FQGII, 0.5 mg/500 µl) in sodium phosphate buffer (0.2 M, pH 8) was added to an aqueous solution of gold NPs (0.5 ml, 5 nM), whilst stirring. The reaction mixture was sonicated for 20 min. at room temperature, then incubated overnight at 4 °C. Colloids were purified from the excess ligands by triple centrifugation (16’400 rpm, 15 min.) followed by decantation, then redispersed in sodium phosphate buffer (0.5 ml, 0.1 M; 0.1 M sodium chloride; pH 8) prior to the characterisation (see **chapter 4**) and assembly on ODN templates (see **chapter 4**). NPs were stored at 4 °C.

ODNs were synthesised by Dr Eugen Stulz group members: Miss Danielle Coomber, Dr Simon R. Gerrard and Miss Sarah Tyas (School of Chemistry, University of Southampton, Southampton, UK) on an ABI Expedite 8909 synthesiser [60]. Standard solid supported phosphoramidite cycle (1 µmol) of acid catalysed detritylation, coupling, capping and iodine oxidation was used. ODNs were deprotected/cleaved from solid support by heating in concentrated ammonium hydroxide at 35 °C for 15 h, then purified using Glen-Pak purification column following standard protocols (Glen Research or Cambio Ltd.).

NPs (2 nM) and templates ODN_{1+2} or ODN_3 (1 µM or 0.5 µM) were suspended in sodium phosphate buffer (0.1 M, 1 ml; 0.1 M sodium chloride, 1 mM EDTA, pH 8).

An approximate 1:1 molar ratio between single AT binding region within ODN and FQGII was achieved (Note: assuming 80 % of NPs surface covarage [61,69], 2000 surface atoms would be bound to CALNN or c-FQGII, which is equal to 500 c-FQGII's for 25 % c-FQGII content). Heating up to 85 °C and cooling down to 18 °C cycle was performed to ensure the formation of ODN-NPs assemblies. The formation of assemblies was monitored by transmission electron microscopy and UV-visible spectroscopy techniques (see **chapter 4** for results).

3.2.4. Further modifications of NPs surface.

Three different octa-peptides (P1, P2 and P3; see **chapter 2** for chemical structures) were conjugated to OEG-coated gold NPs using EDC/s-NHS coupling method [64-66]. In this method, an amide bond was formed between an amine and a carboxylic group; hence, between carboxy terminated OEG NPs (see **chapter 2** for a schematic illustration and the reaction mechanism) and amine containing octa-peptides. EDC/s-NHS coupling resulted in the formation of peptide-OEG conjugated colloids.

In detail, a peptide solution (100 µl, 1 mg/ml, $MW_{P1/P2}$ = 922.1, MW_{P3} = 968.2, in 0.01 M sodium borate buffer, pH 9) was added to OEG-coated NPs solution (5 ml, 1.5 nM for spherical or OD = 0.3 for anisotropic; in 0.01 M sodium borate buffer, pH 9) and mixed. To which, aqueous solutions of coupling agents: EDC (1-(3-(dimethylamino)propyl)-3-ethyl-carbodiimidemethiodide, 50 µl, 0.2 M) and s-NHS (N-hydroxysulfosuccinimide, 100 µl, 0.2 M) were introduced. The reaction mixture was stirred for 24 h at room temperature. Conjugates were purified by triple centrifugation/decantation (16'400 rpm, 15 min.) and redispersed in sodium borate buffer (100 µl, 0.01 M, pH 9) prior to physicochemical characterisation (see **chapter 4**) or in growth media (100 µl) prior to experiments with cells (see **chapter 6** and **chapter 7**). NPs were stored at 4 °C.

Further functionalisation of P1-OEG conjugated spherical NPs with HiLyte Fluor 680 amine fluorescent dye (HiLyte, Anna Spec Inc.) was conducted using the same EDC/s-NHS coupling method. Briefly, HiLyte dye solution (100 µl, 1 mg/ml, MW = 1197.5; 0.01 M borate buffer, pH 9) and coupling agents (50 µl, 0.2 M of EDC and 100 µl, 0.2 M of s-NHS) were added to P1-OEG NPs solution (5 ml, 1.5 nM, in 0.01 M borate buffer, pH 9) and stirred for 24 h at room temperature. HiLyte-P1-OEG conjugates were purified by triple centrifugation/decantation (16'400 rpm, 15 min.) and redispersed in phosphate

buffered saline (1 x PBS, 100 µl, 0.1 M, pH 7.2) prior to characterisation (see **chapter 4**) and experiments with cells (see **chapter 6**). NPs were stored at 4 °C in the dark.

3.3. NPs characterisation techniques.

Several complimentary techniques were employed to characterise gold NPs, including: Raman, UV-vis-NIR and fluorescence spectroscopy (**section 3.3.1.**), transmission electron microscopy, dynamic light scattering, ξ-potential (zeta potential) and gel electrophoresis (**section 3.3.3.**) [48,60,70-74]. NPs surface coverage with ligands was quantified (**section 3.3.2.**) and the colloids stability against aggregations was tested (**section 3.3.4.**) [48,75,76].

3.3.1. Spectroscopy techniques.

UV-visible and fluorescence spectra of gold NPs were collected from aqueous colloidal solutions, using a black quartz cuvette (1 cm, Hellma).

UV-visible spectra were measured using a Cary 300 Bio UV-vis spectrophotometer from 400 to 900 nm or Jasco UV/VIS/NIR spectrophotometer from 400 to 1300 nm. Emission spectra of HiLyte tagged NPs were collected using Varian Cary Eclipse Fluorescence Spectrophotometer from 650 to 800 nm with 633 nm excitation wavelength.

The concentration of spherical gold colloid was estimated from the maximum absorbance value, following the Beer-Lambert law and the subsequent equation [44,45,73,74,77]:

$$c = \frac{Abs^{max} \cdot D \cdot 1}{\varepsilon}$$, where

c – concentration of NPs [mol/l]

Abs^{max} – maximum absorbance value

1 – light pathway [cm]

D – sample dilution factor

ε – extinction coefficient [$l \cdot mol^{-1} \cdot cm^{-1}$]; $3.64 \cdot 10^8$ for 15 nm gold NPs

Raman spectra were collected using a Renishaw Raman 2000 equipped with a 633 nm helium-neon (He-Ne) laser with a maximum power of 5 mW and spectral resolution of 4 cm^{-1}. A 50 x objective was used. Spectra were recorded from 400 cm^{-1} to 3400 cm^{-1} wavenumber shift with a maximum 10 s accumulation time. Surface enhanced Raman

spectra (SERS) of gold NPs were collected from air dried aqueous samples deposited on colloidal crystal templated 'inverse opal' nanostructured gold films [78].

3.1.1. NPs surface coverage quantification.

The number of OEGs per one nanoparticle was estimated using Ellman's thiol quantification method (**Scheme 31)** [75]. In this method, Ellman's reagent (5,5'-dithiobis(2-nitrobenzoic acid), DTNB) reacts with a thiol and releases a chromogenic compound (5-thio-2-nitrobenzoic acid, TNB), which absorbs at 412 nm at pH 7.6 ÷ 8.6.

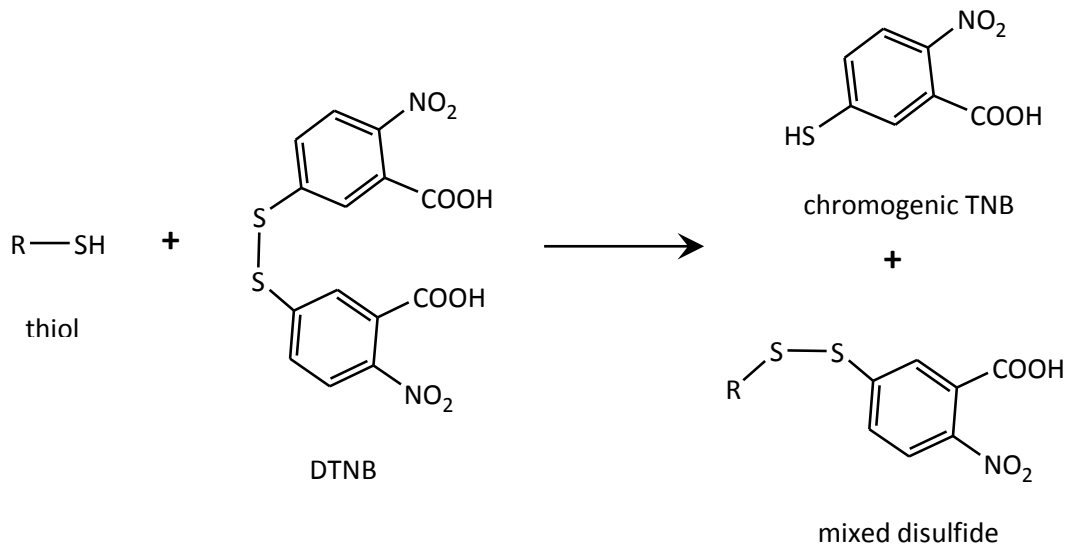

Scheme 31. Schematic illustration of the Ellman's method.

The quantification buffer (0.5 ml, 0.1 M sodium phosphate, pH 8; 1 mM ethylenediaminetetraacetic acid – EDTA) was mixed with Ellman's reagent (10 µl, of solid DTNB dissolved in 1 ml of quantification buffer). To which, the thiol containing solution (50 µl of combined supernatants, left after each step of purification; 0.1 ÷ 1 mM range) was introduced and mixed. The reaction mixture was incubated for 15 min. at room temperature and the maximum absorbance value was measured at 412 nm. Thiol content was calculated from the calibration curve (prepared by measuring a series of dilutions with a given concentration of the quantified thiol, ranging from 0 ÷ 1.5 mM). Since, the pH of a quantified solution affects the intensity of the maximum absorbance [79,80], two separate calibration curves were prepared. One for DA-PEG and the other for OEG ligand, each with the same type of buffer (see **section 3.2.** for NPs surface capping details) as used in the capping procedure. Calibration curves are shown in **Fig. 4**.

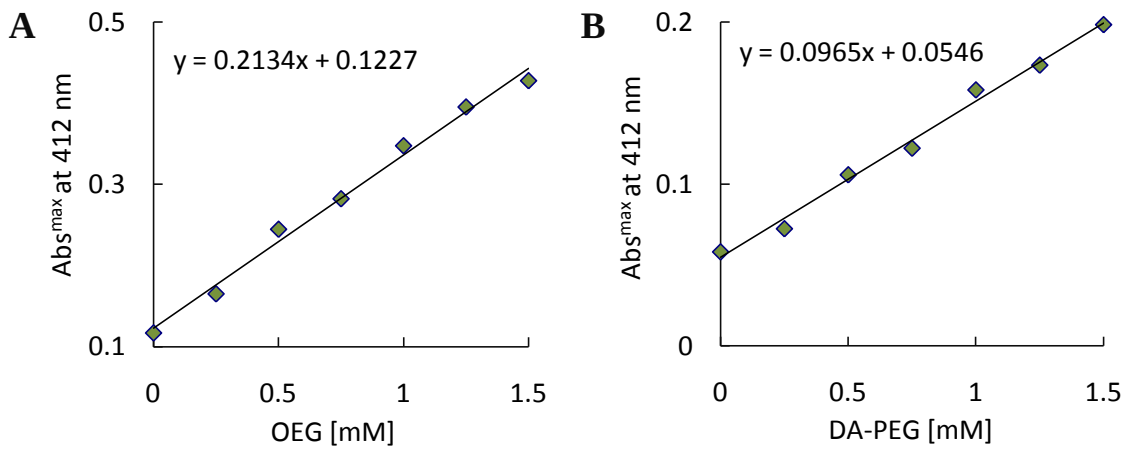

Figure 4. Calibration curves for Ellman's quantification of OEG (A) and DA-PEG (B) ligands.

From the appropriate calibration curve, the concentration of ligand in a quantified sample (supernatant) was estimated. The moles of ligand were calculated from the total volume of the supernatant. The initial amount of ligand introduced into the NPs solution (see **section 3.2.**) was known, thus the quantity of ligand which was chemisorbed onto the NPs surface was deliberated. Taking the molecular weight of ligand, allowed the actual number of ligand molecules chemisorbed on NPs, to be calculated. The concentration of NPs (as well as the number of moles) was calculated using UV-vis spectroscopy (spherical NPs, see **section 3.3.1.**) or mass spectroscopy (anisotropic NPs, ICP-MS, see **section 3.5.3.**). Having estimated the average number of atoms per nanoparticle (see **chapter 4** and **Appendix B**), the total number of NPs in the sample was calculated. The number of chemisorbed ligands was divided by the number of NPs in the sample, to give the number of ligands per each nanoparticle.

The number of peptides per nanoparticle was estimated using FluoroProfile Protein Quantification Kit (Sigma-Aldrich) [76]. In this method, a fluorescent regent called the epicocconone, reacts with a side chain of lysine residues from peptides or proteins (**Scheme 32**), resulting in a shift of the fluorescent signal from 530 nm to 600 nm.

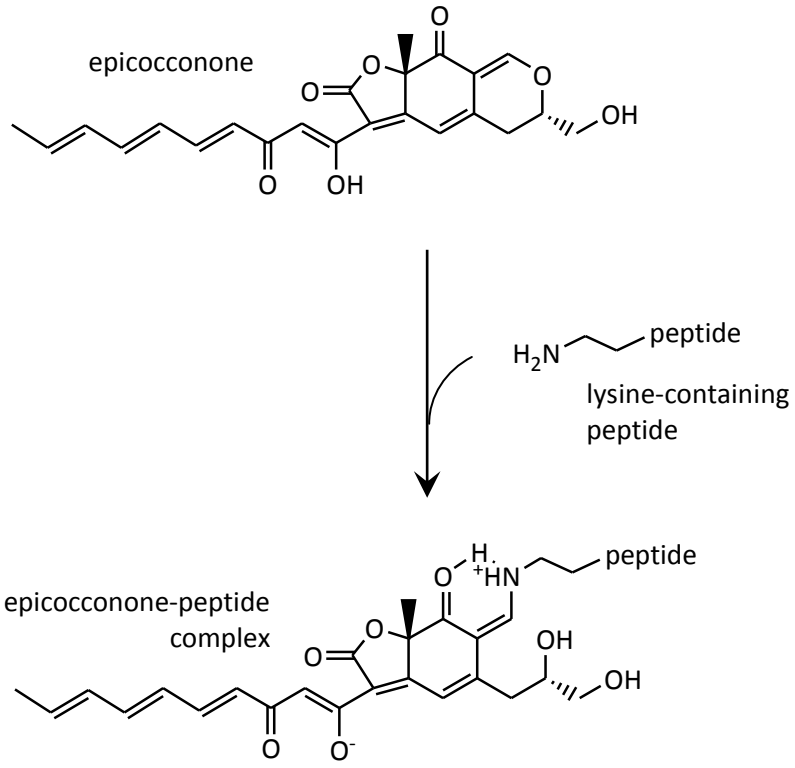

Scheme 32. Schematic illustration of the FluoroProfile method, taken from [76].

As suggested by the manufacturer of FluoroProfile (Sigma-Aldrich), the 'working reagent' was prepared by mixing the fluorescent reagent, quantification buffer and water in the ratio volume: 1:1:8. The 'working reagent' (50 µl) was added to the quantified solution (50 µl, supernatant left after colloids purification, see **section 3.2.**) and shaken. The reaction mixture was incubated for 30 min. at room temperature in the dark. The maximum emission value at 620 nm was measured with 510 nm excitation wavelength and used to calculate the number of peptides from the calibration curve (**Fig. 5**). Since, FluoroProfile reagent reacts selectively with the side chain of lysine residues [76] and each of the octa-peptide sequences contained only one N-terminus lysine, the quantities of all three octa-peptides in solutions were estimated from the same calibration curve, following analogues strategy as in the above thiol quantification method.

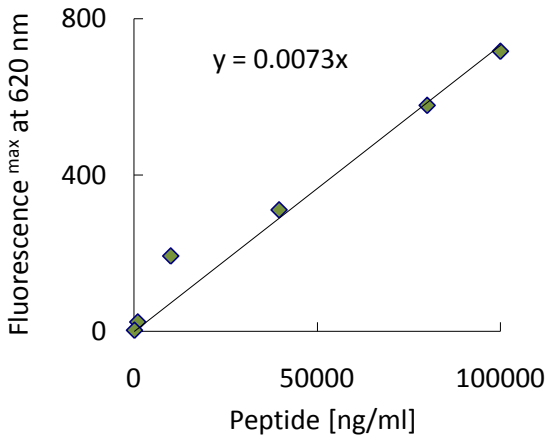

Figure 5. Calibration curves for FluoroProfile quantification of P1, P2 and P3 octa-peptides.

3.1.1. NPs size, shape and net charge measurements.

The shape and size of the metallic core of NPs was determined by transmission electron microscopy (TEM). Images were obtained with Hitachi H7000 transmission electron microscope operating at a bias voltage of 75 kV. All samples were prepared by deposition of a colloid droplet, which was then air dried, onto a Carbon Film 400 Mesh Copper (50) grid. Several images of each sample were taken. Statistical analyses of representative images were drawn onto size distribution histograms.

Hydrodynamic diameters of NPs and their net charge were measured with a Zetasizer Nano ZS (Malvern Instruments Ltd.) using colloids dispersed in Milli-Q water or buffer. Disposable cuvettes (Malvern Instruments Ltd.) were employed in dynamic light scattering (DLS) measurements or disposable capillary cells in ζ-potential measurements. DLS measurements (overall diameter of NPs) in conjunction with histograms representing the size of an inorganic core allowed, the thickness of organic layers: OEG, DA-PEG and octa-peptides (**chapter 4**), to be calculated.

Gel electrophoresis was also employed to determine the differences in charge and size, deriving from the outer shell of NPs [70,71]. A horizontal agarose gel system was used in all experiments. The agarose gel (0.75 %) was prepared by dissolving agarose (0.45 g, Sigma-Aldrich) in Tris-Borate-EDTA buffer (0.5 x TBE, 60 ml, pH 8) by heating up to 90 °C in a microwave and shaking. Liquid agarose was poured into a gel-tray (10 x 7 cm, Bio-Rad) fixed within the gel-caster (Bio-Rad). Next, an 8-teeth comb (Bio-Rad) was placed in the middle slot, the gel was left to cool and solidify for 30 min. at room

temperature. The gel caster was levelled up, ensuring formation of evenly thick (1 cm) matrix with 8 identical wells (well capacity 41.6 µl). The solidified gel was placed in Mini-Sub Cell GT Base (Bio-Rad) along with sufficient TBE buffer (0.5 x) for submersion of the gel, beneath 5 mm of liquid. The colloids (16 µl, 50 nM, in 0.5 x TBE buffer) mixed with glycerol (4 µl, 30 %, in 0.5 x TBE buffer) were gently loaded into the wells. The safety lid was placed onto the base, and electrical cables were plugged into the power supply (Bio-Rad). The gel was run for 1 h, using 10 V (steady current) per 1 cm of gel. Digital images of gels were taken with a Cannon Power Shot A480 digital camera.

3.3.4. Stability tests of colloids.

The stability of spherical colloids was tested at a range of pH and temperatures, as well as in the presence of thiol containing molecules [39,40,48]. The formation of NPs aggregates was monitored by colorimetric assays. These included macroscopic observations of the solution colour change and UV-visible spectroscopy [43,44,48,81].

The stability of NPs against ligand exchange reactions was studied in prolonged incubation with thiol containing molecules, such as: mercaptoethanol, dithiothreitol, cysteamine, cysteine, α-lipoic acid and 11-amino-1-undecanethiol. In a typical experiment, the colloidal solution (100 µl, 1.5 nM) was incubated for 72 h in 10 % mercaptoethanol (1:1, Milli-Q water : methanol), at room temperature, between pH 3 ÷ 9. The stability of colloids (100 µl, 1.5 nM) at variable pH, ranging from 1.2 ÷ 12, was tested over a 48 h incubation time at room temperature.

The stability of colloids at high temperatures was tested in five repeated heating/cooling (100 °C / room temperature) cycles. Low temperature stability was monitored over three freezing (down to -20 °C) / thawing (room temperature) cycles. Extinction spectra of NPs were collected after each cycle.

3.4. Cells isolation and culturing.

Research efforts of this project were focused on the interactions between colloidal gold NPs and human umbilical vein endothelial cells (HUVECs, see **chapter 2** for theoretical background). Primary HUVECs were obtained from umbilical cords. Cells isolation (and culturing) will be described in the following sub-section. Except of HUVECs, malignant cell line (HeLa) was employed in some experiments (flow cytometry, **chapter 6**). These cells show very different physiology compared to HUVECs (see **chapter 2** for theoretical

background), therefore were cultured according to an individual protocol, described in **section 3.4.3.**

3.4.1. HUVECs isolation.

HUVECs were harvested from human umbilical veins by Dr Timothy M. Millar from the School of Medicine, University of Southampton, Southampton, UK. The isolation method involved collagenase digestion, as previously reported [82,83] .

Umbilical cords and placentas were harvested at term following natural delivery at the Princess Anne Hospital, Southampton, UK following local ethically approved procedures (Ethics submission number: 07/H0502/83). Umbilical cords were typically stored at 4 °C until use, within 24 h of delivery. Cords were perfused with Type 1 collagenase solution (1 mg/ml, Worthington) for 10 min. at 37 °C, before endothelial cells were harvested by centrifugation, then seeded onto T-75 cm flasks. Flasks and subsequent culture plastic were pre-coated with porcine gelatin (0.2 % in Hank's Buffered Salt Solution – HBSS, Sigma-Aldrich). Cells were passaged by trypsin digestion and grown to confluence in M199 (Invitrogen) media containing 20 % human serum (Autogen Bioclear) and penicillin / streptomycin (Invitrogen) at 37 °C in a humidified 5 % carbon dioxide (CO_2) balanced air incubator. Endothelial lineage was confirmed by cobblestone appearance in culture, by distinct punctate expression of von Willebrand factor (vWF) and by Cluster of Differentiation molecule number 31 (CD31) expression (data not shown).

3.4.2. HUVECs culturing.

HUVECs were grown on porcine gelatin (0.2 % in HBSS) pre-coated culture dishes, in a media growth (M199) containing 20 % human serum (full-serum). Typically, HUVECs were seeded onto a culture dish, filled with a sufficient volume of growth media (**Table 1**) and incubated in 5 % CO_2 air balanced incubator at 37 °C. Every two to three days, the old medium was decanted, cells were gently washed twice with PBS buffer (1 x) and fresh medium growth was poured into the culture dish. All reagents were pre-warmed to 37 °C before use and kept sterile.

Table 1. HUVECs culturing.

Culture dish	Number of cells	Growth media volume [ml]
Petri dish, 10 cm	$2.0 \cdot 10^6$	10.0
12-well plate	$1.0 \cdot 10^5$	1.0
96-well plate	$2.5 \cdot 10^4$	0.2

HUVECs grown to a confluence on a Petri dish were passaged by trypsinisation. After medium growth was decanted, cells were washed three times with PBS buffer (1 x) and trypsin solution (1.5 ml, 0.25 % trypsin 0.01 % EDTA solution, Sigma-Aldrich) was added. Cells were incubated at 37 °C in 5 % CO_2. The harvesting time was approximately 5 min. To block trypsin and prevent further digestion of cells, serum containing medium growth (5 ml) was added. The cell suspension was transferred into a plastic tube and centrifuged (2'000 rpm, 5 min., 4 °C). Cells were resuspended in medium growth (1 ml) and counted. The desired number of cells was placed in a fresh culture dish along with the sufficient volume of growth media. HUVECs only from second passage were used in all experiments.

3.4.3. HeLa cells culturing.

HeLa cells (see **chapter 2** for theoretical background) were used as a negative control in several experiments (flow cytometry, **chapter 6**). These cells were grown as attached to culture dishes in DNEM media growth (Gibco) supplemented with 10 % fetal bovine serum (FBS, Sigma-Aldrich), and penicillin / streptomycin (Invitrogen) at 37 °C in a humidified CO_2 balanced air incubator. Typically, HeLa were grown to 80 % confluence, then passaged by trypsinisation (see the previous section). The doubling time of HeLa is approximately 24 h [85-89], therefore cells were split few times a week in small portions. In all experiments, cells from the second to tenth passage were used.

3.5. Biological samples characterisation techniques and experimental methods.

Standard techniques commonly used in biomedical and physicochemical sciences were applied to study the interactions of colloidal gold NPs and cells. These included

transmission electron microscopy (**section 3.5.1.**), flow cytometry (**section 3.5.2**), inductively coupled plasma mass spectrometry (**section 3.5.3.**), laser treatment (**section 3.5.4.**), *in vitro* angiogenesis (**section 3.5.5.**) and gene expression profiling (**section 3.5.6.**) assays.

3.5.1. Transmission electron microscopy of biological specimens incubated with NPs.

For electron microscopy purposes, HUVECs were either grown on membrane culture inserts, then fixed with the membrane, or on gelatin pre-coated culture dishes, then harvested and fixed as a pellet [90,91]. All samples were embedded in resin, cut to ultra-thin sections, then stained and imaged with Hitachi H7000 transmission electron microscope operating at a bias voltage of 75 kV.

In detail, HUVECs ($1 \cdot 10^5$) grown on porcine gelatin (0.2 % in HBSS) pre-coated 12-well micro-plate, were incubated with OEG-coated NPs (1000 µl, $5 \cdot 10^{12}$ NP, in a full-serum growth media) for 4 h at 37 °C in a humidified 5 % CO_2 balanced air incubator. After treatment, cells were washed three times with PBS (1 x), then trypsinised (0.75 ml, 0.25 % trypsin 0.01 % EDTA solution, Sigma-Aldrich) for 5 min. at 37 °C in 5 % CO_2. The cell suspension was transferred to a plastic tube (1.5 ml, Eppendorf) and centrifuged (2'500 rpm, 5 min, 4 °C). The solution was decanted and the cell pellet was redispersed in a main fixative: glutaraldehyde / formaldehyde (3 % / 4 %, in 0.1 M piperazine-1,4-bis(2-ethanesulfonic acid – PIPES buffer, pH 7.2), then incubated for 15 min. at room temperature. Cells were centrifuged (2'500 rpm, 5 min, 4 °C) and decanted. To the cell pellet a drop of sodium alginate (5 % in water) was introduced with a mixture of PIPES buffer (0.5 ml, 0.2 M) and calcium chloride solution (0.5 ml, 0.2 M in water). When the alginate settled (15 min.), the supernatant was removed and the embedded cell pellet was transferred into a glass vial and fixed with post fixative: osmium tetroxide (1 %, 0.1 M PIPES buffer) for 1 h. The fixed pellet was washed twice with water (for 5 min.) and stained with uranyl acetate (2 %, in water) for 20 min. The specimen was then washed with 30 %, 50 %, 70 % and 95 % ethanolic solutions for 10 min. each, then absolute ethanol for 20 min. twice. Dehydrated cells were embedded in TAAB resin (Agar Scientific Ltd.) and polymerised at 60 °C for 24 h. Resin blocks were cut using Leica RM 2255 microtome to obtain ultrathin sections (~ 100 nm thickness). Sections were deposited on TEM grids and stained with Reynolds lead stain [92] prior to imaging.

HUVECs in experiments with pep-OEG NPs were processed according to a modified protocol. Firstly, cells ($2.5 \cdot 10^4$) were grown on polyethylene terephthalate (PET) inserts (BD Biosciences) pre-coated with poly-D-lysine (10 μg/ml in 1 x PBS) and incubated with pep-OEG NPs for 4 h at 37 °C in full-serum media growth in a humidified 5 % CO_2 balanced air incubator. The colloidal solution (1000 μl, $1 \cdot 10^{12}$ NPs, in a medium growth) was placed in a well under the PET insert along with additional volume of colloid (300 μl, same solution) placed inside the insert. After treatment, cells were washed three times with PBS (1 x) and fixed before imaging using the main fixative: glutaraldehyde / formaldehyde (3 % / 4 %, in 0.1 M PIPES buffer) and post fixative: osmium tetroxide (1 %, in tetradecafluorohexane – FC-72 solvent). Fixed specimens were washed with absolute ethanol, stained with uranyl acetate (1 %, in ethanol), embedded in Spurr resin (Agar Scientific Ltd.) and polymerised at 60 °C for 24 h. Resin blocks were cut using Leica RM 2255 microtome to obtain ultrathin sections (~ 100 nm thickness). Sections were deposited on TEM grids and stained with Reynolds lead stain [92] prior to imaging.

3.5.2. Flow cytometry.

LL-RPE tagged P1 peptides (P1-LL-RPE) and HiLyte-P1-OEG NPs were employed in flow cytometry assays. HiLyte-P1-OEG NPs were prepared according to a protocol described in **section 3.2.4.**, while P1 peptides were labelled with LL-RPE (Innova Biosciences Ltd.) fluorescent molecules according to a standard protocol supplied by the manufacturer [93].

Typically, live cells ($1 \cdot 10^5$) suspended in a blocker (0.2 ml, 0.1 % sodium azide, 5 % FBS, in 1 x PBS) were incubated with P1-LL-RPE (15 μl, 8.7 μM) or HiLyte-P1-OEG NPs (10 μl, 1 μM, in 1 x PBS) for 1 h on ice. In competition experiments, free P1 or P2 peptide solutions (15 μl, 1 mg/ml, in 1 x PBS, MW = 922.1) were introduced 15 min. before incubation with P1-LL-RPE or HiLyte-P1-OEG NPs. Cells were washed twice with PBS (1 x) and gently redispersed in PBS (0.2 ml, 1 x) prior to measurements.

Scattered and emitted light was recorded with FACS calibur (BD BioSciences) flow cytometer, using 488 nm excitation wavelength and orange channel detector or 633 nm excitation wavelength and infrared channel detector for P1-LL-RPE or HiLyte-P1-OEG NPs, respectively.

All results deriving from the measurements of emitted light were presented simultaneously as one parameter, known as the binding index (BI).

$$BI = \frac{Fl \cdot Mn \cdot 100}{BI^{max}}$$, where

BI – binding index [%]

Fl – measured fluorescence value [a.u]

Mn – measured mean value [a.u.]

100 – factor deriving from referring to BI^{max} [%]

BI^{max} – maximum BI value related to cells incubated with HiLyte-P1-OEG NPs

3.5.3. Inductively coupled plasma mass spectrometry (ICP-MS).

ICP-MS measurements were performed by Dr Simone Nitti from Istituto Italiano Di Tecnologia (IIT), Nanobiotechnology Department, Genova, Italy and by Dr J. Andy Milton from the National Oceanography Centre (NOC), School of Ocean and Earth Science, University of Southampton, Southampton, UK.

Prior to measurements, HUVECs ($1 \cdot 10^5$) were grown on porcine gelatin (0.2 % in HBSS) pre-coated 12-well micro-plate and incubated with OEG-coated NPs (1000 µl, $5 \cdot 10^{12}$ NP, in a full-serum media growth) for 4 h at 37 °C in a humidified 5 % CO_2 balanced air incubator. After treatment, cells were washed three times with PBS (1 x) and trypsin solution (0.75 ml, 0.25 % trypsin 0.01 % EDTA solution, Sigma-Aldrich) was added. HUVECs were incubated for 5 min. at 37 °C in 5 % CO_2, then PBS (5 ml, 1 x) was added and the cell suspension was transferred into a plastic tube (15 ml) and centrifuged (2'500 rpm, 5 min., 4 °C). The cell pellet was redispersed in PBS (1 ml, 1 x), counted and transferred into a glass vial. Sealed vials were transported to IIT or NOC, where Dr Nitti or Dr Milton performed digestion of cells (and NPs) with aqua regia (9 ml) and ICP-MS measurements of a series of dilution using gold standards.

The amount of gold atoms in each sample was measured in ppm, while the number of cells was counted. This was referred to the total amount of introduced NPs and the background level of gold in cells, both measured by ICP-MS. The number of gold atoms per nanoparticle was 'roughly' estimated from the average size of NPs (measured by TEM, see **Appendix B**), the distances between atoms in the fcc crystal structure and the volume of a gold atom. The average number of NPs per cell was then calculated. At least three independent experiments were performed to estimate these average numbers.

3.5.4. Photo-thermal treatment (laser-hyperthermia).

The experimental set-up (**Scheme 33**) consisted of two major components: Supercontinuum SC450 Laser light source (Fianium) and IX81 Motorized Inverted Microscope (Olympus), equipped with an environmental chamber, temperature controller, CO_2 controller, as well as bright field and phase contrast imaging system. The set-up was assembled in the Biomedical Imaging Unit, General Hospital, Southampton, UK by Dr Otto L. Muskens from the School of Physics and Astronomy, University of Southampton, UK.

In a typical experiment, HUVECs ($2.5 \cdot 10^4$) were seeded on porcine gelatin pre-coated 96-well microplate and incubated for 24 h at 37 °C in full-serum growth media in a humidified 5 % CO_2 balanced air incubator. Cells were treated for 4 h with OEG-coated or P1-OEG anisotropic NPs (100 μl, $1 \cdot 10^{13}$, in a medium growth). After treatment, cells were washed twice with PBS (1 x) and kept in PBS (1 x) prior to the laser illumination.

Cells were first imaged (phase contrast filter, 4 x objective) and then illuminated with near-infrared (NIR) laser light for 10 min. using variable laser power density (5 ÷ 32 W/cm^2) and 200 μm laser spot size. Bandpass filters were employed to cut off any wavelength shorter than 680 and longer than 720 nm, to create a narrow (40 nm) band gap falling within NIR region (suitable for photo-thermal treatment of biological tissue [94-98]; see **chapter 2** for theoretical background). SC450 Laser is a powerful pulsed laser, sending 4 ps pulses. The repetition rate is 40 MHz.

After laser illumination, buffer was removed from the wells and the cells were incubated for 1 h or 24 h in fresh medium growth, prior to viability studies. Cells washed once with PBS (1 x) were stained with trypan blue [99] (10 min., 0.1 % in 1 x PBS at 37 °C in a humidified 5 % CO_2 balanced air incubator). Stained cells were washed twice with PBS (1 x) prior to phase contrast and bright field imaging with 4 x objective. The same spot was imaged before and after treatment. Stained (damaged) and unstained (intact) cells were counted. Cell viability was presented as a percent of stained cells to the total number of cells and plotted on a graph against the increasing laser power density (see **chapter 7**).

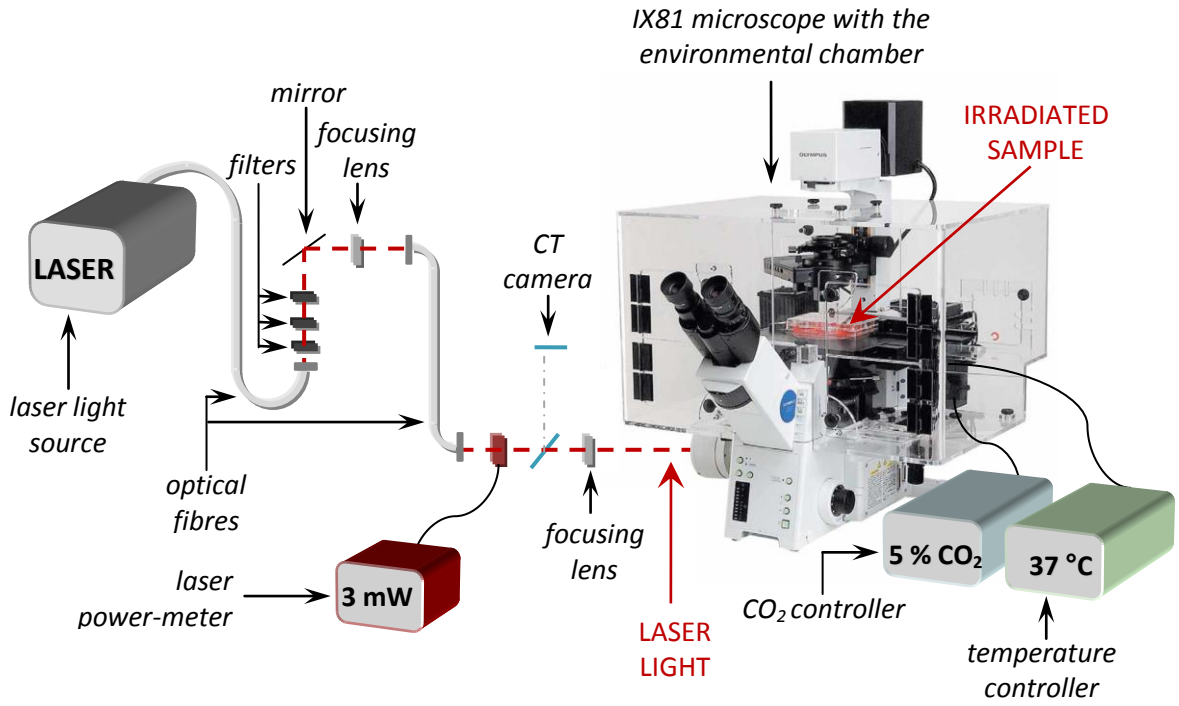

Scheme 33. Schematic illustration of the laser set-up.

3.5.5. Gene expression profiling.

Gene expression profiling assays (see **chapter 6** and **7** for results) involved four major steps: a) treatment of cells with NPs; b) mRNA isolation (the product of activated genes); c) reverse transcriptase polymerase chain reaction (RT-PCR, synthesis of c-DNA on the mRNA templates) and d) quantitative polymerase chain reaction (Q-PCR) using specific primers (oligodeoxynucleotides complimentary to the sequence encoding selected gene) equipped with a fluorescent TaqMan probe [100]. Since, RT-PCR, Q-PCR and TaqMan primers are well-established and commonly used in genes products quantification, associated reaction mechanisms will not be discussed in this thesis.

For treatment with pep-OEG spherical NPs, HUVECs ($1 \cdot 10^5$) were seeded on porcine gelatin pre-coated 12-well micro-plates and incubated for 24 h at 37 °C in serum-depleted growth media (0.2 % of human serum, 100 times less than full-serum growth media) or additionally hypoxia mimicked (100 μM, cobalt II chloride – $CoCl_2$ [101]) conditions in a humidified 5 % CO_2 balanced air incubator. Cells were treated for 6 h with VEGF-B_{167} (150 ng, 10 μl, in 1 x PBS; PeproTech, Inc.), free P1 and P2 (7.3 ng, 10 μl, in 1 x PBS, MW = 922.1), free P3 (7.7 ng, 10 μl, in 1 x PBS, MW = 968.2) or pep-OEG conjugated to spherical NPs (1.5 nM, 10 μl in 1x PBS), prior to mRNA isolation.

Cells, washed twice with PBS (1 x) were lysed directly in a culture dish by adding TRIzol reagent (0.5 ml, Sigma-Aldrich). Homogenised samples were incubated with chloroform (0.1 ml) at room temperature for 5 min. and centrifuged (13'300 rpm, 30 min., 4 °C). The aqueous phase was transferred to a fresh tube and mixed with isopropanol (0.25 ml) and glycogen (5 µl, 20 mg/ml). Samples were incubated for 10 min. at room temperature, 10 min. at -80 °C, then centrifuged (13'300 rpm, 30 min., 4 °C). RNA pellets were washed once with chilled ethanol (75 %), incubated on ice for 10 min. and centrifuged (13'300 rpm, 15 min., 4 °C). Washed pellets were air-dried and dissolved in nuclease-free water (100 µl).

RNA solution (10 µl, 10 ng) was mixed with 10 x RT buffer (2 µl), random primers (2 µl), RNAsin (1 µl), dNTPs (0.8 µl), nuclease-free water (3.2 µl) and reverse transcriptase (1 µl, Applied Biosystems). Samples were incubated for 10 min. at 25 °C, 30 min. at 45 °C and then for 5 min. at 95 °C. RT-PCR was then followed by Q-PCR. In detail, 10 times diluted c-DNA (2.5 µl, in nuclease-free water) was mixed with nuclease-free water (2 µl), 2 x PCR mix (5 µl) and TaqMan primer (0.5 µl, Applied Biosystems) in 384-well microplate. DNA was amplified (35 cycles) and quantified using Thermo-cycler equipped with the TaqMan probe.

For the treatment with P1-OEG or OEG anisotropic NPs followed by laser-hyperthermia, HUVECs ($2.5 \cdot 10^4$) were seeded on porcine gelatin pre-coated 96-well microplate and incubated for 24 h in media growth at 37 °C in a humidified 5 % CO_2 balanced air incubator. Next, the old medium was removed and OEG-coated or P1-OEG conjugated anisotropic NPs were introduced (100 µl, $1 \cdot 10^{13}$ in a medium growth). Cells were incubated for 4 h, then washed twice with PBS (1 x) and kept in PBS (1 x) prior to laser irradiation.

Four spots per sample were exposed to laser light to maximise the surface area of treatment, thus the number of irradiated cells. After the irradiation, buffer was removed and cells were stimulated with TNF-α (100 ng/ml) for 5 h [102,103] in fresh growth media prior to mRNA isolation, RT-PCR and Q-PCR (detailed above).

3.5.6. *In vitro* angiogenesis.

The formation of capillary-like structures by HUVECs on basement membrane matrix gel (Geltrex, Gibco; according to a protocol supplied by the manufacturer [104]) was studied after treatment with pep-OEG NPs.

The matrix gel was thawed overnight on ice, then mixed gently by pipette (avoiding air bubbles). The homogenous gel (50 µl) was placed in a well (48-wells micro-plate) and polymerised at 37 °C in a humidified 5 % CO_2 air balanced incubator for 30 min. HUVECs ($4 \cdot 10^4$) suspended in growth media (200 µl, serum-depleted) mixed with VEGF-B_{167} (150 ng/well), octa-peptides (7.3 ng/well of P1 or P2, MW = 922.1; 7.7 ng/well of P3, MW = 968.2) or pep-OEG conjugated spherical gold NPs (15 fmol/well) were seeded per well and incubated at 37 °C in a humidified 5 % CO_2 air balanced incubator for 2 ÷ 20 h. Phase contrast images of capillary-like structures were taken with IX81 Olympus microscope using 4 x objective.

Statistical analysis of the capillaries formed were performed by measuring the overall length of capillaries per image (the field of view was 0.216 mm^2) using ImageJ software (see **chapter 6**). The number of branching points per each image was counted manually. At least three view points per well were analysed. Variations in tubules morphologies were reflected by error bars on associated graphs (see **chapter 6**). Assuming that untreated cells (control) represent the background level of regulation (minimal capillaries length), while VEGF-B_{167} stimulated cells show the maximum level of regulation (maximum capillaries length; hence equal to 100 %), the regulation index (RI) was calculated from the subsequent equation:

$$RI = \frac{(CL - CL^{cont}) \cdot 100}{(CL^{max} - CL^{cont})}$$, where

RI – regulation index [%]

CL – capillaries length

CL^{cont} – background subtraction (capillaries length quantified in untreated cells; control)

100 – factor deriving from referring to CL^{max} [%]

CL^{max} – maximum CL value quantified in cells treated with VEGF-B_{167}

Analogously, if untreated cells formed the background number of branching points (minimal), while VEGF-B_{167} stimulated cells the maximum, the branching index (BrI) was calculated following the subsequent equation:

$$BrI = \frac{(BPs - BPs^{cont}) \cdot 100}{(BPs^{max} - BPs^{cont})}$$, where

BrI – branching index [%]

BPs – branching points

BPs^{cont} – background subtraction (number of BPs in untreated cells; control)

100 – factor deriving from referring to BPs^{max} [%]

BPs^{max} – maximum BPs number obtain in cells treated with VEGF-B_{167}

References:

[1] Faraday, M. *Philos Trans R Soc London* **1857**, *147*, 145-181.
[2] Frens, G. *Nature-Phys Sci* **1973**, *241*, 20-22.
[3] Turkevich, J.; Stevenson, P. C.; Hillier, J. *J Phys Chem* **1953**, *57*, 670-673.
[4] Kumar, S.; Gandhi, K. S.; Kumar, R. *Ind Eng Chem Res* **2006**, *46*, 3128-3136.
[5] Ji, X.; Song, X.; Li, J.; Bai, Y.; Yang, W.; Peng, X. *J Am Chem Soc* **2007**, *129*, 13939-13948.
[6] Turkevich, J.; Stevenson, P. C.; Hillier, J. *Disc Faraday Soc* **1951**, *11*, 55-75.
[7] Murphy, C. J.; Sau, T. K.; Gole, A. M.; Orendorff, C. J.; Gao, J.; Gou, L.; Hunyadi, S. E.; Li, T. *J Phys Chem B* **2005**, *109*, 13857-13870.
[8] Huang, X.; Neretina, S.; El-Sayed, M. A. *Adv Mater* **2009**, *21*, 4880-4910.
[9] Pérez-Juste, J.; Pastoriza-Santos, I.; Liz-Marzán, L. M.; Mulvaney, P. *Coord Chem Rev* **2005**, *249*, 1870-1901.
[10] Smith, D. K.; Korgel, B. A. *Langmuir* **2008**, *24*, 644-649.
[11] Busbee, B.; Obare, S.; Murphy, C. *Adv Mater* **2003**, *15*, 414-416.
[12] Rayavarapu, R. G.; Ungureanu, C.; Krystek, P.; van Leeuwen, T. G.; Manohar, S. *Langmuir* **2010**, *26*, 5050-5055.
[13] Smith, D. K.; Miller, N. R.; Korgel, B. A. *Langmuir* **2009**, *25*, 9518-9524.
[14] Nikoobakht, B.; El-Sayed, M. A. *Chem Mater* **2003**, *15*, 1957-1962.
[15] Orendorff, C. J.; Murphy, C. J. *J Phys Chem B* **2006**, *110*, 3990-3994.
[16] Sau, T. K.; Murphy, C. J. *Philos Mag* **2007**, *87*, 2143-2158.
[17] Gole, A.; Murphy, C. J. *Chem Mater* **2004**, *16*, 3633-3640.
[18] Jana, N. R.; Gearheart, L.; Murphy, C. J. *J Phys Chem B* **2001**, *105*, 4065-4067.
[19] Stöber, W.; Fink, A.; Bohn, E. *J Colloid Interface Sci* **1968**, *26*, 62-69.
[20] Wu, Y.; Chen, C.; Liu, S. *Anal Chem* **2009**, *81*, 1600-1607.
[21] Westcott, S. L.; Oldenburg, S. J.; Lee, T. R.; Halas, N. J. *Langmuir* **1998**, *14*, 5396-5401.
[22] Van Blaaderen, A.; Van Geest, J.; Vrij, A. *J Colloid Interface Sci* **1992**, *154*, 481-501.
[23] Oldenburg, S. J.; Averitt, R. D.; Westcott, S. L.; Halas, N. J. *Chem Phys Lett* **1998**, *288*, 243-247.
[24] Duff, D. G.; Baiker, A.; Edwards, P. P. *Langmuir* **1993**, *9*, 2301-2309.
[25] Duff, D. G.; Baiker, A.; Gameson, I.; Edwards, P. P. *Langmuir* **1993**, *9*, 2310-2317.
[26] Halas, N. *MRS Bulletin* **2005**, *30*, 362-368.
[27] Phonthammachai, N.; Kah, J. C. Y.; Jun, G.; Sheppard, C. J. R.; Olivo, M. C.; Mhaisalkar, S. G.; White, T. J. *Langmuir* **2008**, *24*, 5109-5112.
[28] Arkhireeva, A.; Hay, J. N. *J Mater Chem* **2003**, *13*, 3122-3127.
[29] Yong, K.-T.; Sahoo, Y.; Swihart, M. T.; Prasad, P. N. *Colloids Surf, A* **2006**, *290*, 89-105.
[30] Au, L.; Lu, X.; Xia, Y. *Adv Mater* **2008**, *20*, 2517-2522.
[31] Skrabalak, S. E.; Au, L.; Li, X.; Xia, Y. *Nat Protocols* **2007**, *2*, 2182-2190.
[32] Wang, H.; Qiao, X.; Chen, J.; Wang, X.; Ding, S. *Mater Chem Phys* **2005**, *94*, 449-453.
[33] Lu, X.; Tuan, H.-Y.; Chen, J.; Li, Z.-Y.; Korgel, B. A.; Xia, Y. *J Am Chem Soc* **2007**, *129*, 1733-1742.
[34] Sun, Y.; Xia, Y. *J Am Chem Soc* **2004**, *126*, 3892-3901.
[35] Lee, G.-J.; Shin, S.-I.; Kim, Y.-C.; Oh, S.-G. *Mater Chem Phys* **2004**, *84*, 197-204.
[36] Siekkinen, A. R.; McLellan, J. M.; Chen, J.; Xia, Y. *Chem Phys Lett* **2006**, *432*, 491-496.
[37] Sun, Y.; Xia, Y. *Science* **2002**, *298*, 2176-2179.
[38] Cobley, C.; Skrabalak, S.; Campbell, D.; Xia, Y. *Plasmonics* **2009**, *4*, 171-179.
[39] Pengo, P.; Pasquato, L. In *The supramolecular chemistry of organic - inorganic hybrid materials*; Rurak, K., Martinez-Manez, R., Eds.; John Wiley & Sons, Inc. : Hoboken, New Jersey, **2010**, p 113-154.

[40] Cortie, M. B.; McDonagh, A. In *Gold Chemistry: Applications and future directions in life sciences*; Mohr, F., Ed.; WILLEY-VCH Verlag GmbH & Co. KGaA Weinheim, **2009**, p 321-343.
[41] Loweth, C. J.; Caldwell, W. B.; Peng, X.; Alivisatos, A. P.; Schultz, P. G. *Angew Chem, Int Ed* **1999**, *38*, 1808-1812.
[42] Yang, J.; Lee, J. Y.; Too, H.-P. *Anal Chim Acta* **2005**, *546*, 133-138.
[43] Burns, C.; Spendel, W. U.; Puckett, S.; Pacey, G. E. *Talanta* **2006**, *69*, 873-876.
[44] Mie, G. *Ann Phys* **1908**, *330*, 377-445.
[45] Kreibig, U.; Vollmer, M. *Optical Properties of Metal Clusters*; Springer: Berlin, **1995**; Vol. 25.
[46] Link, S.; El-Sayed, M. A. *J Phys Chem B* **1999**, *103*, 8410-8426.
[47] Halas, N. *Opt Photon News* **2002**, *13*, 26-30.
[48] Bartczak, D.; Kanaras, A. G. *Langmuir* **2010**, *26*, 7072-7077.
[49] Brust, M.; Fink, J.; Bethell, D.; Schiffrin, D. J.; Kiely, C. *J Chem Soc, Chem Commun* **1995**, 1655-1656.
[50] Kanaras, A. G.; Kamounah, F. S.; Schaumburg, K.; Kiely, C. J.; Brust, M. *Chem Commun* **2002**, 20, 2294-2295.
[51] Prasad, B. L. V.; Stoeva, S. I.; Sorensen, C. M.; Klabunde, K. J. *Chem Mater* **2003**, *15*, 935-942.
[52] Chen, J.; McLellan, J. M.; Siekkinen, A.; Xiong, Y.; Li, Z.-Y.; Xia, Y. *J Am Chem Soc* **2006**, *128*, 14776-14777.
[53] Skrabalak, S. E.; Chen, J.; Sun, Y.; Lu, X.; Au, L.; Cobley, C. M.; Xia, Y. *Acc Chem Res* **2008**, *41*, 1587-1595.
[54] Xia, Y.; Xiong, Y.; Lim, B.; Skrabalak, S. *Angew Chem, Int Ed* **2009**, *48*, 60-103.
[55] Pillai, Z. S.; Kamat, P. V. *J Phys Chem B* **2003**, *108*, 945-951.
[56] Chen, J.; Wiley, B.; Li, Z. Y.; Campbell, D.; Saeki, F.; Cang, H.; Au, L.; Lee, J.; Li, X.; Xia, Y. *Adv Mater* **2005**, *17*, 2255-2261.
[57] Hu, M.; Chen, J.; Li, Z.-Y.; Au, L.; Hartland, G. V.; Li, X.; Marquez, M.; Xia, Y. *Chem Soc Rev* **2006**, *35*, 1084-1094.
[58] Wang, Z.; Levy, R.; Fernig, D. G.; Brust, M. *Bioconjug Chem* **2005**, *16*, 497-500.
[59] Lévy, R. *ChemBioChem* **2006**, *7*, 1141-1145.
[60] Coomber, D.; Bartczak, D.; Gerrard, S. R.; Tyas, S.; Kanaras, A. G.; Stulz, E. *Langmuir* **2010**, *26*, 13760-13762.
[61] Levy, R.; Thanh, N. T. K.; Doty, R. C.; Hussain, I.; Nichols, R. J.; Schiffrin, D. J.; Brust, M.; Fernig, D. G. *J Am Chem Soc* **2004**, *126*, 10076-10084.
[62] You, C.-C.; Chompoosor, A.; Rotello, V. M. *Nano Today* **2007**, *2*, 34-43.
[63] Love, J. C.; Estroff, L. A.; Kriebel, J. K.; Nuzzo, R. G.; Whitesides, G. M. *Chem Rev* **2005**, *105*, 1103-1170.
[64] Hermanson, G. T. *Bioconjugate Techniques*; 2nd ed.; Elsevier Inc. , **2008**.
[65] Eck, W.; Craig, G.; Sigdel, A.; Ritter, G.; Old, L. J.; Tang, L.; Brennan, M. F.; Allen, P. J.; Mason, M. D. *ACS Nano* **2008**, *2*, 2263-2272.
[66] Chan, W. C. W.; Nie, S. *Science* **1998**, *281*, 2016-2018.
[67] Alam, M. R.; Maeda, M.; Sasaki, S. *Nucleic Acids Symp Ser (Oxf)* **1999**, *42*, 173-174.
[68] Alam, M. R.; Maeda, M.; Sasaki, S. *Bioorg Med Chem* **2000**, *8*, 465-473.
[69] Hill, H. D.; Millstone, J. E.; Banholzer, M. J.; Mirkin, C. A. *ACS Nano* **2009**, *3*, 418-424.
[70] Sperling, R.; Pellegrino, T.; Li, J.; Chang, W.; Parak, W. *Adv Funct Mater* **2006**, *16*, 943-948.
[71] Hanauer, M.; Pierrat, S.; Zins, I.; Lotz, A.; Sonnichsen, C. *Nano Lett* **2007**, *7*, 2881-2885.
[72] Day, H. A.; Bartczak, D.; Fairbairn, N.; McGuire, E.; Ardakani, M.; Porter, A. E.; Kanaras, A. G. *CrystEngComm* **2010**, *12*, 4312-4316.

[73] Jain, P. K.; Lee, K. S.; El-Sayed, I. H.; El-Sayed, M. A. *J Phys Chem B* **2006**, *110*, 7238-7248.
[74] Haiss, W.; Thanh, N. T. K.; Aveyard, J.; Fernig, D. G. *Anal Chem* **2007**, *79*, 4215-4221.
[75] Ellman, G. L. *Arch Biochem Biophys* **1959**, *82*, 70-77.
[76] Sigma-Aldrich. FluoroProfile Protein Quantification Kit TECHNICAL BULLETIN http://www.sigmaaldrich.com/etc/medialib/docs/Sigma/Bulletin/fp0010bul.Par.0001.File.tmp/fp0010bul.pdf (last accessed 13-09-2010).
[77] Liu, X.; Atwater, M.; Wang, J.; Huo, Q. *Colloid Surface B* **2007**, *58*, 3-7.
[78] Abdelsalam, M. E.; Bartlett, P. N.; Baumberg, J. J.; Cintra, S.; Kelf, T. A.; Russell, A. E. *Electrochem Commun* **2005**, *7*, 740-744.
[79] Riddles, P. W.; Blakeley, R. L.; Zerner, B. *Anal Biochem* **1979**, *94*, 75-81.
[80] Riddles, P. W.; Blakeley, R. L.; Zerner, B.; C.H.W. Hirs, S. N. T. In *Methods in Enzymology*; Academic Press: **1983**; Vol. 91, p 49-60.
[81] Kelly, K. L.; Coronado, E.; Zhao, L. L.; Schatz, G. C. *J Phys Chem B* **2002**, *107*, 668-677.
[82] Cassie, S.; Masterson, M. F.; Polukoshko, A.; Viskovic, M. M.; Tibbles, L. A. *Free Radic Biol Med* **2004**, *36*, 1102-1111.
[83] Jaffe, E. A.; Nachman, R. L.; Becker, C. G.; Minick, C. R. *J Clin Invest* **1973**, *52*, 2745-2756.
[84] Semmler-Behnke, M.; Kreyling, W. G.; Lipka, J.; Fertsch, S.; Wenk, A.; Takenaka, S.; Schmid, G.; Brandau, W. *Small* **2008**, *4*, 2108-2111.
[85] Lewis, W. H. *Harvey Lect* **1936**, *31*, 214-234.
[86] Masters, J. R. W. *Nature Rev Mol Cell Biol* **2000**, *1*, 233-236.
[87] Nelson-Rees, W. A.; Flandermeyer, R. R. *Science* **1976**, *191*, 96-98.
[88] Masters, J. R. *Nat Rev Cancer* **2002**, *2*, 315-319.
[89] Jones, H. W.; McKusick, V. A.; Harper, P. S.; Wuu, K. D. *Obstet Gynecol* **1971**, *38*, 945-949.
[90] Page, A. M. PhD Dissertation, University of London, 1999.
[91] Page, A. M.; Lagnado, J. R.; Ford, T. W.; Place, G. *J Microsc* **1994**, *175*, 166-170.
[92] Reynolds, E. S. *J Cell Biol* **1963**, *17*, 208-212
[93] InnovaBiosciences. Lightning-Link™ R-Phycoerythrin Conjugation Kit, Technical bulletin 7058. **2008**, http://www.innovabiosciences.com/technicalresources/protocols/LL_rpe_release_004.pdf Cambridge, (last accessed 14-09-2010).
[94] Huang, X.; Jain, P.; El-Sayed, I.; El-Sayed, M. *Lasers Med Sci* **2008**, *23*, 217-228.
[95] Hale, G. M.; Querry, M. R. *Appl Opt* **1973**, *12*, 555-563.
[96] Prahl, S. Optical Absorption of Hemoglobin. **1999**, http://omlc.ogi.edu/spectra/hemoglobin/ Oregon Medical Laser Center Oregon (last accessed: 04-09-2010).
[97] Govorov, A. O.; Richardson, H. H. *Nano Today* **2007**, *2*, 30-38.
[98] Kim, J. G.; Mengna, X.; Hanli, L. *IEEE Eng Med Biol* **2005**, *24*, 118-121.
[99] Strober, W. *Trypan Blue Exclusion Test of Cell Viability*; John Wiley & Sons, Inc., **2001**.
[100] Rapley, R.; Harborn, S. *Molecular Analysis and Genome Discovery*; John Wiley & Sons Ltd.: Chichester, **2004**.
[101] Grasselli, F.; Basini, G.; Bussolati, S.; Bianco, F. *Reprod Fertil Dev* **2005**, *17*, 715-720.
[102] Brand, K.; Lubbe, A. S.; Justus, D. J. *Int J Hyperthermia* **1996**, *12*, 527-538.
[103] Srinivasan, J. M.; Fajardo, L. F.; Hahn, G. M. *J Natl Cancer Inst* **1990**, *82*, 1904-1910.
[104] GIBCOinvitrogen. Geltrex™ Reduced Growth Factor Basement Membrane Matrix. **2007**, http://tools.invitrogen.com/downloads/5012_pdf_final.pdf (last accessed 14-09-2010).

4. Synthesis, surface capping and assembly of NPs.

Over the course of the presented research a variety of water soluble nanomaterials were synthesised. Water solubility along with stability against aggregations in buffered media is required for every appliance of nanocomposites in biomedicine [1-19].

Nanocomposites were prepared according to well-established protocols, described in **chapter 3**. The size and shape of NPs and effectively the physicochemical properties of nanomaterials [20-24] (see **chapter 2** for theoretical background) were manipulated chemically. Spherical, rod-like, hollow gold NPs, as well as silica/gold core/shell hetero-nanostructures (composed of more than one element) were prepared [25-33] (**section 4.1.**). The surface of NPs was coated with various organic molecules [2,4,6,34-36] (**section 4.2.**). Previously reported capping ligands (e.g. CALNN peptide [4], **section 4.2.1.**) and newly developed diacetylene based molecule [6] (**section 4.2.3.**) were utilised during this project. The resulted mono-layer of ligands was further modified with bioactive peptides [37] (**section 4.2.2.**). Surface capping led to stable and water soluble colloids [6] (see **section 4.2.4.**).

4.1. Synthesis of NPs.

The citrate reduction method, developed by Turkievich [26,30,31,38-40] was utilised in the synthesis of spherical gold NPs (**section 4.1.1.**). Gold nanorods (**section 4.1.2.**) were prepared either by a method introduced by El-Sayed's group [28] (method I) or a protocol reported by Murphy [25] (method II). Following a synthetic route introduced by Halas and co-workers led to silica/gold core/shell hetero-structures [29] (**section 4.1.3.**). Gold NPs with hollow interiors were produced according to a method developed by Xia [32,33] (**section 4.1.4.**). One more type of anisotropic gold NPs with multiple arms (branched shape) was obtained with a new method, established during a master project of Mr Hugo Day (the University of Southampton, School of Physics and Astronomy, Southampton, UK). The author of this thesis actively participated in this development, which led to a publication [41] (see **Author's Declaration** for the full list of articles published from this project). These results however, will not be further discussed in the thesis, because branched NPs were not employed in any surface capping experiments nor in the biological part of the research (**chapters 5 ÷ 7**).

4.1.1. Synthesis of spherical gold NPs.

Gold NPs, spherical in shape and relatively mono-dispersed in size, were obtained using the citrate reduction method [26,30,31,38-40] (see **chapter 2** for reaction mechanism and **chapter 3** for protocol). Representative TEM image is shown in **Fig. 6A**. At least five TEM images of a colloid were analysed. Diameters of NPs on each image were measured to determine major size groups. The overall number of NPs in each size group was counted and referred to the overall number of NPs on the micrograph (to give the population as percentage). Obtained populations plotted against size groups (**Fig. 6B**) gave the NPs size distribution in the sample. Estimated average diameter of the colloid was 15 ± 2 nm.

The optical signature of the colloid was determined using UV-vis spectroscopy (**Fig. 6C**). The extinction peak reached maximum at around 520 nm (characteristic feature of 15 nm spherical gold NPs [21-24,42,43]). The single and sharp peak suggested a mono-dispersed colloid [21,23,24].

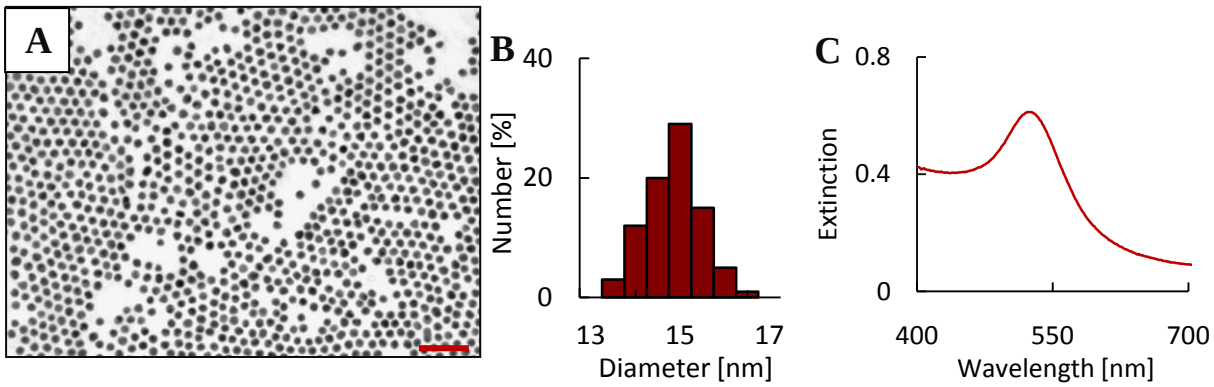

Figure 6. TEM image (A), size distribution histogram (B) and UV-vis spectra of citrate stabilised colloidal gold NPs prepared with 1 : 3.9, Au^{3+} to Ct^{3-} ratio. Scale bar is 100 nm.

It is possible to vary the size of NPs with the citrate reduction method, simply by adjusting the molar ratio between the gold precursor (Au^{3+}) and the citrate reductant (Ct^{3-}) in the reaction mixture [38,39]. When the ratio between Au^{3+} and Ct^{3-} was 1 : 3.9 (see **chapter 3** for experimental details), NPs shown in **Fig. 6** were produced. Larger NPs were prepared with a reduced amount of Ct^{3-}. As an example, TEM images of gold NPs synthesised using 1 : 1.95 and 1 : 0.39 of Au^{3+} to Ct^{3-} ratios are shown in **Fig. 7A** and **B**, respectively.

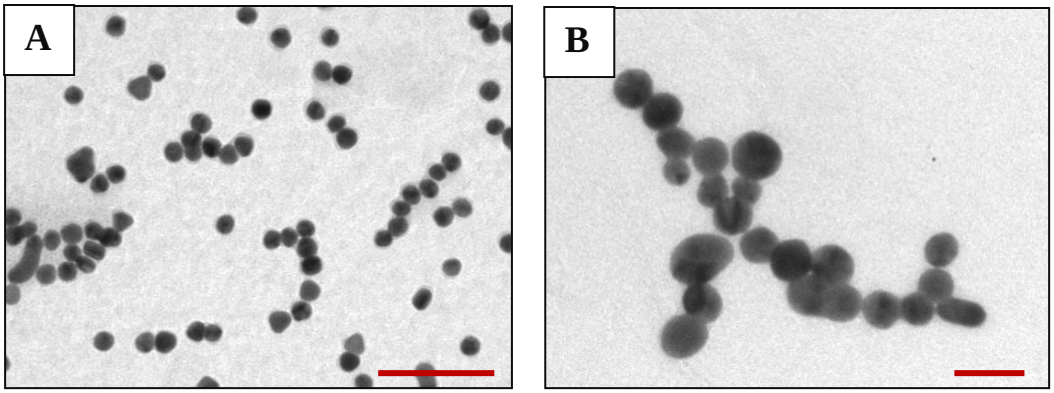

Figure 7. TEM images of citrate stabilised colloidal gold NPs prepared with Au^{3+} to Ct^{3-} ratio of: 1 : 1.95 (A) and 1 : 0.39 (B). Scale bars are 100 nm.

It can be concluded from the images above that, a decrease in the quantity of Ct^{3-} introduced into the reaction mixture, generally leads to the formation of larger particles. One possible explanation is that, decreasing the quantity of citrate reduces the number of nucleation sites [38,39]. The less the gold precursor is involved in the nuclei, the more Au^{3+} is available for growth stage. Larger amount of unconsumed precursor (which remains in solution), can now be employed in further development of NPs, leading to larger structures. Increase in the size of NPs boosts the ratio between the NPs diameter and the ligand length. This, in conjunction with the reduction of the overall number of capping molecules (citrate), can lead to insufficient stabilisation of the NPs surface. Destabilised NPs would clump together and ripen [35,36,38,44,45], which can effectively result in the formation of even larger structures.

In general, the size distribution of NPs produced, increases with decreasing molar ratio between the gold precursor and Ct^{3-}. A decrease in the amount of Ct^{3-} by a factor two, leads to the formation of colloids with a broader plasmon band (**Fig. 8**, **violet line**); possibly attributed to the poly-dispersed (non-uniform) sizes of NPs [21,23,24], as seen on the TEM image (**Fig. 7**). Slight red-shifting of the extinction peak of NPs is most likely derived from their larger size, as in agreement with Mie's theory [24] (see **chapter 2)**.

Further reduction of the amount of Ct^{3-} (factor 10) resulted in a significant decrease in the intensity of the maximum extinction peak (**Fig. 8**, **blue line**). This, along with a significant broadening (possibly light scattering effect [22,46], see **chapter 2** for related theoretical background) and red-shift (to around 540 nm), suggests the formation of larger NPs and/or aggregates of NPs [21-24]. Both can be seen on the associated TEM image (**Fig.**

7B); as explained by the reduced amount of citrate ligand, which cannot sufficiently stabilise the NPs surface.

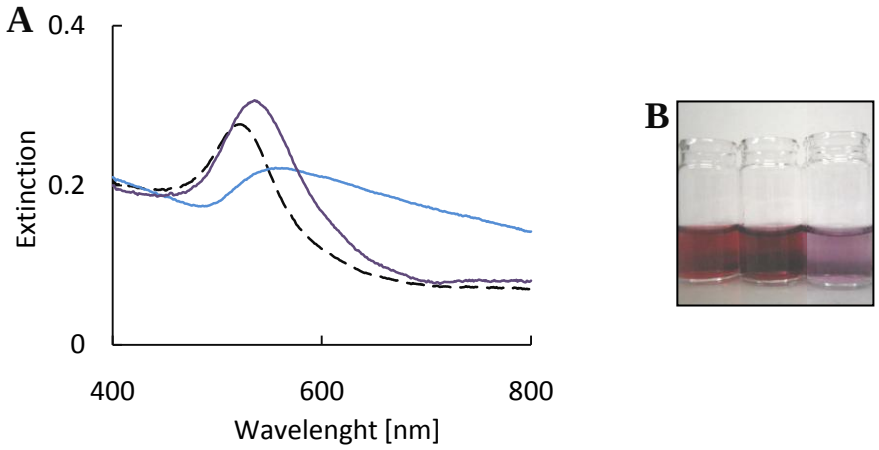

Figure 8. UV-vis spectra (A) and a corresponding digital image (B) of citrate stabilised colloidal gold NPs prepared with Au^{3+} to Ct^{3-} ratio of: 1 : 3.9 (standard protocol, dashed line – A; left vial – B), 1 : 1.95 (violet line – A, middle vial – B) and 1 : 0.39 (blue line – A, right vial – B).

Peng and co-workers proposed that trisodium citrate has a triple role in the citrate reduction [38] (see **chapter 2** for detailed reaction mechanism). Trisodium citrate not only acts as a gold reductant and NPs capping agent, but also as a pH modulator. Reaction pH, according to Peng, has a significant effect on the reaction time and the size of NPs. Below, TEM images of NPs prepared with pH adjusted to pH 6 (**Fig. 9A**) and pH 7 (**Fig. 9B**) are shown. As can be seen, an increase in the pH value to 6 and 7 (images **A** and **B** respectively) generally leads to the formation of larger NPs. At lower pH values, the overall size distribution of NPs seems narrower, as indicated by both, TEM and the extinction peak (shaper peak, **Fig. 9C**, **pink line**). According to Peng and co-workers, depending on the pH, the reaction can undergo one of two possible pathways, with a switching point at pH 6.5 [38]. Slow nucleation and growth occur at high pH, while fast nucleation and intra-particle ripening at low. At low pH (fast reaction) more nuclei are formed leading to smaller NPs.

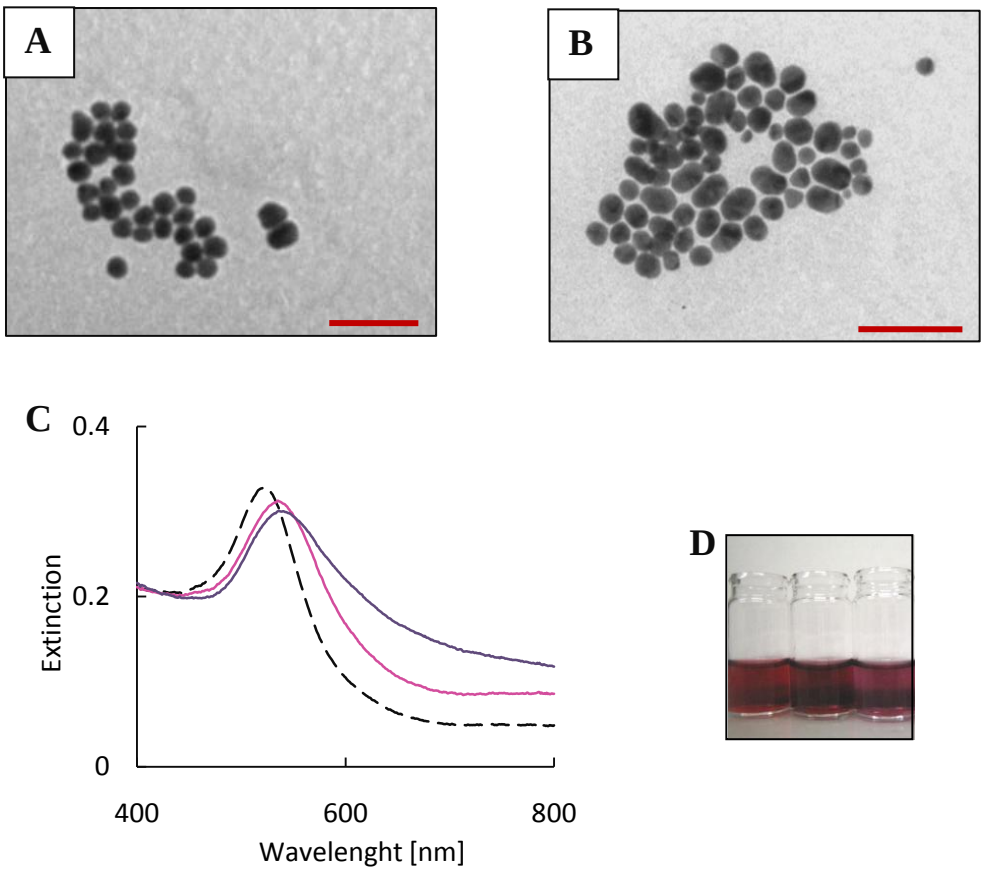

Figure 9. TEM images (A and B), UV-vis spectra (C) and a digital image (D) of citrate stabilised colloidal gold NPs prepared by a standard protocol (dashed line – C, left vial – D) with pH adjusted (with sodium hydroxide) to pH 6 (A, violet line – C, middle vial – D) and pH 7 (B, blue line – C, right vial – D). Scale bars are 100 nm.

In general, citrate stabilised NPs easily aggregate in buffered environments and change their optical properties [7,21,24,35,36,47] (see **chapter 2** for theoretical background). This aggregation is irreversible and is due to a weak electrostatic stabilisation of the NPs surface with the citrate capping agent [35,36]. Negative charge of citrate NPs is screened in a presence of salts (e.g. sodium chloride, NaCl), bringing NPs closer (they no longer repel), until they finally stick together and form aggregates. To increase the stability of NPs, their surfaces can be capped with 'stronger' ligands (interacting more strongly with the gold surface) *via* ligand exchange reactions [7,35,36]; e.g. BSPP ligand (developed by Lehnert's group [48]) provides NPs with a strong electrostatic stabilisation, as demonstrated by Alivisatos and co-workers [49]. As a result, the aggregation of NPs with NaCl is reversible [45,47,49]. NPs can be brought back to solution upon addition of pure water. Most importantly, their optical signatures are fully restored.

Following this idea, to increase the storage stability, spherical citrate stabilised NPs with an average diameter of 15 nm, were capped with BSPP (see **chapter 2** for schematic illustration and **chapter 3** for experimental protocol). The capping with BSPP resulted in a minor change in the refractive index of the colloid. This, as expected from Mie's theory [24], led to a slight red-shift of the plasmon band [21] (from 520 to 522 nm, **Fig. 10C**). Sharpness of the extinction peak suggests that BSPP capped NPs remained dispersed in solution [21-24,42,43,45]. The size and shape of the metallic core of BSPP NPs were not affected, as illustrated by the TEM image (**Fig. 10A**) and a corresponding size distribution histogram (**Fig. 10B**).

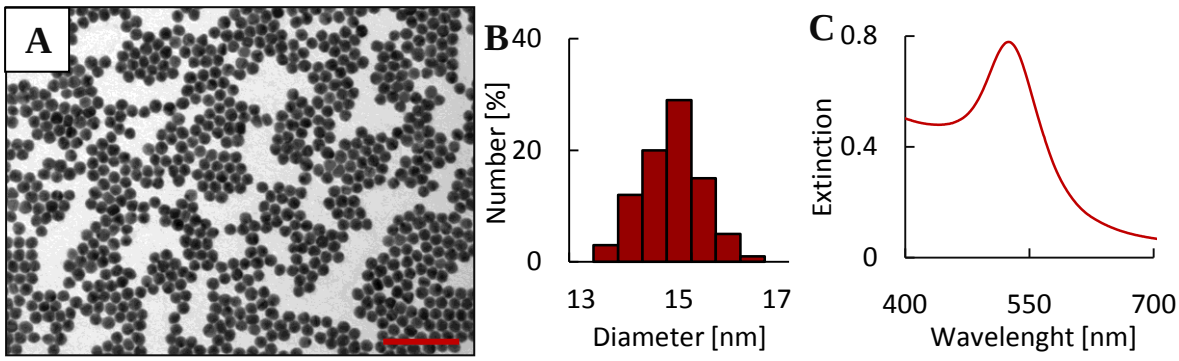

Figure 10. TEM image (A), size distribution histogram (B) and UV-vis spectra of BSPP stabilised colloidal gold NPs. Scale bar is 100 nm.

4.1.2. Synthesis of gold nanorods.

Nanorods were grown in solution from the gold precursor and small gold NPs (seeds), entrapped within micelles formed by surfactant molecules (CTAB) [25,28,50,51]. Two different methods (I [28] and II [25]) were used (see **chapter 3** for details). Method I required additive silver ions (Ag^+), which undergo under-potential deposition (UPD) on the sides of a growing nanorod, promoting longitudinal axis elongation [28,52]. The overall length of the obtained nanorods depends on the introduced quantity of silver, as will be demonstrated in this section.

Gold seeds were prepared by previously reported borohydride reduction method [28]. In this method, gold precursor was reduced with sodium borohydride in the presence of CTAB (see **chapter 2** for reaction mechanism and **chapter 3** for experimental details). Resulting, CTAB stabilised seeds had a typical diameter of 2 ÷ 4 nm (as can be seen on the TEM image, **Fig. 11A**). Colloidal solution had a brown colour and a typical shoulder-like

plasmon band at around 510 nm [21-24,28] (**Fig. 11C and B**, respectively; see also **chapter 2** for theoretical background). These NPs served as seeds in both methods (I and II) used for the preparation of nanorods.

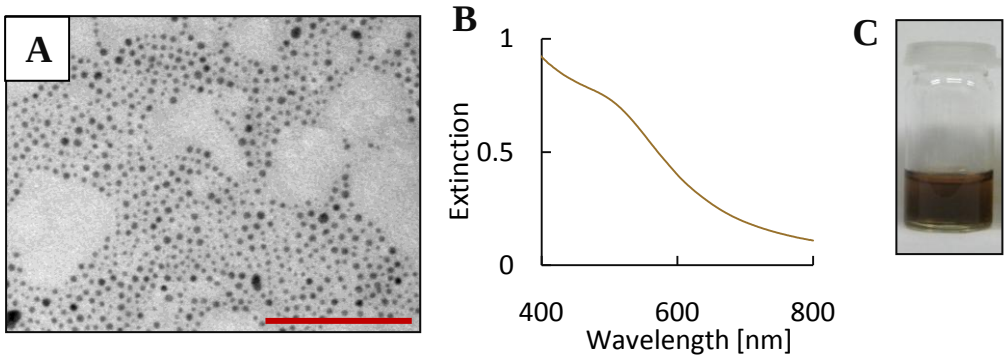

Figure 11. TEM image (A), UV-vis spectra (B) and a digital image (C) of CTAB stabilised colloidal gold NPs. Scale bar is 100 nm.

As already mentioned, the dimensions of NPs synthesised by method I, were controlled by simply varying one reaction parameter – the quantity of introduced silver (silver nitrate solution) into the reaction mixture [28]. An increase of silver nitrate solution volume from .0.15 ml to 0.40 ml resulted in the formation of nanorods with a length-to-width aspect ratio extended from around 2.2 to 5.2 (**Fig. 12A** and **D**, respectively).

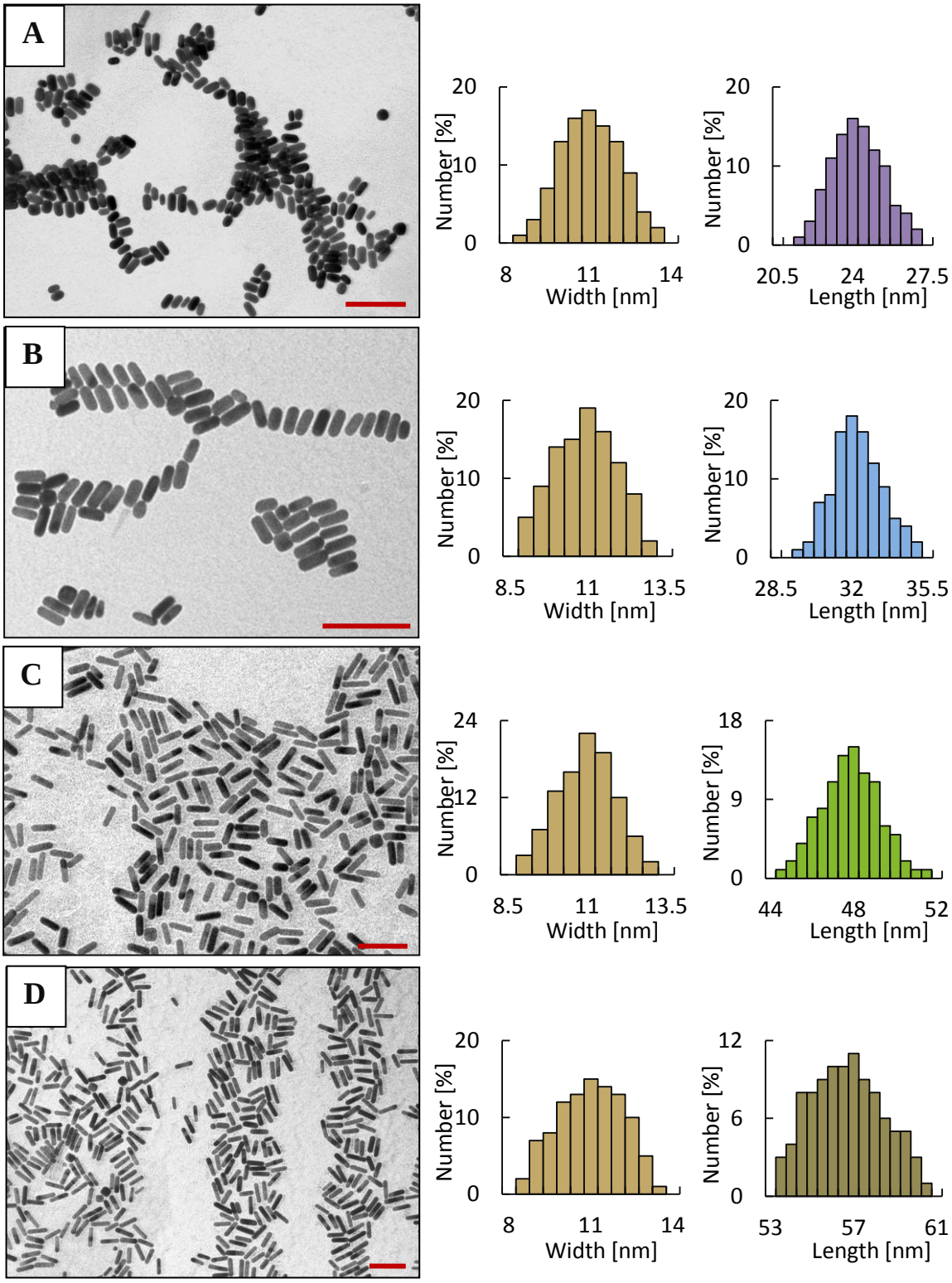

Figure 12. TEM images and the representative size distribution histograms of gold nanorods prepared with: 0.15 ml (A), 0.21 ml (B), 0.30 ml (C) and 0.40 ml (D) of silver nitrate solution. Aspect ratios are around: 2.2 (A), 2.9 (B), 4.4 (C) and 5.2 (D) respectively. Scale bars are 100 nm.

As can be seen on the TEM images, the reaction yield (percent of rod-like structures to the total number of NPs) has reached over 90 %, as the majority of produced NPs were rod-like in shape, with only few spheres (**Fig. 12A**) or cubes (**Fig. 12C**). Synthesised nanorods were narrow in size distribution and had an average dimension of 11 by 24 nm to 11 by 57 nm (size distribution histograms, **Fig. 12**).

It is widely accepted that, the optical properties of NPs strongly depend on their size [21-24,53-55]. In fact, the longitudinal plasmon band of rod-like gold NPs is sensitive to the nanorod aspect ratio and can be red-shifted to the near-infrared (NIR) spectral region [21,22,53-55] (as already explained in **chapter 2**). Consequently, the maximum absorbance peak of nanorods with a width fixed at about 11 nm and length increased from 24 to 57 nm was shifted from 650 to 850 nm in wavelength, respectively (**Fig. 13A**). These variations in the optical properties of rod-like colloids were also perceptible macroscopically, as seen in the solution colour change from violet to brown (**Fig. 13B**).

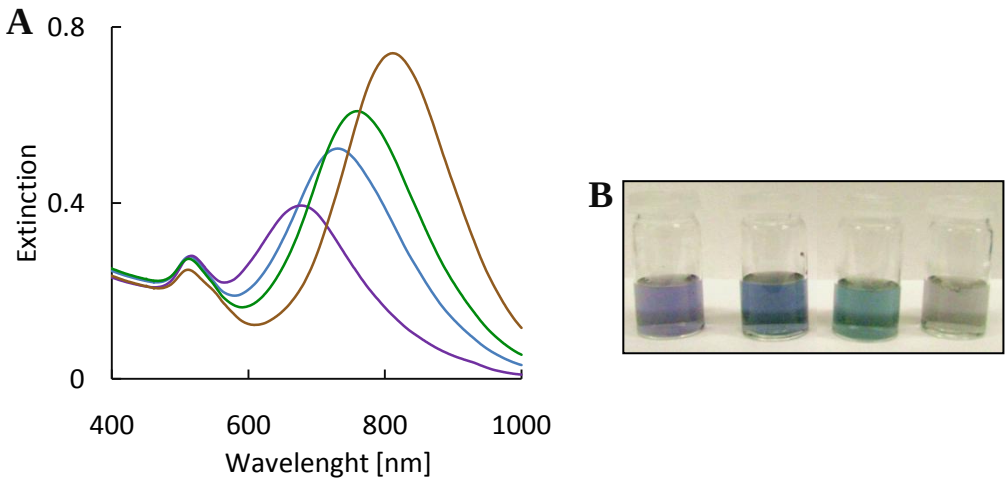

Figure 13. UV-vis spectra (A) and a digital image (B) of gold nanorods prepared with: 0.15 ml (violet: line – A and solution – B), 0.21 ml (blue: line – A and solution – B), 0.3 ml (green: line – A and solution – B) and 0.4 ml (brown: line – A, brown and solution – B) of silver nitrate solution.

More elongated nanostructures, called nanowires were synthesised by a slightly modified reaction scheme [20,25,50,56-59] (method II, see **chapter 3** for experimental details). In method II silver nitrate was discarded from the growth solution and NPs were grown in three steps. This led to the synthesis of gold wires with a high aspect ratio and a length above 100 nm. As an example, up to 300 nm long and 25 nm thick nanowires are shown on TEM micrographs (**Fig. 14A ÷ B**). The corresponding UV-vis spectrum is presented in

Fig. 14D. Clearly, the presence of wire-like structures in colloidal solution resulted in even greater red-shift of the plasmon band (to 1150 nm). Broad longitudinal peak suggests poly-dispersed NPs [21-24,55], as indicated by the TEM images. Higher intensity of the transverse band at 525 nm, along with the red colour of the solution, indicated the presence of spherical NPs [21,23-25]. This was confirmed by the TEM microscopy (**Fig. 14C**). The overall reaction yield was calculated from five representative TEM images with only 10 % of nanowires among shapes of obtained NPs.

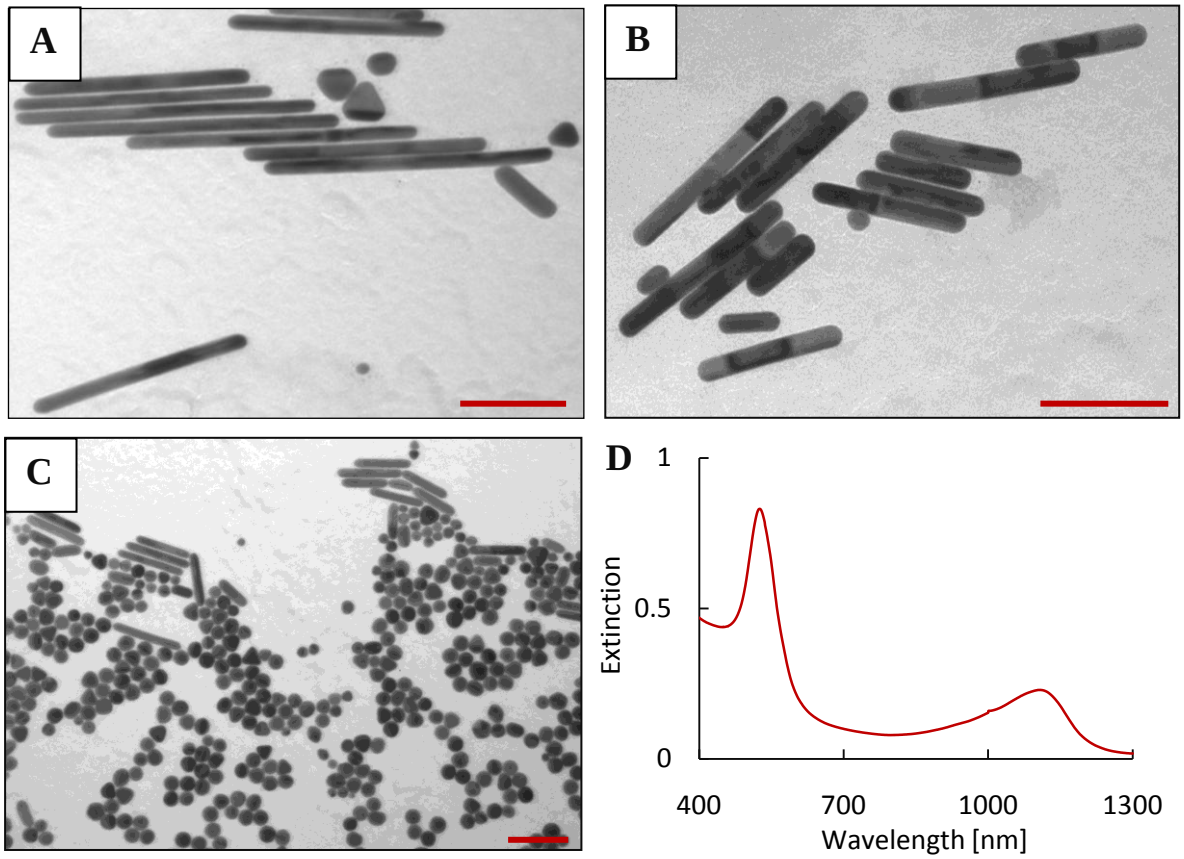

Figure 14. TEM images (A – C) and UV-vis spectrum of gold nanowires. Scale bars are 100 nm.

As explained in **chapter 2**, the growth of nanorods is predominantly controlled by basic components of the reaction mixture: CTAB, seeds and silver nitrate* (*when method I is utilised) [25,28,50-52,56-64]. Murphy's group investigated the effect of different types of seeds on the final product of the reaction [50], e.g. nanorods grown *via* method II from citrate stabilised NPs, had Au{111} facets at the tips and a combination of Au{100} and Au{110} facets on the sides.

The crystal structure of the final reaction product was studied by Guyot-Sionnest and co-workers [52]. They demonstrated that nanorods synthesised by method I exhibit Au {100} facets in the ends and Au {110} on the sides. The different crystal structure was attributed to the UPD of silver, which according to Guyot-Sionnest, is favourable on Au {110} facets (the sides), rather than on Au {100} facets (nanorod ends).

Except of the crystal structure, UPD also explains why the aspect ratio of nanorods produced, can be controlled by adjusting the quantity of the introduced silver nitrate [28,52]. Higher concentrations of silver nitrate result in larger amounts of silver deposited on the nanorod-sides. Larger surface area passivated with silver, leads to more excessive growth of nanorods ends and higher aspect ratio (width-to-length) of synthesised NPs [28,52,58,59]. Elongation of the longitudinal axis is additionally promoted by the strong binding of CTAB to silver (probably *via* bromide [58]), which usually follows the silver UPD [28,52,58,59].

In the absence of silver (method II) the growth is mainly surfactant mediated. As proposed by Mulvaney and co-workers, CTAB micelles form complexes with reduced $AuCl^{2-}$ anions [63,64]. CTAB-$AuCl^{2-}$ complexes collide with CTAB stabilised seeds. The collision rate is faster at tips, rather than sides, thus promoting the growth in one direction. The overall yield of the reaction can be controlled by adjusting the pH of the environment, as demonstrated by Murphy and co-workers [56,58]. A slight increase of the reaction pH results in an increase of the ascorbate mono-anion fraction (effective reductant). Ascorbate binds to the growing nanorod ends and reduces Au^{3+} cations to Au^{+} more efficiently, thus promoting the growth along the longitudinal axis.

4.1.3. Synthesis of silica/gold core/shell NPs.

Silica/gold core/shell hetero-nanocomposites were prepared according to a method developed by Halas and co-workers [29,65,66] (see **chapter 3** for experimental protocol). This method involves three major steps; a) preparation of silica NPs (**Fig. 15A**); b) to which small gold NPs (seeds) are subsequently attached (**Fig. 15B**) and finally c) slow growth of gold shells around silica cores (**Fig. 15C**).

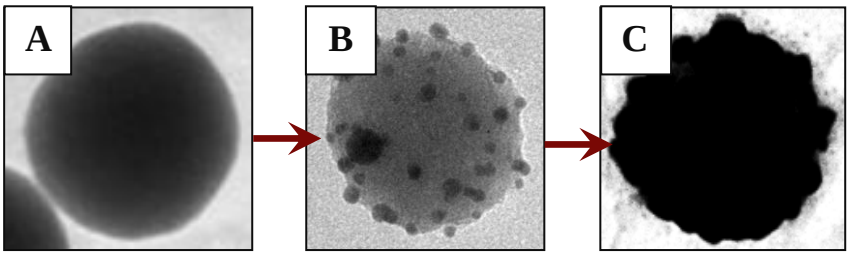

Figure 15. TEM images of: silica nanoparticle (A), silica nanoparticle with attached gold seeds (B) and a complete silica/gold core/shell (C); representing the three major steps in the synthesis of core/shell nanostructures.

Silica NPs, prepared by a standard sol-gel method developed by Stöber *et al.* [67-70], were spherical and uniform in size, with an average diameter around 97 nm, as demonstrated in **Fig. 16A** and **B**. The size of NPs synthesised by this method can be varied by adjusting the amount of water added into the reaction environment [67-70]. Water participates in precursor hydrolysis and condensation (see **chapter 2** for detailed mechanism). The amount of ammonia solution introduced into the reaction also has a strong effect on the final size of NPs [67-70]. As demonstrated by Vrij and co-workers, a synergetic effect of water and ammonia concentration regulate the final diameter and poly-dispersity of silica NPs [68]. Water is a key reagent for the precursor hydrolysis and condensation, therefore reducing the water quantity slows down the reaction rate and leads to the formation of larger NPs. Higher concentrations of ammonia result in larger average diameters and a narrower size distribution. Consequently, smaller silica NPs (around 45 nm in diameter, **Fig. 16C** and **D**) were prepared with increased water and decreased ammonia quantities [68,69] (see **chapter 3** for experimental details).

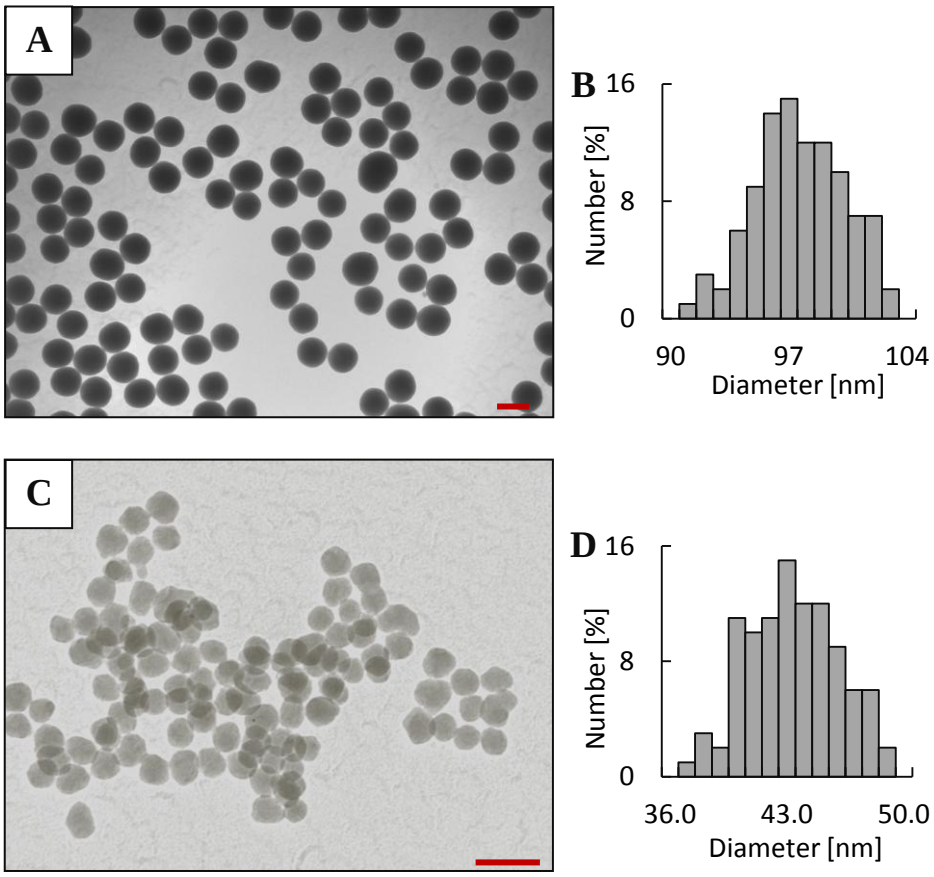

Figure 16. TEM images (A and C) and size distribution histograms (B and D) of silica NPs. Scale bars are 100 nm.

The surface of silica NPs was functionalised with APTMS (see **chapter 3** for experimental details), to generate a monolayer with amine groups extending outwards [29,66]. Available amine groups served as binding sites for small gold NPs in the following step of the synthesis of silica gold hetero-nanostructures.

Three different sizes of gold NPs (seeds) were prepared by the Duff method (see **chapter 3** for experimental details) [71,72]. Simply by changing the amount of the gold precursor (1 % aqueous solution of sodium tetrachloroaurate (III) dihydrate) added into the reaction mixture from 1.5 ml to 0.75 ml, the largest or the smallest seeds were obtained, respectively. UV-vis spectra of seeds solutions are shown in **Fig. 17A**. The largest colloids exhibit a shoulder-like plasmon band (red line), while the maximum absorbance peak of the smallest seeds (yellow line) is nearly invisible [22-24] (see **chapter 2** for theoretical background on the optical properties of gold NPs). A corresponding digital image of colloidal solutions is show in **Fig. 17B**.

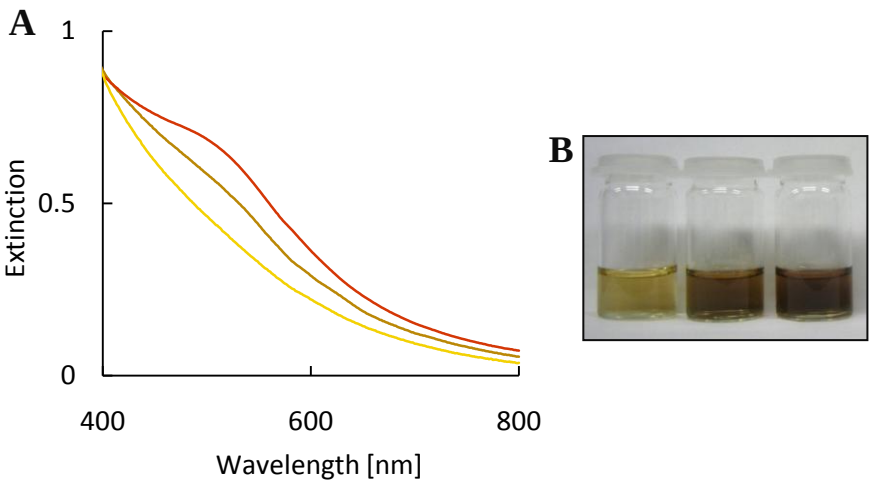

Figure 17. UV-vis spectra (A) and a corresponding digital image (B) of THPC coated gold NPs. Yellow line and solution represent the smallest seeds, brown line and solution – medium size and red line and brownish-red solution – the largest.

As seen on TEM images (**Fig. 18A ÷ C**), the size of produced seeds varied from 3 ÷ 5 nm of the largest (**Fig. 18A**), 2 ÷ 4 nm of the medium size (**Fig. 18B**), to 1 ÷ 3 nm of the smallest colloid (**Fig. 18C**). Moreover, the largest seeds were the least uniform in size and shape, as some larger (up to 10 nm) and elongated structures were also present in solution. Despite that, all three colloids were attached to APTMS-functionalised 100 nm silica NPs (**Fig. 18D ÷ F**) and served as seeds in the synthesis of gold shells. The smallest (yellow) seeds, attached to large silica NPs, were barely visible on the TEM micrograph (**Fig. 18F**), possibly due to their decreased contrast [23].

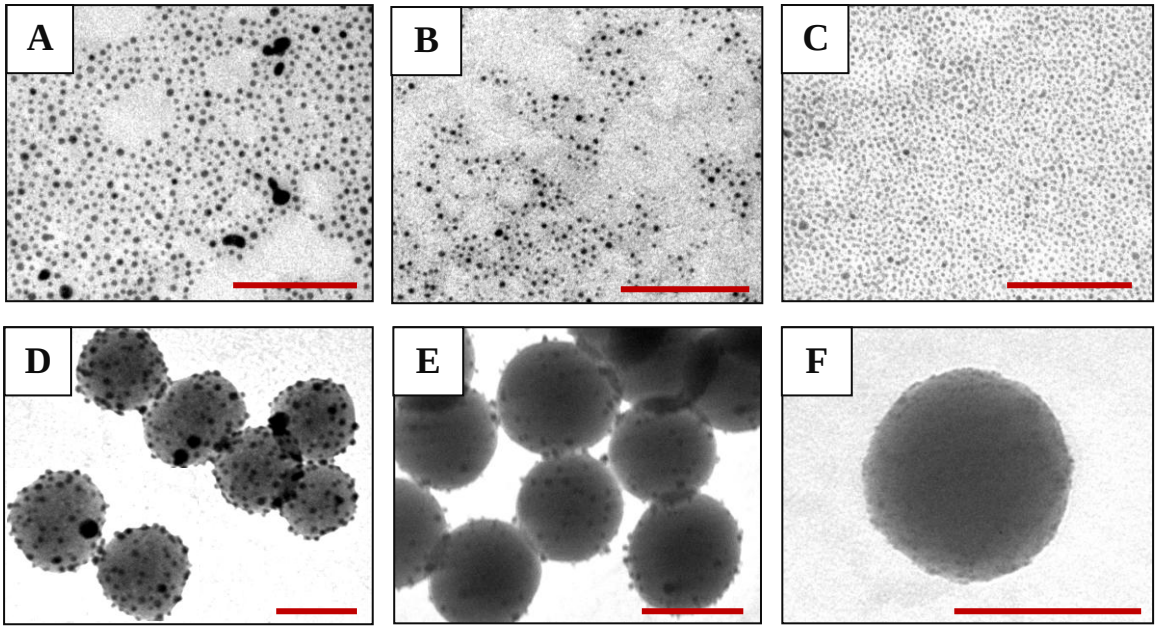

Figure 18. TEM images of THPC coated gold NPs (A ÷ C) and gold seeds attached to silica NPs (D ÷ F); the smallest gold seeds (A, D), medium size (B, E), the largest (C, F). Scale bars are 100 nm.

In the final step of the synthesis of silica/gold hetero-nanocomposites gold shells were grown around silica cores from the gold precursor [29,65,66,73] (sodium tetrachloroaurate (III) dihydrate). Gold seeds attached to the cores served as nucleation sites, therefore their initial size affected the thickness of produced shell and the optical properties of the final core/shell NPs [29,65,66,74]. UV-vis spectra (**Fig. 19A**) of silica/gold hetero-structures showed a significant red-shift of the plasmon band, from around 580 nm to 700 nm, for the core/shells grown from the largest or the smallest seeds, respectively. Silica/gold NPs grown from the medium size seeds absorbed at around 605 nm. The broad shape of extinction peaks can be explained by the scattering effect deriving from the large overall diameter of NPs (100 nm silica cores), possibly in conjunction with the non-uniform size distribution [21,22,46,65]. Changes in the colour of the colloidal solutions were also observed macroscopically, as demonstrated on the associated digital image (**Fig. 19B**).

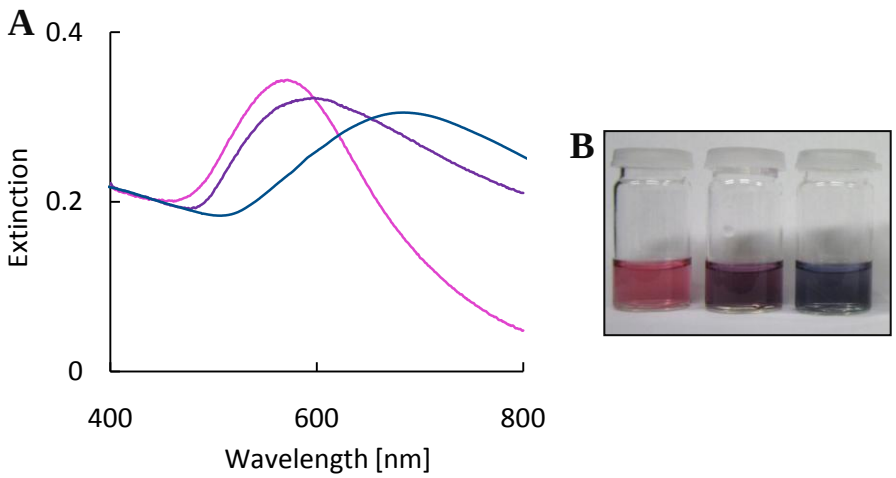

Figure 19. UV-vis spectra (A) and a corresponding digital image (B) of silica/gold core/shell nanostructures. Pink line represents pink solution (thickest shell), violet line – violet solution and blue line – blue solution (thinnest shell).

Significant differences in the optical properties between synthesised colloids derived from the variation in thicknesses of gold shells grown on silica cores. Assuming that the average core size was about 97 nm, the thickest shells (around 45 nm, **Fig. 20A**) were produced from the largest seeds (**Fig. 18**). The medium size seeds resulted in thinner shells (around 33 nm, **Fig. 20B**), while the smallest seeds lead to the formation of the thinnest gold shells (around 20 nm, **Fig. 20C**). It is also worth highlighting that the surfaces of the shells produced were not perfectly smooth, with the thickest shells having the largest bumps.

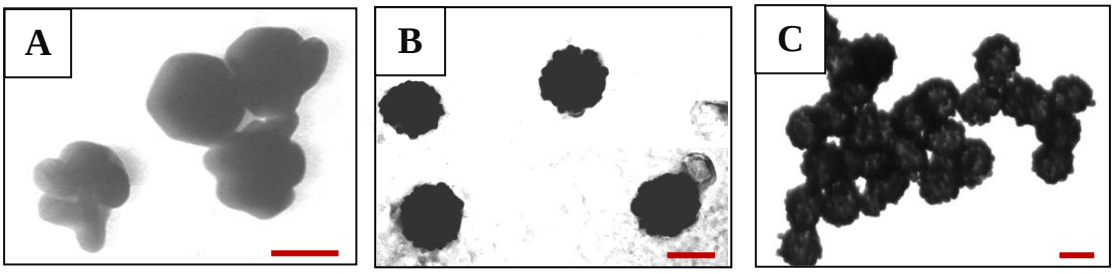

Figure 20. TEM images of silica/gold core/shell nanostructures, with variable thicknesses of gold shell: the thickest (A), medium (B) and the thinnest (C). Scale bars are 100 nm.

It is widely accepted that the optical properties of silica/gold core/shells depend very strongly on three major parameters: the shell thickness, the core size and ratio between them, as described by Halas and co-workers [29,65,66,74]. These parameters can be controlled by slight modifications of the reaction conditions [29,65-74]. As already mentioned, a decrease in the amount of water and an increase in the amount of ammonia in the reaction environment, during the synthesis of silica NPs *via* sol-gel method, result in larger NPs [67-70]. Consequently, larger silica cores lead to larger diameters of gold shells, which results in greater red-shifting of the plasmon band [22,29,65,66,74,75].

Another important parameter is the thickness of the gold shell [22,29,65,76]. Except of the seed sizes (**Fig. 18**), the actual number of seeds attached to each silica core can also affect the thickness of produced gold shell [29,65,66]. This can be controlled by, e.g. the type of functional groups attached to silica NPs. Halas and co-workers showed that thiol or amine terminated silica had the highest number of attached seeds [66]. Larger quantity of seeds per silica nanoparticle results in a thinner shell, because less surface area of silica core is left to cover with gold. As also demonstrated by Halas and co-workers, the thickness of the gold shell can be additionally regulated by adjusting the amount of gold salt present in the growth solution [29,65,66]. Reduced concentration of the precursor leads to the formation of a thinner shell. In general, maximum red-shift of the plasmon band is usually achieved by thin shells (5 to 20 nm) grown around large cores (100 to 200 nm) [65]. However, larger overall size of NPs leads to enhanced scattering properties and a predominantly scattering mode of silica/gold hetero-nanostructures [22,77]. This is particularly important in biomedical applications of NPs, which are based on absorption and scattering properties of silica/gold core/shells (e.g. laser-hyperthermia [78], see **chapter 7**). Consequently, when predominantly absorbing NPs are required, thin gold shells (approximately 5 nm) can be grown around small silica cores (45 nm, see **chapter 3** for experimental protocol) to form silica/gold hetero-structures absorbing in the NIR spectral region (see **section 4.2.2.** for UV-vis spectra of such NPs).

4.1.4. Synthesis of hollow gold NPs.

Hollow gold NPs were synthesised by the method developed by Xia and co-workers and consisting of two steps: preparation of silver NPs (templates), followed by galvanic replacement reaction between templates and the gold precursor [32,33,79-81] (see **chapter 2**

for theoretical background). The shape and size of hollow gold nanostructures are determined by the type and size distribution of the silver templates.

One-step seed mediated protocol developed by Oh and co-workers was employed in the synthesis of silver NPs [82] (see **chapter 3** for experimental details). In this method spherical or rod-like silver NPs can be synthesised in the presence of CTAB from small citrate capped silver NPs. Citrate stabilised silver seeds were prepared by a borohydride reduction method at room temperature. Silver seeds from 4 to 7 nm in diameter were obtained, as demonstrated on a TEM image (**Fig. 21A**).

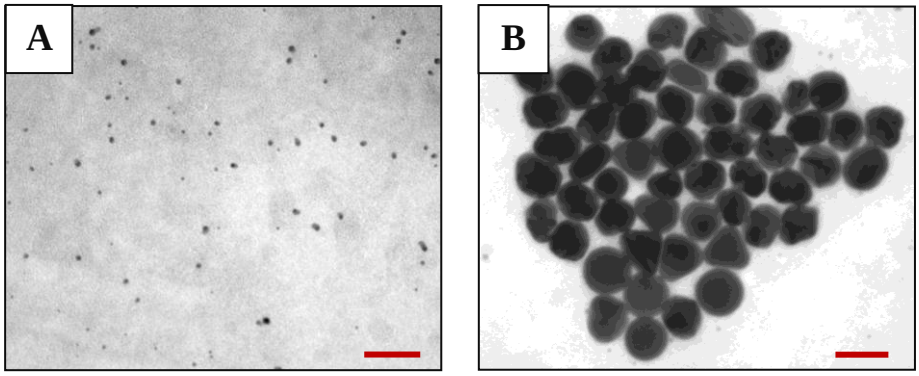

Figure 21. TEM images of citrate stabilised silver seeds (A) and CTAB coated silver NPs (B). Scale bars are 100 nm.

The UV-vis spectrum (**Fig. 22A**) with the characteristic peak (around 400 nm), in conjunction with yellow coloured solution (**Fig. 22B**), indicated the presence of colloidal silver [23,24,32,82]. The final product of the seed mediated synthesis (CTAB stabilised spherical NPs) was orange-yellowish in colour (**Fig. 22B**). NPs were 81 ± 9 nm in diameter (**Fig. 21B**) with an extinction peak around 440 nm (**Fig. 22A**). The broadness of the plasmon band can be attributed to scattering effects and/or wide size distribution of NPs [21,23,24,54].

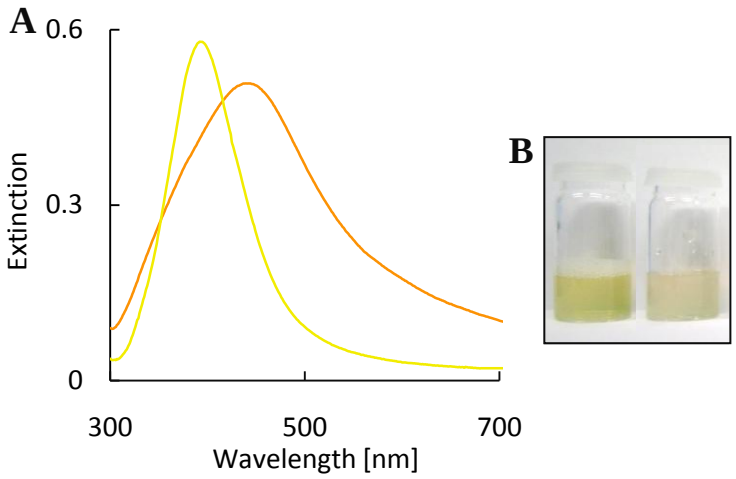

Figure 22. UV-vis spectra (A) and a corresponding digital image (B) of citrate stabilised silver seeds (yellow line – A and solution on the left – B) and CTAB coated silver NPs (orange line – A and solution on the right – B).

In the final stage of the synthesis of hollow gold NPs silver atoms were exchanged to gold during the galvanic replacement reaction [32,33,79,83]. The optical properties of the resulting gold NPs depend strongly on type of nanostructures produced, thus can be adjusted chemically [10,22,27,32,33,76,79-81,83-87]. The quantity of the gold precursor (1 mM sodium tetrachloroaurate (III) dihydrate) injected into the boiling solution of silver nanocrystals was crucial. A decrease from 0.5 to 0.25 ml resulted in the formation of nanoshells or nanocages, respectively (**Fig. 23A ÷ C**) with around 10 nm wall thickness. The presence of holes in the wall resulted in a red-shift of the plasmon band from around 700 nm (for nanoshells) to 800 nm (for nanocages, **Fig. 23D**). Significant differences in the optical properties of colloids were also observed macroscopically, as demonstrated on the associated digital image (**Fig. 23E**).

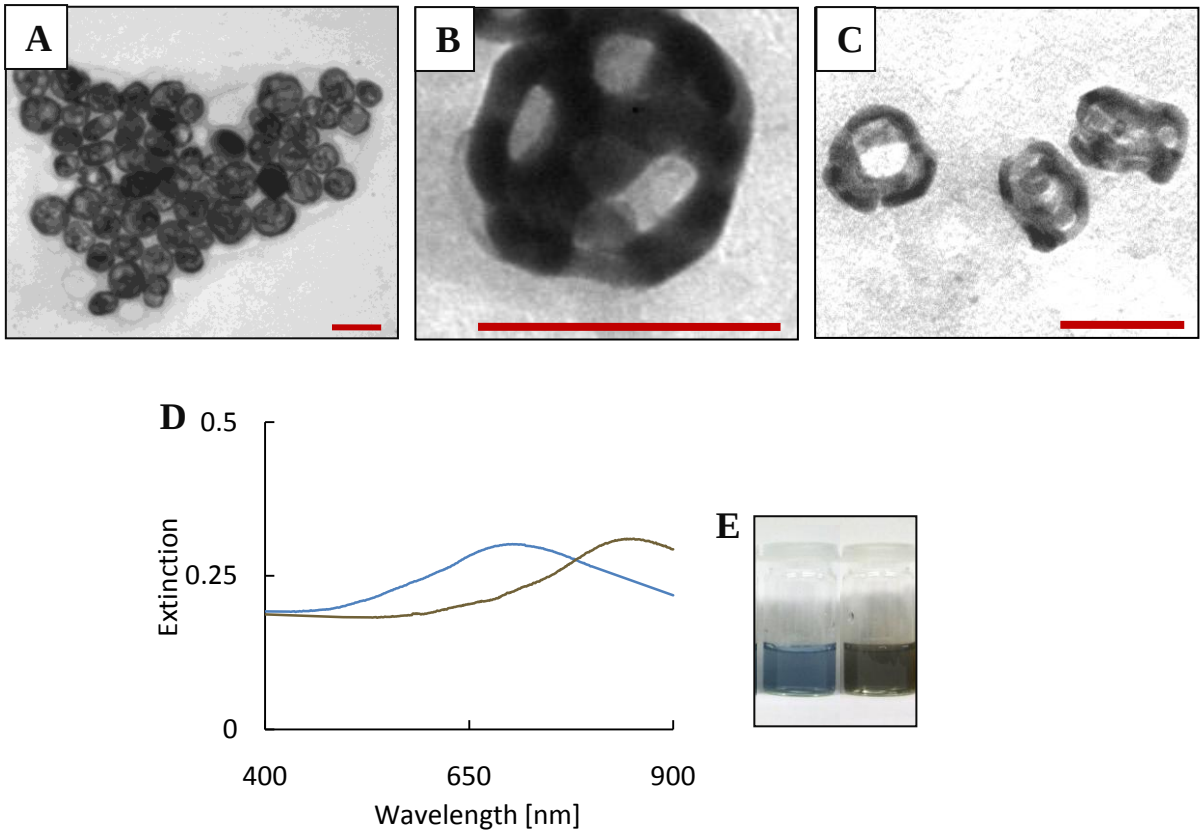

Figure 23. TEM images (A ÷ C), UV-vis spectra (D) and a corresponding digital image (D) of hollow gold NPs; nanoshells (A, blue line on D and solution on the left on E) and nanocages (B and C, brown line on D and solution on the right on E). Scale bars are 100 nm.

Several different methods of the synthesis of monodispersed silver NPs have been developed in recent years, e.g. Xia and co-workers reported a polyol method, which lead to the formation of a variety of shapes of silver NPs, from spherical, cube-like to rice-like [27,81,84,86-88]. This method however, involves high temperatures (up to 160 °C). As an alternative, Oh and co-workers developed a seed mediated surfactant guided method, which was initially designed to synthesise silver nanorods [82]. Nonetheless, as demonstrated in this section, with minor modifications (see **chapter 3** for experimental protocol) this method can be employed in the synthesis of relatively monodispersed spherical NPs.

The very simple method of synthesising hollow gold NPs (developed by Xia and co-workers) involves only two reagents: gold precursor and silver NPs [32,33,79,83]. A type of the final product and its optical properties can be easily modified, by varying the amount of precursor or by using different silver templates; e.g. Oh and co-workers demonstrated the

use of silver nanorods, which led to the formation of hollow gold nanorods with a plasmon band around 800 nm [82]. Whilst the utilisation of silver nanocubes resulted in hollow gold nanocubes or nanocages with plasmon band shift to 1000 nm, as demonstrated by Xia and co-workers [14,27,32,33,79-81,83-85,87,89].

4.2. Surface capping and assembly of NPs.

Gold NPs were coated with three types of ligands: CALNN based peptides [4,34], oligoethylene glycol (OEG) based ligands [2] and diacetylene based molecules [6,90,91]. NPs capped with diacetylene based monomers were photo-polymerised (**section 4.2.3.**) to create firm polymeric shell, which protects the metallic core and enhances NPs stability in aqueous environments [6]. Gold colloids coated with CALNN based peptides were utilised in the formation of NPs assemblies (**section 4.2.1.**) on oligodeoxynucleotide templates [34]. OEG capped NPs were further modified with octa-peptides [37] (**section 4.2.2.**) and employed in the selective targeting of HUVECs (see **chapter 5 and 7**) towards regulation of basic cellular functions (**chapter 6 and 8**). Stability tests of gold colloids are shown in **section 4.2.4.**

4.2.1. NPs surface capping with CALNN based peptides and assembly on oligodeoxynucleotide templates.

Gold NPs were capped with CALNN based [4,92] oligopeptides and assembled on short synthetic oligodeoxynucleotides (ODNs) [34]. Selective binding between FQGII penta-peptide and AT-rich regions of ODNs [93,94] resulted in a range of gold NPs arrays. The size and shape of NPs assemblies were adjusted by changing the composition of NPs capping layer and varying the architecture of ODN templates. Specifically, short self-complementary sequences of ODN_3 contained two AT-regions, while long staggered duplex of ODN_{1+2} had AT-rich regions at regular intervals along its entire length (see **chapter 2** for theoretical background and **chapter 3** for schematic illustration).

Spherical 15 nm gold NPs were coated with a mixture of CALNN and CALNN-Ahex-FQGII (c-FQGII, see **chapter 2** for chemical structures and **chapter 3** for experimental details) peptides [34]. As reported by Brust and co-workers, the CALNN moiety provides NPs with sufficient stability in buffered environments [4,9,92,95] (see **chapter 2** for schematic illustration and more details on CALNN capping ligand). The percentage of c-FQGII to CALNN attached to the surface of gold NPs was varied between 0 and 25 % to obtain

increasing ODN binding sites per nanoparticle. UV-visible spectra of gold colloids (**Fig. 24A**) with varying c-FQGII content showed sharp plasmon bands with typical peaks (around 525 nm), representing stable and dispersed in solution 15 nm NPs [21-24,42]. A decrease in electrophoretic mobility (**Fig. 24B**) of colloids represented an increase in the amount of c-FQGII attached to NPs [96,97].

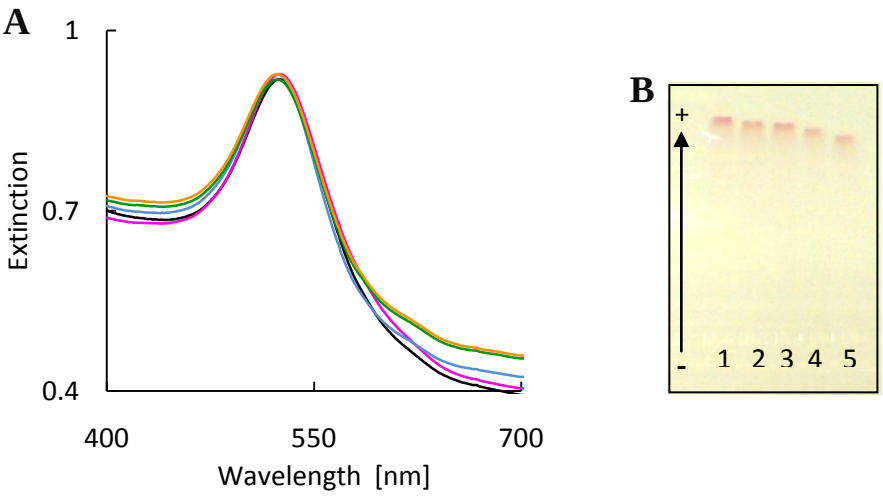

Figure 24. UV-visible spectra (A) and a gel electrophoresis image (B) of gold NPs with: 0 % (black line, lane 1), 5 % (pink line, lane 2), 10 % (blue line, lane 3), 15 % (green line, lane 4) and 25 % (orange line, lane 5) c-FQGII content.

The formation of gold NPs assemblies on ODN templates was monitored by electron microscopy and UV-vis spectroscopy. TEM micrographs (**Fig. 25**) of NPs, incubated with ODN templates, showed clear organisation of NPs-ODN complexes. Dimers and trimers were formed on both templates (ODN_3 and ODN_{1+2}), when 5 % c-FQGII coated NPs were used. Short chains of NPs were formed on both templates when the number of ODN binding sites increased to 10 % c-FQGII. Longer, single chain-like arrangements of 15% c-FQGII coated NPs can be observed on ODN_3, while double chains of NPs were formed on ODN_{1+2} duplexes. Up to 3 µm long chains showed about 100 nm long helical twists, as indicated by red arrows. Much shorter double chains of NPs were formed with 25 % c-FQGII on ODN_{1+2} templates, while when ODN_3 templates were employed, highly complex three dimensional networks of NPs were created (for more TEM images, see related publication listed in **Author's Declaration**).

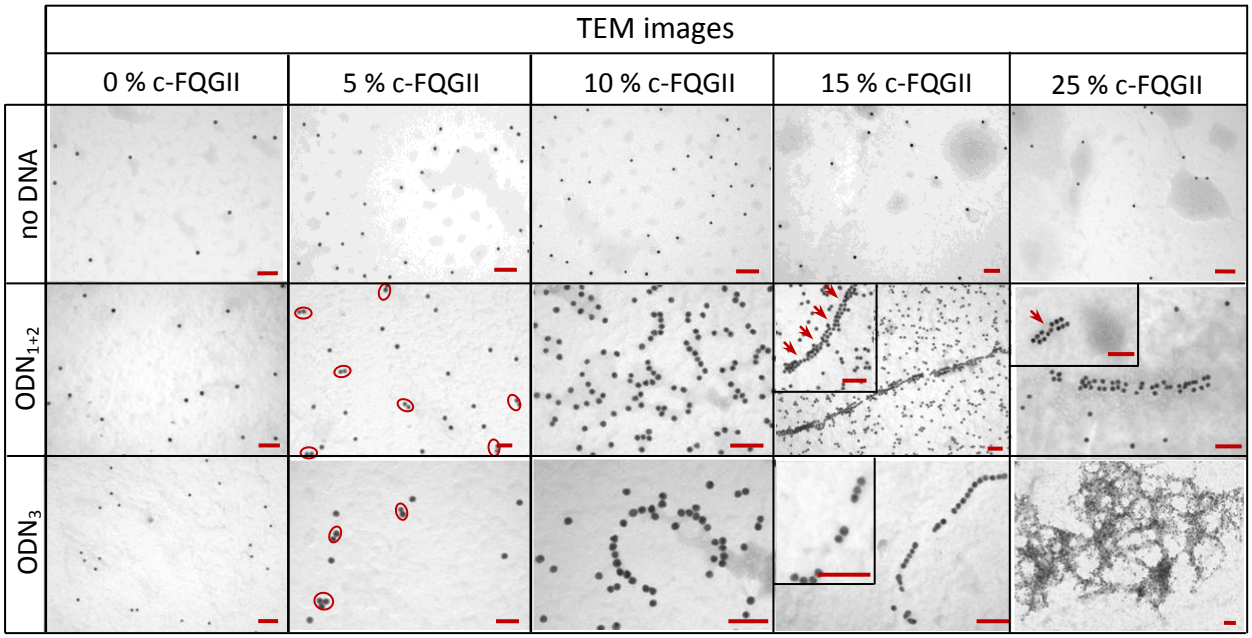

Figure 25. TEM images of gold NPs with variable amount of c-FQGII assembled on ODN templates. Scale bars are 100 nm.

Table 2. Statistical analysis of the NPs assemblies.

c-FQGII [%]	Assembled NPs [%]	
	ODN_{1+2}	ODN_3
5	32 ± 5	42 ± 3
10	53 ± 4	64 ± 4
15	67 ± 7	95 ± 6
25	84 ± 6	100 ± 2

Statistical analysis of TEM micrographs showed a gradual increase in the number of assembled NPs, with an increase in the amount of binding sites per nanoparticle (**Table 2**). Consequently, it can be hypothesised that the probability of binding is directly correlated with the c-FQGII content.

The optical properties of NPs assembled on ODN templates depend strongly on the size and shape of aggregates, as well as distances between NPs [21-24,54,98]. The presence of small structures (e.g. dimers and trimers) is usually indicated by broadening and/or decreasing intensity of the plasmon band, while additional red-shifting suggests the

formation of larger aggregates (**Fig. 26**). Plasmon bands of 5% and 10% c-FQGII coated NPs assembled on ODNs do not show any notable shifts. In contrast, major decrease in the intensity, broadening and red-shifting of plasmon bands, can be observed for NPs with higher c-FQGII content. Red-shifts of up to 11 nm were observed for 25 % c-FQGII NPs assembled on ODN_{1+2} templates, while up to 21 nm for ODN_3, albeit the UV-vis spectra represent an average between NPs involved in assemblies and those remaining free in solution.

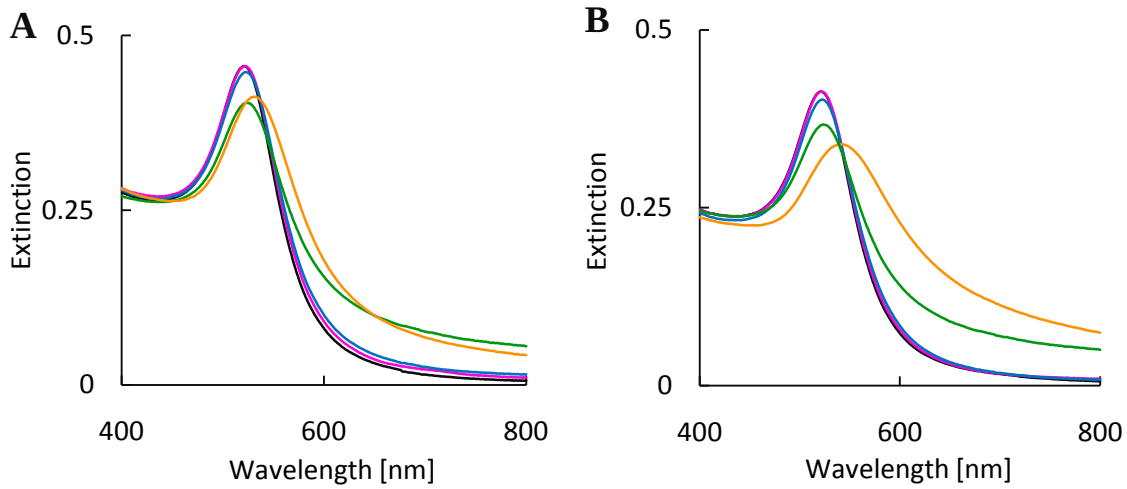

Figure 26. UV-visible spectra of gold NPs with: 0 % (black line), 5 % (pink line), 10 % (blue line), 15 % (green line) and 25 % (orange line) c-FQGII content assembled on ODN_{1+2} (A) and ODN_3 (B) templates.

DNA based scaffolds have been employed in the past to arrange NPs, as reported by several research groups [49,98-101]. These approaches either require a high level of sophistication in design and synthesis, or are limited to fabrication of small quantities of material. A system developed during this project, is based on specific recognition between penta-peptide and short ODN based sequences. It is simple in design and easy in preparation (see **chapter 3** for experimental protocols). Sasaki and co-workers demonstrated that the FQGII sequence selectively binds to an AT-rich region of a short target DNA duplex with high binding constants [93,94]. This idea was employed in the fabrication of NPs assemblies. Hence, FQGII penta-peptide was used in the preparation of the minimal NPs-ODN building blocks. This new strategy of NPs assembly was developed over the course of this project in a close collaboration with Stulz's group from the School of Chemistry, University of Southampton, Southampton, UK.

4.2.2. NPs surface capping with OEG ligand and further modifications.

Brust and co-workers developed a method for preparation of water soluble and stable in buffered environments gold NPs, capped with amphiphilic thioalkyl based ligand: monohydroxy (1-mercaptoundec-11-yl) tetraethylene glycol [2]. A slightly modified molecule, extended by two steps of ethylene glycol and terminated with a functional carboxylic group (OEG, see **chapter 3** for structure and capping protocol) was employed here as a capping ligand for spherical (15 nm in diameter) and anisotropic (rod-like, hollow and core/shell) gold NPs (see **chapter 2** for schematic illustration).

NPs were capped with OEG (monocarboxy (1-mercaptoundec-11-yl) hexaetylene glycol) through the thiol anchoring group [2,35,36]. The long (C_{11}) carbon chain of OEG provided NPs with a uniform hydrophobic layer, due to Van der Waals interactions between neighbouring ligands [2,7]. The hydrophilic part of OEG (-$(EG)_6$-OCH_2-COOH) ensured water solubility and a functional carboxylic group [2,7,36,102,103]. Carboxyl was employed in further modifications of NPs with octa-peptides (P1, P2 or P3, see **chapter 2** for chemical structures) and a fluorescent tag (HiLyte) *via* the EDC/s-NHS coupling method [37] (see **chapter 2** for reaction mechanism and **chapter 3** for experimental protocols). This conjugation technique was employed in the past to couple transferrin and antibodies to mercaptoacetic acid coated quantum dots or carboxy terminated PEG dithiol capped gold NPs, as reported by Nie and co-workers and Mason's group, respectively [104,105]. The reaction conditions used here (see **chapter 3**) were adjusted and optimised, to match the requirements of the octa-peptide based system, which resulted in up to 31 % reaction yield, as will be discussed further in the text.

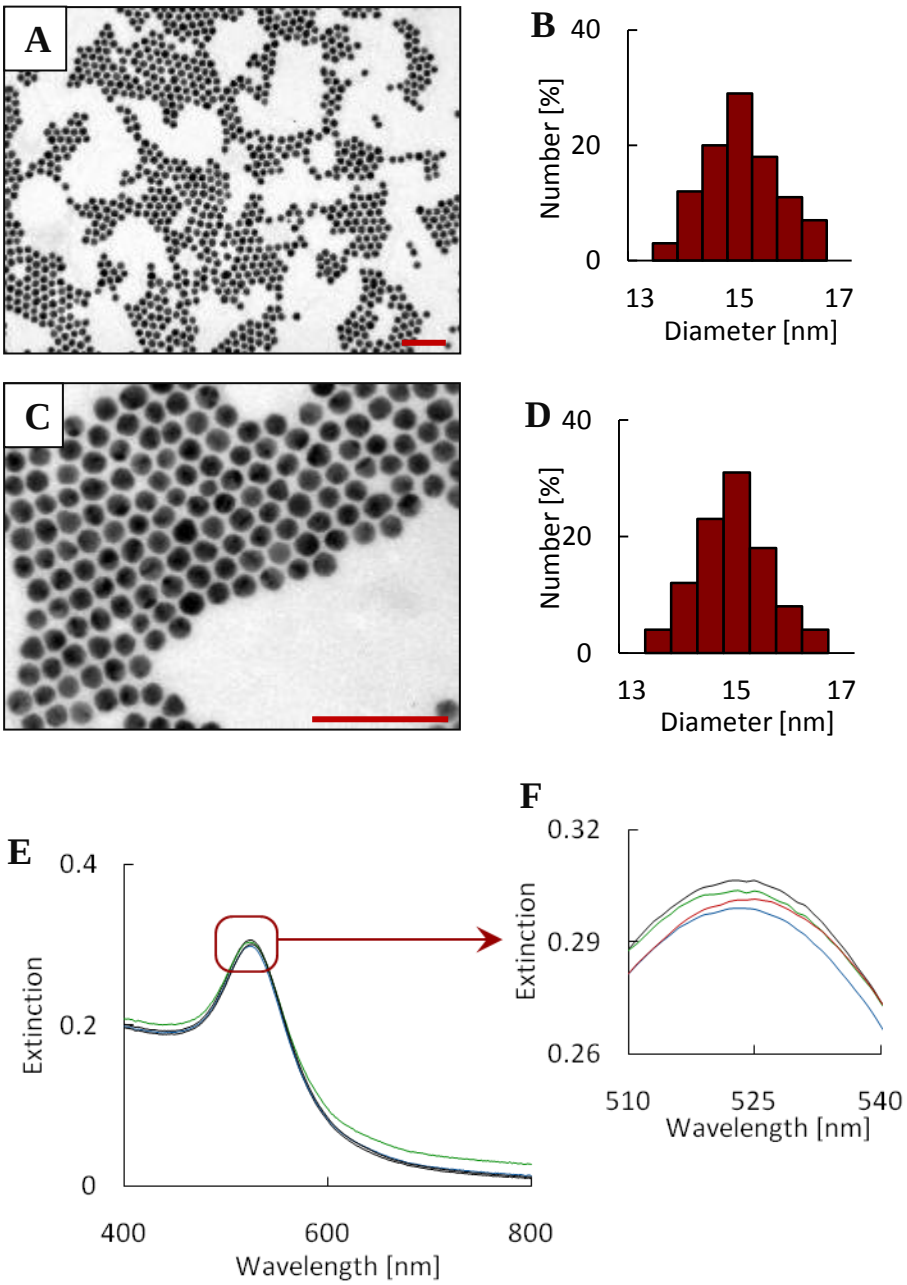

Figure 27. TEM images (A and C), size distribution histograms (B and D) and UV-vis spectra (E and F) of: OEG NPs (A, B and red line) and P1-OEG NPs (C, D and green line), P2-OEG NPs (blue line) and P3-OEG NPs (black line). Scale bars are 100 nm.

OEG coated NPs, as well as P1-OEG, P2-OEG, P3-OEG and HiLyte-P1-OEG conjugates, were stable in buffered environments and did not form any large aggregates. As an example, TEM micrographs and size distribution histograms of OEG coated and P1-OEG conjugated 15 nm spherical NPs are shown in **Fig. 27A ÷ D** (see **section 4.1.1.** for BSPP caped NPs). It is evident that the metallic core has not been affected by the ligand

exchange or EDC/s-NHS coupling procedures. In addition, sharp plasmon bands without shoulders (**Fig. 27E** and **F**) suggested dispersed NPs of typical sizes in solution [21-24]. Slight shifts between peaks representing OEG coated and peptide conjugated (pep-OEG) colloids were observed. This indicated minor changes in the refractive indexes, most likely derived from the presence of an additional organic layer composed of octa-peptide [21,24,42].

Spherical NPs served as a model system and were employed in studies regarding non-specific interactions with mammalian cells (see **chapter 5**), specific targeting of desired cell types and regulation of certain cellular functions (see **chapter 6**). However, because of the optoelectronic properties of spherical NPs (plasmon band around 520 nm), they could not be applied in laser induced photo-thermal treatment [106-108] (see **chapter 2** for theoretical background). Instead, anisotropic NPs (rod-like, hollow and core/shell) absorbing in the NIR spectral region were used [78,80,109-111] (see **chapter 7**). All three types of anisotropic NPs were successfully stabilised with OEG capping ligand and conjugated to P1 peptide. UV-visible spectra (**Fig. 28**) indicated stable colloids of typical shapes and sizes [21-24,42,43]. The character of the peaks was not affected, suggesting that the metallic cores of OEG NPs and P1-OEG NPs remained unaltered and that the NPs did not form any aggregates.

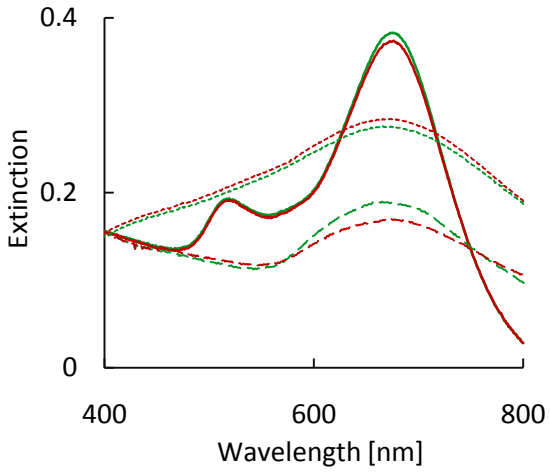

Figure 28. UV-visible spectra of OEG NPs – red line and P1-OEG NPs – green line. Nanorods – full line, hollow NPs – dotted line and core/shells – dashed line.

Both, UV-vis spectroscopy and TEM imaging cannot give sufficient information about the exact overall size of NPs, including the organic shell and the net charge of the particle. Therefore dynamic light scattering (DLS) and ζ-potential measurements were performed to

determine these parameters (see **chapter 3** for experimental details). Changes in the hydrodynamic diameter between OEG and pep-OEG coated NPs are shown in **Fig. 29**. OEG NPs had an average size of 24.7 ± 1.8 nm, while the average size of P1-OEG NPs was 30.7 ± 0.9 nm. Assuming that the average diameter of the gold core was 15 nm (TEM images, **Fig. 27**), the width of OEG monolayer was calculated at 4.85 nm, while the peptide layer was found to be 3 nm thick. The layers of P2 and P3 octa-peptides had similar thicknesses. A strong negative charge (-27.53 ± 1.5 mV) of OEG coated NPs derived from the presence of carboxylic groups in the organic layer. The net charge of P1-OEG conjugates changed by 4 mV (-23.40 ± 2.3 mV), due to the formation of amide bonds between carboxylic groups from the outer shell of OEG and N-terminus lysines form positively charged peptides. P2-OEG conjugates had a similar ζ-potential, while P3-OEG NPs had slightly lower, which might be a result of a slightly smaller number of peptides attached to each nanoparticle.

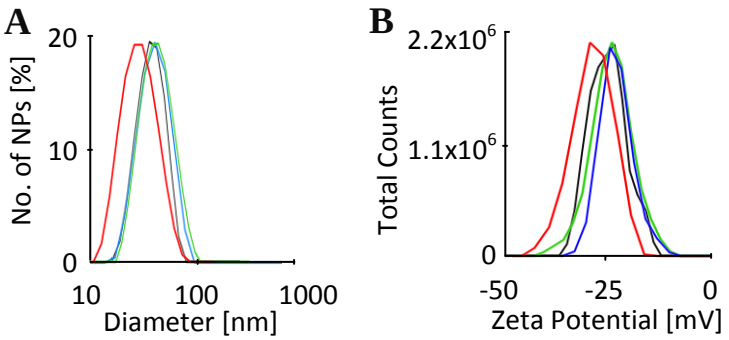

Figure 29. Dynamic light scattering (A) and ζ-potential (B) of: OEG coated NPs – red line, P1-OEG NPs – green line, P2-OEG NPs – blue line and P3-OEG NPs – black line.

This is in a good agreement with quantitative analysis of OEG NPs and pep-OEG NPs. The average number of OEGs attached to each nanoparticle was estimated with Ellman's method [112,113] and the amount of conjugated peptides was found with a lysine specific, FluoroProfile protein quantification kit [114] (see **chapter 3** for experimental details). Overall, it was calculated that 1876 ± 156 OEG ligands (see **Appendix B** for tables with data from 10 independent measurements) were chemisorbed on the surface of 15 nm spherical NPs. An average of 436 ± 44 P1 or P2 and 417 ± 10 P3 octa-peptides was conjugated to the outer shell of each nanoparticle. Variable peptide coverage can be derived from differences in amino acids content between P1 (or P2) and P3 (see **chapter 2** for chemical

structures), possibly affecting the diffusion rate in an aqueous environment and the yield of the coupling reaction [37,115]. P3 peptide consist of 25 % hydrophilic residues and its average hydrophilicity is 0, while P1 and its scrambled (mutated) version P2 contain twice as much (50 %) hydrophilic amino acids, what makes them slightly more hydrophilic (average 0.6). Nevertheless, all three pep-OEG NPs showed equally good water solubility.

Similar measurements (DLS and ζ-potential) and quantification assays were performed on anisotropic core based NPs. DLS and ζ-potential spectra are shown in **Fig. 30**. However, the hydrodynamic width and length of nanorods could not have been measured with this method, due to the difficulty of distinguishing the peaks representing longitudinal axis from the nanorod thickness.

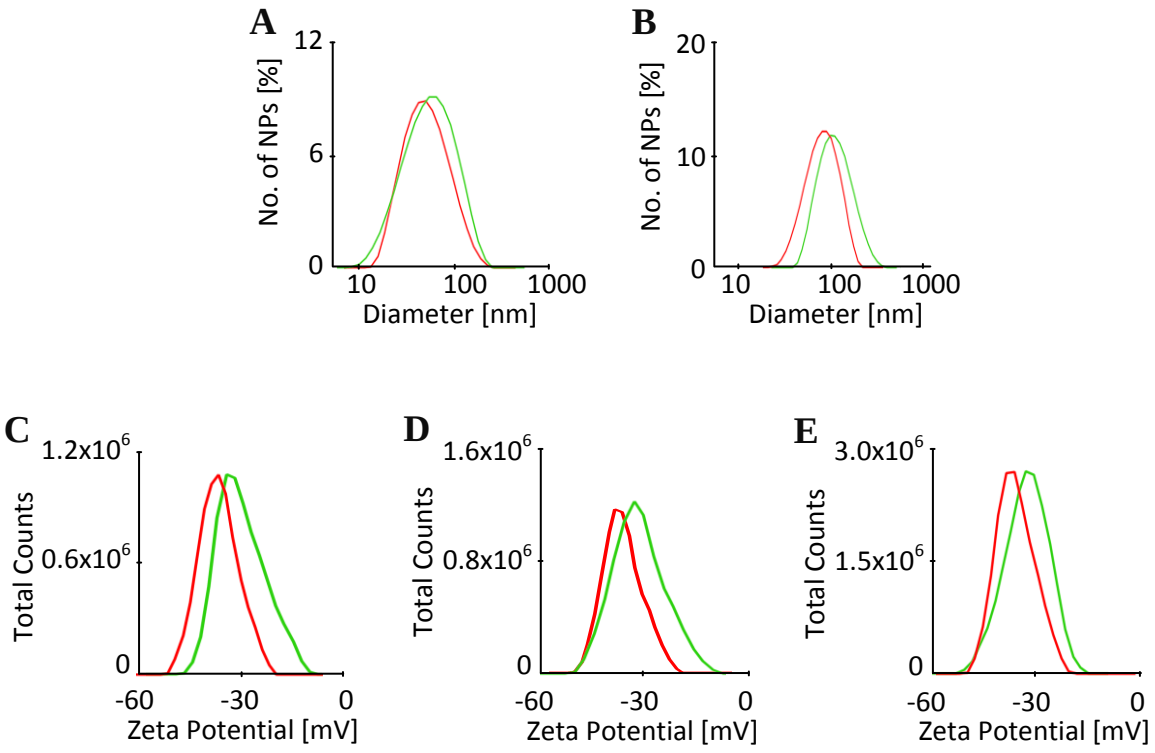

Figure 30. Dynamic light scattering (A – C) and ζ-potential (D – F) of: OEG coated NPs – red line and P1-OEG NPs – green line. Core/shells (A, D), hollow NPs (B, E) and nanorods (C).

The average number of OEGs and P1 peptides attached to anisotropic core based NPs was estimated following Ellman's [112,113] and FluoroProfile [114] methods, respectively. In all cases the number of capping ligands seemed to be sufficient to provide appropriate surface stabilisation. Between 21 to 32 % of the available carboxylic groups on the outer shell of NPs were consumed for the covalent attachment of P1 peptides. This can be

considered as a relatively good reaction yield. All measured and calculated values of spherical and anisotropic NPs are shown in **Table 3**.

Table 3. A summary of physiochemical properties of P1-OEG NPs.

P1-OEG NPs type	Metallic core [nm]	Hydrodynamic diameter [nm]	Net charge [mV]	Number of OEGs	Number of P1s
spherical	15 ± 2	31 ± 1	-23 ± 2	1876 ± 156	436 ± 44
rod-like	16 ± 3/47 ± 3	-	- 26 ± 1	6820 ± 877	1457 ± 149
hollow	92 ± 8/9 ± 3	98 ± 4	-32 ± 2	55871 ± 570	17514 ± 1904
core/shells	43 ± 6/6 ± 3	56 ± 3	-29 ± 2	21368 ± 830	6931 ± 300

Gel electrophoresis was used for qualitative examination of the EDC/s-NHS coupling products to determine the differences in size and net charge between the resulting colloids [96,97] (**Fig. 31**). Notable delay of colloid in lane 4 (**Fig. 31A**) in comparison to OEG NPs (lane 1) and control samples (lanes 2 and 3), indicated successful conjugation of P1 peptides to OEG NPs. There are no significant differences between P1, P2 and P3 pep-OEG NPs (**Fig. 31B**), which indicates similar yields of these coupling reactions, as the sizes and net charges of these colloids are comparable.

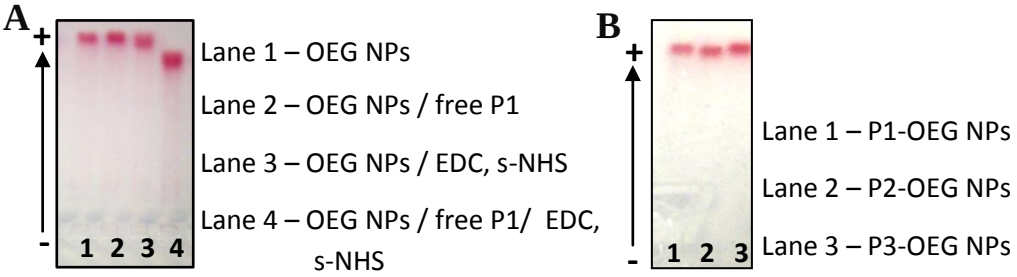

Figure 31. Gel electrophoresis showing: qualitative analysis of EDC/s-NHS coupling (A) and the differences between pep-OEG NPs (B).

Gel electrophoresis was also performed on anisotropic core based OEG and P1-OEG NPs (**Fig. 32**). As expected OEG NPs (lanes 1, 3, 5 and 7) showed higher electrophoretic mobility than P1 conjugates (lanes 2, 4, 6 and 8) and travelled further in the gel for all types the NPs cores. On the other hand, it is evident that the smallest spherical NPs (lanes

1 and 2) migrated the furthest, while the largest hollow NPs (lanes 5 and 6) delayed the most in the gel. Hollow NPs smeared in the gel, rather than migrated as one homogenous band, which can be a size related effect.

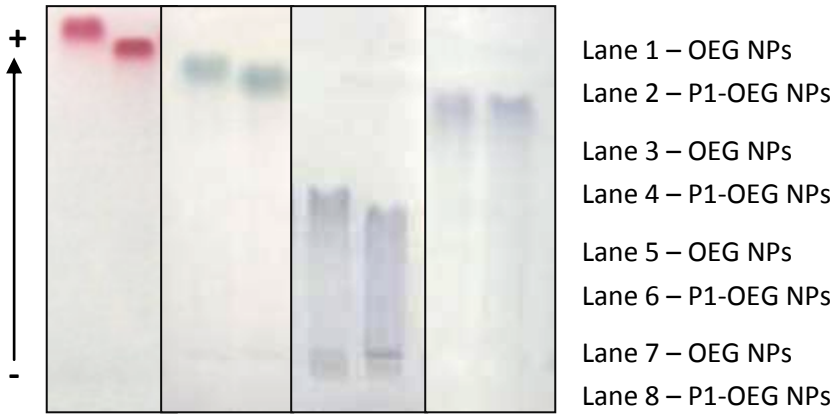

Figure 32. Gel electrophoresis of colloidal gold NPs: spherical (1, 2), rod-like (3, 4), hollow (5, 6) and core/shell NPs (7, 8).

Presence of the fluorescent tag on HiLye-P1-OEG NPs (see **chapter 3** for experimental details) was confirmed by fluorescence spectroscopy (**Fig. 33A**) and gel electrophoresis (**Fig. 33C**). A slight red-shift in the emission spectra of HiLyte-P1-OEG NPs (around 695 nm) in a comparison to free fluorescent dye (680 nm) [116] was observed. This slight shift in emission can be attributed to stretching, deriving from covalent attachment of HiLyte molecules [117]. Distances from 4.85 to 7.85 nm (OEG or P1-OEG layers, respectively) between fluorophore and the gold surface sufficiently prevented quenching of the fluorescent signal. No changes in visible light absorption characteristics (**Fig. 33B**) suggest the HiLyte-P1-OEG NPs remained stable and dispersed in solution after conjugation [21-24,42]. Significant differences in electrophoretic mobility between colloids in lanes 1 ÷ 3 (**Fig. 33C**) provide an additional confirmation of successful conjugation between HiLyte dye molecules and P1-OEG NPs.

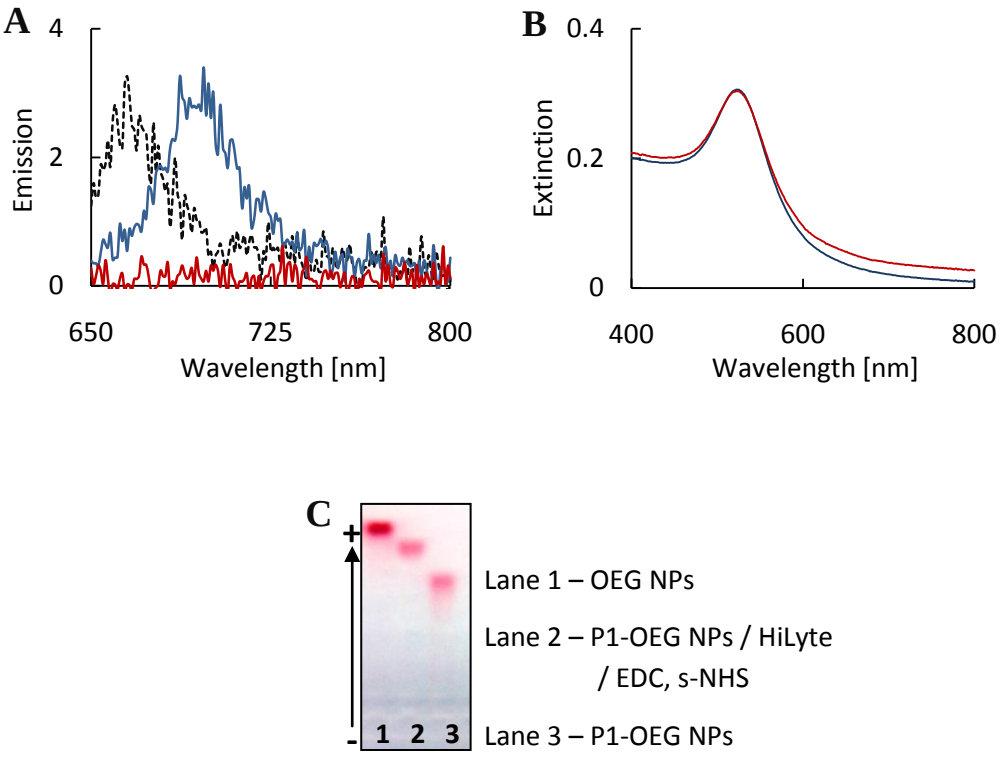

Figure 33. Emission (A) and extinction spectra (B); P1-OEG NPs (red line), HiLyte-P1-OEG NPs (blue line) and free HiLyte dye (black dashed line, emission only). A digital image of a gel electrophoresis (C).

Kamat and co-workers showed that the deactivation of excited states in fluorophore-gold NPs composites most likely derives from electron or energy transfer from fluorophore to the metallic core, or inter-molecular interactions between fluorophores [117]. Within the HiLyte-P1-OEG NPs, the quenching of the fluorescent signal was sufficiently prevented using appropriate selection of critical parameters. Fluorophore molecules were separated from the gold surface (quencher) by 4.85 ÷ 7.85 nm distance created by OEG or OEG-P1 layers. Relatively high flexibility of P1 and hexa-ethylene glycol moieties [7,102,118] in conjunction with discrete positions of HiLyte dyes on the outer shell of the organic corona, prevented inter-molecular quenching of fluorophores. Since, HiLyte dye emits (and is excited) in NIR region, the fluorescent signal could not be disrupted by NPs, absorbing in the visible range.

4.2.3. NPs surface capping with diacetylene based (DA-PEG) ligand.

A new type of capping ligand (DA-PEG, see **chapter 3** for structure) based on diacetylene group was employed in the NPs surface capping [6]. DA-PEGs were attached to the surface of NPs through thiol anchoring groups [35,36] and polymerised by UV-irradiation [91,119,120] (see **chapter 2** for schematic illustration and **chapter 3** for experimental details). Fine packing between neighbouring monomers was assured by the hydrophobic part of DA-PEGs, where long carbon chains interacted with each other *via* van der Waals forces [7,35,36,121,122]. The hydrophilic unit containing oligoethylene glycol ensured water solubility and provided a functional carboxylic group for further modifications [2,7,37,102,103].

The idea to use diacetylene based molecules as NPs capping ligands only recently appeared in the literature, e.g. Dellepiane and co-workers reported that thiolalkyl-diacetylenes can be utilised in the synthesis of small gold NPs in organic solvents [91,120,123,124]. Here, diacetylene based ligands (DA-PEG) were employed in the capping of water soluble 15.5 nm spherical gold NPs (BSPP stabilised; see **section 4.1.1.**).

After photo-polymerisation NPs remained dispersed in solution, showing no sign of aggregation, as can be seen on TEM micrographs (**Fig. 34A** and **C**). No changes in the average diameter of NPs after photo-crosslinking (size distribution histograms, **Fig. 34B** and **D**) indicated that the inorganic core remained stable under the irradiation conditions. Another proof of the core stability comes from the sharpness of the extinction spectrum of photo-polymerised NPs [23,24] (**Fig. 34E** and **F**). Dispersed colloids of typical sizes are indicated by a single extinction peak in the visible spectral range [21-24]. Slight red-shifting in the plasmon band position from 522 to 526 nm (in comparison to BSPP NPs) suggested only minor changes in the refractive index after capping [21,24,42]. The polymerised form of the diacetylene moiety does not show any feature on the UV-vis spectra of colloids, because the extinction coefficient of gold NPs is much higher than of polymerised diacetylenes ($\geq 10^3$) [42,125].

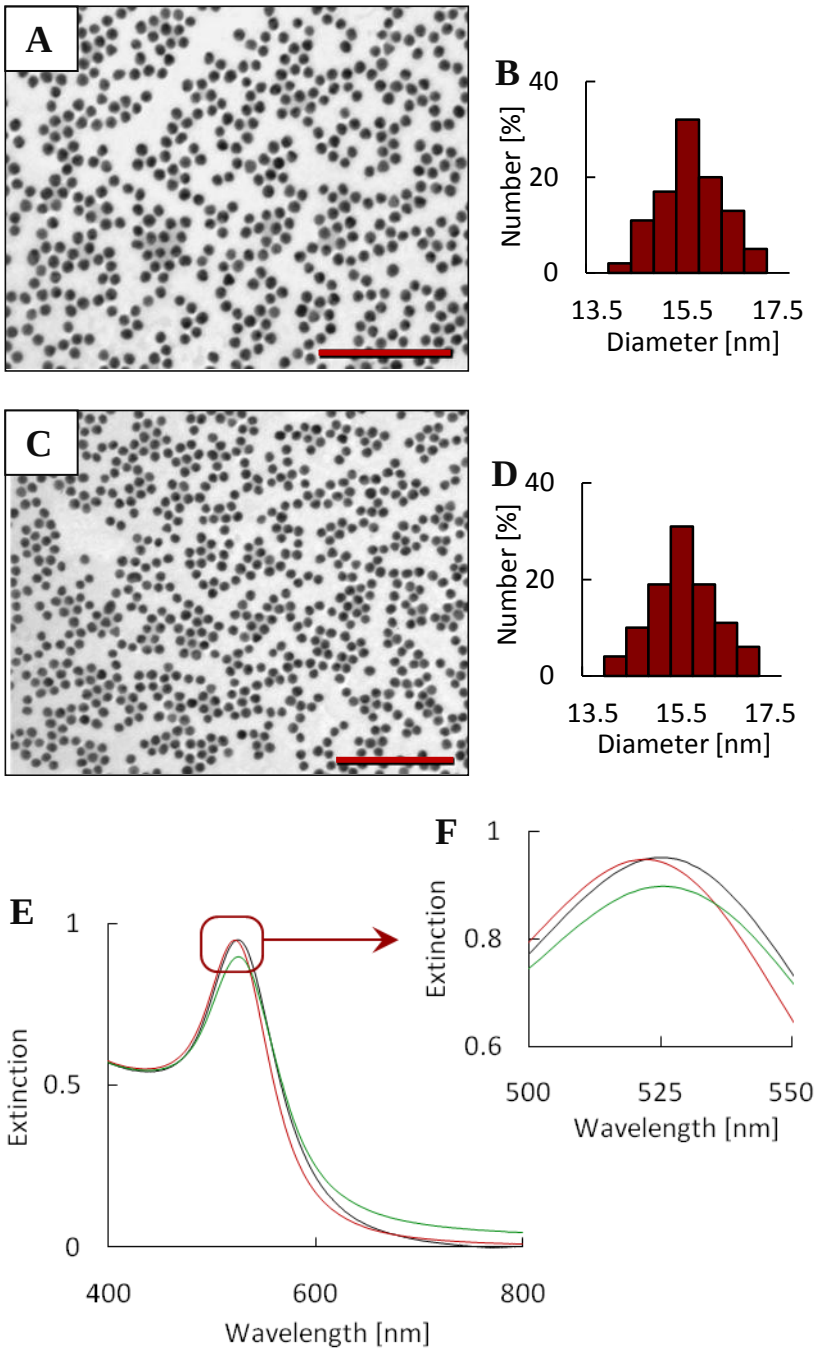

Figure 34. TEM images (A, C), size distribution histograms (B, D) and UV-vis spectra (E, F) of 15.5 ± 1.5 nm, DA-PEG coated gold NPs before (A, B and green line) and after (C, D and black line) UV-polymerisation; BSPP capped NPs – red line. Scale bars are 100 nm.

The overall size of DA-PEG capped NPs (including the organic corona) was determined by DLS, while the net charge by ζ-potential measurements (see **chapter 3** for experimental details). It was possible to detect changes in the hydrodynamic diameter of DA-PEG capped NPs before and after photo-polymerisation (**Fig. 35**). Monomeric NPs

had an average size of 25.9 ± 1.9 nm, while DA-PEG NPs after polymerisation were 24.3 ± 1.0 nm. Assuming that the gold core was 15.5 nm in diameter (from TEM images, **Fig. 34**), the width of the monomeric shell was calculated at 5.2 nm, while the polymeric shell was found to be 4.4 nm thick. The decrease in size of photo-crosslinked NPs can be attributed to stretching and bending of photo-crosslinked poly-diacetylenes in comparison to the monomeric form [91,119,120,123,126,127]. DA-PEG capped NPs were in general negatively charged. The strong charge was derived from the presence of carboxylic groups in the outer shell of ligands. Notable increases in the charge strength of photo-crosslinked NPs (-30.4 ± 1.5 mV) in comparison to unpolymerised NPs (-28.6 ± 1.5 mV) can be attributed to an additional amount of ligands attached to NPs throughout the second step of capping (see **chapter 3** for experimental details).

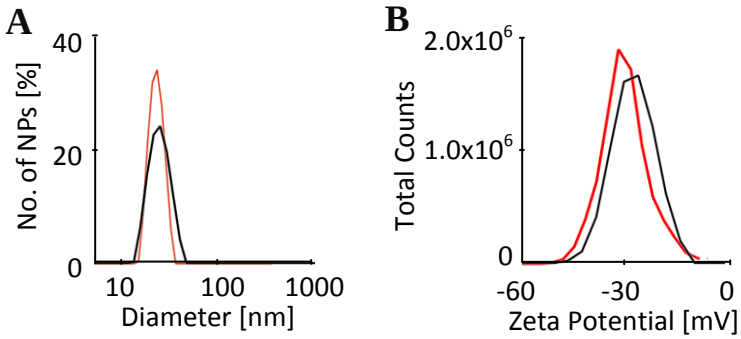

Figure 35. Dynamic light scattering (A) and ζ-potential (B) of DA-PEG coated NPs, before – black line and after – red line photo-polymerisation.

The average number of DA-PEG monomers per each 15.5 ± 1.5 nm nanoparticle was quantified with Ellman's method [112,113] at 2073 ± 250 DA-PEGs (see **chapter 3** for experimental details and **Appendix B** for a table with data from 10 independent measurements). Consequently, more than 80 % of NPs surface was covered with DA-PEG, resulting in high proximity between diacetylene groups. According to the literature, only distances not exceeding 5 Å (Angstrom), lead to successful polymerisation of diacetylenes [119,120]. Polymerisation criteria were met within the presented system, as indicated by surface enhanced Raman spectroscopy (SERS, **Fig. 36**).

The SERS spectrum (**Fig. 36**) of a colloid capped with DA-PEG monomers clearly presented typical fingerprints of the non-polymerised diacetylene group (**b –** diacetylene vibrations; **a –** carbon-carbon triple bonds) [91,120,124]. The polymeric form of DA-PEG can be seen on a SERS spectrum of UV-irradiated colloid (remaining **a** band), while no

characteristic feature can be attributed to the non-polymerised diacetylene stretch (**b**). The additional peak at around 1556 cm^{-1} (**c**) was assigned to carbon-carbon double bond vibrations, produced upon the polymerisation process (see **chapter 2** for schematic illustration). It can be concluded that most of the available diacetylene groups were successfully photo-crosslinked on the surface of NPs. Tight photo-crosslinked shell provided NPs with enhanced stability against aggregation in aqueous environments, as demonstrated by stability tests in the following section.

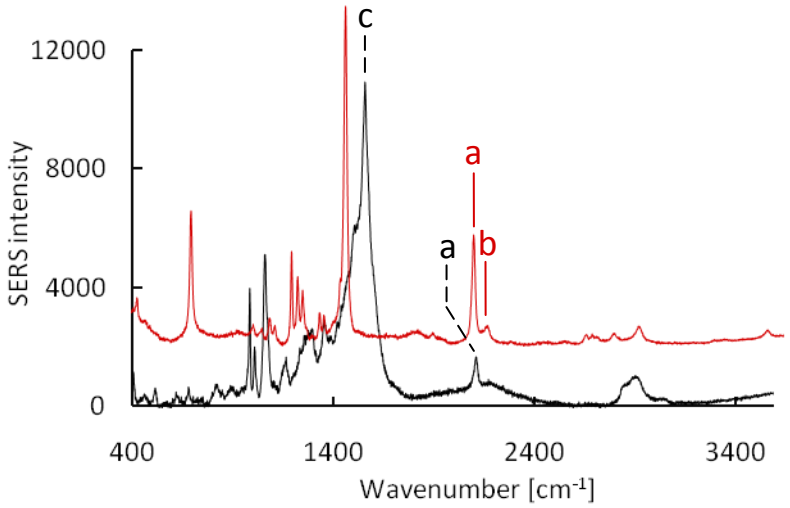

Figure 36. SERS spectra of DA-PEG coated gold NPs before (red line) and after (black line) UV-irradiation, where (a) [2150 cm^{-1}] represents the stretching vibration of carbon-carbon triple bonds, (b) [2257 cm^{-1}] a feature band of the diacetylene group and (c) [1556 cm^{-1}] the stretching vibration of carbon-carbon double bond.

DA-PEG ligands can be employed to coat the surfaces of other types of NPs, e.g. small 2 ÷ 4 nm spherical gold NPs (related publication is listed in **Author's Declaration**) were capped with DA-PEG monomers. In this case however, the polymerisation process was not fully completed. Partial polymerisation was attributed to the high surface curvature of small NPs [118], which possibly resulted in larger distances between neighbouring diacetylene groups (Note: distances between neighbouring monomers are critical for the polymerisation process). Nonetheless, DA-PEG capped NPs both, polymerised (15 nm NPs, see the next section) and partially polymerised (3.25 ± 1.5 nm NPs, see related publication) showed very good stability in aqueous environments.

4.2.4. Stability tests of colloids.

The efficiency of several capping strategies, including BSPP, OEG and DA-PEG ligands in NPs surface stabilisation was assessed [6]. Specifically, capped colloids were exposed to various chemical conditions, including low pH, high concentration of thiol containing molecules and elevated temperatures.

Stability of 15 nm spherical gold NPs coated with BSPP (**A**), OEG (**B**) and DA-PEG (monomeric – **C** and polymerised – **D**) was tested over a wide range of pH (see **chapter 3** for experimental details). Changes in the colour of colloidal solutions upon aggregation [22-24,45,49,128] (blue colour) were observed macroscopically, as shown on a digital image (**Fig. 37**) and by UV-visible spectroscopy (**Fig. 38**).

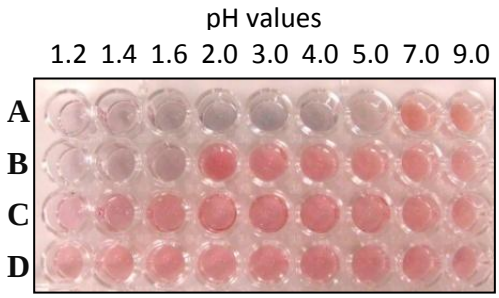

Figure 37. A digital image of gold NPs coated with: BSPP (A), OEG (B), monomeric DA-PEG (C) and polymerised DA-PEG (D). NPs were incubated at various pH for 48 h.

It is evident that at pH lower than 2, DA-PEG was the only ligand capable of providing NPs with sufficient surface stabilisation. It can be hypothesised that enhanced stability of colloids derived from a presence of diacetylene groups, which in conjunction with long carbon chains can maximise the Van der Waals interactions between ligands. This would lead to a higher surface coverage (see **sections 4.2.3.** for physicochemical characterisation) and better stability. Improved stability of polymeric over non-polymerised DA-PEG coated NPs was reviled at pH lower than 1.6. Here, the presence of an additional covalent bond between neighbouring ligands seems to be necessary for the ultimate stabilisation of colloids.

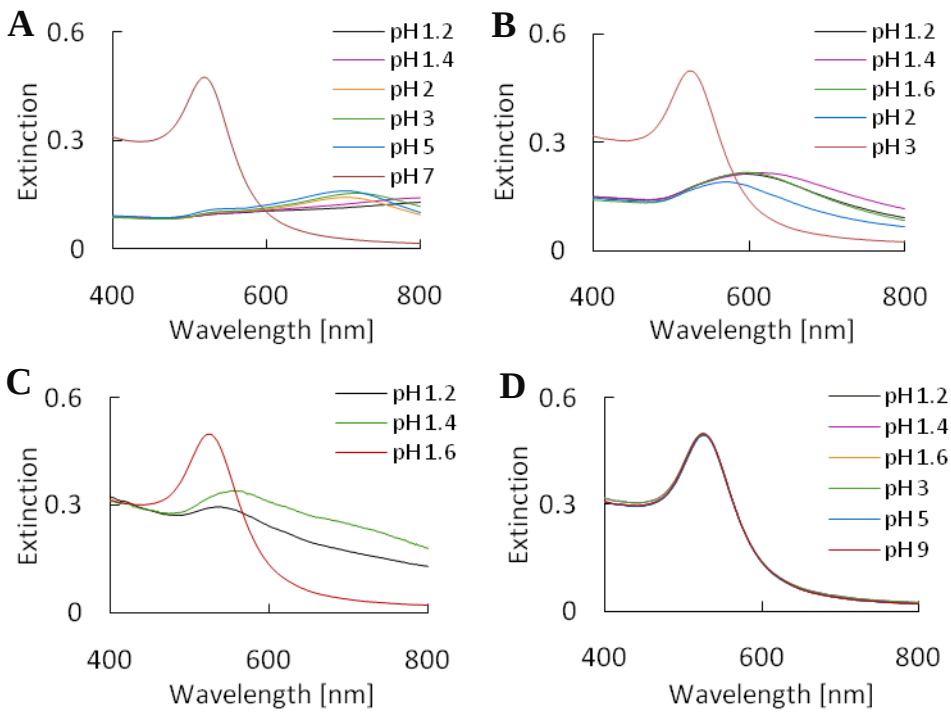

Figure 38. UV-visible spectra of gold NPs coated with: BSPP (A), OEG (B), monomeric DA-PEG (C) and polymerised DA-PEG (D). NPs were incubated at various pH for 48 h.

Stability of colloids against ligand exchange reactions with thiol containing molecules was tested in the presence of 10 % mercaptoethanol at pH 3 to 9 (**Fig. 39**). After 72 h incubation, monomeric DA-PEG NPs (**C**), OEG coated (**B**) and BSPP stabilised NPs (**A**) aggregated, while polymerised DA-PEG NPs (**D**) remained stable. Once again, firm polymeric shell with additional covalent bonds between ligands provided enhanced resistance to thiolated ligands in exchange reactions.

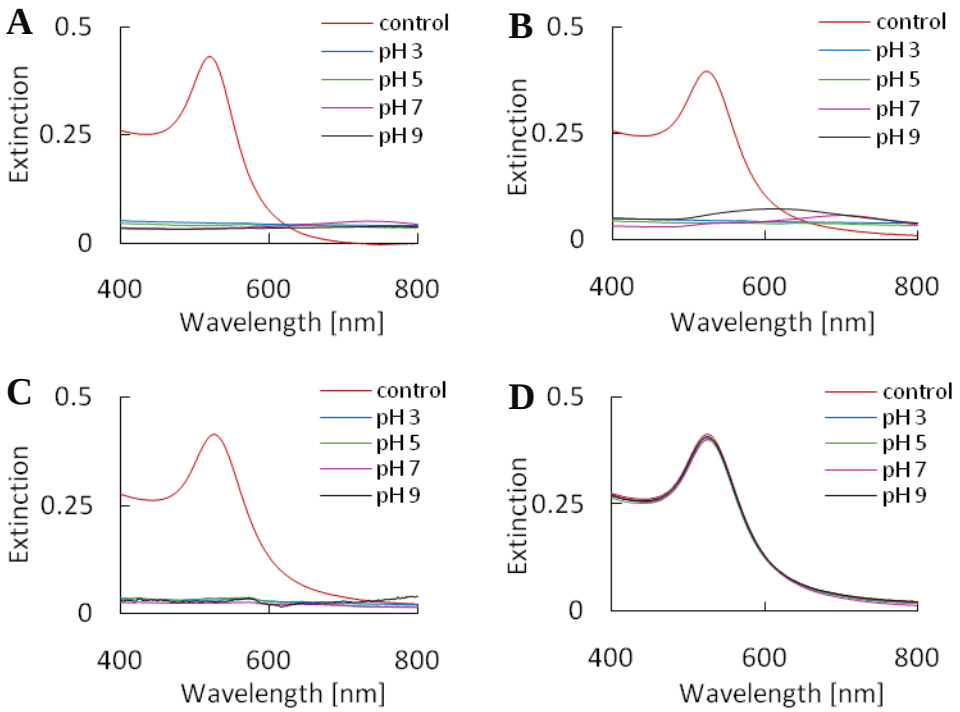

Figure 39. UV-visible spectra of gold NPs coated with: BSPP (A), OEG (B), monomeric DA-PEG (C) and polymerised DA-PEG (D). NPs were incubated with 10 % mercaptoethanol, at various pH for 72 h; control – NPs in water.

In addition to pH and ligand exchange stability tests, temperature stability analysis were performed on the most stable DA-PEG coated polymerised NPs. Repeated heating/cooling and freezing/thawing cycles were carried out (see **chapter 3** for experimental details) and the stability of colloid was monitored by UV-visible spectroscopy (**Fig. 40**). Polymeric DA-PEG NPs remained stable even after five heat/cool (100/25 °C) cycles, as no red-shifting of the plasmon band was observed. DA-PEG capped NPs were also frozen then thawed and showed no sign of aggregation in at least 3 cycles.

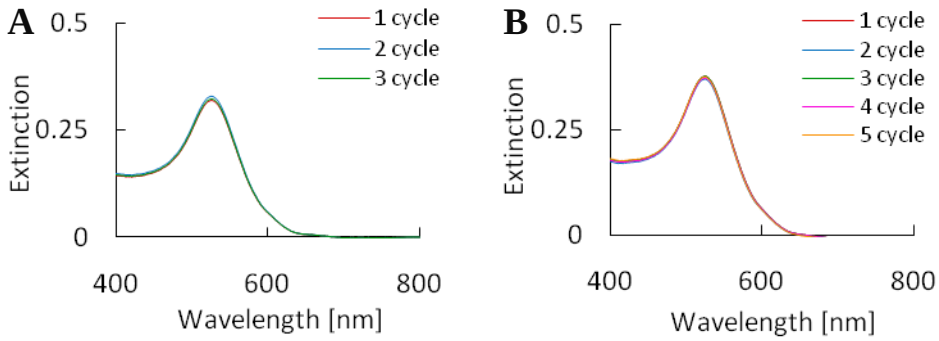

Figure 40. UV-visible spectra of gold NPs coated with polymerised DA-PEG after freeze/thaw (A) and heat/cool (B) cycles.

A variety of capping ligands for NPs surface stabilisation have been reported in recent years, including: oligonucleotides [49,118,129], peptides [4,92,95], lipids [130], polyethylene glycols [102-104,121], silica shells [131] and amphiphilic molecules such as alkylthiols [122], poly(acrylic acid) [132] and poly(maleic anhydride *alt*-1-tetradecene) [133]. However, research efforts were focused on searching for universal capping ligand for the preparation of unconditionally stable colloids. DA-PEG ligand established during this project meets some of the stability criteria. NPs coated with polymerised shell of DA-PEG are stable at elevated temperatures, low pH and in the presence of high concentration of thiols. Despite such enhanced stability, the preparation of DA-PEG capped colloids is fairly simple, fast and does not require any sophisticated equipment (see **chapter 3** for experimental details).

Clearly, polymeric DA-PEG NPs show an opportunity for a number of applications that require storage in a frozen form, reactions at high temperatures or low pH environments. However, NPs capped with other thiolated ligands (e.g. OEG) show satisfactory stability in standard buffered environments, thus can still be utilised in biomedical sciences (see **chapters 5** and **6**).

References:

[1] Gentilini, C.; Evangelista, F.; Rudolf, P.; Franchi, P.; Lucarini, M.; Pasquato, L. *J Am Chem Soc* **2008**, *130*, 15678-15682.

[2] Kanaras, A. G.; Kamounah, F. S.; Schaumburg, K.; Kiely, C. J.; Brust, M. *Chem Commun* **2002**, 20, 2294-2295.

[3] Duchesne, L.; Gentili, D.; Comes-Franchini, M.; Fernig, D. G. *Langmuir* **2008**, *24*, 13572-13580.

[4] Levy, R.; Thanh, N. T. K.; Doty, R. C.; Hussain, I.; Nichols, R. J.; Schiffrin, D. J.; Brust, M.; Fernig, D. G. *J Am Chem Soc* **2004**, *126*, 10076-10084.

[5] Zhang, T.; Ge, J.; Hu, Y.; Yin, Y. *Nano Lett* **2007**, *7*, 3203-3207.

[6] Bartczak, D.; Kanaras, A. G. *Langmuir* **2010**, *26*, 7072-7077.

[7] You, C.-C.; Chompoosor, A.; Rotello, V. M. *Nano Today* **2007**, *2*, 34-43.

[8] Rouhana, L. L.; Jaber, J. A.; Schlenoff, J. B. *Langmuir* **2007**, *23*, 12799-12801.

[9] Nativo, P.; Prior, I. A.; Brust, M. *ACS Nano* **2008**, *2*, 1639-1644.

[10] Jain, P. K.; Huang, X.; El-Sayed, I. H.; El-Sayed, M. A. *Acc Chem Res* **2008**, *41*, 1578-1586.

[11] Rosi, N. L.; Mirkin, C. A. *Chem Rev* **2005**, *105*, 1547-1562.

[12] Murphy, C. J.; Gole, A. M.; Stone, J. W.; Sisco, P. N.; Alkilany, A. M.; Goldsmith, E. C.; Baxter, S. C. *Acc Chem Res* **2008**, *41*, 1721-1730.

[13] Levy, R.; Shaheen, U.; Cesbron, Y.; See, V. *Nano Rev* **2010**, *1*, 4889-4907.

[14] Chen, J.; Wiley, B.; Li, Z. Y.; Campbell, D.; Saeki, F.; Cang, H.; Au, L.; Lee, J.; Li, X.; Xia, Y. *Adv Mater* **2005**, *17*, 2255-2261.

[15] Gil, P. R.; Parak, W. J. *ACS Nano* **2008**, *2*, 2200-2205.

[16] Chen, C. S. *Nat Nano* **2008**, *3*, 13-14.

[17] Sperling, R. A.; Rivera Gil, P.; Zhang, F.; Zanella, M.; Parak, W. J. *Chem Soc Rev* **2008**, *37*, 1896-1908.

[18] Salata, O. V. *J Nanobiotechnology* **2004**, *2*, 3-9.

[19] Gao, J.; Xu, B. *Nano Today* **2009**, *4*, 37-51.

[20] Orendorff, C.; Sau, T.; Murphy, C. *Small* **2006**, *2*, 636-639.

[21] Kelly, K. L.; Coronado, E.; Zhao, L. L.; Schatz, G. C. *J Phys Chem B* **2002**, *107*, 668-677.

[22] Jain, P. K.; Lee, K. S.; El-Sayed, I. H.; El-Sayed, M. A. *J Phys Chem B* **2006**, *110*, 7238-7248.

[23] Kreibig, U.; Vollmer, M. *Optical Properties of Metal Clusters*; Springer: Berlin, **1995**; Vol. 25.

[24] Mie, G. *Ann Phys* **1908**, *330*, 377-445.

[25] Jana, N. R.; Gearheart, L.; Murphy, C. J. *J Phys Chem B* **2001**, *105*, 4065-4067.

[26] Turkevich, J.; Stevenson, P. C.; Hillier, J. *Disc Faraday Soc* **1951**, *11*, 55-75.

[27] Xia, Y.; Xiong, Y.; Lim, B.; Skrabalak, S. *Angew Chem, Int Ed* **2009**, *48*, 60-103.

[28] Nikoobakht, B.; El-Sayed, M. A. *Chem Mater* **2003**, *15*, 1957-1962.

[29] Oldenburg, S. J.; Averitt, R. D.; Westcott, S. L.; Halas, N. J. *Chem Phys Lett* **1998**, *288*, 243-247.

[30] Frens, G. *Nature-Phys Sci* **1973**, *241*, 20-22.

[31] Faraday, M. *Philos Trans R Soc London* **1857**, *147*, 145-181.
[32] Sun, Y.; Xia, Y. *Science* **2002**, *298*, 2176-2179.
[33] Sun, Y.; Xia, Y. *J Am Chem Soc* **2004**, *126*, 3892-3901.
[34] Coomber, D.; Bartczak, D.; Gerrard, S. R.; Tyas, S.; Kanaras, A. G.; Stulz, E. *Langmuir* **2010**, *26*, 13760-13762.
[35] Cortie, M. B.; McDonagh, A. In *Gold Chemistry: Applications and future directions in life sciences*; Mohr, F., Ed.; WILLEY-VCH Verlag GmbH & Co. KGaA Weinheim, **2009**, p 321-343.
[36] Pengo, P.; Pasquato, L. In *The supramolecular chemistry of organic - inorganic hybrid materials*; Rurak, K., Martinez-Manez, R., Eds.; John Wiley & Sons, Inc. : Hoboken, New Jersey, **2010**, p 113-154.
[37] Hermanson, G. T. *Bioconjugate Techniques*; 2nd ed.; Elsevier Inc. , **2008**.
[38] Ji, X.; Song, X.; Li, J.; Bai, Y.; Yang, W.; Peng, X. *J Am Chem Soc* **2007**, *129*, 13939-13948.
[39] Kumar, S.; Gandhi, K. S.; Kumar, R. *Ind Eng Chem Res* **2006**, *46*, 3128-3136.
[40] Turkevich, J.; Stevenson, P. C.; Hillier, J. *J Phys Chem* **1953**, *57*, 670-673.
[41] Day, H. A.; Bartczak, D.; Fairbairn, N.; McGuire, E.; Ardakani, M.; Porter, A. E.; Kanaras, A. G. *CrystEngComm* **2010**, *12*, 4312-4316.
[42] Liu, X.; Atwater, M.; Wang, J.; Huo, Q. *Colloid Surface B* **2007**, *58*, 3-7.
[43] Haiss, W.; Thanh, N. T. K.; Aveyard, J.; Fernig, D. G. *Anal Chem* **2007**, *79*, 4215-4221.
[44] Prasad, B. L. V.; Stoeva, S. I.; Sorensen, C. M.; Klabunde, K. J. *Chem Mater* **2003**, *15*, 935-942.
[45] Burns, C.; Spendel, W. U.; Puckett, S.; Pacey, G. E. *Talanta* **2006**, *69*, 873-876.
[46] Purcell, E. M.; Pennypacker, C. R. *Astrophys J* **1973**, *186*, 705-714.
[47] Yang, J.; Lee, J. Y.; Too, H.-P. *Anal Chim Acta* **2005**, *546*, 133-138.
[48] Schmid, G.; Lehnert, A. *Angew Chem, Int Ed* **1989**, *28*, 780-781.
[49] Loweth, C. J.; Caldwell, W. B.; Peng, X.; Alivisatos, A. P.; Schultz, P. G. *Angew Chem, Int Ed* **1999**, *38*, 1808-1812.
[50] Gole, A.; Murphy, C. J. *Chem Mater* **2004**, *16*, 3633-3640.
[51] Tornblom, M.; Henriksson, U. *J Phys Chem B* **1997**, *101*, 6028-6035.
[52] Liu, M.; Guyot-Sionnest, P. *J Phys Chem B* **2005**, *109*, 22192-22200.
[53] Gans, R. *Ann Phys* **1915**, *352*, 270-284.
[54] Link, S.; El-Sayed, M. A. *J Phys Chem B* **1999**, *103*, 8410-8426.
[55] Kooij, E. S.; Poelsema, B. *Phys Chem Chem Phys* **2006**, *8*, 3349-3357.
[56] Busbee, B.; Obare, S.; Murphy, C. *Adv Mater* **2003**, *15*, 414-416.
[57] Murphy, C. J.; Sau, T. K.; Gole, A. M.; Orendorff, C. J.; Gao, J.; Gou, L.; Hunyadi, S. E.; Li, T. *J Phys Chem B* **2005**, *109*, 13857-13870.
[58] Sau, T. K.; Murphy, C. J. *Philos Mag* **2007**, *87*, 2143-2158.
[59] Orendorff, C. J.; Murphy, C. J. *J Phys Chem B* **2006**, *110*, 3990-3994.
[60] Smith, D. K.; Miller, N. R.; Korgel, B. A. *Langmuir* **2009**, *25*, 9518-9524.
[61] Rayavarapu, R. G.; Ungureanu, C.; Krystek, P.; van Leeuwen, T. G.; Manohar, S. *Langmuir* **2010**, *26*, 5050-5055.
[62] Smith, D. K.; Korgel, B. A. *Langmuir* **2008**, *24*, 644-649.

[63] Pérez-Juste, J.; Pastoriza-Santos, I.; Liz-Marzán, L. M.; Mulvaney, P. *Coord Chem Rev* **2005**, *249*, 1870-1901.
[64] Pérez-Juste, J.; Liz-Marzán, L.; Carnie, S.; Chan, D.; Mulvaney, P. *Adv Func Mater* **2004**, *14*, 571-579.
[65] Halas, N. *Opt Photon News* **2002**, *13*, 26-30.
[66] Westcott, S. L.; Oldenburg, S. J.; Lee, T. R.; Halas, N. J. *Langmuir* **1998**, *14*, 5396-5401.
[67] Arkhireeva, A.; Hay, J. N. *J Mater Chem* **2003**, *13*, 3122-3127.
[68] Van Blaaderen, A.; Van Geest, J.; Vrij, A. *J Colloid Interface Sci* **1992**, *154*, 481-501.
[69] Wu, Y.; Chen, C.; Liu, S. *Anal Chem* **2009**, *81*, 1600-1607.
[70] Stöber, W.; Fink, A.; Bohn, E. *J Colloid Interface Sci* **1968**, *26*, 62-69.
[71] Duff, D. G.; Baiker, A.; Gameson, I.; Edwards, P. P. *Langmuir* **1993**, *9*, 2310-2317.
[72] Duff, D. G.; Baiker, A.; Edwards, P. P. *Langmuir* **1993**, *9*, 2301-2309.
[73] Phonthammachai, N.; Kah, J. C. Y.; Jun, G.; Sheppard, C. J. R.; Olivo, M. C.; Mhaisalkar, S. G.; White, T. J. *Langmuir* **2008**, *24*, 5109-5112.
[74] Halas, N. *MRS Bulletin* **2005**, *30*, 362-368.
[75] Yong, K.-T.; Sahoo, Y.; Swihart, M. T.; Prasad, P. N. *Colloids Surf, A* **2006**, *290*, 89-105.
[76] Hao, E.; Li, S.; Bailey, R. C.; Zou, S.; Schatz, G. C.; Hupp, J. T. *J Phys Chem B* **2004**, *108*, 1224-1229.
[77] Draine, B. T.; Flatau, P. J. *J Opt Soc Am A* **1994**, *11*, 1491-1499.
[78] O'Neal, D. P.; Hirsch, L. R.; Halas, N. J.; Payne, J. D.; West, J. L. *Cancer Lett* **2004**, *209*, 171-176.
[79] Lu, X.; Tuan, H.-Y.; Chen, J.; Li, Z.-Y.; Korgel, B. A.; Xia, Y. *J Am Chem Soc* **2007**, *129*, 1733-1742.
[80] Skrabalak, S. E.; Chen, J.; Sun, Y.; Lu, X.; Au, L.; Cobley, C. M.; Xia, Y. *Acc Chem Res* **2008**, *41*, 1587-1595.
[81] Chen, J.; McLellan, J. M.; Siekkinen, A.; Xiong, Y.; Li, Z.-Y.; Xia, Y. *J Am Chem Soc* **2006**, *128*, 14776-14777.
[82] Lee, G.-J.; Shin, S.-I.; Kim, Y.-C.; Oh, S.-G. *Mater Chem Phys* **2004**, *84*, 197-204.
[83] Au, L.; Lu, X.; Xia, Y. *Adv Mater* **2008**, *20*, 2517-2522.
[84] Skrabalak, S. E.; Au, L.; Li, X.; Xia, Y. *Nat Protocols* **2007**, *2*, 2182-2190.
[85] Hu, M.; Chen, J.; Li, Z.-Y.; Au, L.; Hartland, G. V.; Li, X.; Marquez, M.; Xia, Y. *Chem Soc Rev* **2006**, *35*, 1084-1094.
[86] Siekkinen, A. R.; McLellan, J. M.; Chen, J.; Xia, Y. *Chem Phys Lett* **2006**, *432*, 491-496.
[87] Cobley, C.; Skrabalak, S.; Campbell, D.; Xia, Y. *Plasmonics* **2009**, *4*, 171-179.
[88] Wang, H.; Qiao, X.; Chen, J.; Wang, X.; Ding, S. *Mater Chem Phys* **2005**, *94*, 449-453.
[89] Chen, J.; Saeki, F.; Wiley, B. J.; Cang, H.; Cobb, M. J.; Li, Z.-Y.; Au, L.; Zhang, H.; Kimmey, M. B.; Li; Xia, Y. *Nano Lett* **2005**, *5*, 473-477.

[90] Alloisio, M.; Demartini, A.; Cuniberti, C.; Dellepiane, G.; Muniz-Miranda, M.; Giorgetti, E. *Vib Spectrosc* **2008**, *48*, 53-57.
[91] Alloisio, M.; Demartini, A.; Cuniberti, C.; Petrillo, G.; Thea, S.; Giorgetti, E.; Giusti, A.; Dellepiane, G. *J Phys Chem C* **2006**, *111*, 345-353.
[92] Wang, Z.; Levy, R.; Fernig, D. G.; Brust, M. *Bioconjug Chem* **2005**, *16*, 497-500.
[93] Alam, M. R.; Maeda, M.; Sasaki, S. *Nucleic Acids Symp Ser (Oxf)* **1999**, *42*, 173-174.
[94] Alam, M. R.; Maeda, M.; Sasaki, S. *Bioorg Med Chem* **2000**, *8*, 465-473.
[95] Lévy, R. *ChemBioChem* **2006**, *7*, 1141-1145.
[96] Sperling, R.; Pellegrino, T.; Li, J.; Chang, W.; Parak, W. *Adv Funct Mater* **2006**, *16*, 943-948.
[97] Hanauer, M.; Pierrat, S.; Zins, I.; Lotz, A.; Sonnichsen, C. *Nano Lett* **2007**, *7*, 2881-2885.
[98] Seeman, N. C. *Nano Lett* **2010**, *10*, 1971-1978.
[99] Sharma, J.; Chhabra, R.; Cheng, A.; Brownell, J.; Liu, Y.; Yan, H. *Science* **2009**, *323*, 112-116.
[100] Park, S. Y.; Lytton-Jean, A. K. R.; Lee, B.; Weigand, S.; Schatz, G. C.; Mirkin, C. A. *Nature* **2008**, *451*, 553-556.
[101] Zheng, J.; Constantinou, P. E.; Micheel, C.; Alivisatos, A. P.; Kiehl, R. A.; Seeman, N. C. *Nano Lett* **2006**, *6*, 1502-1504.
[102] Liu, Y.; Shipton, M. K.; Ryan, J.; Kaufman, E. D.; Franzen, S.; Feldheim, D. L. *Anal Chem* **2007**, *79*, 2221-2229.
[103] Wuelfing, W. P.; Gross, S. M.; Miles, D. T.; Murray, R. W. *J Am Chem Soc* **1998**, *120*, 12696-12697.
[104] Eck, W.; Craig, G.; Sigdel, A.; Ritter, G.; Old, L. J.; Tang, L.; Brennan, M. F.; Allen, P. J.; Mason, M. D. *ACS Nano* **2008**, *2*, 2263-2272.
[105] Chan, W. C. W.; Nie, S. *Science* **1998**, *281*, 2016-2018.
[106] Kim, J. G.; Mengna, X.; Hanli, L. *IEEE Eng Med Biol* **2005**, *24*, 118-121.
[107] Prahl, S. Optical Absorption of Hemoglobin. **1999**, http://omlc.ogi.edu/spectra/hemoglobin/ Oregon Medical Laser Center Oregon (last accessed: 04-09-2010).
[108] Hale, G. M.; Querry, M. R. *Appl Opt* **1973**, *12*, 555-563.
[109] Huang, X.; Neretina, S.; El-Sayed, M. A. *Adv Mater* **2009**, *21*, 4880-4910.
[110] Huang, X.; Jain, P.; El-Sayed, I.; El-Sayed, M. *Lasers Med Sci* **2008**, *23*, 217-228.
[111] Link, S.; El-Sayed, M. A. *Int Rev Phys Chem* **2000**, *19*, 409-453.
[112] Ellman, G. L. *Arch Biochem Biophys* **1959**, *82*, 70-77.
[113] Riddles, P. W.; Blakeley, R. L.; Zerner, B. *Anal Biochem* **1979**, *94*, 75-81.
[114] Sigma-Aldrich. FluoroProfile Protein Quantification Kit TECHNICAL BULLETIN http://www.sigmaaldrich.com/etc/medialib/docs/Sigma/Bulletin/fp0010bul.Par.0001.File.tmp/fp0010bul.pdf (last accessed 13-09-2010).
[115] INNOVAGEN. Peptide property calculator. **2010**, http://www.innovagen.se/custom-peptide-synthesis/peptide-property-calculator/peptide-property-calculator.asp (last accessed: 11-09-2010).

[116] AnaSpec. HiLyte Fluor™ 680 amine, Product Data Sheet. http://www.anaspec.com/pdfs/81262.pdf (last accessed 14-09-2010).
[117] Thomas, K. G.; Kamat, P. V. *Acc Chem Res* **2003**, *36*, 888-898.
[118] Hill, H. D.; Millstone, J. E.; Banholzer, M. J.; Mirkin, C. A. *ACS Nano* **2009**, *3*, 418-424.
[119] Kricheldorf, H. R.; Schwarz, G. *Handbook of Polymer Synthesis*; Marcel Dekker Inc.: New York, **1992**.
[120] Alloisio, M.; Demartini, A.; Cuniberti, C.; Muniz-Miranda, M.; Giorgetti, E.; Giusti, A.; Dellepiane, G. *Phys Chem Chem Phys* **2008**, *10*, 2214-2220.
[121] Kanaras, A. G.; Kamounah, F. S.; Schaumburg, K.; Kiely, C. J.; Brust, M. *Chem Commun* **2002**, 2294-2295.
[122] Brust, M.; Fink, J.; Bethell, D.; Schiffrin, D. J.; Kiely, C. *J Chem Soc, Chem Commun* **1995**, 1655-1656.
[123] Demartini, A.; Alloisio, M.; Cuniberti, C.; Dellepiane, G.; Jadhav, S. A.; Thea, S.; Giorgetti, E.; Gellini, C.; Muniz-Miranda, M. *J Phys Chem C* **2009**, *113*, 19475-19481.
[124] Alloisio, M.; Demartini, A.; Cuniberti, C.; Dellepiane, G.; Muniz-Miranda, M.; Giorgetti, E. *Vib Spectrosc* **2008**, *48*, 53-57.
[125] Deschamps, J.; Balog, M.; Boury, B.; Ben Yahia, M.; Filhol, J.-S.; van der Lee, A.; Al Choueiry, A.; Barisien, T.; Legrand, L.; Schott, M.; Dutremez, S. G. *Chem Mater* **2010**, *22*, 3961-3982.
[126] Song, J.; Cheng, Q.; Stevens, R. C. *Chem Phys Lipids* **2002**, *114*, 203-214.
[127] Jung, Y. K.; Kim, T. W.; Kim, J.; Kim, J. M.; Park, H. G. *Adv Funct Mater* **2008**, *18*, 701-708.
[128] Slocik, J. M.; Zabinski, J. S.; Phillips, D. M.; Naik, R. R. *Small* **2008**, *4*, 548-551.
[129] Yin, Y.; Alivisatos, A. P. *Nature* **2005**, *437*, 664-670.
[130] Dubertret, B.; Skourides, P.; Norris, D. J.; Noireaux, V.; Brivanlou, A. H.; Libchaber, A. *Science* **2002**, *298*, 1759-1762.
[131] Mine, E.; Yamada, A.; Kobayashi, Y.; Konno, M.; Liz-Marzán, L. M. *J Colloid Interface Sci* **2003**, *264*, 385-390.
[132] Hussain, I.; Brust, M.; Papworth, A. J.; Cooper, A. I. *Langmuir* **2003**, *19*, 4831-4835.
[133] Di Corato, R.; Quarta, A.; Piacenza, P.; Ragusa, A.; Figuerola, A.; Buonsanti, R.; Cingolani, R.; Manna, L.; Pellegrino, T. *J Mater Chem* **2008**, *18*, 1991-1996.

5. Cellular fate of OEG NPs.

As emphasised in the introductory part of the thesis (**chapter 1**), key motivation of this research was to achieve highly controllable regulation of biological functions in selected type of mammalian cells (HUVECs) with colloidal gold NPs. The first mile stone towards realisation of this aim was to identify and understand the basic mechanisms controlling common interactions between colloids and HUVECs.

Hence, the use of OEG capped NPs (Note: synthesis and physicochemical characterisation of OEG capped colloidal NPs was demonstrated in **chapter 4**). These NPs can interact with cells only in a non-selective manner, since no molecules showing any biological activity were incorporated in the capping layer [1-7] (see **Scheme 34**). The employed mono-layer of OEG provides NPs with a strong negative charge, which determines the cellular fate of the colloid [8]. As will be demonstrated in this chapter, OEG NPs were taken-up by cells. To realise how the uptake rate is affected by other parameters, e.g. size and shape of NPs, four types of OEG capped NPs were employed in these studies: spherical gold NPs (SP, 15 ± 2 nm), gold nanorods (NR, 16 ± 3 / 47 ± 3 nm), hollow gold NPs (HG, 92 ± 8 / 9 ± 3 nm) and silica/gold core/shell nanostructures (CS, 43 ± 7 / 6 ± 3 nm). Previously, 15 nm SP have been used to investigate the interactions of NPs with various types of cells [1,2,5,6,8-17]. Consequently, OEG capped SP served here as a 'reference' NPs for an easier comparison with the literature data.

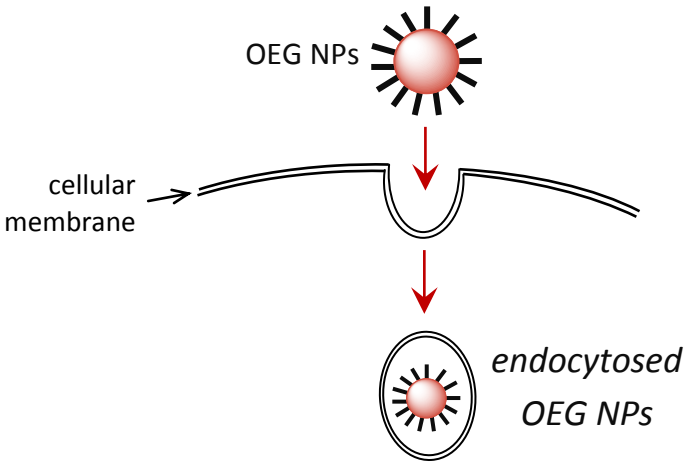

Scheme 34. Schematic illustration of non-specific uptake of OEG NPs by HUVECs.

Chen and co-workers demonstrated that the uptake of NPs (citrate stabilised, spherical gold NPs) by HeLa cells (see **chapter 2** for more information about HeLa) reached a plateau after 4 ÷ 7 h of treatment [9]. Based on these findings, the minimal 4 h treatment time of HUVECs with OEG NPs was selected. Cells were treated with OEG capped SP, NR, HG or CS in serum containing (20 % serum proteins – full-serum) growth media ($5 \cdot 10^{12}$ NPs in 1 ml; see **chapter 3** for more details). After treatment with NPs cells were either imaged live with an inverted light microscope (OEG SP only), or fixed and imaged with a transmission electron microscope (all types of NPs). For electron microscopy purposes cells were fixed according to the protocol described in **chapter 3**.

TEM micrographs of HUVECs incubated with OEG coated SP are shown in **Fig. 41**. NPs were taken-up by the cells, since they are confined within cytoplasmic vesicles (**circles**); most likely endosomes [17,18]. The well-preserved double membrane of these vesicles is indicated by arrows. There are no OEG SP outside endosomes 'free' in the cytoplasm. Since OEG SP did not contain any bioactive molecules, specific interactions between them and the cells were unlikely to happen. Consequently, non-selective (charge mediated) endocytosis can be considered as the most probable pathway of internalisation. The internalisation of colloidal NPs by mammalian cells by engulfing with the cellular membrane (endocytosis) was previously reported by many research groups [6-9,12,17-24].

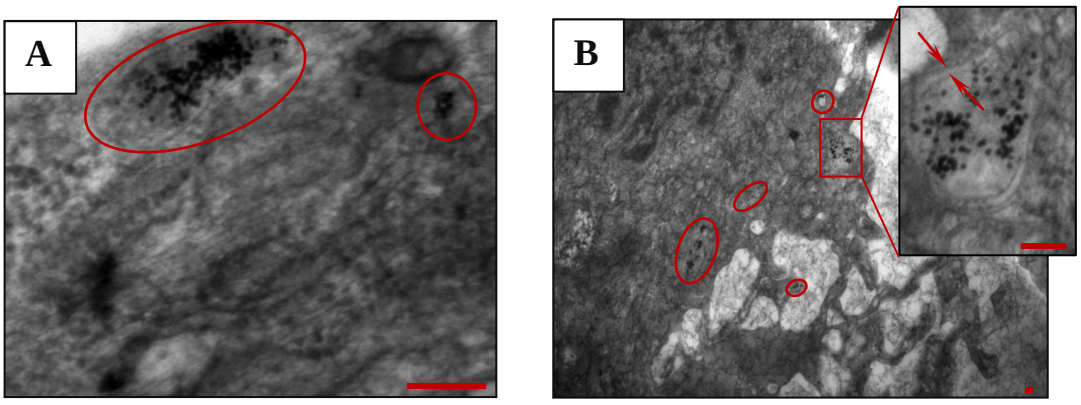

Figure 41. TEM images of HUVECs after 4 h incubation with OEG coated NPs (A and B). Circles represent NPs locked inside the organelles. A square indicates magnified area of an image (B, insert). Double membrane is shown by arrows. Scale bars are 100 nm.

High ionic strength and acidic pH can be found within intra-cellular vesicles, like endosomes [25]. In the endosomes, thiolated biomolecules, e.g. proteins or peptides can

also be present [25,26] (Note: side chain of cysteine contains thiol group, which can bind to gold surface [27-29]; see **chapter 2** for theoretical background). Such conditions can affect the stability of colloids, in extreme cases leading to aggregation and changes in NPs properties (e.g. optical signatures) [30-33]. Pacey and co-workers observed colour changes of citrate stabilised gold SP solutions from red to blue (aggregation) deriving from the adsorption of various cationic salts [32]. Brust and co-workers reported the uptake of citrate stabilised gold SP by HeLa cells and their aggregation within endosomes [17]. In both cases, instability of gold colloids in biological environments derived from insufficient (electrostatic) NPs surface stabilisation with sodium citrate. To enhance the stability against aggregation of gold NPs, their surfaces can be capped covalently [27,28,30], e.g. with OEG ligand (see **chapter 2** for schematic illustration and **chapter 3** for experimental details). As demonstrated in **chapter 4**, OEG capped NPs remain stable in buffered and low pH (down to pH 3) environments. Therefore, it was expected that the OEG capping layer would provide NPs with sufficient stability against aggregations inside endosomes.

Within endosomes, mostly single (non-aggregated) OEG SP were found (TEM images, **Fig. 41**). However, larger groups and/or agglomerates of NPs were also denoted. The presence of these on TEM micrographs can be explained by NPs overlaying on two dimensional images. In theory, up to four OEG SP (hydrodynamic diameter around 25 nm, see **chapter 4**) can be fitted on top of each other in 100 nm thick cell sections, which were imaged by TEM (see **chapter 3** for experimental methods). To verify whether observed groups of NPs are indeed just overlaid NPs, or rather real aggregates, colour changes of uptaken NPs were observed (Note: changes in NPs colour suggest aggregation [31-34]). The simplest method involved macroscopic observations of the cell suspension. A more advanced technique based on phase contrast and bright field microscopy of cells grown on a surface was also employed (see **chapter 3** for experimental details).

A digital image of HUVECs suspension after treatment with OEG SP is shown in **Fig. 42**. Prior to imaging, cells (with NPs) were washed with buffer (until the solution was colourless) to remove excess of non-internalised (or non-interacting) OEG NPs, then harvested from the culture dish and suspended in a buffered solution (see **chapter 3** for experimental details). Differences between untreated cells (**left**) and cells, which have uptaken NPs (**right**) are evident. Reddishness of the cell suspension, indicating the presence of stable NPs [33,35,36], was perceivable to the naked-eye. Since colloidal gold has a high extinction coefficient value [35,37] ($\varepsilon = 3.64 \cdot 10^8$ for 15 nm SP), even pico-molar

(pM) concentration of OEG SP can be detected. Possibly, the colour intensity of cells loaded with NPs was additionally enhanced, due to increased local concentration of OEG NPs within endosomes.

Figure 42. A digital image of HUVECs suspension: control sample (cells only, left) and cells treated with OEG coated NPs for 4 h (right).

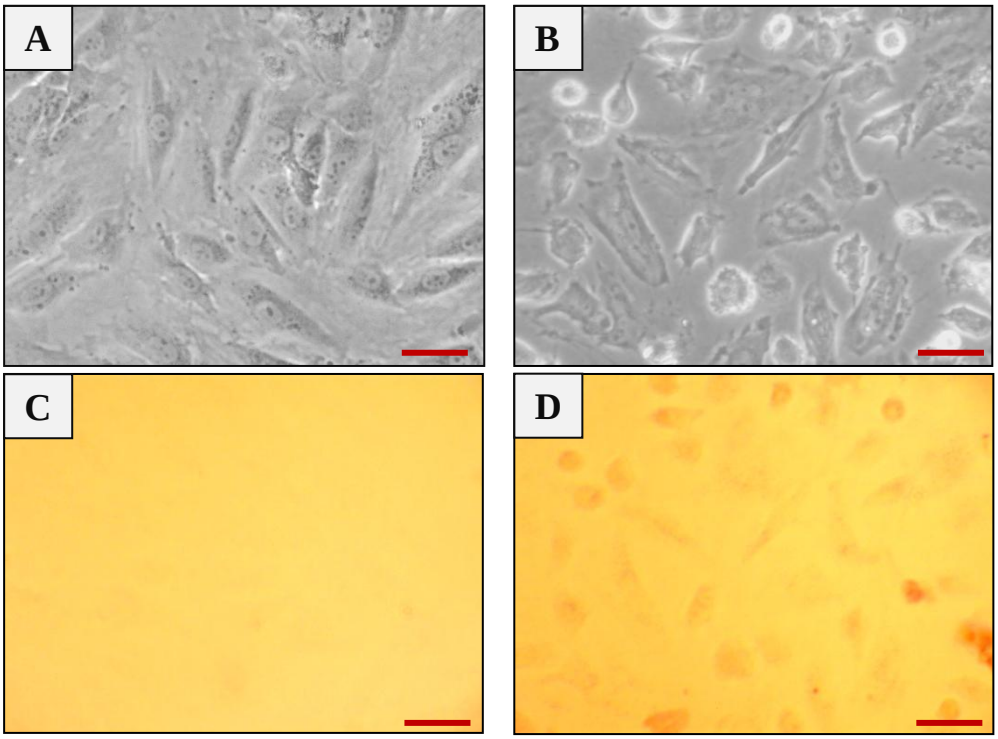

Figure 43. Phase contrast (A and B) and bright field (C and D) images of HUVECs after 4 h treatment with: OEG coated NPs (B and D); control sample (HUVECs only, A and C). Scale bars are 10 μm.

Moreover, the intense colour of HUVECs (with associated NPs) was observed by light microscopy techniques. The quantity of endocytosed OEG coated NPs was high enough to permit detection by bright field microscopy. Phase contrast images of cells and bright field images of the same area of the culture dish are presented in **Fig. 43**. The differences

between control sample (**C**) and HUVECs loaded with NPs (**D**) are evident. The red colour (**D**) deriving from uptaken OEG NPs indicated that NPs remained stable within cellular matrix [32,33,35,36].

As suggested recently by Levy and co-workers, even though there are many reports on the uptake of NPs by cells, some questions regarding the role of basic parameters such as: size, shape and surface chemistry of NPs, still remain answered [6]. Consequently, additional experiments following systematic approaches were recommended. Following this idea, after the uptake of OEG SP and the colloidal stability inside endosomes were confirmed, the studies were extended to other types of NPs. The intracellular fate of OEG capped anisotropic core based NPs (NR, HG and CS) in HUVECs was investigated. As shown on TEM images (**Fig. 44A** and **B**), OEG NR were taken-up by HUVECs. Double membrane surrounding NR is clearly presented on the image **A**, suggesting that OEG NR were locked inside organelles (endosomes). As in case of OEG SP, endocytosis would be the most likely cell entry pathway. Interestingly, it seems that the orientation of OEG NR within vesicles was random. Some nanorods were aligned horizontally to the TEM grid and appeared as elongated structures on the image (**white circle**), while others were lined-up vertically, giving the impression of more spherical shape (**orange circle**).

OEG HG were also taken-up by HUVECs (TEM images, **Fig. 44C** and **D**). A double membrane (arrows) surrounding NPs, suggesting their presence in the endosomal vesicles, was well preserved. As expected, the fourth type of NPs: OEG CS was also confirmed inside HUVECs by the TEM microscopy (**Fig. 44E** and **F**). It is clear that NPs were confined within organelles (**arrows**), even though the double membrane was not clearly presented. Also, endocytosis seemed to be the most probable explanation of entrance route into the cells by both, OEG HG and OEG CS.

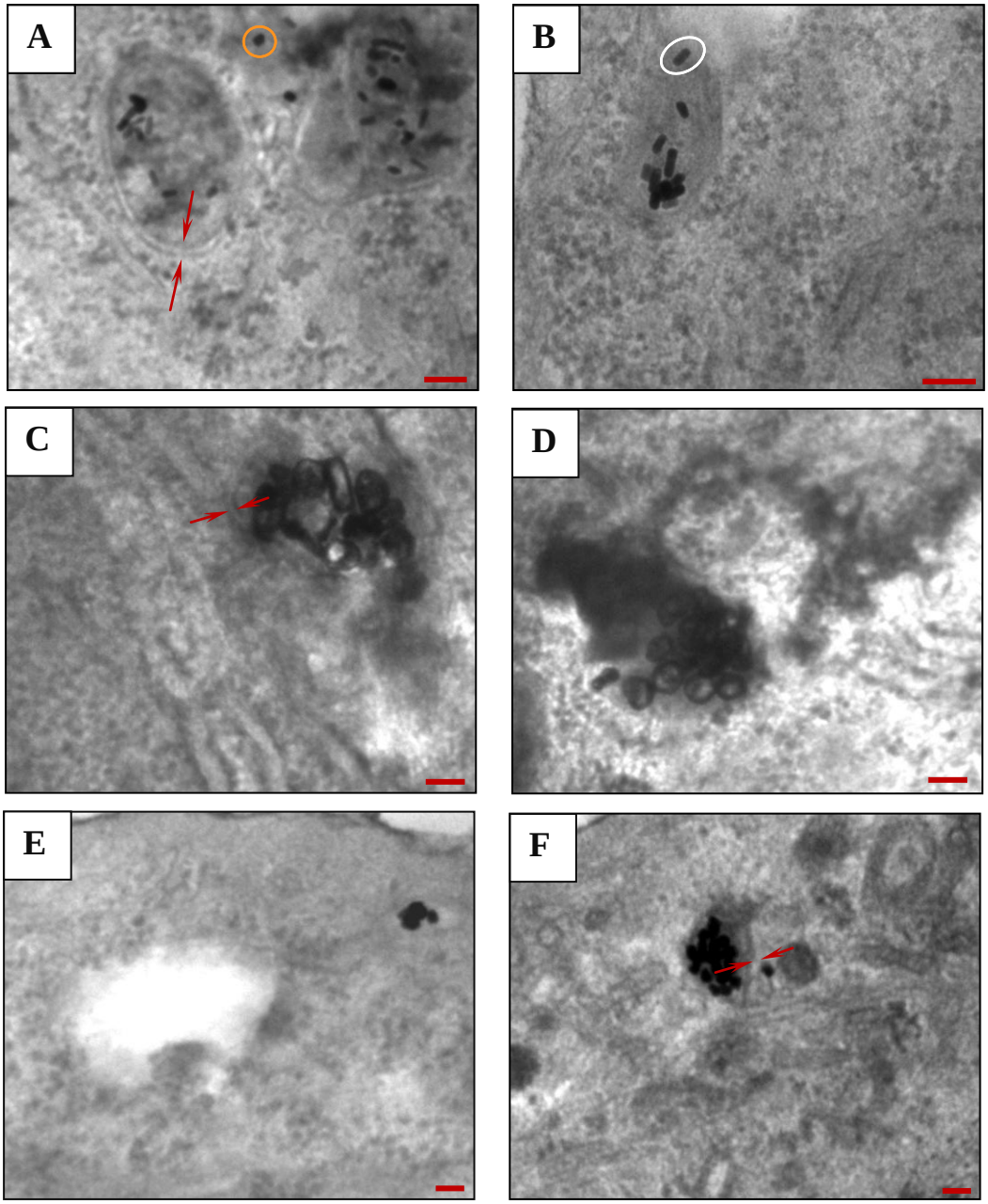

Figure 44. TEM images of HUVECs after 4 h incubation with OEG NR (A and B), OEG HG (C and D) and OEG CS (E and F). Double membrane is indicated by arrows. White circle represents NR aligned horizontally, while orange circle – vertically. Scale bars are 100 nm.

As seen from the TEM images above, the number of vesicles per cell, as well as the number of NPs locked within each endosome varied. Only thin (around 100 nm, see **chapter 3** for experimental details) slices of cells were imaged at a time (around 1 % of a cell). Due to these reasons, it was unlikely to foresee the average number of uptaken NPs (per cell) with high accuracy, based only on statistical analysis of TEM images. Therefore,

another relevant, relatively simple and efficient technique: inductively coupled plasma mass spectrometry (ICP-MS, see **chapter 3** for more experimental details) was used [38]. First, the number of cells in the sample was counted (100'000 cells). The number of gold atoms per nanoparticle and the weight of a single nanoparticles were calculated (e.g. 105'448 gold atoms, equals to $3.45 \cdot 10^{-17}$ g per 15 nm spherical NPs, see **Appendix B** for detailed calculations also for other types of NPs), while the weight of gold atoms in the sample was given by ICP-MS (ppm). Taking the weight of gold atoms in the nanoparticle and the weight of gold atoms in the sample, the number of NPs in the sample was calculated, then divided by the number of cells in the sample, to give the number of NPs in each cell. The results from three independent experiments are shown in **Table 4**.

It is widely accepted that the cellular ability to uptake NPs depends on the size, shape and the net charge of NPs (positive, negative or neutral) [2,6-9,12,17-19,21,24,39-42]. Here, all types of OEG coated NPs were negatively charged, however larger NPs (e.g. OEG HG) had a slightly stronger charge than smaller ones (e.g. OEG SP). This can be attributed to a larger number of OEG ligands chemisorbed on the surface of larger HG (see **Table 4** and **chapter 4** for physicochemical characterisation). It seems that strongly charged OEG HG (-40 mV) were taken-up by HUVECs less effectively than OEG SP (-28 mV). One can hypothesise that the stronger negative charge of HG makes it difficult for them to physically approach the cells, probably because HG were repelled (even stronger than OEG SP) from negatively charged cellular membrane of HUVECs [9,42]. However, these differences in the charge strength between NPs can be treated as minor and not necessarily considered as a predominantly controlling constraint. OEG NPs were significantly varied in other parameters, e.g. size and shape (**Table 4**). These two parameters (rather than the charge strength) probably play a dominating role in regulating of the uptake rate.

The smallest, OEG SP (hydrodynamic diameter around 25 nm) were most efficiently taken-up by HUVECs, while the largest OEG HG (96 nm) the least. On the other hand, OEG NR were endocytosed in much larger numbers than OEG CS with a diameter comparable to the NR length. The uptake rate of OEG NR and OEG SP with the same diameter as the NR width was similar.

Table 4. A summary of physiochemical properties of OEG NPs.

OEG NPs type	Metallic core [nm]	Hydrodynamic diameter [nm]	Net charge [mV]	Number of NPs per cell
spherical	15 ± 2	25 ± 2	-28 ± 2	2551 ± 343
rod-like	16 ± 3/47 ± 3	-	-30 ± 1	2486 ± 460
hollow	92 ± 8/9 ± 3	96 ± 4	-40 ± 2	363 ± 82
core/shells	44 ± 7/6 ± 3	51 ± 3	-36 ± 2	901 ± 99

Chan and co-workers were investigating the shape dependent differences in the uptake of citrate stabilised gold NPs by HeLa cells and found that, NR (14 x 74 nm) were taken-up less efficiently than both, 14 or 74 nm SP [9,21]. Chan's group performed a direct comparison between NR and their spherical length and width equivalents [9,21]. They found that HeLa took-up 500 and 375 % more of 74 and 14 nm SP than 74 x 14 nm rods, respectively. The much lower uptake of NR was attributed to the CTAB capping layer, which may be toxic to cells. Chan's group also reported that 50 nm spherical gold citrate capped NPs were taken-up by HeLa cells more efficiently that 14 nm and 74 nm SP, also the uptake rate reached its half-life the fastest [9,21]. In case of HUVECs (**Table 4**), 50 nm (core/shells) were taken-up more efficiently than the largest NPs (HG), but less efficiently than the smallest 15 nm NPs. Only slightly higher uptake rate of OEG NR, than their length equivalent (OEG CS), was observed. While, very similar numbers of OEG NR and their width equivalent (OEG SP) were internalised by HUVECs. Such variations can be explained by: a) the differences in cell type physiology (Note: HUVECs are primary culture cells, healthy mammalian non-malignant cells, as opposed to an immortalised and transformed cell line, like HeLa [43-45]); b) the differences in charge strength within OEG NPs and/or c) the type of NPs surface capping layer (here OEG). This hypothesis is supported by more recent literature reports, demonstrating the dependence of the uptake rate on the composition of the organic corona of NPs and the type of cells [2,3,5,6,9,11,14,15,17,19-21,23,24,40-42,46-53].

Several groups have investigated the differences in NPs uptake that derive from their functionality, e.g. Ghandehari and co-workers demonstrated that the uptake of 30 ÷ 90 nm 'bare' gold SP (meaning citrate capped, natively charged) by prostate cancer cells (PC-3)

was much higher than 'PEGylated' ones (meaning polyethylene glycol coated) [19]. On the contrary, Brust and co-workers reported that 'PEGylated' 16 nm SP (meaning 1-mercaptoundec-11-yl tetraethylene glycol coated) were not taken-up by HeLa cells at all and showed that the same NPs but citrate or CALNN capped were endocytosed very effectively [17]. The differences in the uptake of 'PEGylated' NPs observed by Ghandehari's and Brust's groups can be attributed to the cell type (PC-3 and HeLa, respectively). Mirkin and co-workers investigated the differences in NPs uptake deriving purely from the cell type [14]. They tested the uptake of antisense oligonucleotide modified 13 nm gold SP (ASNPs) by a mouse cell line (C-166) and two human cell models (HeLa and A594). It was found that NPs were taken-up by all three cell types, but the absolute number of uptaken NPs varied by a factor of 20.

The closest example of studies showing the behaviour of HUVECs in contact with NPs, is the work reported by McGrath's group on 100 nm polystyrene SP, with various functional groups attached to the outer shell of the capping layer (e.g. carboxylic, methyl, lysine) [23]. It was demonstrated that the uptake rate of 'carboxy' NPs was the highest (up to 200 NPs per cell after 80 h of incubation), presumably because of the adsorption of serum proteins – albumin (Note: the adsorption of serum proteins was also demonstrated by Mirkin for ASNPs [14]). McGrath reported that the proteins stayed adsorbed to NPs even after a wash [23]. On the contrary, ζ-potential measurements of OEG capped NPs (**Fig. 45**) after 24 h incubation with growth medium (20 % human serum, see **chapter 3** for cell culturing protocol) and one wash (1 x PBS, centrifugation/decantation: 16'400 rpm, 15 min.) did not show any changes in the net charge, which could have been assigned to the presence of serum proteins. Consequently, it can be hypothesised that a very firm organic shell formed by OEG ligands (see **chapter 4** for physicochemical characterisation and stability tests), sufficiently prevented the adsorption of serum proteins on the surface of gold NPs. However, proteins can still interact with the negatively charged outer shell of OEG capping layer (e.g. weak electrostatic interactions), while NPs are suspended in a growth media (before wash and centrifugation steps).

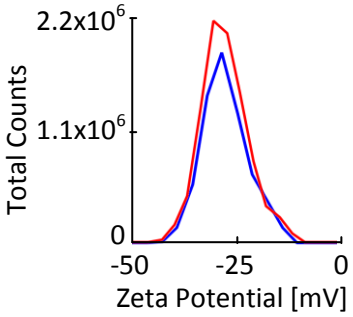

Figure 45. ζ-potential of: OEG coated NPs (red line) and OEG coated NPs incubated with growth media (blue line).

Another method of controlling the uptake rate of NPs, is to coat their surface with appropriate biomolecules, e.g. cell penetrating peptides [16,17,54,55], proteins [5,21,56,57], antibodies [1,58-60], bacterial toxins [6], oligonucleotides [14,61] or liposomes [62,63]. A good example would be a family of octa-peptides, as developed during this research (see **chapter 2** for chemical structures). High control upon the cellular fate of colloids was gained (see the following chapter) with octa-peptide conjugated OEG NPs (pep-OEG NPs), even though pep-OEG NPs showed very similar physicochemical properties and varied only in the amino acid arrangement (see **chapter 4** for physicochemical characterisation).

Referrences:

[1] Eck, W.; Craig, G.; Sigdel, A.; Ritter, G.; Old, L. J.; Tang, L.; Brennan, M. F.; Allen, P. J.; Mason, M. D. *ACS Nano* 2008, *2*, 2263-2272.

[2] Liu, Y.; Shipton, M. K.; Ryan, J.; Kaufman, E. D.; Franzen, S.; Feldheim, D. L. *Anal Chem* 2007, *79*, 2221-2229.

[3] Gao, J.; Xu, B. *Nano Today* 2009, *4*, 37-51.

[4] Salata, O. V. *J Nanobiotechnology* 2004, *2*, 3-9.

[5] You, C.-C.; Chompoosor, A.; Rotello, V. M. *Nano Today* 2007, *2*, 34-43.

[6] Levy, R.; Shaheen, U.; Cesbron, Y.; See, V. *Nano Rev* 2010, *1*, 4889-4907.

[7] Decuzzi, P.; Ferrari, M. *Biomaterials* 2007, *28*, 2915-2922.

[8] Minchin, R. *Nat Nano* 2008, *3*, 12-13.

[9] Chithrani, B. D.; Ghazani, A. A.; Chan, W. C. W. *Nano Lett* 2006, *6*, 662-668.

[10] Krpetic, Z.; Nativo, P.; Porta, F.; Brust, M. *Bioconjug Chem* 2009, *20*, 619-624.

[11] Hosta-Rigau, L.; Olmedo, I.; Arbiol, J.; Cruz, L. J.; Kogan, M. J.; Albericio, F. *Bioconjug Chem* 2010, *21*, 1070-1078.

[12] Jiang, W.; Kim, B. Y. S.; Rutka, J. T.; Chan, W. C. W. *Nat Nano* 2008, *3*, 145-150.

[13] Huang, Y.-F.; Liu, H.; Xiong, X.; Chen, Y.; Tan, W. *J Am Chem Soc* 2009, *131*, 17328-17334.

[14] Giljohann, D. A.; Seferos, D. S.; Patel, P. C.; Millstone, J. E.; Rosi, N. L.; Mirkin, C. A. *Nano Lett* 2007, *7*, 3818-3821.

[15] Dixit, V.; Van den Bossche, J.; Sherman, D. M.; Thompson, D. H.; Andres, R. P. *Bioconjug Chem* 2006, *17*, 603-609.

[16] de la Fuente, J. M.; Berry, C. C. *Bioconjug Chem* 2005, *16*, 1176-1180.

[17] Nativo, P.; Prior, I. A.; Brust, M. *ACS Nano* 2008, *2*, 1639-1644.

[18] Zhang, S.; Li, J.; Lykotrafitis, G.; Bao, G.; Suresh, S. *Adv Mater* 2009, *21*, 419-424.

[19] Arnida; Malugin, A.; Ghandehari, H. *J Appl Toxicol* 2010, *30*, 212-217.

[20] Mandal, D.; Maran, A.; Yaszemski, M.; Bolander, M.; Sarkar, G. *J Mater Sci: Mater Med* 2009, *20*, 347-350.

[21] Chithrani, B. D.; Chan, W. C. W. *Nano Lett* 2007, *7*, 1542-1550.

[22] Connor, E.; Mwamuka, J.; Gole, A.; Murphy, C.; Wyatt, M. *Small* 2005, *1*, 325-327.

[23] Ehrenberg, M. S.; Friedman, A. E.; Finkelstein, J. N.; Oberdörster, G.; McGrath, J. L. *Biomaterials* 2009, *30*, 603-610.

[24] Liu, R.; Kay, B. K.; Jiang, S.; Chen, S. *MRS Bulletin* 2009, *34*, 432-440.

[25] Pierre J., C. *Endocytosis: from cell biology to health, disease and therapy*; Springer-Verlag: Berlin, 1992.

[26] See, V.; Free, P.; Cesbron, Y.; Nativo, P.; Shaheen, U.; Rigden, D. J.; Spiller, D. G.; Fernig, D. G.; White, M. R. H.; Prior, I. A.; Brust, M.; Lounis, B.; Levy, R. *ACS Nano* 2009, *3*, 2461-2468.

[27] Pengo, P.; Pasquato, L. In *The supramolecular chemistry of organic - inorganic hybrid materials*; Rurak, K., Martinez-Manez, R., Eds.; John Wiley & Sons, Inc. : Hoboken, New Jersey, 2010, p 113-154.

[28] Cortie, M. B.; McDonagh, A. In *Gold Chemistry: Applications and future directions in life sciences*; Mohr, F., Ed.; WILLEY-VCH Verlag GmbH & Co. KGaA Weinheim, 2009, p 321-343.
[29] Levy, R.; Thanh, N. T. K.; Doty, R. C.; Hussain, I.; Nichols, R. J.; Schiffrin, D. J.; Brust, M.; Fernig, D. G. *J Am Chem Soc* 2004, *126*, 10076-10084.
[30] Bartczak, D.; Kanaras, A. G. *Langmuir* 2010, *26*, 7072-7077.
[31] Slocik, J. M.; Zabinski, J. S.; Phillips, D. M.; Naik, R. R. *Small* 2008, *4*, 548-551.
[32] Burns, C.; Spendel, W. U.; Puckett, S.; Pacey, G. E. *Talanta* 2006, *69*, 873-876.
[33] Mie, G. *Ann Phys* 1908, *330*, 377-445.
[34] Kelly, K. L.; Coronado, E.; Zhao, L. L.; Schatz, G. C. *J Phys Chem B* 2002, *107*, 668-677.
[35] Jain, P. K.; Lee, K. S.; El-Sayed, I. H.; El-Sayed, M. A. *J Phys Chem B* 2006, *110*, 7238-7248.
[36] Kreibig, U.; Vollmer, M. *Optical Properties of Metal Clusters*; Springer: Berlin, 1995; Vol. 25.
[37] Liu, X.; Atwater, M.; Wang, J.; Huo, Q. *Colloid Surface B* 2007, *58*, 3-7.
[38] Scheffer, A.; Engelhard, C.; Sperling, M.; Buscher, W. *Anal Bioanal Chem* 2008, *390*, 249-252.
[39] Verma, A.; Uzun, O.; Hu, Y.; Hu, Y.; Han, H.-S.; Watson, N.; Chen, S.; Irvine, D. J.; Stellacci, F. *Nat Mater* 2008, *7*, 588-595.
[40] Semmler-Behnke, M.; Kreyling, W. G.; Lipka, J.; Fertsch, S.; Wenk, A.; Takenaka, S.; Schmid, G.; Brandau, W. *Small* 2008, *4*, 2108-2111.
[41] Hauck, T.; Ghazani, A.; Chan, W. *Small* 2008, *4*, 153-159.
[42] Green, J. J.; Chiu, E.; Leshchiner, E. S.; Shi, J.; Langer, R.; Anderson, D. G. *Nano Lett* 2007, *7*, 874-879.
[43] Michiels, C. *J Cell Physiol* 2003, *196*, 430-443.
[44] Masters, J. R. W.; Palsson, B. O. *Human Cell Culture*, 1999.
[45] Masters, J. R. *Nat Rev Cancer* 2002, *2*, 315-319.
[46] Bastus, N. G.; Sanchez-Tillo, E.; Pujals, S.; Farrera, C.; Lopez, C.; Giralt, E.; Celada, A.; Lloberas, J.; Puntes, V. *ACS Nano* 2009, *3*, 1335-1344.
[47] Chen, J.; Wiley, B.; Li, Z. Y.; Campbell, D.; Saeki, F.; Cang, H.; Au, L.; Lee, J.; Li, X.; Xia, Y. *Adv Mater* 2005, *17*, 2255-2261.
[48] Cheng, J.; Teply, B. A.; Sherifi, I.; Sung, J.; Luther, G.; Gu, F. X.; Levy-Nissenbaum, E.; Radovic-Moreno, A. F.; Langer, R.; Farokhzad, O. C. *Biomaterials* 2007, *28*, 869-876.
[49] Huff, T. B.; Hansen, M. N.; Zhao, Y.; Cheng, J.-X.; Wei, A. *Langmuir* 2007, *23*, 1596-1599.
[50] Gil, P. R.; Parak, W. J. *ACS Nano* 2008, *2*, 2200-2205.
[51] Choi, M.-R.; Stanton-Maxey, K. J.; Stanley, J. K.; Levin, C. S.; Bardhan, R.; Akin, D.; Badve, S.; Sturgis, J.; Robinson, J. P.; Bashir, R.; Halas, N. J.; Clare, S. E. *Nano Lett* 2007, *7*, 3759-3765.
[52] Hirak, K. P.; Shuvojit, B.; Utpal, C.; Prabir, L.; Anjan Kr, D. *Nanomedicine* 2007, *3*, 111-119.
[53] Jain, P. K.; El-Sayed, I. H.; El-Sayed, M. A. *Nano Today* 2007, *2*, 18-29.

[54] Oyelere, A. K.; Chen, P. C.; Huang, X.; El-Sayed, I. H.; El-Sayed, M. A. *Bioconjug Chem* 2007, *18*, 1490-1497.
[55] Rhee, M.; Davis, P. *J Biol Chem* 2006, *281*, 1233-1240.
[56] Buranda, T.; Jones, G. M.; Nolan, J. P.; Keij, J.; Lopez, G. P.; Sklar, L. A. *J Phys Chem B* 1999, *103*, 3399-3410.
[57] Li, J. L.; Day, D.; Gu, M. *Adv Mater* 2008, *20*, 3866-3871.
[58] El-Sayed, I. H.; Huang, X.; El-Sayed, M. A. *Nano Lett* 2005, *5*, 829-834.
[59] Sokolov, K.; Follen, M.; Aaron, J.; Pavlova, I.; Malpica, A.; Lotan, R.; Richards-Kortum, R. *Cancer Res* 2003, *63*, 1999-2004.
[60] Au, L.; Zheng, D.; Zhou, F.; Li, Z.-Y.; Li, X.; Xia, Y. *ACS Nano* 2008, *2*, 1645-1652.
[61] Dhar, S.; Daniel, W. L.; Giljohann, D. A.; Mirkin, C. A.; Lippard, S. J. *J Am Chem Soc* 2009, *131*, 14652-14653.
[62] Dubertret, B.; Skourides, P.; Norris, D. J.; Noireaux, V.; Brivanlou, A. H.; Libchaber, A. *Science* 2002, *298*, 1759-1762.
[63] Park, S.-H.; Oh, S.-G.; Mun, J.-Y.; Han, S.-S. *Colloid Surface B* 2006, *48*, 112-118.

6. Cell targeting and regulation with pep-OEG NPs.

As explained in **chapter 2**, within the human body, interior layers of blood vessels in the circulatory system are formed by endothelial cells [1-3]. These cells are involved in important biological processes, including: the formation of blood vessels (angiogenesis and vasculogenesis), maintaining blood homeostasis, as well as regulating and being a part of the immune response against pathogens [2,4-7]. New blood vessels (angiogenesis), are grown during physiological processes (e.g. wound healing), but also in many pathological developments, like cancer [2,5,7-9]. Tumour progression, according to literature reports, can be suppressed by angiogenesis regulation [5,7,9-18].

In the presented research gold NPs were employed to achieve selective regulation of angiogenesis. NPs were designed to target endothelial cells (HUVECs) *via* membrane receptors, specifically VEGFR-1 and NRP-1. Selective targeting of VEGFR-1 or NRP-1 was achieved with synthetic peptides attached to NPs (see **section 6.1.**). VEGFR-1 was chosen because of its anti-apoptotic and pro-angiogenic functions [5,7,19-25]. Its selective targeting is a challenging task, since this receptor is less abundant than e.g. VEGFR-2. NRP-1 serves as a co-receptor regulating the formation of VEGFR-1-ligand complexes [5,7,19,23,24,26-28].

As described in **chapter 3**, NPs were prepared by standard wet chemistry methods, then capped with OEG ligand and further functionalised with peptides (see **chapter 4** for results). Each of the peptides: P1, P2 or P3 showed similar length, charge and hydrophilicity, but was comprised of a unique primary structure (see **chapter 2** for chemical structures). Different sequences of P1, P2 and P3 determined their bioactivity. P1 peptide (wild type) showed binding affinity towards VEGFR-1 (see **section 6.1.1.** for flow cytometry studies), while P3 preferably bound to NRP-1. P2 peptide (mutant), a scrambled version of P1 could not form any active complexes with VEGFR-1 (see **chapter 2** for theoretical background).

Once selective binding of pep-OEG NPs to HUVECs was confirmed by transmission electron microscopy (**section 6.1.2.**), the cellular response following the binding event was studied (**section 6.2.**). A capability of pep-OEG NPs to activate or inhibit basic cellular functions was studied at the molecular level (gene expression profiling assay, **section 6.2.1.**) and by *in vitro* angiogenesis (capillaries formation assay, **section 6.2.2.**). See **Scheme 35** for schematic illustration of the scientific content of this chapter.

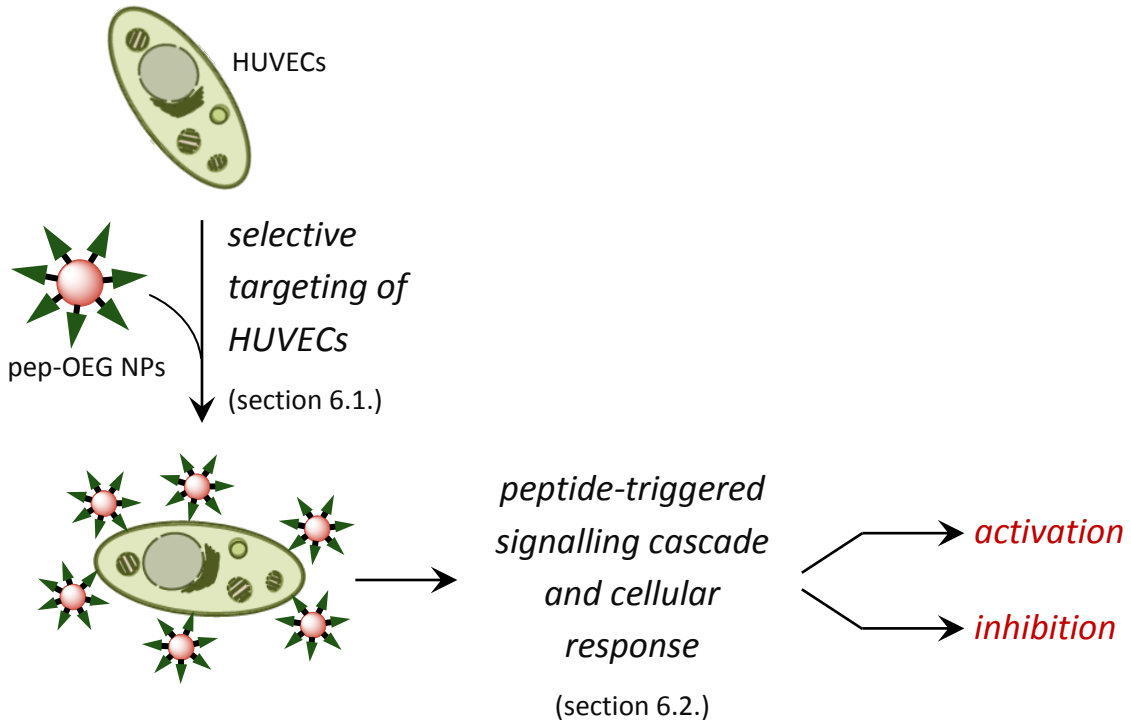

Scheme 35. Schematic illustration of selective targeting of HUVECs with pep-OEG NPs resulting in controlled regulation of cellular functions.

6.1. Selective targeting of HUVECs.

HUVECs were targeted with NPs through octa-peptides (incorporated in the organic corona of NPs). The level of selectivity (specificity) in binding of P1 and its mutated version (P2), as well as P1-OEG NPs to membrane receptors over-expressed by HUVECs was assessed by flow cytometry assays (**section 6.1.1.**). Once binding activity of the peptides was confirmed, the cellular fate of P1-OEG NPs, P2-OEG NPs and P3-OEG NPs in HUVECs was studied by transmission electron microscopy. Differences between specific (P1 or P3 mediated) and non-specific (P2 mediated) interactions between cells and NPs are demonstrated in **section 6.1.2**.

6.1.1. Cell receptors binding.

To assess whether the newly designed artificial P1 octa-peptide exhibited binding affinity towards VEGFR-1 receptors, the peptide was labelled with a LL-RPE fluorescent tag [29] (see **chapter 3** for experimental details) and employed in flow cytometry assays. P1-LL-RPE conjugates were incubated with live HUVECs, to allow binding to appropriate

cellular receptors. The selectivity of binding was studied in a series of competition experiments with untagged P1 and with respect to untreated cells. HUVECs labelled with P1-LL-RPE conjugates were excited at 488 nm wavelength. The orange channel was used to detect fluorescent signal and count positive cells. Both, fluorescence intensity and the mean values were presented as one parameter, called the binding index (BI, see **chapter 3** for subsequent equation).

To study only receptor mediated interactions between HUVECs and fluorescent conjugates, while eliminating non-specific interactions between them and a charged cellular membrane, cells were blocked with serum proteins [30-32] (FBS, see **chapter 3** for experimental details). HUVECs were incubated with conjugates on ice to avoid uptake of P1-LL-RPE and in the presence of sodium azide to prevent receptor circulation within cells [33-36].

Overlaid, LL-RPE intensity spectra and binding indexes are shown in **Fig. 46**. It is evident that P1-LL-RPE were bound to HUVECs with high affinity, as BI of conjugates was 100 % referred to 0.5 % background coming from unlabelled cells. The competition for binding sites allocated on the cellular membrane of HUVECs with free (unlabelled) P1 resulted in a significant decrease of the BI value. This indicated that P1-LL-RPE conjugates and P1 peptides bind to the same spots on the cellular membrane in a sequence specific manner (P1 mediated). It can be hypothesised that as designed, VEGFR-1 were indeed the binding sites for P1 sequence (RPL motif [37]).

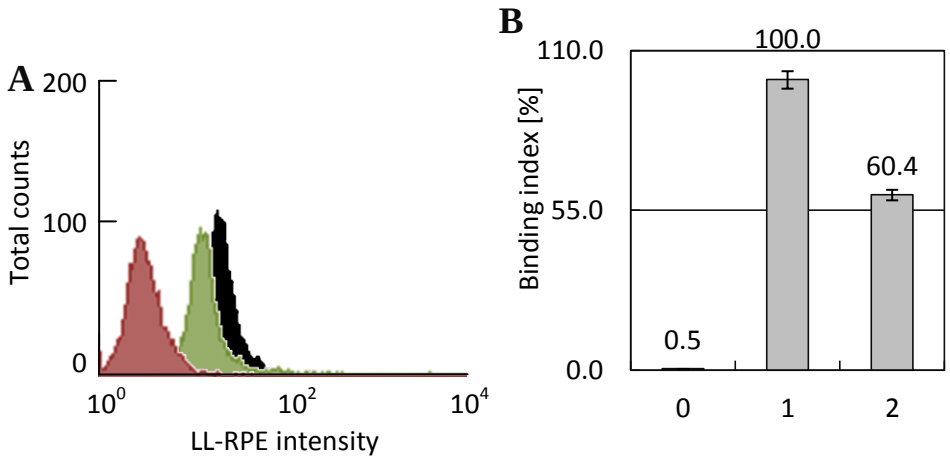

Figure 46. Overlaid LL-RPE intensity histograms (A) and binding index values (B) of unlabelled cells (red; 0), HUVECs incubated with LL-RPE-P1 conjugates (black; 1) and competition with free P1 (green; 2).

To verify whether P1 conjugated to OEG NPs have the same activity as free P1, P1-OEG NPs were tagged with a fluorescent HiLyte dye (see **chapter 3** for experimental protocol). The intensity of a fluorescent signal of HiLyte-P1-OEG NPs bound to HUVECs, as well as the number of positive cells were measured using infrared channel detector (633 nm excitation wavelength). These results are presented as BI's.

The population of HUVECs (blocked for non-specific interactions) incubated with HiLyte-P1-OEG NPs showed high binding index (BI = 100 %). Around two hundred times higher than the background signal (BI = 0.5 %), coming from unlabelled cells (**Fig. 47**). To confirm whether binding of HiLyte-P1-OEG NPs to membrane receptors was indeed peptide dependent, a series of competition experiments with free P1 peptide and a scrambled (mutated) P2 sequence was performed. P1 peptide was expected to compete HiLyte-P1-OEG NPs, whilst P2 should not (since the P2 peptide consists of the same amino acids as P1 but arranged in a different order; see **chapter 2** for theoretical background).

In the first series of competition experiments (**Fig. 47A**), HUVECs were incubated with free P1, followed by the fluorescent colloid. Considerably lower binding index showing a 30 % decrease (in comparison to the maximum value of **sample 1**), suggested that P1 peptides were successfully competed out by HiLyte-P1-OEG NPs. In contrast, the presence of P2 octa-peptide had no major effect on the binding (**sample 3**, BI = 95.3 %). Suggesting that both, florescent colloid and free untagged P1 peptide bind to the same receptors, while as expected, the mutated (P2) sequence shows no significant binding activity.

In the second series of competition experiments (**Fig. 47B**), HUVECs were incubated first with a fluorescent colloid and then with free octa-peptides (P1 or P2). Competition with P1 peptides resulted in approximately 11.2 % decrease of the binding index (BI = 88.8 %), referred to the maximum signal of **sample 1**. Clearly, in this case the competition was by far less effective, as the BI index was 18.8 % higher (referred to **sample 1**) than in the series **A** competition experiments; possibly steric hindrance related effects. Specifically, it can be hypothesised that VEGFR-1 were no longer accessible for the peptides, because of a 'blocking' derived from the considerably larger HiLyte-P1-OEG NPs (over 33 nm, see **chapter 4** for physicochemical characterisation) than P1 (P1 peptides are only about 3 nm) attached to them. It is also possible for HiLyte-P1-OEG NPs to bind to more than one receptor (since HiLyte-P1-OEG NPs contain multiple binding sites). Thus, even if one of the occupied (by a fluorescent nanoparticle) binding

sites was replaced with P1, the nanoparticle would still be attached to the cellular membrane (*via* other receptors). Another possibility is that, NPs bind stronger to the receptors because of this multiplexing, thereby preventing competition with peptides. The problem of steric hindrance to 'incoming' ligands from 'resident' ligands (bound to the receptors) was also reported by Sklar and co-workers, for the binding studies on fluorescein-biotin conjugates to streptavidin coated polystyrene beads [38].

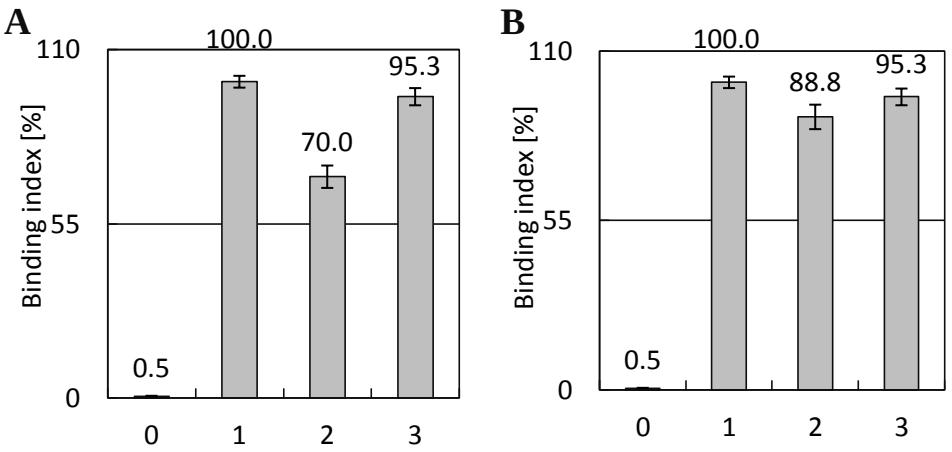

Figure 47. Binding index values of unlabelled cells (0), or incubated with HiLyte-P1-OEG NPs (1) and in a competition with free P1 (2) or P2 (3) peptides. HUVECs incubated with HiLyte-P1-OEG NPs first (A) or with free peptides (B).

Besides the emitted light, flow cytometry also allows measurements of the scattered light. Both, side scattered (SSC) and forward scattered (FSC) light of unlabelled HUVECs and cells incubated with HiLyte-P1-OEG NPs were measured. As shown in **Fig. 48**, the population of HUVECs incubated with a fluorescent colloid moved with a respect to untreated cells. Both, the inner complexity (SSC) and the cell volume (FSC) values increased. Indicating, HiLyte-P1-OEG NPs were attached to the cellular membrane of cells, rather than internalised and allocated within the cellular matrix (Note: experiment was performed on ice and in the presence of sodium azide).

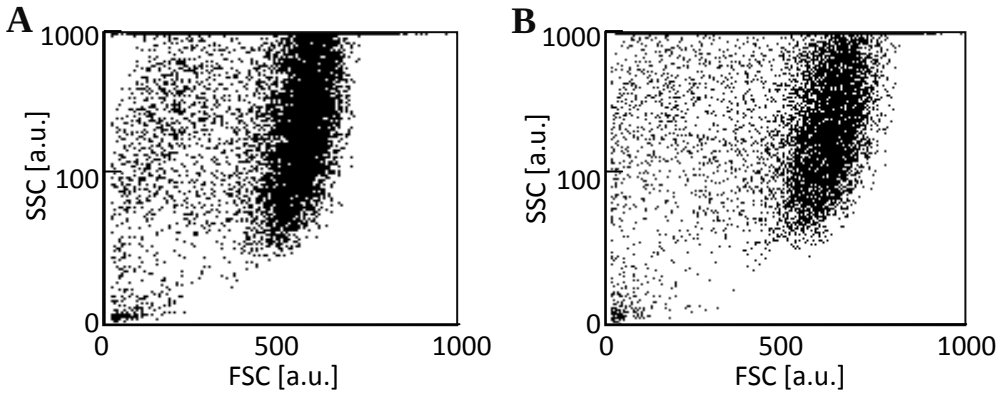

Figure 48. Forward (FSC) and side (SSC) scattered light by HUVECs (A) and cells incubated with HiLyte-P1-OEG NPs (B).

To confirm that the binding of P1 (and P1-OEG NPs) to HUVECs was based on the affinity towards the specific growth factor receptor, HeLa cells which do not over-express VEGFR-1 were employed as a negative control (see **chapter 2** for more information about HeLa). HeLa cells were incubated with a fluorescent colloid, as well as with free P1 or P2 peptides in competition studies. The background BI of HeLa cells (**Fig. 49**, **sample 0**) reached nearly 50 %, while the maximal BI value of cells incubated with HiLyte-P1-OEG NPs was double (BI = 100 %, **sample 1**). HUVECs were approximately one hundred times more effectively labelled with a fluorescent colloid than HeLa cells. It could be concluded that HiLyte-P1-OEG NPs bind to receptors, which are over-expressed by HUVECs, but are infrequent in HeLa, like VEGFR-1 [2,19,22,39,40]. Therefore, it was assumed that the binding event was selective to these receptors.

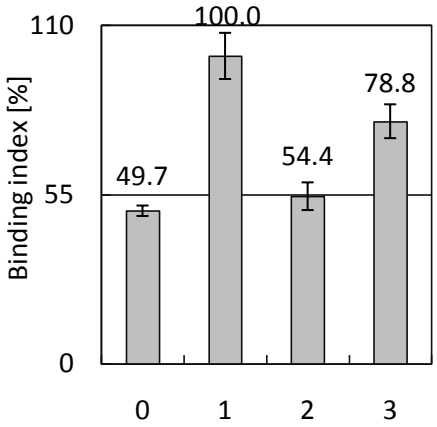

Figure 49. Binding index values of unlabelled HeLa cells (0), or incubated with HiLyte-P1-OEG NPs (1) and in a competition with free P1 (2) or P2 (3) peptides.

As already discussed in **chapter 2**, Arap and co-workers developed a cyclic peptide (CPQPRPLC), which binds to the growth factor receptors [37]. The binding to VEGFR-1 was attributed to arginine and leucine residues in RPL motif, based on a series of experiments with RPL tri-peptide. These findings were implicated in a design of P1 octa-peptide (KPQPRPLS, see **chapter 2** for details). As demonstrated by flow cytometry assays, P1 peptide and P1-OEG NPs were capable of selective binding to receptors over-expressed by HUVECs, presumably VEGFR-1.

As demonstrated by Arap's group, RPL tri-peptide (so as the cyclic peptide) binds to NRP-1 receptors, where the proline residue plays an important role [37]. On the contrary, Perret and co-workers reported the ATWLPPR sequence, which possess anti-angiogenic activity deriving from the inhibition of the $VEGF_{165}$ binding to NRP-1 [41]. It was found that this peptide bound to NRP-1 through LPPR motif and demonstrated that the C-terminus arginine was crucial for its activity, deriving from its side chain (guanidine group) and free negatively charged carboxylic group (C-end peptide residue). Also, both prolines were participating in binding to NRP-1. The RPL sequence reported by Arap does not contain a C-terminus arginine (with free carboxylic group) [37], however an easy accessible guanidine group may still be involved in binding. The unique conformation of a cyclic peptide may also help in the presentation of the side chain of arginine and allowing the binding to NRP-1; despite the strong statement made by authors about the lack of importance of the secondary structure of this peptide. Possibly the proline and lysine residues play a similar role in determination of the structure of the RPL tri-peptide and a cyclic peptide, as both prolines in LPPR motif and proline and lysine residues in the exon 8 peptide (bicyclic), developed by Zachary and co-workers [28]. It is worth highlighting, that the non-cyclised version of the bicyclic peptide shows significantly reduced activity.

The ATWLPPR sequence developed by Perret and co-workers [41] was used in a design of NRP-1 binding P3 peptide (KATWLPPR, see **chapter 2** for details). The following sections will show that P3-OEG NPs and P1-OEG NPs interact with HUVECs in a very different way, presumably *via* NRP-1 and VEGFR-1, respectively. Meaning that, even though P1-OEG NPs contained the RPL motif, predominant binding was to VEGFR-1 and not to NRP-1. Another hypothesis (except these presented in the previous paragraph) is related to the conformation of peptides attached to the surface of NPs. Dense packing of OEG ligands and high loading of peptides (see **chapter 4** for ligand quantification) may result in a three dimensional structure of P1-OEG NPs that prevents good presentation of the side chain guanidines, between neighbouring ligands/peptides.

This hypothesis can also explain why the flow cytometry competition between LL-RPE-P1 and free P1 was slightly more effective (**Fig. 46**) than between HiLyte-P1-OEG NPs and P1 (**Fig. 47**). Specifically, free P1 and LL-RPE-P1 conjugates may still present a slight affinity towards NRP-1, even though P1 does not have a unique cyclic conformation [28]. Here, the guanidine group may not be as easily accessible as in case of the cyclic peptide [28,37] or tri-peptide [37], but perhaps it was not completely masked, as was possibly happening in case of P1-OEG NPs.

6.1.2. Receptor mediated targeting.

Possible interactions between pep-OEG NPs and HUVECs were investigated by transmission electron microscopy, using spherical NPs as a 'model' system. As explained earlier (see **chapter 2** for details), P1-OEG NPs were designed to bind to VEGFR-1 endogenously over-expressed by HUVECs, while P3-OEG NPs were expected to bind to NRP-1. A mutated peptide (P2), conjugated to OEG capped NPs were unable to bind to any of these receptors.

The formation of a receptor-NPs complex with a typical tyrosine kinase VEGFR-1 receptors activates the transduction of the signalling cascade within the cell, while the complex stays attached to the cellular membrane [22,24] (**Scheme 36**). In contrast, the formation of NRP-1-NPs complexes is followed by their trafficking on the cellular membrane and internalisation [26-28,41]. These differences in mechanistic pathways of receptor complexes were reflected on TEM images. Specifically, P1 conjugated colloids were found on the outer membrane of HUVECs, while P3 colloids within the cellular matrix. P2-OEG NPs were interacting with cells non-specifically (endocytosis).

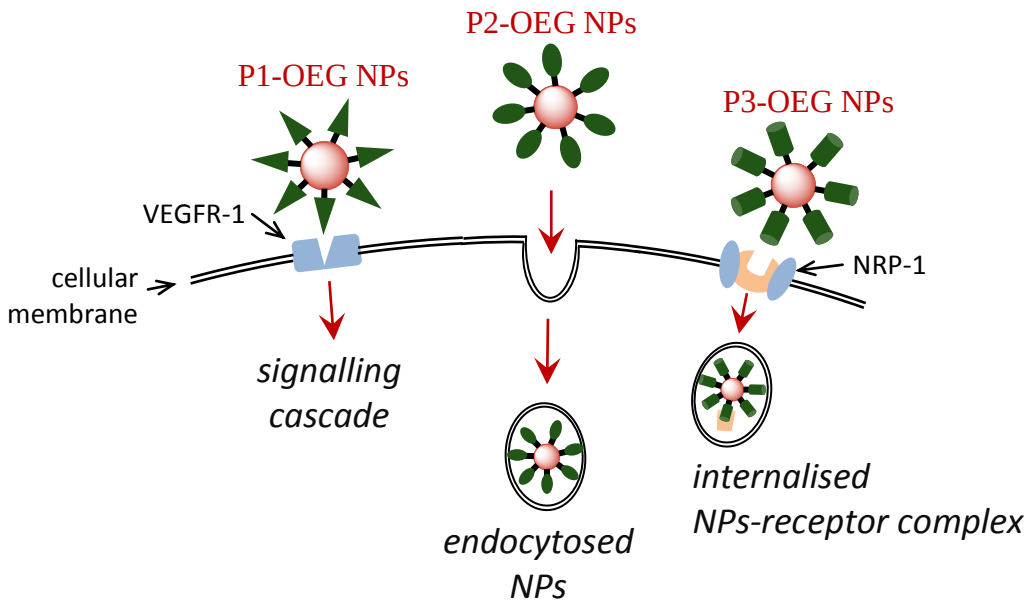

Scheme 36. Schematic illustration of the possible interactions between pep-OEG NPs and cells.

HUVECs were incubated with spherical pep-OEG NPs ($5 \cdot 10^{12}$ NPs / 1 ml, 1.3 ml) in human serum containing (20 %, full-serum) growth media for 4 h. Cells were grown on removable PET (polyethylene terephthalate) membrane inserts to avoid harvesting cells from the culture dish by trypsinisation (see **chapter 3** for experimental details). This was to prevent possible cleavage (by trypsin digestion) of membrane receptors with attached NPs (P1-OEG NPs), or dissociation of peptides from P1-OEG NPs. After treatment with NPs, cells were fixed with PET membranes and imaged with the transmission electron microscope.

TEM images (**Fig. 50A**) show that the spherical P1-OEG NPs were clearly bound to the cellular membrane of HUVECs (orange circles). As expected, conjugated NPs mainly interacted with the external surface of HUVECs (VEGFR-1, see also **section 6.1.1.**) and rarely internalised (NPs pointed by white arrow).

In contrast, P3-OEG NPs can be seen either agglomerated on the cellular membrane (most likely attached to NRP-1, **Fig. 50C left**), or internalised and locked inside cytoplasmic vesicles (**red arrow**). Even though the double membrane of vesicles was not clearly presented on the image, it can be assumed that NPs were presumably confined within endosomes. Most likely, P3-OEG NPs were taken-up by cells through specific receptor mediated endocytosis (RME, NRP-1 mediated [26-28,41]), since all stages of this

process are presented on images. Binding to the receptors and trafficking on the surface of HUVECs is showed in **Fig. 50C left**, **orange circle**. The formation of vesicles and their internalisation is clearly presented in **the middle**, **red circle**. Finally, travelling of the vesicles loaded with NPs inside the cell can be seen on **the right**, **red circles**.

As presented on TEM images (**Fig. 50B**), P2-OEG NPs interacted with HUVECs in a very different way. There were no NPs attached to the cellular membrane, while a vast number of P2-OEG NPs were seen within cellular matrix, locked inside vesicles. The double membrane (**red arrows**) was clearly presented, suggesting endosomes as cytoplasmic vesicles. NPs were probably internalised, following the non-selective endocytosis pathway (no NPs were bound to membrane receptors) and confined in endosomes. Clear similarities between the cellular fate of P2-OEG NPs and OEG NPs presented in **chapter 5**, suggest an analogues, non-selective mechanisms of uptake. These are very different from both, RME (observed with P3-OEG NPs) and the receptor binding with P1-OEG NPs. As previously mentioned, pep-OEG NPs were designed to show very similar physicochemical properties (size, charge, hydrophilicity and stability). Only the amino acids arrangement and content was varied within octa-peptides, resulting in sequence dependent differences, which regulated the cellular fate of colloids. The fate of NPs was qualitatively analysed using TEM. Quantitfication experiments (e.g. competition with free peptides or cytokines) could not be performed with this technique, because: a) some NP might have been lost during the harsh and complex procedure of TEM fixation (see **chapter 3**); b) only small section of cell (and cellular membrane) can be seen per image, possibly leading to large errors.

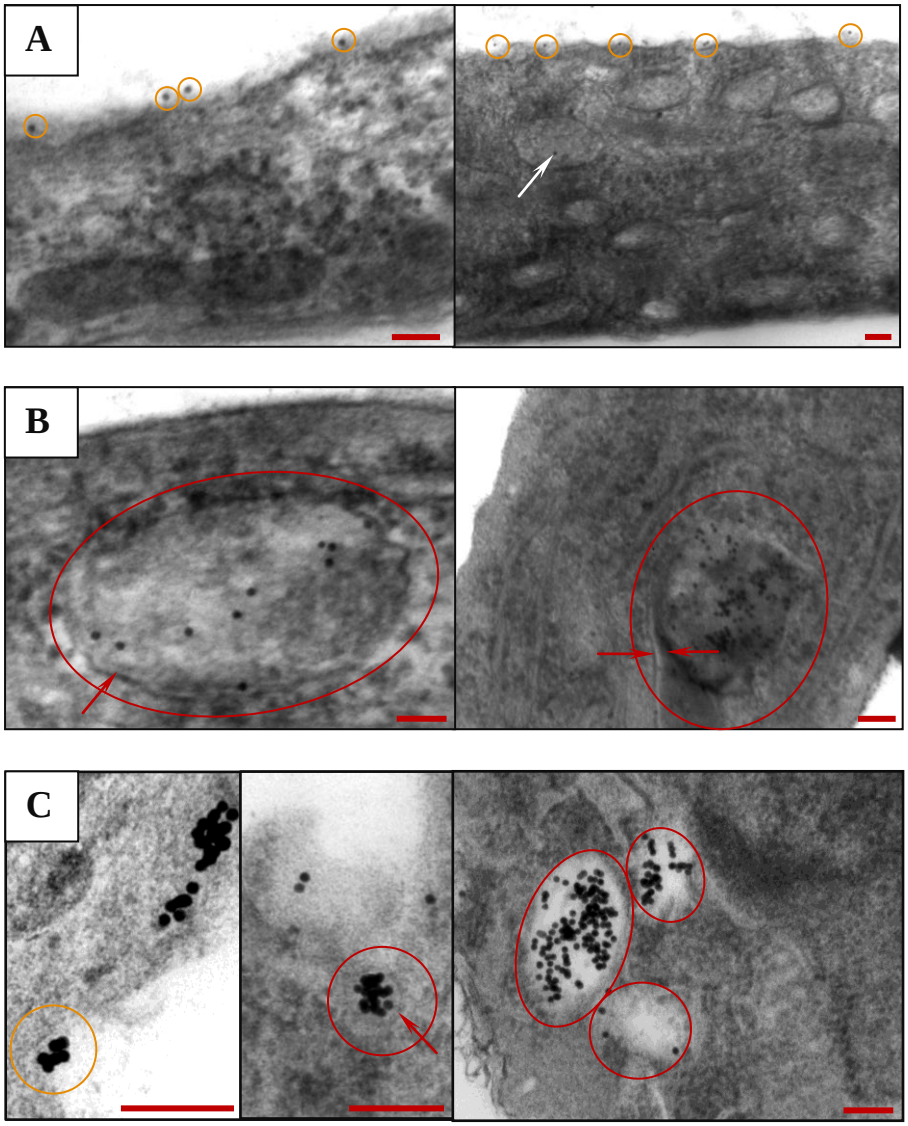

Figure 50. TEM images of HUVECs incubated with: P1-OEG NPs (A), P2-OEG NPs (B) and P3-OEG NPs (C). Scale bars are 100 nm. Orange circles indicate NPs bound to the external membrane of cells, while red represent internalised NPs. Double membrane is pointed by red arrows. Internalised NPs are pointed by white arrows.

Specific targeting of cells with NPs *via* receptor mediated interactions has been intensively investigated in recent years [42-65]. A number of strategies following both, intra- and extracellular approaches, utilising either large (e.g. antibodies) or small (e.g. peptides, folic acid) molecules, have been reported. Richards-Kortum and co-workers and El-Sayed's group established spherical gold NPs directly capped with anti-epidermal growth factor receptor antibodies (anti-EGFR) [45,46,64]. They demonstrated that anti-EGFR-coated NPs selectively bound to EGFR over-expressing (endogenously) cells (e.g.

SiHa cells) and stayed attached to the surface of cells, rather than internalised, as observed for P1-OEG NPs and HUVECs (**Fig. 50**). Except of antibodies, other large proteins were also employed in the receptor mediated uptake of NPs [66,67] (the intracellular approach). Gu and co-workers showed that transferrin/PEG mixed layer capped gold nanorods were efficiently taken-up by HeLa cells expressing transferrin receptors [66].

However, the use of small molecules in selective targeting of cells seems to be more advantageous, mainly because of reduced immunogenicity and simplicity of their production, which could be easily scaled-up (e.g. solid phase synthesis) [12,53,68,69]. As demonstrated by Andres and co-workers, thioctic acid-PEG-folic acid capped spherical gold NPs were selectively taken-up by foliate receptor positive cancer cells, while their uptake was minimal in cells, which do not over-express these receptors [44]. Moreover, the presence of thiolated-PEG compartment within the organic layer, enhanced the stability of NPs in buffered environments; another advantage upon protein or antibodies stabilised NPs (electrostatic stabilisation [64,70-72]). Often NPs based cellular targeting probes are designed to serve as imaging agents, therefore it is extremely important that the uptaken NPs retain their properties, e.g. luminescent quantum dots and nanorods (QDs, QNRs) [56,73]. As reported by Pellegrino and co-workers, 'PEGylated' folic acid conjugated QNRs remained stable (and fluorescent) after selective uptake (mediated by foliate receptors) [73]. Presented here OEG capping layer provided NPs with a substantial stability in buffered environments, as demonstrated in **chapters 4** and **5**.

Besides folic acid, the use of other small molecules (like peptides), for the preparation of cell targeting nanocomposites, gained popularity in recent years [47,53-55,57,62,74-80]; especially cell penetrating peptides (CPP) are very attractive biomolecules and were employed by several groups in the preparation of bioactive NPs [74,75,77]. Berry and co-workers and Brust's group demonstrated that TAT peptide functionalised NPs were not only taken-up by cells (e.g. HeLa) but were capable of escaping the endosomes, as they were found dispersed in the cytosol [74,75]. Except of that, the receptor targeting peptides have also been used to prepare NPs-peptide conjugates. Very recently, Albericio and co-workers reported that gold NPs capped with a mixed layer of targeting (bombesin gastrin releasing receptor peptide, BN/GRP) and drug (RAF) peptide analogues were successfully taken-up by GRP receptors expressing HeLa cells [53], while no NPs were found in the SHSY5Y cell line, which does not over-express GRP receptors. As another example, RGD peptide was used by several research groups to functionalise NPs (e.g. QDs, magnetic NPs)

[13,81-83]. RGD-functionalised NPs were specifically taken-up by interleukin $\alpha_v\beta_v$ expressing cells.

As recently demonstrated by Levy and co-workers, endocytosis is usually followed by proteolytic digestion of peptides or proteins conjugated to NPs, carried out by cathepsin L protease in the endosome [84]. Bearing in mind that the properties of NPs should be retained even after digestion, to preserve their function (e.g. fluorescence) [56, 73, 83] and to avoid any intoxication (e.g. cadmium release from QDs) [85], the use of e.g. thiolated-PEG or OEG compartments in the organic layer is advantageous [73, 86] (Note: OEG capping layer provide NPs with sufficient stability in endosomes; see **chapter 5**). Another way to solve the digestion issue [84] might be the utilisation of an extracellular approach in cell targeting and regulation. P1 conjugated OEG NPs developed during this project meet both of these criteria (good stability and extracellular method). Also, P3-OEG NPs were capable of triggering desired cellular response (even though they were internalised; **section 6.2.**) simply by receptor binding (ahead of RME), which can also be considered as the extracellular approach.

6.1.2.1. Anisotropic pep-OEG NPs in selective interactions with HUVECs.

As explained previously (see **chapter 2**), the applications of pep-OEG conjugates based on spherical gold cores (15 nm) in biomedicine are limited [87-90]. These limitations purely derive from the optical properties of NPs [91, 92] (e.g. plasmon band in the visible spectral range; see **chapter 4** for physicochemical properties). Therefore, these nanomaterials were only utilised to assess general bioactivity of pep-OEG NPs (**section 6.2.**) and were not used in laser induced photo-thermal treatment of cells (**chapter 7** for results, **chapter 2** for theoretical background). For this purpose, pep-OEG NPs with anisotropic cores were selected in respect to their optical signatures [92-97], including NIR extinction, which is required for *in vivo* treatment of a deeper tissue (see **chapter 4** for physicochemical properties of these nanomaterials).

Three types of anisotropic NPs were used: nanorods (NR), hollow gold (HG) and silica/gold core/shell (CS) nanostructures. Their surfaces were capped with the OEG ligands, and further modified with P1 or P2 octa-peptides (see **chapter 3** for experimental details) to form P1-OEG and P2-OEG NPs (NR, HG and CS, see **chapter 4** for physicochemical characterisation).

To confirm that anisotropic P1 conjugates interacted with HUVECs in the same way as spherical core based nanocomposites, a series of experiments was performed. Representative TEM images (**Fig. 51**) clearly demonstrated P1-OEG NPs attached to the cellular membrane HUVECs, most likely *via* VEGFR-1 receptors. All three types (NR, HG and CS) of P1 conjugated NPs were found attached to the outer membrane of cells.

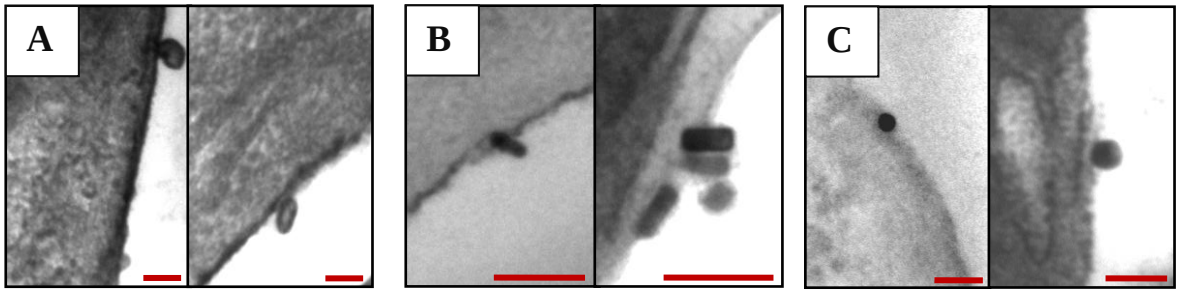

Figure 51. TEM images of HUVECs incubated with: P1-OEG HG NPs (A), P1-OEG NR (B) and P1-OEG CS (C). Scale bars are 100 nm.

The average number of P1-OEG NPs interacting with a single cell can be approximated from TEM images, assuming that the receptors were evenly distributed on the surface of cells [98]. Taking the thickness of the imaged specimen (100 nm slice) and the dimensions of the picture (scale bars), the surface area of the cell (cellular membrane) shown on the image can be calculated. Simply by counting the number of NPs on the image (average from at least 10 representative images) and referring this to the observed membrane area (e.g. 1 nanoparticle per 0.018 ÷ 0.075 μm^2) and to the total area of HUVECs membrane (150 μm^2 was assumed, as the average diameter of cells in suspension – 'rounded shaped cells' was 6.9 μm), the average number of NPs per cell was approximated. Specifically, the average number of P1-OEG NPs (for all types of metallic cores) attached to each cell was found to be in a region between 2000 ÷ 8000.

To show that the binding of P1-OEG NPs to cellular membrane is not random (non-selective), but programmed, receptor selective type of interactions, a series of control experiments was conducted. Hence, HUVECs were incubated with P2-OEG NPs, unable to bind to VEGFR-1, but which can interact with cells non-specifically (demonstrated in the previous sections). TEM images (**Fig. 52**) confirmed NPs within the intracellular matrix, locked inside vesicles – endosomes, as designated by **circles**. **Arrows** indicated the double membrane of vesicles. Rod-like, hollow and core/shell NPs have entered cells most likely following the endocytosis pathway.

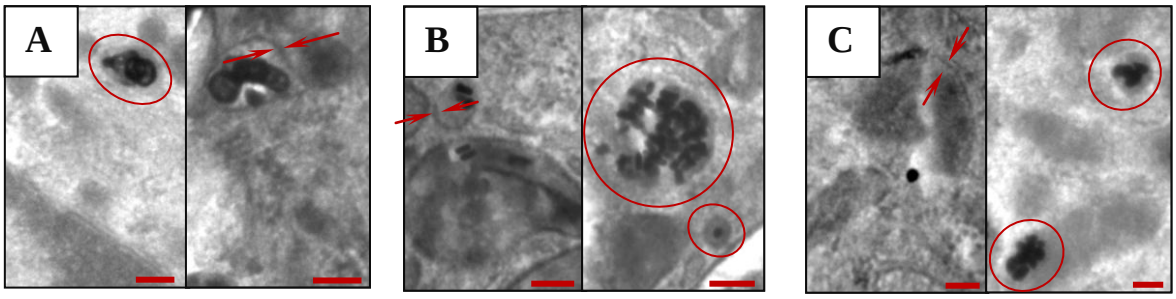

Figure 52. TEM images of HUVECs incubated with: P2-OEG HG NPs (A), P2-OEG NR (B) and P2-OEG CS (C). Scale bars are 100 nm.

6.2. Regulation of basic biological functions of HUVECs.

As demonstrated in **section 6.1.**, spherical pep-OEG NPs (P1 and P3) selectively bind to receptors (VEGFR-1 and NRP-1, respectively) allocated on the cellular membrane of HUVECs. Both receptors play a fundamental role in the regulation of basic physiological functions of HUVECs [2,5,7,19,22,23,26-28], therefore it was anticipated that following the binding event, pep-OEG NPs would induce a certain cellular response. P1-OEG NPs were expected to act as activators, while P3-OEG NPs as inhibitors (see **chapter 2** for theoretical background).

The bioactivity of pep-OEG NPs was studied by gene expression profiling assays. Three genes related to angiogenesis (blood vessels growth, basic function of HUVECs, see **chapter 2** for more details) and/or hypoxia (oxygen deprivation, see **chapter 2**) and regulated by the binding of growth factors to appropriate receptors [5,10,37,41,84,85] were examined. Specifically, vascular endothelial growth factor A gene (VEGF A), hypoxia inducible factor 1 gene α subunit (HIF-1α), myelocytomatosis oncogene (C-MYC) were selected. Since the selected genes are critical to angiogenesis, regulation of their expression levels in HUVECs (following treatment with pep-OEG NPs) would allow a control over cell physiology.

On the other hand, even if a successful regulation of gene transcription in a population of cells is achieved, a control upon the whole physiological processes (e.g. angiogenesis) conducted by these cells [86] may not necessarily be gained. Therefore, once it was confirmed that pep-OEG NPs regulate the cellular response at the molecular level (**section 6.2.1.**), the capability of colloids to stimulate or suppress the entire angiogenesis process was examined by *in vitro* capillary-like structures formation assays (**section 6.2.2.**).

6.2.1. Overview at the molecular level: gene expression profiling.

As described in **chapter 3** prior to gene expression profiling assays, HUVECs were treated for 6 h with pep-OEG NPs. Environmental conditions, e.g. the quantity of serum proteins in growth media, were varied during treatment, to achieve the highest possible expression of VEGF A, HIF-1α and C-MYC genes. The amount of expressed mRNA was quantified by Q-PCR reaction (see **chapter 3** for experimental details) using primers equipped with TaqMan probes and c-DNA; c-DNA was synthesised by reverse transcription (RT) on mRNA templates isolated from cells [87].

To optimise environmental conditions for VEGF A, HIF-1α and C-MYC genes expression assay, a series of control experiments was performed. In these experiments HUVECs were stimulated with a naturally existing cytokine – VEGF-B_{167} (see **chapter 2** for more information about VEGF-B_{167} and **chapter 3** for experimental protocol). As reported by Eriksson and co-workers, VEGF-B_{167} selectively binds to VEGFR-1 [85]. VEGF-B_{167} can also bind to NRP-1, as demonstrated by Alitalo's group [27]. Following the binding event, activation of several genes, including VEGF A, HIF-1α and C-MYC in HUVECs was shown by Li and co-workers [10]. On account of previously reported up-regulation of selected genes [10], as well as the binding affinity towards both chosen receptors [19-21,23] (Note: other cytokines, e.g. VEGF-A_{165}, bind to different sets of growth factor receptors, see **chapter 2**), this cytokine was selected to serve as a positive control.

VEGF A, HIF-1α and C-MYC genes expression profiling after treatment with VEGF-B_{167} is shown in **Fig. 53**. Presented values were normalised according to glyceraldehyde 3-phosphate dehydrogenase (GAPDH, standard used in data normalisation [88], which is not regulated by VEGF-B_{167}) expression levels and referred to untreated HUVECs, which were incubated in full-serum (20 % human serum, see **chapter 3** for cells culturing protocol) growth media. In all tested conditions (**Fig. 53**, conditions **1** ÷ **3**) three genes were up-regulated. The highest up-regulation (nearly 60 fold, **Fig. 53**, conditions **1**) was achieved for VEGF A gene, whilst the lowest (around 3 fold, same conditions) for C-MYC gene. It is evident that cells were the most effectively stimulated in serum-depleted (0.2 % human serum, 100 times less than in a standard growth media) and hypoxia mimicked conditions (by the presence of cobalt II chloride, $CoCl_2$ [89]; see **chapter 3** for experimental details). Moderate regulation (over 10 fold of VEGF A) was achieved in serum-depleted environment, while only minor effects on genes (0.7 fold of VEGF A) were observed, when cells were incubated in full-serum growth media.

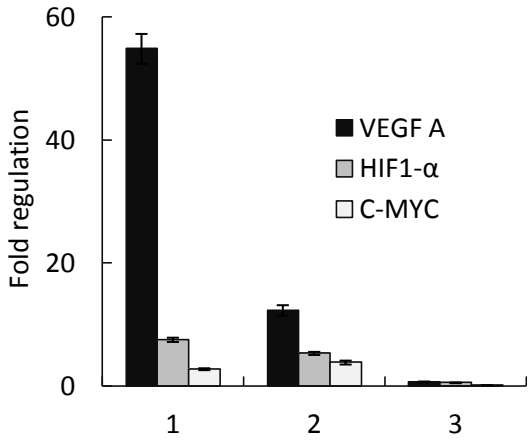

Figure 53. VEGF A, HIF-1α and C-MYC genes fold regulation in HUVECs after 6 h treatment with VEGF-B_{167} in reduced-serum with $CoCl_2$ (1), reduced-serum (2) and full-serum (3) media growth.

It can be concluded (based on a graph; **Fig. 53**) that HUVECs were the most effectively stimulated in serum-depleted conditions and this effect was additionally enhanced by a $CoCl_2$ mimicked hypoxia. Consequently, it was anticipated that P1-OEG NPs would have similar activating effects on tested genes, even though P1-OEG NPs most likely bind to VEGFR-1, as demonstrated in **section 6.1.** (Note: VEBF-B_{167} binds to both, VEGFR-1 and NRP-1 [19-23,26-28,85]). Therefore, in response to P1-OEG NPs binding to HUVECs, optimum levels of genes expression were expected in serum-depleted and hypoxia mimicked environmental conditions.

As already mentioned, P3-OEG NPs (NRP-1 binding) were expected to inhibit the expression of monitored genes. Since hypoxic conditions (here, mimicked by $CoCl_2$) can activate several genes, including VEGF A as demonstrated by Keshet's group [90], there was a concern that in the presence of $CoCl_2$, P3-OEG NPs mediated inhibition can be undermined or even masked. To overcome this issue, a series of control experiments with HUVECs treated with free P3 octa-peptide under various conditions (**Fig. 54**, conditions **1** ÷ **3**) was performed first. The same conditions, showing a maximum gene inhibition with P3, would then be chosen and used in the cells treatment with colloidal P3-OEG NPs.

P3 peptide showed inhibitory effects on all three angiogenesis related genes. In the tested conditions VEGF A gene was down-regulated the most efficiently, while the C-MYC gene was the least affected (as in case of VEGF-B_{167} mediated activation). It is evident that the most efficient down-regulation (around -9 for VEGF A, and -8 for HIF-1α) was achieved in serum-depleted conditions (**Fig. 54**, conditions **2**). As predicted, the addition of $CoCl_2$ had a positive effect on genes expression levels. Joint outcome of both:

serum starvation and hypoxia (conditions number **1**), led to less effective down-regulation of VEGF A, HIF-1α (-8.5 and -7, respectively) and C-MYC genes (**Fig. 54**, conditions **1**), than in conditions number **2**. Incubation in full-serum growth media (**Fig. 54**, conditions **3**) resulted in a minor down-regulation of tested genes (minimum -0.6 for VEGF A). Moreover, the maximum effect on HUVECs (-9 down-regulation of VEGF A) was nearly 6 times lower than VEGF-B_{167} induced effect (over 50 fold up-regulation of VEGF A) in number **1** conditions. Possibly explained by the activation of the VEGF A gene in hypoxic conditions (here mimicked by $CoCl_2$), which was also demonstrated by Keshet's group [90].

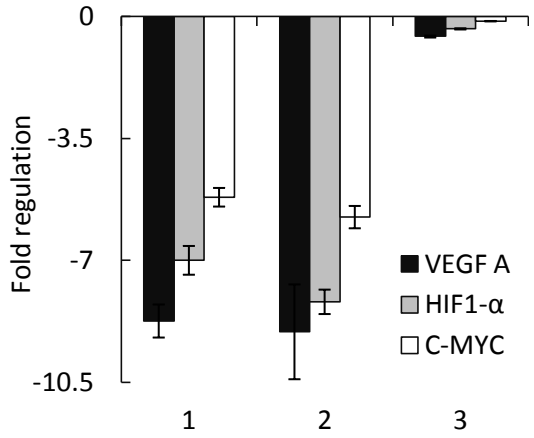

Figure 54. VEGF A, HIF-1α and C-MYC genes fold regulation in HUVECs after 6 h treatment with P3 in reduced-serum with $CoCl_2$ (1), reduced-serum (2) and full-serum (3) media growth.

The activity of P1 and mutated P2 octa-peptides (activator, or no effect, respectively), as well as pep-OEG NPs (P1, P2 and P3) were assessed next. The expression levels of VEGF A, HIF-1α and C-MYC genes in HUVECs, treated either with VEGF-B_{167} or free (P1, P2 or P3) peptides and their analogous pep-OEG NPs, were tested in the presence of $CoCl_2$ in serum-depleted (**Fig. 55**), or without $CoCl_2$ in serum-depleted (**Fig. 56**) or full-serum (**Fig. 57**) growth media. All three environmental conditions were applied in the experimentation assays, to fully assess the efficacy of both, inhibitory and activating effects on cells, in respect to each other.

Overall, the VEGF A gene was affected the most by treatment with all tested gene regulators (see **Fig. 55**, natural cytokine, octa-peptides and pep-OEG NPs), while the smallest effect was observed on C-MYC gene. Maximum up-regulation (nearly 50 fold) was observed for VEGF A gene after the cells treatment with VEGF-B_{167} cytokine. Synthetic P1 octa-peptide and P1-OEG NPs up-regulated VEGF A gene by nearly 26 and

over 15 fold, respectively. Interestingly, HIF-1α and C-MYC genes were stimulated more efficiently with P1 and P1-OEG NPs analogues than with the natural cytokine.

On the contrary, all three genes were significantly down-regulated with P3 octa-peptides and P3-OEG NPs. VEGF A reached maximum down-regulation after treatment with P3-OEG NPs (over -10 fold). The incubation with free P3 resulted in nearly -8 fold inhibition. It is worth noticing that both, P1-OEG and P3-OEG NPs presented slightly stronger effects on tested genes, than free P1 and P3 octa-peptides, respectively (Note: the total quantity of introduced octa-peptides, those free in solution or attached to NPs was kept constant; see **chapter 3** for experimental details). One possible hypothesis which may explain this, can be an effect deriving from a higher local concentration of receptor binding epitopes on NPs (over 500 per each NP, see **chapter 4** for peptide quantification) than on free peptides (only one binding site per each octa-peptide). Meaning that, once a pep-OEG nanoparticle is bound to the appropriate receptor *via* one of its 500 octa-peptides, other epitopes are brought close to the surface of a cell, possibly inducing an additional binding event between the neighbouring receptor and another peptide (out of 499 still available for binding). By this way the binding rate and the resulting gene expression levels can be increased.

As predicted, a mutated P2 sequence and P2-OEG NPs did not induce any notable gene response. This is because P2 octa-peptide cannot interact with any of the listed receptors.

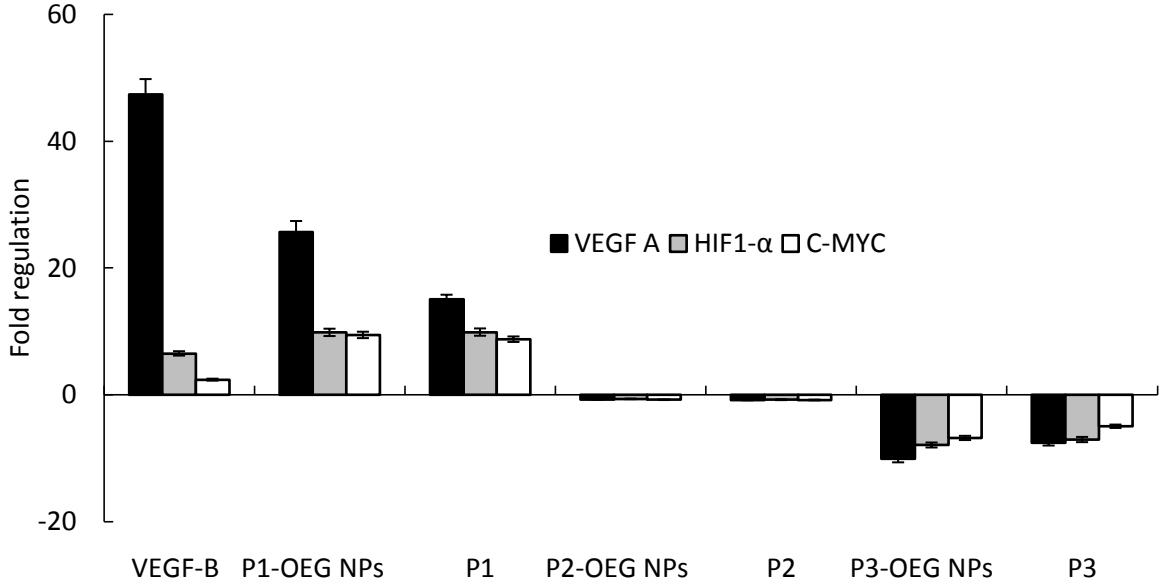

Figure 55. VEGF A, HIF-1α and C-MYC genes fold regulation in HUVECs after 6 h treatment in serum-reduced growth media and with $CoCl_2$.

In serum-depleted conditions (**Fig. 56**) similar trends were observed. VEGF-B_{167} cytokine, as well as P1-OEG NPs and free P1 octa-peptide up-regulated, while P3-OEG NPs and free P3 octa-peptides down-regulated VEGF A, HIF1-α and C-MYC genes. Both, P2 and P2-OEG NPs had no effect on the genes tested. VEGF A gene responded the strongest to the tested factors, while C-MYC gene the least. The highest fold regulation (over 14 fold up-regulation of VEGF A) was achieved after treatment with the natural cytokine. Overall inhibitory effects seem to be much stronger in these conditions, than in the presence of $CoCl_2$. Over -12 fold down-regulation of VEGF A gene (and -8 fold of HIF1-α; -3 of C-MYC) was observed after treatment with P3-OEG NPs. At the same time, the relative value of activation was much weaker, than in $CoCl_2$ containing environment. Here, only 10 fold up-regulation of VEGF A (and 5 fold of HIF1-α; 1.5 of C-MYC) was achieved with P1-OEG NPs. Possibly explained by the activation deriving from $CoCl_2$, which mimics the hypoxic conditions, as already suggested in the text and previously demonstrated by several research groups [89,90]. $CoCl_2$ based activation could have enhanced the VEGF-B_{167}, P1 and P1-OEG NPs mediated induction and at the same time suppressed the P3 or P3-OEG NPs mediated inhibition.

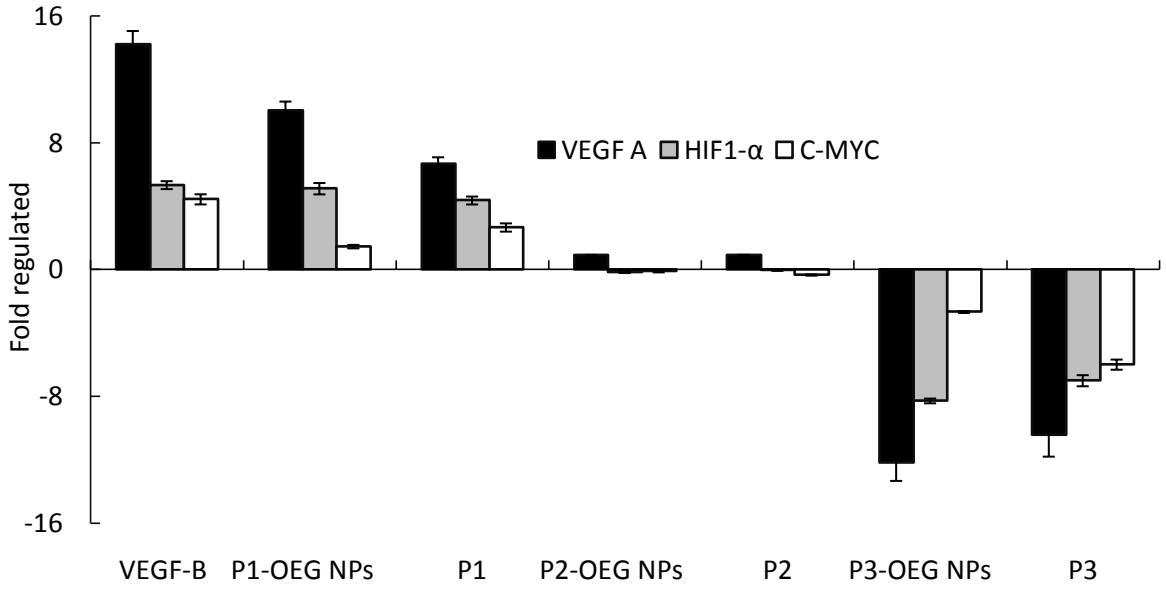

Figure 56. VEGF A, HIF-1α and C-MYC genes fold regulation in HUVECs after 6 h treatment in serum-reduced growth media.

The natural cytokine, as well as octa-peptides and pep-OEG NPs showed only minor level of genes fold (between 0.7 and -0.7 fold) regulation in full-serum conditions (**Fig. 57**). However, the general trends (genes up-regulation with VEGF-B_{167}, P1 and P3-

OEG NPs and down-regulation with P3 and P3-OEG NPs), observed after treatment in serum-depleted (**Fig. 56**) and serum-depleted with $CoCl_2$ (**Fig. 55**) growth media, were preserved.

Minor effect on genes in full-serum conditions can be attributed to the presence of growth factors among serum proteins. Consequently, the control sample (cells only), which served as a reference point (background correction) for data normalisation, as well as samples treated with gene regulators were stimulated. That is why relative heights of bars representing genes fold regulation are not as elevated as in case of the serum-depleted environment.

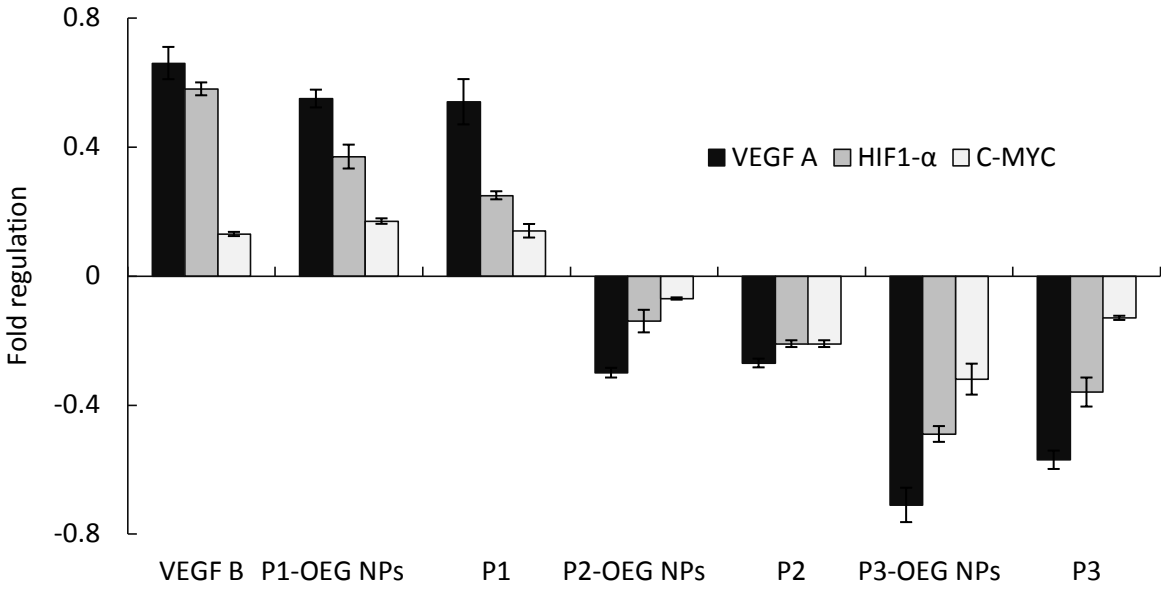

Figure 57. VEGF A, HIF-1α and C-MYC genes fold regulation in HUVECs after 6 h treatment in full-serum growth media.

To summarise, generally the strongest effects on genes were observed in hypoxia ($CoCl_2$ mimicked) and serum-depleted conditions (**Fig. 55**). However, down-regulation with P3 octa-peptide or analogues P3-OEG NPs seemed to be more efficient in the serum-depleted environment only (**Fig. 56**). Moreover, in $CoCl_2$ free environment the effects deriving from P3 and P3-OEG NPs treatment are stronger than P1 and P1-OEG NPs mediated stimulation. Treatment in full-serum conditions did not lead to any notable effects on tested genes [10,84]. Nonetheless, it was successfully demonstrated that both synthetic sequences (P1 and P3), as well as P1-OEG and P3-OEG NPs conjugates show desired activity and can regulate the response of HUVECs at the molecular level.

A different cell line, which does not over-express VEGFR-1 and/or NRP-1 (e.g. HeLa) was not used as an additional control in gene profiling assays. In these assays, regulatory effects of colloids on cell metabolism (following the receptor binding event) were studied. Since no receptor binding was denoted in HeLa (flow cytometry, see the previous section), no major effects on genes could have been observed. Consequently, HeLa were discarded from gene expression profiling experiments.

As previously reported by Li and co-workers, treatment with VEGF-B_{167} cytokine up-regulates many post-survival genes, including VEGF A, HIF1-α and C-MYC in a number of vascular cells [84]. Similar effects (activation) were observed in HUVECs treated with P1 or P1-OEG NPs. It can be hypothesised that the binding of cytokine or octa-peptide derivatives to VEGFR-1 receptor induces tyrosine kinase phosphorylation cascade and a signal transduction within cells, which led to up-regulation of monitored genes. The activation of VEGF A gene could have resulted in the secretion of VEGF-A protein, e.g. VEGF-A_{165} and its isoforms (see **chapter 2** for more details). Consequently, produced VEGF-A factor (along with growth factors present in growth media; serum-depleted environment still contained 0.2 % serum proteins) could have bound to growth factor receptors (e.g. VEGFR-1 and VEGFR-2) and further activated the signalling cascade and increased the expression levels of selected genes.

In general, tested genes were activated slightly stronger with VEGF-B_{167} than by P1 derivatives. A possible explanation could be that the natural cytokine can bind to both, VEGFR-1 and NRP-1 receptors [10,19,27,84,85] (and perhaps with higher affinity), while P1 octa-peptide and P1-OEG NPs predominantly to VEGFR-1 (see **section 6.1.**). Activated NRP-1 (by cytokine) can mediate more stable physical association between VEGF-A_{165} and VEGFR-2, as demonstrated by Zachary and co-workers [28]. This is required for full activation of the receptor and its signaling pathways [27,28,91], thus can enhance the expression levels of the tested genes. It is also worth highlighting that the increased fold up-regulation of VEGF A gene after treatment with VEGF-B_{167} in serum-depleted growth media with $CoCl_2$, can be explained by the stimulating effects of hypoxia (mimicked by $CoCl_2$) on this gene [89,90] (already mentioned in the text).

The mechanism of P3 and P3-OEG NPs mediated inhibition seems to be more complicated and harder to explain than the regulatory effects of P1 and analogous P1-OEG NPs. One can hypothesise that the association of P3 and P3-OEG NPs with NRP-1 can prevent the binding of growth factors (present in the growth media; serum-depleted contained 0.2 % serum proteins) to this receptor. Consequently, since co-binding to NRP-

1 is required for stable binding of VEGF-A to VEGFR-2 (shown by Zachary's group) [28], the effective blocking of NRP-1 (with P3 or P3-OEG NPs) could inhibit the phosphorylation signalling cascade within cells, thus the expression of associated genes. On the other hand, the formation of complexes between NRP-1 and VEGFR-2 enhances the binding of growth factors, as reported by Klagsbrun and co-workers [91]. Therefore, it is possible that, if NRP-1 is bound to P3 or P3-OEG NPs, the formation of complexes with another growth factor receptor is suppressed and so is the efficiency of the growth factor binding events. Consequently, it can be hypothesised that genes tested, including VEGF A, could not have been effectively stimulated and that growth factors could not have been secreted. This resulted in genes down-regulation (referred to untreated cells). It seems to be in agreement with hypoxia related effects on genes in HUVECs treated with P3 or P3-OEG NPs. Less effective gene fold regulation was indeed observed in the presence of $CoCl_2$. However, $CoCl_2$ induction could not outweigh inhibition by P3 derivatives, because of binding to NRP-1, which (as already explained) possibly suppressed the association of growth factors with VEGFR-2 and the phosphorylation cascade.

6.2.2. *In vitro* angiogenesis regulation.

As demonstrated in the previous section, pep-OEG colloids regulate several angiogenesis related genes in HUVECs. This section will assess whether analogues regulation of the whole physiological process (angiogenesis) can be achieved.

Soker and co-workers previously reported the inhibition of angiogenesis with gold NPs [92]. In their work, the inhibition of VEGF-A_{165} induced *in vivo* angiogenesis (in mice) using uncoated, spherical and around 5 nm diameter gold colloids. Anti-angiogenic action was attributed to the binding of VEGF-A_{165} to the surface of gold NPs. It was hypothesised that the binding occurred *via* the side chain thiol group of cysteine residues (Note: cysteines are critical to the activity of VEGF-A_{165}, as they are allocated within the active site). Inactivated VEGF-A_{165} cannot induce angiogenesis. The authors have utilised the affinity of gold NPs towards thiol containing molecules. Introduced into mice NPs themselves did not possess any angiogenic activity. In such an approach, it is difficult to fully control the action of NPs, since in the organism (e.g. mice), there is a number of thiol containing molecules (e.g. glutathione), which can also bind to gold NPs [70,71,93,94]. Consequently, it is hard to predict which molecules and in what ratio (in respect to each other) will bind to NPs and what percentage of them will remain unbound. This rises the

following questions: a) will every VEGF-A_{165} molecule be blocked?; b) will the activity of other molecules (which ones?) be affected by binding to NPs? and c) if so, what are the consequences (side effects) on other (which ones?) physiological processes in the organism? One way to overcome these issues would be the use of capped NPs [48,50,52,53,58,64,72,74,76,95,96]. Such NPs will not covalently bind (*via* thiol-gold interactions) to any biomolecules in the organism. The angiogenic activity will come from pro- or anti-angiogenic molecules incorporated in the organic corona. Newly developed family of pep-OEG NPs meet those criteria.

The capability of pep-OEG NPs to regulate the angiogenesis process (conducted by HUVECs) was examined by *in vitro* capillary-like structures formation assay [15,50] (see **chapter 3** for experimental details). Hence, cells were grown on a basement membrane matrix gel (thin layer method, see **chapter 3**) and stimulated with pep-OEG NPs in serum-depleted growth media (0.2 % serum proteins). The selection of such conditions was based on the genes profiling assay, as shown in the previous section. Specifically, the maximum inhibition of genes in cells, treated with P3-OEG NPs were observed in serum-depleted environment, as well as their sufficient induction with P1-OEG NPs. On the contrary, in serum-depleted and hypoxia mimicked conditions, enhanced induction (with P1-OEG NPs) and reduced inhibition (with P3-OEG NPs) was denoted. In the full-serum growth media no major effects on the genes was observed. Since, it was anticipated to study both regulatory effects (induction and inhibition) on the *in vitro* angiogenesis simultaneously, using the same conditions, the assay was performed in a serum-depleted environment. The reduced growth factor gel (Geltrex) was employed in all experiments, so that the stimulation of capillary formation by the matrix components was minimal. The incubation time of cells with NPs was varied between $2 \div 20$ h. VEGF-B_{167} was chosen to serve as a positive control and a reference point; at which maximum stimulation was expected (this will be further discussed by the end of this section).

After the cell treatment with gold colloids or VEGF-B_{167}, phase contrast images were taken. The length of capillaries formed by HUVECs was quantified per image area of 0.216 mm^2, using ImageJ software (see **chapter 3** for more details). Also, the number of branching points (BPs) was counted. The overall length of capillaries developed after stimulation with each type of gold colloid was referred to untreated (but incubated in the same conditions – control) and VEGF-B_{167} treated cells, then presented as a regulation index (RI, see **chapter 3** for equation). Branching indexes (BrI) were calculated in an analogues way (see **chapter 3** for equation).

Only recently, Anderson and co-workers reported that HUVECs with anchored 'nanoparticulate patches' retained their ability to form capillaries on matrix gels [50]. In their work, the cellular membrane of living HUVECs was first biotinylated then decorated with commercially available NeutrAvidin labelled 40 nm fluoSpheres. Cells modified with NPs were forming multi-cellular structures as fast as unmodified HUVECs. Hence, any delay (inhibition) or induction of the capillaries formation by cells with pep-OEG NPs should be assigned to the specific activity possessed by NPs.

As an example, phase contrast images showing HUVECs after 4 h stimulation are presented in **Fig. 58**. Neo-vascular sprouting by untreated cells (**A**) was marginal, while upon stimulation with VEGF-B_{167} (**B**) or P1-OEG NPs (**C**), HUVECs were forming capillaries. Hence, the pro-angiogenic activity of P1 based gold colloid was determined. P2-OEG and P3-OEG colloids did not induce any notable spouting, either as a result of anti-angiogenic activity (as expected for P3-OEG NPs, see the previous section), or a lack of any activity. To verify if P3-OEG NPs possess any anti-angiogenic activity, the assay conditions were optimised to achieve neo-vascularisation of the untreated cells. Instead of using a matrix gel with a higher quantity of growth factors (to stimulate tubules formation), the assay duration time was extended (up to 20 h). Such an approach was chosen to avoid masking any possible inhibitory effects of P3-OEG NPs with antagonistic action (pro-angiogenic) of growth factors.

Phase contrast images of HUVECs were taken after 2, 4, 8 and 20 h of treatment (Note: exactly the same areas of culture dishes were imaged at each time point). As already mentioned, quantitative analysis of the images were performed for data clarification (see **chapter 3** for equations). The measured overall length of capillaries after 2, 4 and 8 h of treatment are shown in **Fig. 59A**, while in **B**, calculated values of RI's are presented (Note: RI's are relative to the maximum regulation with VEGF-B_{167} achieved after 4 h – equals to 100 % RI and referred to the background sprouting observed in the control sample). After 20 h of treatment cell apoptosis was observed. Hence, this set of images was discarded from statistical analysis. Rapid apoptosis of endothelial cells in the matrix gel assays is quite common, as was previously reported by, e.g. Riese's and Brodsky's research groups [97,98].

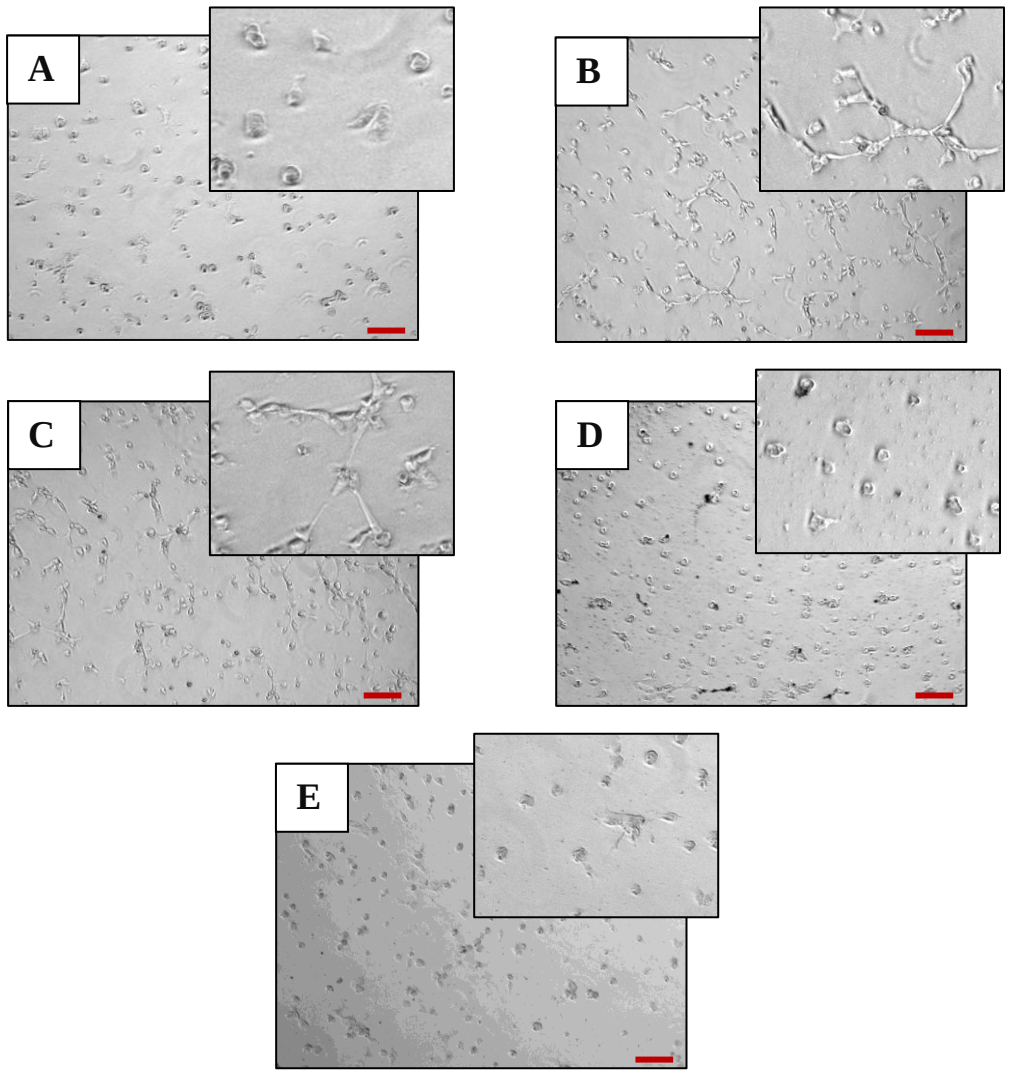

Figure 58. Phase contrast images of capillaries formed by HUVECs after 4 h treatment with: VEGF-B_{167} (B), P1-OEG NPs (C), P2-OEG NPs (D) and P3-OEG NPs (E) in serum-depleted growth media. Untreated cells are shown in (A). Inserts represent magnified fragments of images. Scale bars are 50 μm.

Significant pro-angiogenic activity of P1-OEG NPs can be seen on both graphs, after 2 and 4 h of treatment. The maximum activity was observed after 4 h (over 2 mm tubules – graph **A** and over 90 % RI – graph **B**). These effects were almost as strong as the neo-vascularisation induced with the natural cytokine (VEGF-B_{167}, positive control). After 8 h of treatment the overall tubules length and RI decreased in both, P1-OEG NPs and VEGF-B_{167} stimulated cells; possibly attributed to cell apoptosis, which usually follows capillary formation [97,98]. Nonetheless, the pro-angiogenic effects of P1-OEG NPs were still notable, especially when presented as RI (**Fig. 59B**). After 8 h of incubation neo-

vascular sprouting was also observed in the control sample (untreated cells, **Fig. 59A**). This however, did not outweigh the pro-angiogenic effects deriving from P1-OEG NPs and VEGF-B_{167}. The neo-vascularisation of untreated cells was probably induced by the small amount of growth factors present in the matrix.

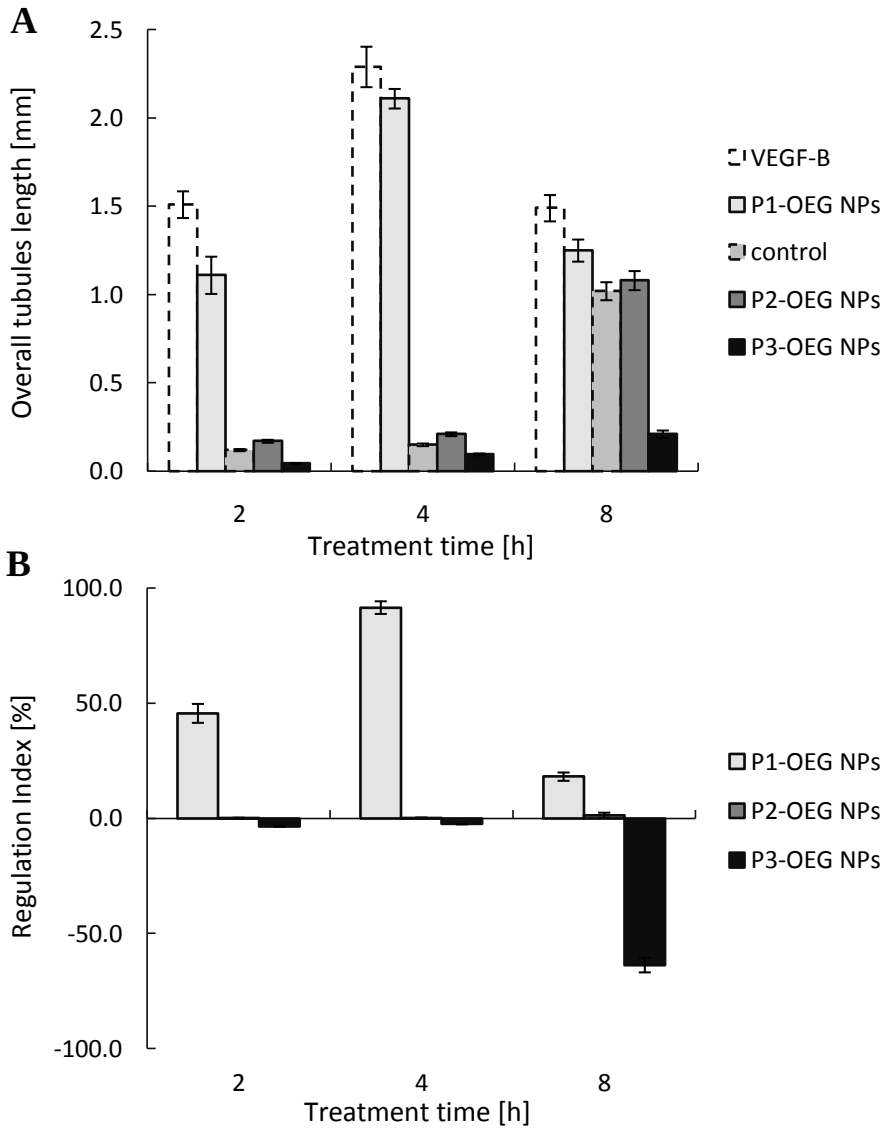

Figure 59. Statistical analysis of capillaries formed by HUVECs, after 2, 4 or 8 h treatment. The total length of tubules per image area (0.216 mm^2) is shown in (A). The regulation index (RI) is shown in (B).

The differences in angiogenic activity between P2-OEG and P3-OEG NPs were barely distinguishable after 2 and 4 h treatment. However, it seemed that P3-OEG NPs showed minor anti-angiogenic activity (**Fig. 59B**, negative value of RI), whilst P2-OEG NPs (based on a mutated sequence) did not show any significant effects on neo-vascular

sprouting. These effects became much clearer after 8 h treatment. Hence, HUVECs treated with P3-OEG NPs did not form capillaries (**Fig. 59A**), while cells incubated with P2-OEG NPs showed a relatively high (similar to the control) level of neo-vascularisation. When RI's (**Fig. 59B**) were taken under consideration, it was evident that P3-OEG NPs acted as anti-angiogenic factors (over -50 % RI), while P2-OEG NPs did not show any activity. Pro-angiogenic action of P1-OEG NPs was still noticeable (around 25 % RI).

As suggested by Ribatti and co-workers, when the inhibitory effects on the neo-vascularisation (or the early stage of this process) are to be assessed, the quantification of BPs can be useful [99]. Hence, the number of BPs (and BrI's) formed by sprouting cells was determined (**Fig. 60**). The maximum number of BPs was found after 4 h of cell treatment with the natural cytokine. After 4 h of stimulation with P1-OEG NPs a relatively high (over 75 % BrI) level of branching was achieved, which additionally confirmed the pro-angiogenic activity of this colloid. Strong inhibition of the BPs formation with P3-OEG NPs was revealed after 8 h treatment (nearly -25 % BrI). Here, the positive effect on BPs formation with P1-OEG NPs decreased, but remained apparent (around 25 % BrI). At all times no major effects of the BPs development was achieved with P2-OEG NPs, which gave further evidence to the lack of any major activity of this colloid upon angiogenesis regulation.

Slightly stronger pro-angiogenic activity of VEGF-B_{167} than P1-OEG NPs can be a consequence of the stronger gene up-regulation with VEGF-B_{167} (see the previous section), related to the receptor binding affinities (Note: as already described in the previous sections, VEGF-B_{167} bind to both, VEGFR-1 and NRP-1 receptors, while P1-OEG NPs predominantly binds to VEGFR-1).

On the other hand, the actual concentration of introduced VEGF-B_{167} was 500 times higher than P1-OEG NPs. This was to keep the number of receptor binding sites constant (assuming that each VEGF-B_{167} can bind to one receptor, while each nanoparticle contains around 500 receptor binding sites; see **chapter 4** for peptide quantification). Despite the lower concentration of NPs, the local concentration of peptides bound to the NPs surface was much higher. Possibly, peptides were more accessible for receptors when presented on the surface of NPs. Consequently, relatively high pro-angiogenic action (nearly as high as with cytokine) was achieved with P1 colloid.

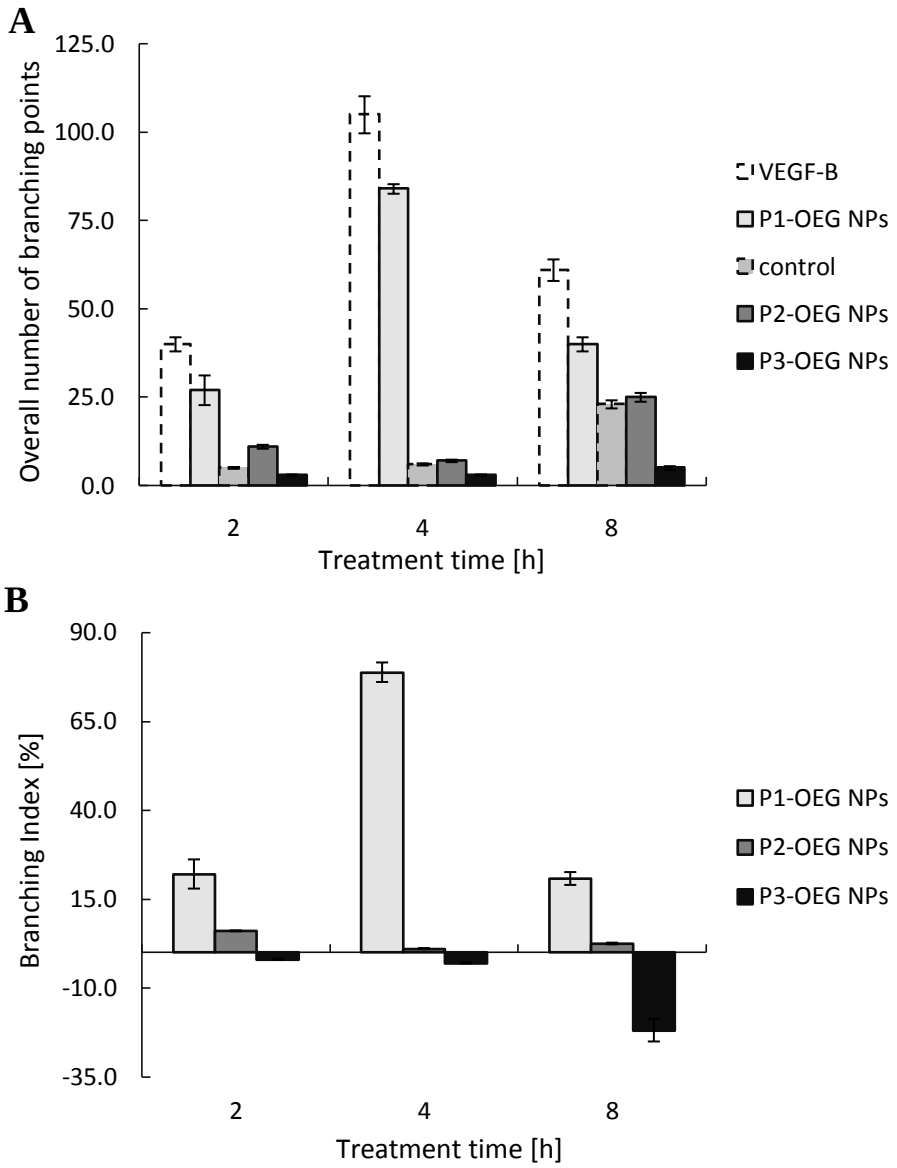

Figure 60. Statistical analysis of capillaries formed by HUVECs, after 2, 4 or 8 h treatment. Overall number of branching points (BPs) per image area (0.216 mm^2) is shown in (A). The branching index (BrI) is shown in (B).

Kay and co-workers suggested that VEGF-B_{167} potentiates, rather than induces angiogenesis in endothelial cells [100]. This is not denied (nor supported) by the results presented in this thesis. However, it can be hypothesised that since the matrix gel contained a reduced amount of growth factor, these could have induced the capillaries formation. The sprouting process was definitely enhanced by the presence of VEGF-B_{167} (or P1-OEG NPs) as shown in **Fig. 59** and **60**. Hence, the pro-angiogenic activity of P1 colloid (as well as the natural cytokine) was confirmed, which was the aim of performed experiments. On the other hand, Li and co-workers reported that VEGF-B_{167} up-regulates

several angiogenesis related genes in HUVECs, including VEGF A [10]. Such activity of both, VEGF-B_{167} and P1 colloids was demonstrated in the previous section. Consequently, even in the absence of other pro-angiogenic molecules (other than VEGF-B_{167} or P1 colloids), the angiogenesis can still be induced (as long as the gene activation is followed by the secretion of VEGF-A isoforms). Therefore, VEGF-B_{167} and P1-OEG NPs can be considered as self-sufficient angiogenesis inductors, even if only indirect (*via* VEGF A gene activation).

In general, P3-OEG NPs showed slightly lower angiogenic activity than P1-OEG NPs. The highest denoted RI value achieved with P1-OEG NPs reached over 90 %, while P3-OEG NPs showed -64 %. One possible explanation can be the presence of growth factors in the matrix gel, which can mask some of the anti-angiogenic activity of P3 based colloids, at the same time enhancing the pro-angiogenic action of P1 colloids.

Generally, colloids acted slightly stronger on the overall length of tubules than the branching process. Specifically, P3-OEG NPs showed over double inhibition of RI than BrI, while the BrI of P1-OEG NPs was over 20 % lower than the RI. It can be hypothesised that this is related to the narrow selectivity in receptor binding (and angiogenic activity) of colloids, when assuming that BPs (and BrI's) represent the early stage of angiogenesis [99]. As already discussed, the early angiogenesis can be initiated by VEGF-A; since VEGF-B_{167} binds to NRP-1 and mediates more stable association between VEGF-A and VEGFR-2 (required for the signalling) [28], possibly enhancing (promoting) the early neo-vascularisation stage. On the contrary, such enhancement did not occur with the P1 colloid, since it predominantly binds to VEGFR-1 (rather than NRP-1).

On the other hand, P3-OEG NPs mediated angiogenesis inhibition was measured with respect to the tubules formed by untreated cells. In control cells, the branching process was only ¼ as effective as in VEGF-B_{167} stimulated cells, while the tubules were formed with ½ efficiency of VEGF-B_{167} treatment (Note: this is based on comparison between overall tubules length and BPs number in cells stimulated for 4 h with VEGF-B_{167} or untreated cells after 8 h incubation). Since the BrI of P3 colloid was referred to the control sample (with a high background, smaller number of BPs), achieved value of BrI not necessarily means less pronounced (inhibitory) effects on the early angiogenesis, with respect to VEGF-B_{167} or P1-OEG NPs (pro-angiogenic) activities.

References:

[1] Risau, W. *Nature* **1997**, *386*, 671-674.

[2] Michiels, C. *J Cell Physiol* **2003**, *196*, 430-443.

[3] Sumpio, B. E.; Timothy Riley, J.; Dardik, A. *Int J Biochem Cell Biol* **2002**, *34*, 1508-1512.

[4] Schnittler, H. J. *Basic Res Cardiol* **1998**, *93*, 30-39.

[5] Clauss, M.; Breier, G. *Mechanisms of angiogenesis*; Brikhauser Verlag, Basel-Boston-Berlin, **2005**.

[6] Dejana, E. *J Clin Invest* **1996**, *98*, 1949-1953.

[7] Cliff, W. J. *Blood vessels (Biological structure and function; 6)*; Cambridge University Press: Cambridge, **1976**.

[8] Carmeliet, P.; Jain, R. K. *Nature* **2000**, *407*, 249-257.

[9] Folkman, J. *Semin Cancer Biol* **2003**, *13*, 159-167.

[10] Zhang, F.; Tang, Z.; Hou, X.; Lennartsson, J.; Li, Y.; Koch, A. W.; Scotney, P.; Lee, C.; Arjunan, P.; Dong, L.; Kumar, A.; Rissanen, T. T.; Wang, B.; Nagai, N.; Fons, P.; Fariss, R.; Zhang, Y.; Wawrousek, E.; Tansey, G.; Raber, J.; Fong, G.-H.; Ding, H.; Greenberg, D. A.; Becker, K. G.; Herbert, J.-M.; Nash, A.; Yla-Herttuala, S.; Cao, Y.; Watts, R. J.; Li, X. *Proc Natl Acad Sci USA* **2009**, *106*, 6152-6157.

[11] Hood, J. D.; Bednarski, M.; Frausto, R.; Guccione, S.; Reisfeld, R. A.; Xiang, R.; Cheresh, D. A. *Science* **2002**, *296*, 2404-2407.

[12] D'Andrea, L. D.; Del Gatto, A.; Pedone, C.; Benedetti, E. *Chem Biol Drug Des* **2006**, *67*, 115-126.

[13] Kobayashi, H.; Lin, P. C. *Nanomedicine* **2006**, *1*, 17-22.

[14] Kim, K. J.; Li, B.; Winer, J.; Armanini, M.; Gillett, N.; Phillips, H. S.; Ferrara, N. *Nature* **1993**, *362*, 841-844.

[15] Goodwin, A. M. *Microvasc Res* **2007**, *74*, 172-183.

[16] Vincent, L.; Kermani, P.; Young, L. M.; Cheng, J.; Zhang, F.; Shido, K.; Lam, G.; Bompais-Vincent, H.; Zhu, Z.; Hicklin, D. J.; Bohlen, P.; Chaplin, D. J.; May, C.; Rafii, S. *J Clin Invest* **2005**, *115*, 2992-3006.

[17] Shanafelt, T. D.; Kay, N. E. *Semin Oncol* **2006**, *33*, 174-185.

[18] Teicher, B. A. *Crit Rev Oncol/Hematol* **1995**, *20*, 9-39.

[19] Veikkola, T.; Alitalo, K. *Semin Cancer Biol* **1999**, *9*, 211-220.

[20] Michael, K.; Patricia, A. D. A. *Cytokine Growth Factor Rev* **1996**, *7*, 259-270.

[21] Neufeld, G.; Cohen, T.; Gengrinovitch, S.; Poltorak, Z. *FASEB J* **1999**, *13*, 9-22.

[22] Shibuya, M. *Int J Biochem Cell Biol* **2001**, *33*, 409-420.

[23] Li, X.; Eriksson, U. *Int J Biochem Cell Biol* **2001**, *33*, 421-426.

[24] Mustonen, T.; Alitalo, K. *J Cell Biol* **1995**, *129*, 895-898.

[25] Ferrara, N.; Davis-Smyth, T. *Endocr Rev* **1997**, *18*, 4-25.

[26] Salikhova, A.; Wang, L.; Lanahan, A. A.; Liu, M.; Simons, M.; Leenders, W. P. J.; Mukhopadhyay, D.; Horowitz, A. *Circ Res* **2008**, *103*, 71-79.

[27] Makinen, T.; Olofsson, B.; Karpanen, T.; Hellman, U.; Soker, S.; Klagsbrun, M.; Eriksson, U.; Alitalo, K. *J Biol Chem* **1999**, *274*, 21217-21222.

[28] Jia, H.; Bagherzadeh, A.; Hartzoulakis, B.; Jarvis, A.; Lohr, M.; Shaikh, S.; Aqil, R.; Cheng, L.; Tickner, M.; Esposito, D.; Harris, R.; Driscoll, P. C.; Selwood, D. L.; Zachary, I. C. *J Biol Chem* **2006**, *281*, 13493-13502.

[29] InnovaBiosciences. Lightning-Link™ R-Phycoerythrin Conjugation Kit, Technical bulletin 7058. **2008**, http://www.innovabiosciences.com/technicalresources/protocols/LL_rpe_release_004.pdf Cambridge, (last accessed 14-09-2010).

[30] Glasmästar, K.; Larsson, C.; Höök, F.; Kasemo, B. *J Colloid Interface Sci* **2002**, *246*, 40-47.

[31] Satulovsky, J.; Carignano, M. A.; Szleifer, I. *Proc Natl Acad Sci USA* **2000**, *97*, 9037-9041.

[32] Ehrenberg, M. S.; Friedman, A. E.; Finkelstein, J. N.; Oberdörster, G.; McGrath, J. L. *Biomaterials* **2009**, *30*, 603-610.

[33] Cui, Z.; Hsu, C.-H.; Mumper, R. J. *Drug Dev Ind Pharm* **2003**, *29*, 689-700.

[34] Verma, A.; Uzun, O.; Hu, Y.; Hu, Y.; Han, H.-S.; Watson, N.; Chen, S.; Irvine, D. J.; Stellacci, F. *Nat Mater* **2008**, *7*, 588-595.

[35] Lichstein, H. C.; Soule, M. H. *J Bacteriol* **1944**, *47*, 231-238.

[36] Lu, J.; Liong, M.; Sherman, S.; Xia, T.; Kovochich, M.; Nel, A.; Zink, J.; Tamanoi, F. *NanoBioTechnology* **2007**, *3*, 89-95.

[37] Giordano, R. J.; Anobom, C. D.; Cardó-Vila, M.; Kalil, J.; Valente, A. P.; Pasqualini, R.; Almeida, F. C. L.; Arap, W. *Chem Biol* **2005**, *12*, 1075-1083.

[38] Buranda, T.; Jones, G. M.; Nolan, J. P.; Keij, J.; Lopez, G. P.; Sklar, L. A. *J Phys Chem B* **1999**, *103*, 3399-3410.

[39] Nelson-Rees, W. A.; Flandermeyer, R. R. *Science* **1976**, *191*, 96-98.

[40] Masters, J. R. *Nat Rev Cancer* **2002**, *2*, 315-319.

[41] Starzec, A.; Ladam, P.; Vassy, R.; Badache, S.; Bouchemal, N.; Navaza, A.; du Penhoat, C. H.; Perret, G. Y. *Peptides* **2007**, *28*, 2397-2402.

[42] Gu, F. X.; Karnik, R.; Wang, A. Z.; Alexis, F.; Levy-Nissenbaum, E.; Hong, S.; Langer, R. S.; Farokhzad, O. C. *Nano Today* **2007**, *2*, 14-21.

[43] Kim, G. J.; Nie, S. *Mater Today* **2005**, *8*, 28-33.

[44] Dixit, V.; Van den Bossche, J.; Sherman, D. M.; Thompson, D. H.; Andres, R. P. *Bioconjug Chem* **2006**, *17*, 603-609.

[45] El-Sayed, I. H.; Huang, X.; El-Sayed, M. A. *Nano Lett* **2005**, *5*, 829-834.

[46] Sokolov, K.; Follen, M.; Aaron, J.; Pavlova, I.; Malpica, A.; Lotan, R.; Richards-Kortum, R. *Cancer Res* **2003**, *63*, 1999-2004.

[47] Yu, D.-H.; Lu, Q.; Xie, J.; Fang, C.; Chen, H.-Z. *Biomaterials* **2010**, *31*, 2278-2292.

[48] Eck, W.; Craig, G.; Sigdel, A.; Ritter, G.; Old, L. J.; Tang, L.; Brennan, M. F.; Allen, P. J.; Mason, M. D. *ACS Nano* **2008**, *2*, 2263-2272.

[49] Giljohann, D. A.; Seferos, D. S.; Patel, P. C.; Millstone, J. E.; Rosi, N. L.; Mirkin, C. A. *Nano Lett* **2007**, *7*, 3818-3821.

[50] Cheng, H.; Kastrup, C. J.; Ramanathan, R.; Siegwart, D. J.; Ma, M.; Bogatyrev, S. R.; Xu, Q.; Whitehead, K. A.; Langer, R.; Anderson, D. G. *ACS Nano* **2010**, *4*, 625-631.

[51] Huang, Y.-F.; Liu, H.; Xiong, X.; Chen, Y.; Tan, W. *J Am Chem Soc* **2009**, *131*, 17328-17334.
[52] Liu, R.; Kay, B. K.; Jiang, S.; Chen, S. *MRS Bulletin* **2009**, *34*, 432-440.
[53] Hosta-Rigau, L.; Olmedo, I.; Arbiol, J.; Cruz, L. J.; Kogan, M. J.; Albericio, F. *Bioconjug Chem* **2010**, *21*, 1070-1078.
[54] Krpetic, Z.; Nativo, P.; Porta, F.; Brust, M. *Bioconjug Chem* **2009**, *20*, 619-624.
[55] von Maltzahn, G.; Ren, Y.; Park, J.-H.; Min, D.-H.; Kotamraju, V. R.; Jayakumar, J.; Fogal, V.; Sailor, M. J.; Ruoslahti, E.; Bhatia, S. N. *Bioconjug Chem* **2008**, *19*, 1570-1578.
[56] Gao, X.; Cui, Y.; Levenson, R. M.; Chung, L. W. K.; Nie, S. *Nat Biotech* **2004**, *22*, 969-976.
[57] Bastus, N. G.; Sanchez-Tillo, E.; Pujals, S.; Farrera, C.; Lopez, C.; Giralt, E.; Celada, A.; Lloberas, J.; Puntes, V. *ACS Nano* **2009**, *3*, 1335-1344.
[58] Levy, R.; Shaheen, U.; Cesbron, Y.; See, V. *Nano Rev* **2010**, *1*, 4889-4907.
[59] Cheng, J.; Teply, B. A.; Sherifi, I.; Sung, J.; Luther, G.; Gu, F. X.; Levy-Nissenbaum, E.; Radovic-Moreno, A. F.; Langer, R.; Farokhzad, O. C. *Biomaterials* **2007**, *28*, 869-876.
[60] Green, J. J.; Chiu, E.; Leshchiner, E. S.; Shi, J.; Langer, R.; Anderson, D. G. *Nano Lett* **2007**, *7*, 874-879.
[61] Gil, P. R.; Parak, W. J. *ACS Nano* **2008**, *2*, 2200-2205.
[62] Mandal, D.; Maran, A.; Yaszemski, M.; Bolander, M.; Sarkar, G. *J Mater Sci: Mater Med* **2009**, *20*, 347-350.
[63] Choi, M.-R.; Stanton-Maxey, K. J.; Stanley, J. K.; Levin, C. S.; Bardhan, R.; Akin, D.; Badve, S.; Sturgis, J.; Robinson, J. P.; Bashir, R.; Halas, N. J.; Clare, S. E. *Nano Lett* **2007**, *7*, 3759-3765.
[64] Jain, P. K.; El-Sayed, I. H.; El-Sayed, M. A. *Nano Today* **2007**, *2*, 18-29.
[65] Hauck, T.; Ghazani, A.; Chan, W. *Small* **2008**, *4*, 153-159.
[66] Li, J. L.; Day, D.; Gu, M. *Adv Mater* **2008**, *20*, 3866-3871.
[67] Ryan, J. A.; Overton, K. W.; Speight, M. E.; Oldenburg, C. N.; Loo, L.; Robarge, W.; Franzen, S.; Feldheim, D. L. *Anal Chem* **2007**, *79*, 9150-9159.
[68] Lee, S.; Xie, J.; Chen, X. *Biochemistry* **2010**, *49*, 1364-1376.
[69] Pennington, M. W.; Dunn, B. M. *Peptide synthesis protocols*; Humana Press Inc.: New Jersey, **1994**.
[70] Cortie, M. B.; McDonagh, A. In *Gold Chemistry: Applications and future directions in life sciences*; Mohr, F., Ed.; WILLEY-VCH Verlag GmbH & Co. KGaA Weinheim, **2009**, p 321-343.
[71] Pengo, P.; Pasquato, L. In *The supramolecular chemistry of organic - inorganic hybrid materials*; Rurak, K., Martinez-Manez, R., Eds.; John Wiley & Sons, Inc. : Hoboken, New Jersey, **2010**, p 113-154.
[72] You, C.-C.; Chompoosor, A.; Rotello, V. M. *Nano Today* **2007**, *2*, 34-43.
[73] Quarta, A.; Ragusa, A.; Deka, S.; Tortiglione, C.; Tino, A.; Cingolani, R.; Pellegrino, T. *Langmuir* **2009**, *25*, 12614-12622.
[74] Nativo, P.; Prior, I. A.; Brust, M. *ACS Nano* **2008**, *2*, 1639-1644.
[75] de la Fuente, J. M.; Berry, C. C. *Bioconjug Chem* **2005**, *16*, 1176-1180.

[76] Liu, Y.; Shipton, M. K.; Ryan, J.; Kaufman, E. D.; Franzen, S.; Feldheim, D. L. *Anal Chem* **2007**, *79*, 2221-2229.
[77] Oyelere, A. K.; Chen, P. C.; Huang, X.; El-Sayed, I. H.; El-Sayed, M. A. *Bioconjug Chem* **2007**, *18*, 1490-1497.
[78] Lévy, R. *ChemBioChem* **2006**, *7*, 1141-1145.
[79] Wang, Z.; Levy, R.; Fernig, D. G.; Brust, M. *Bioconjug Chem* **2005**, *16*, 497-500.
[80] Ghosh, P. S.; Kim, C.-K.; Han, G.; Forbes, N. S.; Rotello, V. M. *ACS Nano* **2008**, *2*, 2213-2218.
[81] Xavier, M.; Karin, M.-A.; Fred, R.; Ralph, W.; Lee, J. *Neoplasia* **2006**, *8*, 214-222.
[82] Montet, X.; Funovics, M.; Montet-Abou, K.; Weissleder, R.; Josephson, L. *J Med Chem* **2006**, *49*, 6087-6093.
[83] Smith, B. R.; Cheng, Z.; De, A.; Koh, A. L.; Sinclair, R.; Gambhir, S. S. *Nano Lett* **2008**, *8*, 2599-2606.
[84] Li, Y.; Zhang, F.; Nagai, N.; Tang, Z.; Zhang, S.; Scotney, P.; Lennartsson, J.; Zhu, C.; Qu, Y.; Fang, C.; Hua, J.; Matsuo, O.; Fong, G.-H.; Ding, H.; Cao, Y.; Becker, K. G.; Nash, A.; Heldin, C.-H.; Li, X. *J Clin Invest* **2008**, *118*, 913-923.
[85] Olofsson, B.; Korpelainen, E.; Pepper, M. S.; Mandriota, S. J.; Aase, K.; Kumar, V.; Gunji, Y.; Jeltsch, M. M.; Shibuya, M.; Alitalo, K.; Eriksson, U. *Proc Natl Acad Sci USA* **1998**, *95*, 11709-11714.
[86] Johnson, L. R. *Essential Medical Physiology*; 3rd ed.; Elsevier: San Diego, **2003**.
[87] Rapley, R.; Harborn, S. *Molecular Analysis and Genome Discovery*; John Wiley & Sons Ltd.: Chichester, **2004**.
[88] Sawaji, Y.; Sato, T.; Takeuchi, A.; Hirata, M.; Ito, A. *Br J Cancer* **2002**, *86*, 1597-1603.
[89] Grasselli, F.; Basini, G.; Bussolati, S.; Bianco, F. *Reprod Fertil Dev* **2005**, *17*, 715-720.
[90] Shweiki, D.; Itin, A.; Soffer, D.; Keshet, E. *Nature* **1992**, *359*, 843-845.
[91] Soker, S.; Miao, H. Q.; Nomi, M.; Takashima, S.; Klagsbrun, M. *J Cell Biochem* **2002**, *85*, 357-368.
[92] Mukherjee, P.; Bhattacharya, R.; Wang, P.; Wang, L.; Basu, S.; Nagy, J. A.; Atala, A.; Mukhopadhyay, D.; Soker, S. *Clin Cancer Res* **2005**, *11*, 3530-3534.
[93] Gao, J.; Xu, B. *Nano Today* **2009**, *4*, 37-51.
[94] Han, G.; Ghosh, P.; De, M.; Rotello, V. *NanoBioTechnology* **2007**, *3*, 40-45.
[95] Free, P.; Shaw, C. P.; Levy, R. *Chem Commun* **2009**, 33, 5009-5011.
[96] Levy, R.; Thanh, N. T. K.; Doty, R. C.; Hussain, I.; Nichols, R. J.; Schiffrin, D. J.; Brust, M.; Fernig, D. G. *J Am Chem Soc* **2004**, *126*, 10076-10084.
[97] Segura, I.; Serrano, A.; De Buitrago, G. G.; Gonzalez, M. A.; Abad, J. L.; Claveria, C.; Gomez, L.; Bernad, A.; Martinez-A, C.; Riese, H. H. *FASEB J* **2002**, *16*, 833-841.
[98] Mezentsev, A.; Merks, R. M. H.; O'Riordan, E.; Chen, J.; Mendelev, N.; Goligorsky, M. S.; Brodsky, S. V. *Am J Physiol Heart Circ Physiol* **2005**, *289*, 1106-1114.
[99] Guidolin, D.; Vacca, A.; Nussdorfer, G. G.; Ribatti, D. *Microvasc Res* **2004**, *67*, 117-124.

[100] Mould, A. W.; Greco, S. A.; Cahill, M. M.; Tonks, I. D.; Bellomo, D.; Patterson, C.; Zournazi, A.; Nash, A.; Scotney, P.; Hayward, N. K.; Kay, G. F. *Circ Res* **2005**, *97*, 60-70.

7. Laser-hyperthermia with OEG NPs and P1-OEG NPs.

Laser light of the appropriate power and frequency causes no damage to mammalian cells (e.g. HUVECs) [1-3]. NIR frequency is generally considered as safe. In the spectral region between 650 and 900 nm (Biological NIR Window) tissue components show minimal extinction characteristics, resulting in the highest light transitivity (see **chapter 2** for theoretical basis). The tissue penetrating properties of NIR light were utilised in photo-thermal treatment with NPs [4-15]. When NIR absorbing NPs (e.g. gold NPs) are associated with the tissue components (cells), NIR light which passes the cell structure, will be absorbed by NPs. Absorbed light will be then converted into heat [16]. This generated heat will result in an increase of the local temperature, leading to heat induced cellular response or cell death [4-9,11-13,16-22] (hyperthermia, see **Scheme 37**). Laser-hyperthermic treatment of HUVECs was performed with NIR absorbing NPs, which were either capped with OEG ligands or additionally conjugated to peptides.

As demonstrated in **chapter 5**, OEG capped nanocomposites were endocytosed by HUVECs following non-specific mechanisms, deriving from the strong charge of these NPs. The overall number of internalised NPs was strongly dependant on their size and shape (SP, NR, HG or CS). On the other hand, it was possible to gain control upon the cellular fate of colloids by incorporating bioactive peptides (P1 or P3, see **chapter 2** for sequences) in the organic corona of NPs (see **chapter 6**). The resulting NPs interactions with cells were mediated by selective recognition between cell receptors and peptides. It was demonstrated that P1 conjugated colloids (P1-OEG NPs) selectively bind to VEGFR-1 receptors over-expressed by HUVECs. Hence, the number of NPs associated with cells did not depend on the size and shape of nanocomposites, but was determined by the NPs functionality and the number of available cell receptors.

HUVECs, tagged with P1-OEG NPs or with endocytosed OEG NPs, were illuminated with NIR laser light (see **Scheme 37** and **chapter 3** for experimental details). Since P1-OEG NPs bind to the cell surface, whilst OEG NPs are internalised, the differences in thermal effects on the cell physiology, deriving from externally or internally associated NPs, could be studied.

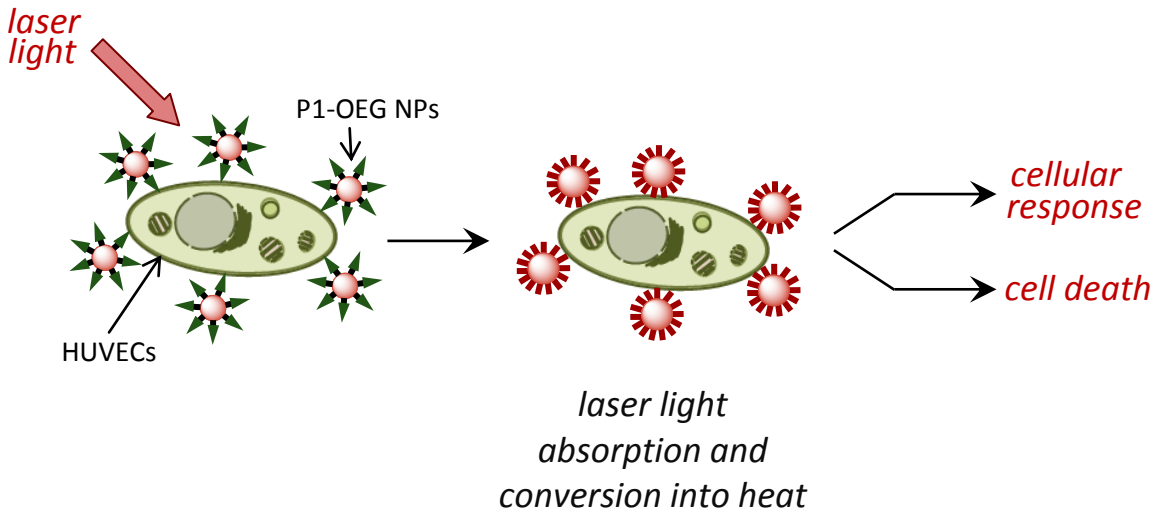

Scheme 37. Schematic illustration of laser induced P1-OEG NPs mediated thermal effects on HUVECs (laser-hyperthermia).

As demonstrated in **chapter 4**, the optical properties (e.g. extinction frequency) of gold colloids can be adjusted by changing the shape and size of NPs. NIR absorbing NPs: NR, HG and CS were synthesised. Their surfaces were capped with OEG ligands then further functionalised with P1 peptides (see **chapter 3** for experimental details and **chapter 4** for physicochemical properties of colloids). P1-OEG NPs were binding to membrane receptors in HUVECs, whilst OEG NPs were internalised by cells. Cells loaded with NPs were exposed to laser light falling within the narrow band gap between 680 and 720 nm (**Fig. 62**, **red lines** and **red shade**). At approximately 700 nm (**Fig. 62**, **black lines**), the plasmon bands of NR, HG and CS were positioned, so that the laser light was absorbed with the highest efficacy.

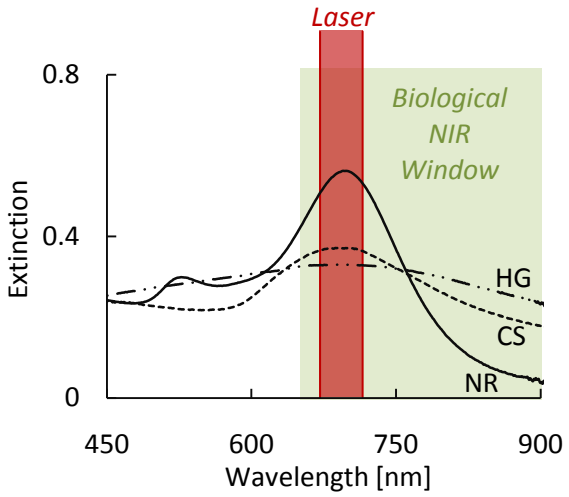

Figure 62. Extinction spectra of OEG capped NPs with absorbance maximum at approximately 700 nm; full line –NR, dashed line – CS and dotted-dashed line – HG. OEG NPs were used in hyperthermia with laser light (700 ± 20 nm) falling within biological NIR window (650 ÷ 900 nm).

It is widely accepted that the efficiency of photo-thermally induced effects on cells depends on the applied laser power [7,8,10,11,13-15,23]. Hence, the laser power was varied over a wide range, from 0.75 to 5 mW (5 ÷ 32 W/cm^2, 200 µm spot size; Note: laser exposure time was kept constant at 10 min. in all experiments). As reported by several research groups, the overall percentage of damaged cells, quantified immediately after laser treatment or after additional post-treatment incubation, can vary [14,24,25]. Consequently, after laser treatment, HUVECs were incubated for 1 or 24 h in fresh growth media (see **chapter 3** for experimental details), prior to studies upon hyperthermia efficiency. The efficiency of photo-induced thermal effects on HUVECs was assessed by two complimentary techniques: cell viability and gene expression profiling. Cell viability studies showing the cell survival rate (see **chapter 3** for experimental protocol) will be demonstrated in **section 7.1**. Gene expression profiling assay, illustrating the heat shock response of HUVECs (see **chapter 3** for experimental protocol) will be demonstrated in **section 7.2**.

7.1. HUVECs survival rate.

HUVECs were treated with two types of colloids: OEG and P1-OEG coated. OEG NPs were internalised by cells (see **chapter 5** for uptake studies), while P1-OEG NPs stayed attached to the outer surface of cells (bound to VEGFR-1, see **chapter 6**). Consequently,

two strategies in laser-hyperthermia: intra- and extracellular, were investigated. As will be demonstrated in this section, laser induced intracellular damage in cells lead to a different overall cell survival rate than membrane injuries (extracellular approach).

To investigate further the role of NPs in laser-hyperthermia, three types of NPs (NR, HG and CS) were employed. It was found that in general, the type of NPs have a strong effect on the cell survival rate. Percent of dead HUVECs to the overall number of treated cells was quantified by cell viability assays (trypan blue staining, see **chapter 3** for experimental). Positively stained cells (damaged), as well as the whole cell population were manually counted on phase contrast and bright field images.

As an example, a set of bright filed and phase contrast images of HUVECs is shown in **Fig. 63**. Rows represent HUVECs without (control) or with P1-OEG NPs (HG, NR or CS). Phase contrast images of HUVECs before laser treatment are shown in **the left column**. After illumination (24 W/cm^2, 200 μm laser spot size designated by red dashed circles, 10 min.), cells were incubated in fresh growth media for 1 h (see **chapter 3** for experimental details) and stained with trypan blue viability stain. Phase contrast images of stained cells are shown in **the middle column**, while bright field in **the right column**. Clearly, the majority of cells within circles was damaged (blue spots), while non-illuminated cells (outside circles) or cells without NPs (control) survived treatment. The cell damage rate was estimated at 86.7 % after treatment with P1-OEG HG, 85.4 % for P1-OEG NR and 49.2 % with P1-OEG CS. Only background level of damage was observed in control sample (1 %).

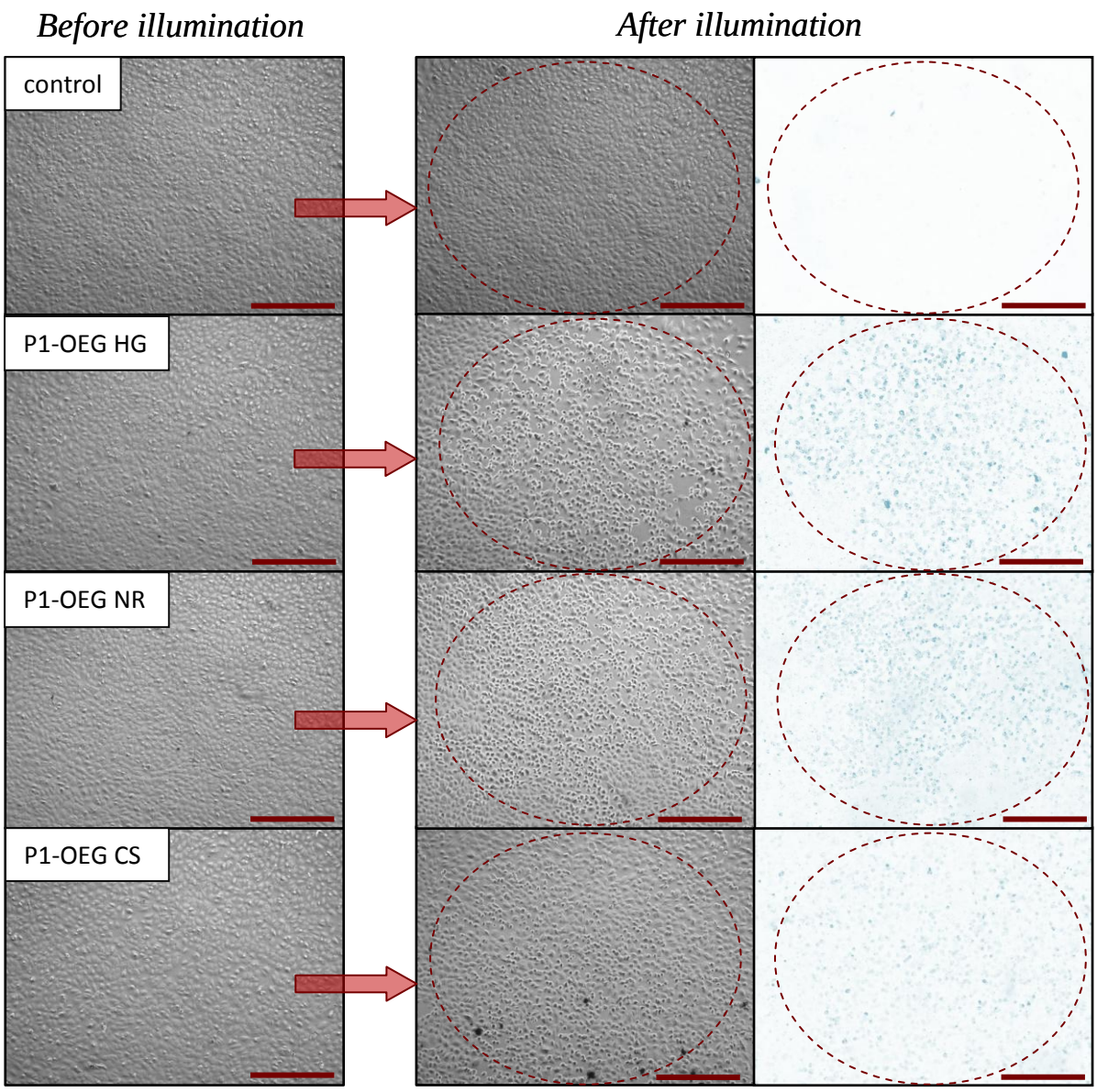

Figure 63. Phase contrast (left and middle) and bright field (right) images of HUVECs before (left) and after (middle and right) exposure to NIR laser (10 min., 24 W/cm^2) and 1 h incubation at 37 °C followed by viability staining. Rows represent HUVECs without NPs (control), and P1-OEG NPs: hollow gold (P1-OEG HG), nanorods (P1-OEG NR), and core/shells (P1-OEG CS). Dashed red circles indicate laser spots. Scale bars are 50 µm.

According to the literature, each type of NPs (meaning the size and shape of metallic cores) shows different energy conversion rate (absorbed light to heat) [6,11-13,16,26]. As already mentioned in **chapter 2**, Richardson and co-workers calculated that a single gold nanoparticle, around 60 nm in diameter, can generate 5 µW of heat if SPR illuminated with 2 mW laser light [16]. However, the overall heating intensity can be significantly enhanced

by collective effects of several NPs, e.g. NPs entrapped in cell endosomes or associated with the cellular membrane. Assuming that comparable numbers of each type of P1-OEG NPs (NR, HG and CS, approximately 5000 ± 3000 per cell; see **chapter 6**) were associated with HUVECs, the least efficient heating (measured by the number of damaged cells) was observed with CS.

As already mentioned, the efficiency of laser-hyperthermia (referred to the percentage of damaged cells in the overall number of treated cells) not only depends on the type of NPs, but can be controlled by adjusting the laser power used during treatment [7,8,10,11,13-15,23] (Note: the illumination time was kept constant). Consequently, laser power density (LPD) in presented studies, was varied between 5 ÷ 32 W/cm^2. To fully investigate the effects of variable LPD (along with the type of nanocomposites) on the cell survival rate, different types of NPs (NR, HG and CS) with different functionality: P1-OEG NPs or OEG NPs, were employed. These studies were further extended by applying variable post-treatment incubation time (1 or 24 h), which can be considered as an additional (third) parameter on which hyperthermia efficiency depends.

HUVECs (without and with NR, HG or CS) before and after laser treatment (followed by viability staining) were imaged. On every image, the number of damaged cells and overall number of treated cells were counted. These numbers were plotted against variable LPD (**Fig. 64**). Separate graphs were prepared for each type of NPs (NR, HG and CS) and functionality (P1-OEG and OEG NPs). Two data-sets are shown on each graph, representing the percentage of damaged cells, quantified after 1 h post-treatment incubation (triangles) or after 24 h (diamonds). Controls, showing the damage in laser-irradiated but NPs-free cells are shown in the **Appendix B**.

Comparative studies of the graphs allowed the determination of major aspects of NPs mediated treatment, as discussed in the following paragraphs. Variations in cell survival rate, deriving from the type (NR, HG and CS) or functionality (OEG and P1-OEG) of NPs were identified. The cell recovery rate after 24 h post-treatment incubation was also assessed.

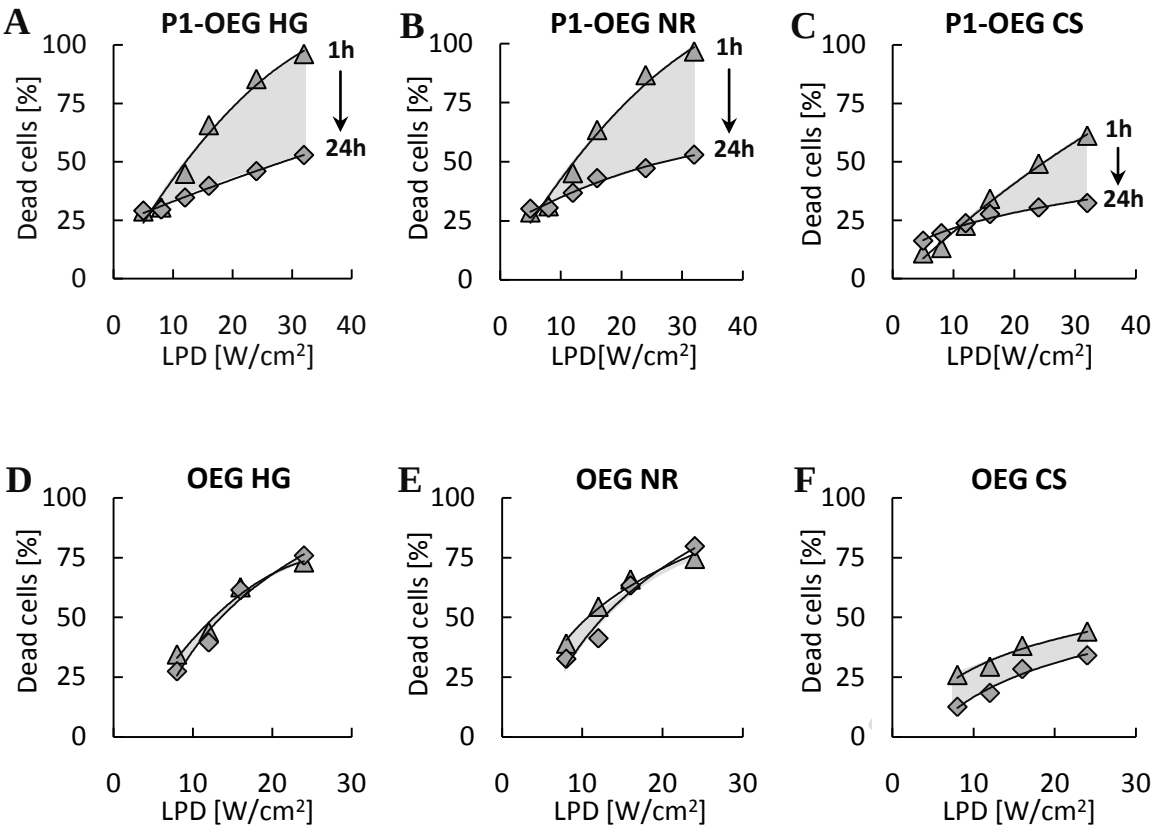

Figure 64. HUVECs number after the treatment with variable laser power density (LPD) and: hollow (A and D), rod-like (B and E) and core/shell (C and D) NPs; P1-OEG NPs (A ÷ C), OEG capped (D ÷ F). Symbols indicate percentage of dead cells determined after 1 h (triangles) and 24 h (diamonds) of incubation, which followed the exposure of the laser light. Grey areas represent changes in the overall number of cells recovered over the post-treatment incubation.

The percentage of injured HUVECs increased with LPD. Clearly, the use of laser light induced damage within cells. Until 24 W/cm^2 LPD was reached, control samples (cells without any NPs) showed only a background level of damage (see **Appendix B**). This significantly lower number (or none) of injured cells in the control samples, compared to cells with associated NPs, indicated NPs mediated damage in cells. Further increase of LPD to 32 W/cm^2 resulted in 25 % of damage in the control samples. Evidently this LPD value is excessively high for selective (NP mediated) hyperthermia. On the other hand, no major effect on cell viability was observed when 5 W/cm^2 LPD or 8 W/cm^2 LPD was applied. Therefore, to simplify further experiments and data analysis, the lowest LPD was

discarded. Consequently, only 8 ÷ 24 W/cm^2 LPD range is presented on graphs in **Fig. 64D ÷ F**.

It can be concluded that in general, cell survival rates decrease with LPD. However, the exact percentage of survived cells (thus, the efficacy of treatment) varies with the type (NR, HG and CS) and functionality (P1-OEG or OEG) of NPs.

The efficacy of treatment, depending on the type of anisotropic cores of NPs, was assessed with P1-OEG functionalised NPs (**Fig. 64A ÷ C**); assuming that the average number of each type of P1-OEG NPs associated with the cellular membrane was comparable. As estimated from TEM images (see **chapter 6**), approximately 5000 ± 3000 of P1-OEG NPs were attached to each cell (*via* VEGFR-1 receptors; Note: HUVECs from the same umbilical cord and the same passage, thus over-expressing similar number of VEGFR-1 were used in each set of experiments). Consequently, from **graphs A ÷ C**, it can be hypothesised that treatment with NR and HG results in a similar degree of damage within cells (similar hyperthermia efficacy). This is considerably higher than after treatment with CS. Low hyperthermia efficacy with CS was previously reported, e.g. Xia's group demonstrated that 1.5 W/cm^2 LPD (5 min.) is required to effectively inactivate SKBR3 breast cancer cells tagged with PEG-antiHER2 capped nanocages [8,14,27], while according to Drezek and co-workers, 35 W/cm^2 LPD (7 min.) is needed to destroy these cells with CS (also PEG-antiHER2 capped) [28].

Treatment efficacy with OEG functionalised NR, HG and CS was also investigated. Here however, direct comparison between each type of NPs was more difficult. Since, as demonstrated in **chapter 5**, the overall number of internalised OEG NPs depends very strongly on their shape and size (Note: 2486 ± 460 OEG NR, 363 ± 82 OEG HG and 901 ± 99 OEG CS per cell were found, see **chapter 5**). Such variations in the quantity of NR, HG and CS endocytosed by HUVECs, might affect the intensity of intracellular damage, caused by each type of NPs. However, as can be seen in **Fig. 64D ÷ F**, it is clear that hyperthermia with CS was not as efficient as when NR or HG were used; even though, e.g. more CS than HG were internalised by HUVECs.

Interestingly, OEG NR showed only slightly higher hyperthermia efficiency than OEG HG, even though over 6 times more NR than HG were internalised by HUVECs (see **chapter 5**). One possible explanation can be a slightly higher energy conversion rate [13,26] (and larger absorption cross-section [26,27]) with HG, than with NR, as reported previously.

Assuming that more heat is generated with HG (than e.g. NR), lower overall number of HG (than e.g. NR) is required to generate a similar temperature increase. However,

other parameters should also be considered here, e.g. distribution of NPs inside cells (referred to the number of endosomes per cell and number of NPs per each vesicle, see **chapter 5** for TEM images), could have an effect on the local temperature increase rate and on the type of cellular compartment damaged the most. The effect of heat level (temperature) on cell survival (more heat equals to more damage) was reported in the past by several research groups [5,6,8,11,16,19,22,24,26], whilst the effect of the type of cellular compartment damaged during hyperthermia on cell survival was not widely investigated.

Hence, the relationship between the type of cell injuries (cell compartment) and treatment efficacy was investigated using OEG and P1-OEG NPs. Treatment with OEG NPs resulted in thermal damages of the inner parts of the cell, while P1-OEG NPs led to cellular membrane injuries.

Initially, the use of P1-OEG NPs (**Fig. 64A ÷ C**) led to a higher death rate (triangles), than the analogous OEG NPs (observed in all types of NPs: NR, HG and CS). However, this trend changed when elongated post-treatment incubation (24 h) was applied (diamonds). Here, treatment with OEG NPs seemed to be more effective in cell inactivation, compared to P1-OEG NPs. Specifically, irreversible damage of cellular organelles leading to 75 % of death was achieved with OEG NR or HG, while irreversible damage of cellular membrane resulting in 50 % of death was observed with P1-OEG NR or HG.

One more aspect of hyperthermia can be identified by cell viability studies. Specifically, the comparison between the number of damaged cells determined after 1 or 24 h of post-treatment incubation shows the cell recovery rate (designated by gray fields). The recovery rate of HUVECs treated with both, OEG NPs (intracellular damage) and P1-OEG NPs (extracellular damage) was studied*. It can be concluded (**Fig. 64**) that HUVECs treated with OEG NPs (NR, HG and CS; intracellular injuries) do not recover after elongated post-treatment incubation time, compared to cells treated with analogues P1-OEG NPs (extracellular injuries). These findings come into agreement with the literature. There are reports showing that cells with a damaged cellular membrane are prone to recovery, after e.g. electroporation (cell transfection technique) [29,30] or trypsinisation (cell passaging method) [31,32].

Based on the presented differences in the cell survival rate after treatment with OEG NPs and analogues P1-OEG NPs, the importance in selecting the appropriate strategy in laser hyperthermia (intra- or extracellular) should be emphasised here. When intended to combine laser-hyperthermia with drug delivery (e.g. into drug resistant cells [25]), the use of

* Note: Cells are considered damaged, when positively stained with trypan blue. Viability stain can penetrate both: dead cells and cells with holes in the outer membrane but still alive, as partially destroyed membrane cannot prevent the penetration of the stain.

P1-OEG NPs seems to be a rational option. This is because the majority (nearly 90 %) of cells becomes accessible to drugs (holes in the cellular membrane; Note: viability stain could penetrate cells), until 1 h after laser illumination. On the other hand, the use of OEG NPs should give better results, when laser hyperthermia is the only method of damaging the unhealthy cells (e.g. tumour) [7,10,12,14]. This is because here, the death rate (treatment efficacy) remains high even after 24 h of post-treatment incubation.

It is also important to highlight that the presented hyperthermia efficiency values, were derived from experiments conducted on healthy mammalian cells, not on malignant cells. As already explained in **chapter 2**, malignant cells are more sensitive to temperature changes than mammalian cells [5,7,9,12,17,19-21,33-36]. This means that if the presented system (both, OEG NPs and P1-OEG NPs) is to be used in tumour treatment, higher cell death rate can be expected.

One may consider additional parameter deriving from cell physiology (cell age), when discussing possible efficiency of hyperthermic treatment, as the cell survival rate depends strongly on the cell division cycle phase [18,33,37,38]. Hahn's group reported the highest thermo-sensitivity of HeLa cells in late S (synthesis phase, DNA replication) and early G-2 phases (growth phase, e.g. synthesis of microtubules), while the lowest thermo-sensitivity was observed in early G-1 phase (growth phase, e.g. synthesis of enzymes) [37]. Hence, higher death rates should be expected among cells in thermo-sensitive phase than cells in thermo-resistant phase.

However, cell physiology deriving from the cell type seems to have a dominating effect not only on the overall cell survival rate, but also on the mechanism of cell inactivation [5,7,9,10,12,17-21,33-35,38-40] (see **chapter 2** for more details biochemical basis of hyperthermia). According to Bouchier-Hayes and co-workers, heat shock stressor in human endothelial cells induces apoptosis (programmed death), rather than necrosis (premature death) [20]. It was also demonstrated that the apoptosis of endothelial cells can be induced when moderate heat treatment is combined with ROS stimuli. Such combination results in enhanced heat shock response (death) by simultaneous oxidative stress response (to ROS). In the presented NPs mediated hyperthermia no additional stressors (besides NPs and heat) were used. Despite that sufficient cell damage leading to cell death was achieved, possibly suggesting a high level of heat generated with NPs and/or releasing of another type of stressor (e.g. toxic species) from nanocomposites upon the laser illumination. One way to determine whether observed effects on cells indeed were driven by the temperature increase is to study the expression levels of genes

selectively regulated by the temperature changes (see **chapter 2** for heat shock response in HUVECs). This will be demonstrated in the following section.

7.2. Matabolism changes in survived HUVECs.

As demonstrated in the previous section, laser-hyperthermia with OEG HG and OEG NR resulted in up to 75 % of dead HUVECs (24 W/cm^2 LPD). Over 50 % of cells were found dead (after 24 h post-treatment incubation) when P1-OEG HG and P1-OEG NR were used. CS based nanocomposites were notably less effective in hyperthermia than HG or NR analogues. One possible explanation of this might be that not enough heat was generated with CS to destroy the majority of cells. Since not all cells were killed during laser treatment (especially when CS and/or low LPD were used) it would be interesting to identify if survived HUVECs were affected in any other way.

It is well-known that increased temperature induces stress response in mammalian cells [17-19,21]. Nonlethal heat induces changes in cell metabolism, including up- or down-regulation of many important genes and protein expression levels (e.g. heat shock proteins – HSPs, see **chapter 2** for more details). Justus and co-workers reported down-regulation of endothelial adhesion molecule 1 (ELAM-1) and inter-cellular adhesion molecule 1 (ICAM-1) genes in HUVECs [39]. These genes encode adhesion molecules, which are critical for angiogenesis (blood vessels growth, primary function of HUVECs, see **chapter 2**) and tumour metastasis [39,41-46]. Both, ELAM-1 and ICAM-1 affect fundamental cellular activities and are regulated by temperature variations. Thus, their expression levels were studied in cells, which survived laser-hyperthermia. By this way it was possible to assess if and how strong the metabolism of cells was affected.

Genes profiling assays (see **chapter 3** for experimental) were performed after cells treatment with OEG NPs or P1-OEG NPs and illumination with 12 or 24 W/cm^2 LPD. Since, 24 W/cm^2 LPD (10 min.) was the highest power used in selective hyperthermia (see the previous section; LPD over 24 W/cm^2 caused damage in control samples), the maximum level of gene regulation in survived HUVECs was expected here. On the contrary, the exposure to 12 W/cm^2 LPD caused only approximately 25 % damage, thus considerably smaller gene regulation was anticipated at this point. Regulatory effects on genes deriving from laser-hyperthermia with three types of NPs (NR, HG and CS) were tested, while NPs-free cells served as controls. All results were normalised to GAPDH expression levels (standard used in data normalisation [47]) and referred to non-treated

HUVECs (no NPs and no laser). As previously reported by Justus and co-workers, to determine inhibitory effect of heat on ELAM-1 and ICAM-1 genes, cells were stimulated with tumour necrosis factor α (TNF-α, see **chapter 2** for more details and **chapter 3** for experimental protocols) for 5 h in fresh growth media (full-serum) straight after laser treatment (also non-treated HUVECs) [39]. The results are shown in **Fig. 65**. Clearly both, ELAM-1 and ICAM-1 genes in survived HUVECs were significantly down-regulated. Fold down-regulation was strongly dependent on LPD (increased with LPD) and type of NP.

Laser-hyperthermia with OEG NPs (**graphs A** and **B**) resulted in a stronger regulation of ELAM-1 than ICAM-1 gene in all tested conditions. Nearly -160 fold regulation of ELAM-1 was achieved after the illumination with 24 W/cm^2 LPD, while 12 W/cm^2 LPD resulted in -80 fold. Clearly, an increase in LPD led to more efficient down-regulation of both genes. ELAM-1 and ICAM-1 were regulated most effectively with OEG NR, while with OEG CS the least. Similar trends were observed in cell survival rate, possibly attributed to the overall number of endocytosed NPs (see **chapter 5**), as explained in the previous section. Low uptake rate of CS along with low energy conversion rate (absorbed light to heat, reported by several research groups [11,13,14,27,28,48]) can be one possible explanation of the least significant effects on gene expression levels, observed after CS mediated hyperthermia. **Graphs C** and **D** represent P1-OEG NPs mediated effects on genes induced by illumination with 12 and 24 W/cm^2 LPD, respectively. Exposure to 12 W/cm^2 LPD resulted in down to -25 fold regulation of tested genes (NR and HG) with only slightly stronger regulation of ICAM-1.

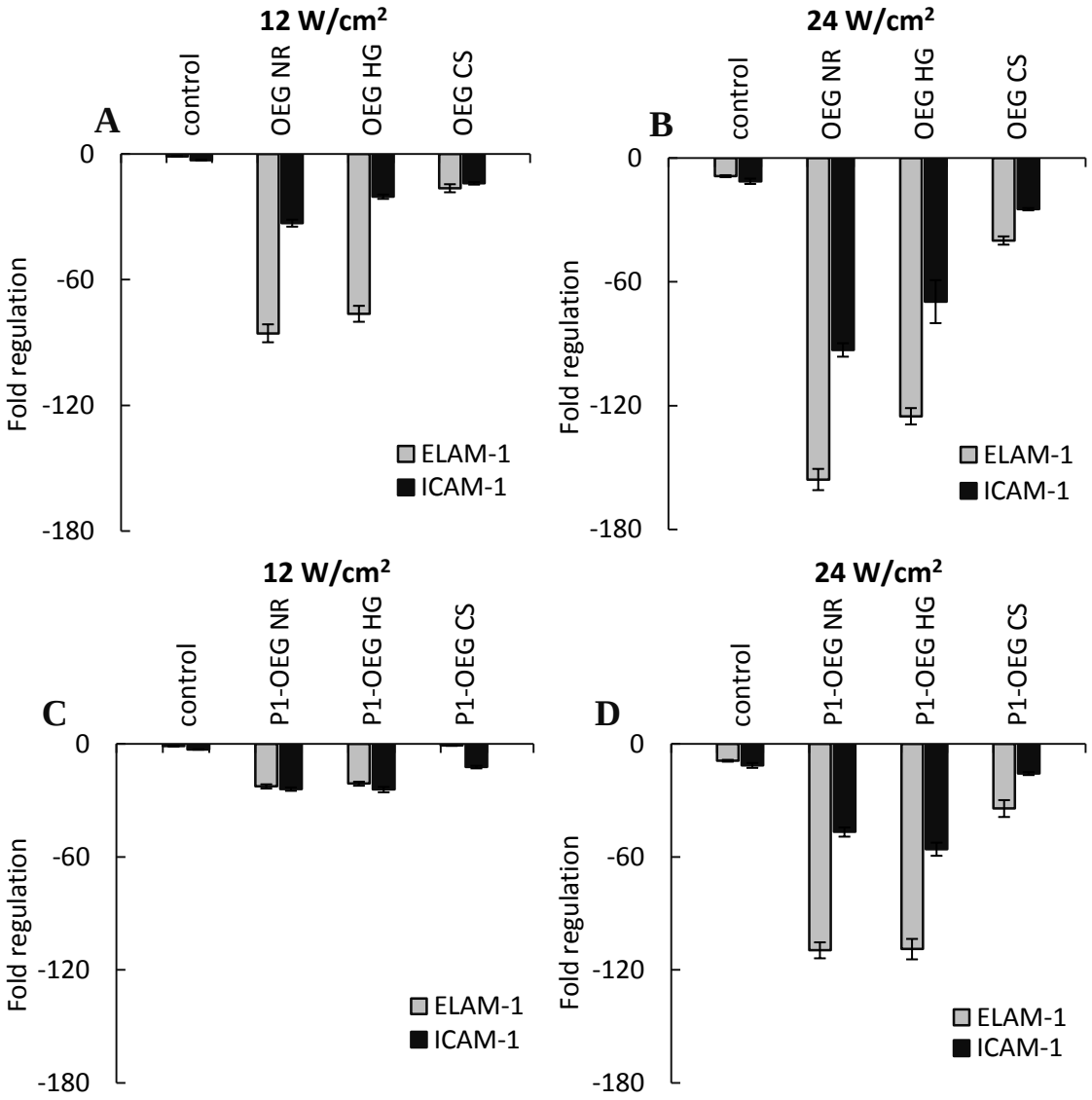

Figure 65. Gene expression profiling in HUVECs after the treatment with low, 12 W/cm^2 (A and C) and high, 24 W/cm^2 (B and D) laser power density and OEG capped (A and B) and P1-OEG NPs (C and D); hollow gold (HG), nanorods (NR) and core/shell (CS) NPs. Control samples did not contain any NPs, but were exposed to the laser.

Justus and co-workers previously reported down-regulation of ELAM-1 and ICAM-1 genes after 1 h exposure of HUVECs to 37 ÷ 44 ºC [39]. Similar expression levels of both genes tested were observed after: a) treatment with 12 W/cm^2 LPD and P1-OEG HG or NR, presented here; and b) temperature-hyperthermia, reported by Justus [39]. Therefore, it can be hypothesised that similar levels of shock response were achieved in HUVECs after both, a) and b). Possibly, illumination with 24 W/cm^2 LPD (HG and NR) generated more extreme conditions (more e.g. heat or other factors, like photoelectron emission or shock

wave [26,27,49,50]), leading to stronger regulation of both genes, with notably higher expression level of ELAM-1.

P1-OEG CS mediated hyperthermia with 12 W/cm^2 LPD had only minor effects on cell metabolism, which was indicated by a negligible inhibition of genes (referred to control samples). This is in agreement with cell viability studies (see the previous section), which showed much stronger effects on HUVECs achieved with NR and HG mediated hyperthermia, than CS. This can be attributed to the smaller shock (e.g. heat shock) generated with CS than NR or HG, since as previously mentioned comparable numbers of CS, NR and HG were attached to each cell (see **chapter 6** for more details).

Importantly, even though over 50 % cells survived treatment with P1-OEG HG or P1-OEG NR and 12 W/cm^2 LPD (see the previous section), their metabolism was significantly affected. Sufficient inhibition of the expression of adhesion proteins can possibly prevent tumour metastasis, if the presented system is to be applied in cancer treatment.

As demonstrated by Ito and co-workers, hyperthermia (42 ºC, 4 h) suppresses the expression of VEGF-A (all isoforms, see **chapter 2** for theoretical background on growth factors) in human fibrosarcoma HT-1080 cells, resulting in the inhibition of proliferation of endothelial cells (ECs) *in vitro* [47]. ECs inhibition was attributed to the lack of sufficient quantity of growth factors in growth media. It is also known that hyperthermia can affect basic functions carried out by ECs *in vivo*, e.g. Kwan and co-workers reported inhibition of angiogenesis in mice [51]. However, hyperthermia mediated inhibition of expression of VEGF A gene in ECs themselves has not been reported so far.

Given that P1-OEG NPs can activate the expression of VEGF A gene in HUVECs, as shown in **chapter 6**, it was critical to assess, whether any effects on the expression of VEGF A gene in HUVECs deriving from P1-OEG NPs binding to receptors along with laser induced hyperthermia, can be observed. As shown in **Fig. 66**, only background levels (below 0.1 fold; Note: the activation of VEGF-A with P1-OEG NPs at 37 ºC was 0.8 ÷ 25 fold; see **chapter 6**) of VEGF A regulation were denoted. Insignificant effects on the VEGF A gene can be attributed to, e.g. thermal inactivation of receptors by localised heat (assuming residual levels of VEGF A in serum; see the previous chapter). On the other hand, the same background level of VEGF A expression after the illumination with 24 W/cm^2 LPD (as 12 W/cm^2 LPD; data not shown) suggests rather marginal role of the temperature itself (assuming that the temperature increases with LPD [25]) on the regulation of VEGF A gene (in agreement with the literature [17,21]).

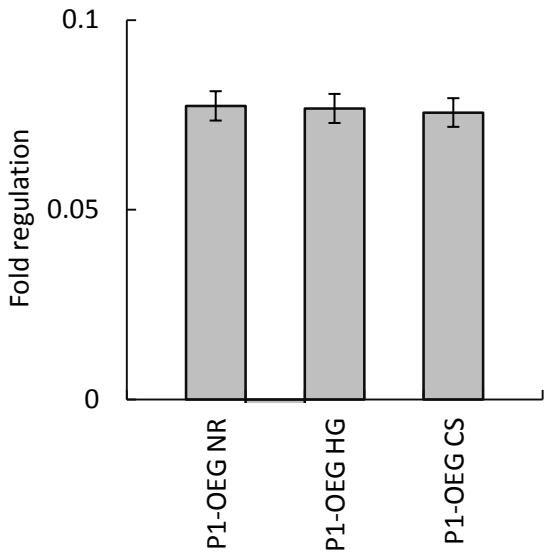

Figure 66. VEGF A gene expression profiling of HUVECs tagged with P1-OEG NPs, after illumination with 12 W/cm^2 LPD.

In general, stronger gene regulation was observed with OEG NPs than with P1-OEG NPs. One possible explanation can be the post-treatment cell recovery. As demonstrated in the previous section, laser and P1-OEG NPs treated cells can recover to an extent, while OEG NPs treated cannot. Consequently, it was hypothesised that HUVECs (after hyperthermia with P1-OEG NPs) can start the recovery process during 5 h of post-treatment incubation [35,40,52], which can result in less significant effects on gene expression levels.

To investigate whether post-treatment incubation has an effect on gene expression levels, HUVECs after laser-hyperthermia were either immediately treated with TNF-α (to induce the expression of ELAM-1 [36,39]) or incubated for 1 h (to allow recovery) before the stimulation. P1-OEG NR and P1-OEG HG were utilised in this experiment, since CS based nanocomposites showed only minor effects on genes (see **Fig. 65**). Thus, it would be hard to observe any changes in gene expression levels deriving from CS mediated treatment.

Clear differences in fold regulation of ELAM-1 (**Fig. 67**) were detected (-120 before and -70 after the recovery), while no major changes in the expression levels of ICAM-1 were denoted; possibly because ELAM-1 is not constituently expressed, but induced upon stimulation with TNF-α [36,39], while ICAM-1 is over-expressed by non-stimulated cells

[43,44]. Consequently, 1 h delay in the cell stimulation after laser treatment resulted in much lower expression levels of ELAM-1 (cell recovery).

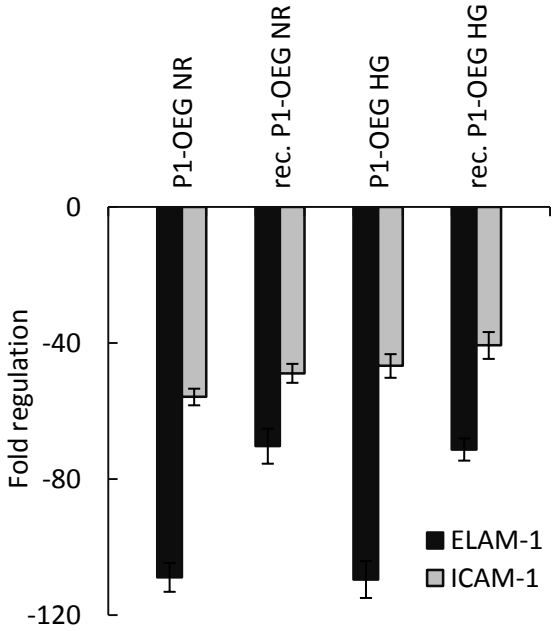

Figure 67. Gene expression profiling of P1-OEG NR and P1-OEG HG tagged HUVECs after illumination with 24 W/cm^2 LPD and after additional 1 h post-treatment incubation: rec. P1-OEG NR and rec. P1-OEG HG.

As already mentioned at the beginning of this section and demonstrated in the previous section, selective (NP mediated) damage in cells can be achieved with a maximum 24 W/cm^2 LPD (Note: above 24 W/cm^2, up to 30 % of cells without NPs 'control samples' was damaged). To investigate if LPD higher than 24 W/cm^2 LPD affects the metabolism of survived cells in the control samples, the expression levels of ELAM-1 and ICAM-1 genes were studied.

As seen in **Fig. 68**, strong down-regulation of both genes (down to -100 fold of ELAM-1) was observed with 32 W/cm^2 LPD. Illumination with 24 W/cm^2 LPD or less resulted in reasonably lower alteration of gene expression levels (compared to cells treated with NPs). Thus, confirming the maximum value of LPD, at which hyperthermia can be considered as selective to cells containing NPs.

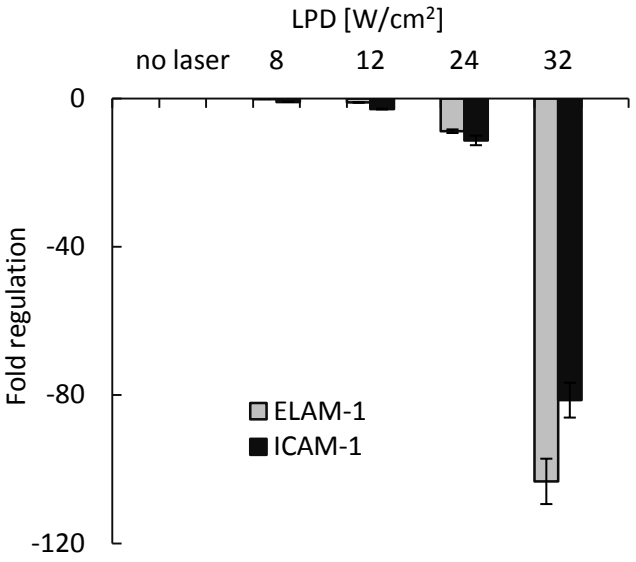

Figure 68. Gene expression profiling of NPs-free HUVECs, after illumination with various LPD (8 ÷ 32 W/cm^2).

Relatively high down-regulation of genes in control samples illuminated with 32 W/cm^2 should be attributed to heat, since no other stressor (NPs) was present. Therefore, it can be hypothesised that the cellular response to treatment with NPs and laser can be also derived from heat, rather than additional stressors coming from NPs (e.g. photoelectron emission or other toxic species released by illuminated NPs [49,50]).

To summarise, laser-hyperthermia with gold colloids led to a down-regulation of ELAM-1 and ICAM-1 genes in survived HUVECs. An increase in LPD resulted in more pronounced down-regulation of both genes, with the highest efficiency achieved using NR and HG, while the lowest with CS. Laser-hyperthermia with OEG NPs (internalised) resulted in more down-regulation than with P1-OEG NPs (associated with cell membrane). In both cases however, cell metabolism was significantly affected. Physical association of P1-OEG NPs with VEGFR-1 did not induce any notable changes in VEGF A gene expression levels, possibly due to the thermal inactivation of receptors by localised heat. Post-treatment cell recovery studies reviled significant differences in the expression level of ELAM-1 gene, while no major effects on ICAM-1 were denoted. Gene expression studies in laser treated control samples (without NPs), confirmed the maximum threshold for selective (NPs mediated) hyperthermic damage in HUVECs, at 24 W/cm^2 LPD or less.

References:

[1] Kim, J. G.; Mengna, X.; Hanli, L. *IEEE Eng Med Biol* **2005**, *24*, 118-121.

[2] Prahl, S. Optical Absorption of Hemoglobin. **1999**, http://omlc.ogi.edu/spectra/hemoglobin/ Oregon Medical Laser Center Oregon (last accessed: 04-09-2010).

[3] Hale, G. M.; Querry, M. R. *Appl Opt* **1973**, *12*, 555-563.

[4] Huang, X.; El-Sayed, I. H.; Qian, W.; El-Sayed, M. A. *J Am Chem Soc* **2006**, *128*, 2115-2120.

[5] Overgaard, J. *Cancer* **1977**, *39*, 2637-2646.

[6] Lukianova-Hleb, E. Y.; Anderson, L. J. E.; Lee, S.; Hafner, J. H.; Lapotko, D. O. *Phys Chem Chem Phys* **2010**, *12*, 12237-12244.

[7] Huff, T. B.; Tong, L.; Zhao, Y.; Hansen, M. N.; Cheng, J.-X.; Wei, A. *Nanomedicine* **2007**, *2*, 125-132.

[8] Chen, J.; Wang, D.; Xi, J.; Au, L.; Siekkinen, A.; Warsen, A.; Li, Z.-Y.; Zhang, H.; Xia, Y.; Li, X. *Nano Lett* **2007**, *7*, 1318-1322.

[9] Lowery, A. R.; Gobin, A. M.; Day, E. S.; Halas, N. J.; West, J. L. *Int J Nanomedicine* **2006**, *1*, 149-154.

[10] Lal, S.; Clare, S. E.; Halas, N. J. *Acc Chem Res* **2008**, *41*, 1842-1851.

[11] Cole, J. R.; Mirin, N. A.; Knight, M. W.; Goodrich, G. P.; Halas, N. J. *J Phys Chem C* **2009**, *113*, 12090-12094.

[12] O'Neal, D. P.; Hirsch, L. R.; Halas, N. J.; Payne, J. D.; West, J. L. *Cancer Lett* **2004**, *209*, 171-176.

[13] Huang, X.; Jain, P.; El-Sayed, I.; El-Sayed, M. *Lasers Med Sci* **2008**, *23*, 217-228.

[14] Au, L.; Zheng, D.; Zhou, F.; Li, Z.-Y.; Li, X.; Xia, Y. *ACS Nano* **2008**, *2*, 1645-1652.

[15] Li, J. L.; Day, D.; Gu, M. *Adv Mater* **2008**, *20*, 3866-3871.

[16] Govorov, A. O.; Richardson, H. H. *Nano Today* **2007**, *2*, 30-38.

[17] Dinh, H.-K. B.; Zhao, B.; Schuschereba, S. T.; Merrill, G.; Bowman, P. D. *Physiol Genomics* **2001**, *7*, 3-13.

[18] Kühl, N. M.; Rensing, L. *Cell Mol Life Sci* **2000**, *57*, 450-463.

[19] Lindquist, S. *Annu Rev Biochem* **1986**, *55*, 1151-1191.

[20] Wang, J. H.; Redmond, H. P.; Watson, R. W.; Bouchier-Hayes, D. *Am J Physiol Cell Physiol* **1997**, *272*, 1543-1551.

[21] Sonna, L. A.; Fujita, J.; Gaffin, S. L.; Lilly, C. M. *J Appl Physiol* **2002**, *92*, 1725-1742.

[22] Huang, H.-C.; Rege, K.; Heys, J. J. *ACS Nano* **2010**, *4*, 2892-2900.

[23] Huang, X.; Neretina, S.; El-Sayed, M. A. *Adv Mater* **2009**, *21*, 4880-4910.

[24] Huang, H.-C.; Barua, S.; Kay, D. B.; Rege, K. *ACS Nano* **2010**, *4*, 1769-1770.

[25] Hauck, T. S.; Jennings, T. L.; Yatsenko, T.; Kumaradas, J. C.; Chan, W. C. W. *Adv Mater* **2008**, *20*, 3832-3838.

[26] Link, S.; El-Sayed, M. A. *Int Rev Phys Chem* **2000**, *19*, 409-453.

[27] Skrabalak, S. E.; Chen, J.; Sun, Y.; Lu, X.; Au, L.; Cobley, C. M.; Xia, Y. *Acc Chem Res* **2008**, *41*, 1587-1595.

[28] Loo, C.; Lowery, A.; Halas, N.; West, J.; Drezek, R. *Nano Lett* **2005**, *5*, 709-711.
[29] Neumann, E.; Schaefer-Ridder, M.; Wang, Y.; Hofschneider, P. H. *EMBO J* **1982**, *1*, 841-845.
[30] Presse, F.; Quillet, A.; Mir, L.; Marchiol-Fournigault, C.; Feunteun, J.; Fradelizi, D. *Biochem Biophys Res Commun* **1988**, *151*, 982-990.
[31] Huang, H.-L.; Hsing, H.-W.; Lai, T.-C.; Chen, Y.-W.; Lee, T.-R.; Chan, H.-T.; Lyu, P.-C.; Wu, C.-L.; Lu, Y.-C.; Lin, S.-T.; Lin, C.-W.; Lai, C.-H.; Chang, H.-T.; Chou, H.-C.; Chan, H.-L. *J Biomed Sci* **2010**, *17*, 36-46.
[32] Kao, K.; Caple, M. Cell Culture, TrypZean™: Recombinant Bovine Trypsin Expressed in Corn – A Non-animal Alternative. http://www.sigmaaldrich.com/etc/medialib/docs/Sigma/General_Information/cell_culture.Par.0001.File.tmp/cell_culture.pdf Sigma-Aldrich: St. Louis, (last accessed 15-09-2010).
[33] Tsuboi, A. *Int J Hyperthermia* **1988**, *4*, 655-664.
[34] Creagh, E. M.; Sheehan, D.; Cotter, T. G. *Leukemia* **2000**, *14*, 1161-1173.
[35] Fujio, N.; Hatayama, T.; Kinoshtta, H.; Yukioka, M. *J Biochem* **1987**, *101*, 181-187.
[36] Srinivasan, J. M.; Fajardo, L. F.; Hahn, G. M. *J Natl Cancer Inst* **1990**, *82*, 1904-1910.
[37] Kim, S. H.; Kim, J. H.; Hahn, E. W. *Radiat Res* **1976**, *66*, 337-345.
[38] Schlag, H.; Lücke-Huhle, C. *Eur J Cancer* **1976**, *12*, 827-831.
[39] Brand, K.; Lubbe, A. S.; Justus, D. J. *Int J Hyperthermia* **1996**, *12*, 527-538.
[40] Flanders, K. C.; Winokur, T. S.; Holder, M. G.; Sporn, M. B. *J Clin Invest* **1993**, *92*, 404-410.
[41] Phillips, M. L.; Nudelman, E.; Gaeta, F. C.; Perez, M.; Singhal, A. K.; Hakomori, S.; Paulson, J. C. *Science* **1990**, *250*, 1130-1132.
[42] Bevilacqua, M. P.; Stengelin, S.; Gimbrone, M. A., Jr.; Seed, B. *Science* **1989**, *243*, 1160-1165.
[43] Dustin, M. L.; Rothlein, R.; Bhan, A. K.; Dinarello, C. A.; Springer, T. A. *J Immunol* **1986**, *137*, 245-254.
[44] Wegner, C. D.; Gundel, R. H.; Reilly, P.; Haynes, N.; Letts, L. G.; Rothlein, R. *Science* **1990**, *247*, 456-459.
[45] Smith, C. W.; Rothlein, R.; Hughes, B. J.; Mariscalco, M. M.; Rudloff, H. E.; Schmalstieg, F. C.; Anderson, D. C. *J Clin Invest* **1988**, *82*, 1746-1756.
[46] Lauri, D.; Needham, L.; Martin-Padura, I.; Dejana, E. *J Natl Cancer Inst* **1991**, *83*, 1321-1324.
[47] Sawaji, Y.; Sato, T.; Takeuchi, A.; Hirata, M.; Ito, A. *Br J Cancer* **2002**, *86*, 1597-1603.
[48] Lukianova-Hleb, E. Y.; Anderson, L. J. E.; Lee, S.; Hafner, J. H.; Lapotko, D. O. *Phys Chem Chem Phys* **ASAP**.
[49] Nolle, E.; Schelev, M. *Tech Phys* **2005**, *50*, 1528-1530.
[50] Letfullin, R. R.; Joenathan, C.; George, T. F.; Zharov, V. P. *Nanomedicine* **2006**, *1*, 473-480.
[51] Fajardo, L. F.; Prionas, S. D.; Kowalski, J.; Kwan, H. H. *Radiat Res* **1988**, *114*, 297-306.

[52] Paidas, C. N.; Mooney, M. L.; Theodorakis, N. G.; De Maio, A. *Am J Physiol Regul Integr Comp Physiol* **2002**, *282*, 1374-1381.

8. Summary and outlook.

For centuries, NPs have held a prime position in the world of alchemy [1,2]. In medieval times, glass staining techniques involving colloidal gold solutions were commonly used. It was not until 1851 however, when gold NPs were properly introduced into the world of science through Faraday's work [3]. In modern chemistry, physics, engineering and biomedicine, inorganic NPs have found a number of applications; all based on the unique properties of nanomaterials, very different to those observed at the macroscopic scale [4-19]. Unlike bulk gold, nanoscale gold colloids exist in a range of colours covering the entire visible spectrum (e.g. red, green and blue). Such properties derive from the resonant interactions of the nanogold with an applied electromagnetic wave (longer than NPs diameter). The size and shape of nanocomposites can be adjusted chemically [1,3,4,11,20-34]. Several methods have been utilised in this project, the summary of which will be given in the following sub-sections. Synthesised 'bare' gold NPs were coated with water soluble organic molecules [35-44]. To the organic corona, bioactive peptides were attached [45]. Appropriate surface functionality enabled biomedical applications of the resulting nanocomposites.

Bioactive nanocomposites were utilised in selective targeting of human cells (HUVECs). These cells cover the internal layer of blood vessels (endothelium) in the circulatory system and conduct important physiological processes, e.g. angiogenesis (formation of new blood vessels) [46-51]. New vessels are excessively formed during severe pathological developments, including cancer [52,53]. Tumours growth and progression can be suppressed by inhibiting angiogenesis [54-59]. Key selectivity was achieved with HUVECs targeting colloids. Bioactive NPs targeted two receptors over-expressed on the cell membrane. The binding event triggered a cellular response, resulting in selective regulation of the angiogenesis process.

On the other hand, HUVECs targeting NPs were employed in photo-thermal therapy (hyperthermia) using laser light illumination [60-67]. The light was absorbed by NPs (associated with cell components) and converted to heat [68]. Heating served as a stressor [69-72], which induced stress response within the cells, or at the extreme led to cell death. Cells with no associated NPs were not affected. This technique can be considered as an alternative way of selective regulation of angiogenesis along with cancer treatment.

Obtained results will be summarised in **section 8.1**. The outlook to future experiments and further developments will be proposed in **section 8.2**.

8.1. Summary of results.

Several methods were utilised in the preparation of gold colloids, capped with previously reported (e.g. CALNN peptide, OEG ligand) [36-38,40,41,73] or novel (e.g. DA-PEG) [35] ligands. CALNN derivative (CALNN-Ahex-FQGII) functionalised NPs were employed in the formation of NPs assemblies [39], while OEG NPs were further modified with octa-peptides [45]. These results will be summarised in **section 8.1.1**. The cellular fate of both, OEG capped and octa-peptide modified (pep-OEG) NPs were studied in HUVECs. OEG NPs were internalised following a non-selective mechanism (see **section 8.1.2.** for summary), while the type of interactions between pep-OEG NPs and cells was determined by peptide sequence (P1, P2 or P3). P1 and P3 based colloids were binding selectively to membrane receptors over-expressed by HUVECs. Receptor binding initiated signalling cascades within cells, resulting in a regulation of certain physiological processes (see **section 8.1.3** for summary). HUVECs tagged with P1-OEG NPs or with associated (internalised) OEG NPs were illuminated with a laser light. This effectively led to hyperthermia and heat shock, which depending on the laser power applied, led to a cellular response or cell death (see **section 8.1.4.** for summary).

8.1.1. Synthesis, surface capping and assembly of NPs.

Gold colloids (spherical and anisotropic) were prepared according to established wet chemistry methods with slight modifications to literature protocols [1,3,11,20,21,23,24,26-30,32-34,74-84] (see **chapter 3** for protocols; related publication is listed in **Author's Declaration**). Citrate reduction was utilised in the synthesis of spherical NPs, while rod-like structures were prepared by seed mediated approaches. A method developed by Hals was employed in the production of spherical gold shells with silica cores, while spherical shells (or cages) with hollow interiors were obtained by a galvanic replacement reaction.

Spherical colloids were capped with a mixed layer of CALNN and CALNN-Ahex-FQGII (c-FQGII) ligands, then utilised in the formation of assembled structures [39]. NPs assembling was achieved with oligodeoxynucleotide based (ODN) templates *via* selective recognition between AT-rich regions in ODNs and FQGII sequence [85,86]. As demonstrated in **chapter 4**, the architecture of NPs assemblies can be controlled by varying the amount of c-FGQII incorporated in the organic corona and/or the type ODNs (short or pseudo-infinite duplexes) used. This led to the formation of dimers, trimers, shorter and longer chains of NPs, or even more complex three dimensional arrays, making

the method highly attractive in the engineering of NPs assemblies (related publication is listed in **Author's Declaration**).

DA-PEG capping ligand was employed in the preparation of new family of spherical gold colloids, showing enhanced stability in aqueous media [35]. Colloidal stability against aggregations was tested in a varied pH range (1.2 ÷ 9), during heat/cool (100 ºC/25 ºC) and freeze/thaw (-20 ºC/25 ºC) cycles. DA-PEG capped NPs also showed resistance to ligand exchange reactions in the presence of high concentration of thiolated molecules. Enhanced stability of DA-PEG colloids derived from photo-polymerised DA-PEG shell, tightly encapsulating inorganic cores (see **chapter 4** for more details; related publication is listed in **Author's Declaration**).

OEG capped and pep-OEG NPs with spherical and inorganic cores (see **chapter 4** for physicochemical properties) were utilised in experiments with HUVECs.

8.1.2. Cellular fate of OEG NPs.

Mechanisms of fundamental interactions between HUVECs and NPs were studied with OEG capped colloids. Strong charge of OEG NPs (see **chapter 4** for physicochemical properties) was identified as a driving force of NPs uptake, based on non-selective endocytosis. The uptake rate was determined by the NPs size and shape, rather than the NPs functionality.

Spherical (SP), rod-like (NR), core/shell (CS) and hollow (HG) NPs employed in OEG system were all negatively charged, but significantly varied in size and shape. These two parameters (rather than the charge strength) were dominant in the regulation of the uptake rate. The smallest OEG SP (hydrodynamic diameter around 25 nm) were most efficiently taken-up by HUVECs, whilst the largest OEG HG (96 nm) the least. OEG NR were endocytosed in greater numbers than OEG CS, with a diameter comparable to the NR length (around 50 nm). OEG NR and OEG SP, with the same diameter as the NR width were similar in uptake rate. These results were presented in **chapter 5** and are to be published in academic press (the manuscript is in preparation).

More efficient control upon cellular fate of gold colloids was gained with bioactive pep-OEG NPs.

8.1.3. Cell targeting and regulation with pep-OEG NPs.

Pep-OEG NPs were prepared by conjugating octa-peptides (either P1 – wild type, P2 – scrambled mutant or P3 – inhibitor) to the outer part of the OEG capping layer [45,87,88] (see **chapter 3** for experimental protocol). Resulting colloids showed similar physicochemical properties (size and charge, see **chapter 4**), but different bioactivity, as determined by the primary structure of the peptide (amino acids arrangements, see **chapter 2**).

HUVECs were targeted with P1-OEG and P3-OEG NPs *via* selective recognition between over-expressed membrane receptors and peptides [89,90]. As demonstrated in **chapter 6**, P1-OEG NPs bind to VEGFR-1, while P3-OEG NPs to NRP-1. The formation of receptor-NPs complexes with NRP-1 was followed by trafficking on the cellular membrane, then complex internalisation. On the contrary, NPs associated with VEGFR-1 remained outside the cellular milieu. The receptor binding event triggered a cellular response, which was monitored by gene expression profiling. Up to 60 fold regulation of three angiogenesis related genes (VEGF A, HIF-1α, C-MYC) was denoted. P1-OEG NPs activated the tested genes; whilst P3-OEG NPs had inhibitory effects (related publication is listed in **Author's Declaration**).

Except of changes in cell metabolism, controlled regulation of physiological processes conducted by HUVECs was also achieved, which was studied with *in vitro* angiogenesis model. Capillaries were formed by cells upon stimulation with P1-OEG NPs; while P3-OEG NPs suppressed neo-vascular sprouting (related manuscript is in preparation, see **Author's Declaration**).

The scrambled version of the wild type peptide (P2 mutant) was also incorporated in the organic corona of NPs. The resulting P2-OEG colloid lost its affinity towards growth factor receptors, was therefore incapable of triggering any angiogenesis related response in HUVECs.

8.1.4. Laser-hyperthermia with OEG NPs and P1-OEG NPs.

HUVECs associated with anisotropic (NR, HG or CS) OEG capped or P1-OEG NPs were exposed to the NIR laser light. At NIR frequency, anisotropic NPs exhibit maximum extinction (see **chapter 4** for physicochemical characterisation), whilst tissue components have the highest transitivity [91-93]. Consequently NIR light can penetrate cells, while being absorbed by associated NPs [60,62,66,67,94]. NPs will then convert the light into heat [68]. This

will induce a heat shock response in the cell, or at the extreme lead to cell death, depending on the applied laser power (LPD, see **chapter 7** for results).

Generally, cell mortality was increasing with LPD. However, the exact percentage of damaged cells was dependent on the type (NR, HG and CS) and functionality (P1-OEG or OEG) of NPs. P1-OEG NPs led to a higher rate of cell damage (up to 90 %), compared to the analogous OEG NPs (quantified after 1 h post-treatment incubation). When the post-treatment incubation time was extended (24 h), OEG NPs resulted in up to 75 % of death, while P1-OEG NPs in only 50 %. Hence, it was concluded that cells with membrane injuries (P1-OEG NPs) can recover, whilst the intracellular damage is potentially irreversible.

Physiological changes in survived cells deriving from heat stimuli were monitored by the expression profiling of two genes (ELAM-1 and ICAM-1), which are responsive to heat stressor and important for angiogenesis (and tumour metastasis). Up to -160 fold inhibition was denoted. Gene regulation was increasing with LPD and was higher with NR or HG than CS, as well as OEG NPs than P1-OEG analogues (related publication is listed in **Author's Declaration**).

8.2. Outlook to future work.

Novel pep-OEG NPs, developed during this project, show promising bioactivity. Selective regulation of several angiogenesis related genes in primary HUVECs along with *in vitro* angiogenesis regulation was demonstrated. However, further experiments aiming to fully appreciate the bioactivity of these novel nanocomposites could be proposed.

One could further extend the presented development by applying pep-OEG NPs *in vivo*. The capability of spherical core based nanocomposites to regulate *in vivo* (e.g. mice) angiogenesis, is to be explored in the presence of naturally existing growth factors, at physiological concentrations. In mice, baring tumours, endothelium around the tumour site can be targeted with anisotropic pep-OEG NPs, then illuminated with the NIR laser, followed by assessing the efficiency of resulting tumour regression (if any) and/or metastasis suppression.

On the other hand, given that another physiological role of HUVECs is to participate in the inflammatory response (to a pathogen) [47,48], it would be interesting to study possible cyto-toxicity related effects, deriving from the prolonged exposure to pep-OEG NPs (and OEG NPs). Assessing the safety of pep-OEG NPs can be considered

as an important step in future real-life applications using these novel nanocomposites, as well as the development of new 'smart' treatments.

The author of the thesis was awarded a one year fellowship, entitled 'PhD plus programme', funded by the EPSRC. Over the course of this PhD-follow-up research, it is intended to investigate the effects of novel pep-OEG NPs on *in vivo* angiogenesis, extended to laser-hyperthermic treatment using NIR absorbing nanocomposites. Cyto-toxicity of applied nanomaterials will be also monitored.

References:

[1] Liz-Marzán, L. M. *Mater Today* **2004**, *7*, 26-31.

[2] Mulvaney, P. The beauty and elegance of Nanocrystals: How invisibly small particles will colour and shape our future. **2003**, http://uninews.unimelb.edu.au/news/791/ The University of Melbourne, UniNews Vol. 12, No. 13 Melbourne, (last accessed: 04-09-2010).

[3] Faraday, M. *Philos Trans R Soc London* **1857**, *147*, 145-181.

[4] Murphy, C. J.; Sau, T. K.; Gole, A. M.; Orendorff, C. J.; Gao, J.; Gou, L.; Hunyadi, S. E.; Li, T. *J Phys Chem B* **2005**, *109*, 13857-13870.

[5] Jain, P. K.; Lee, K. S.; El-Sayed, I. H.; El-Sayed, M. A. *J Phys Chem B* **2006**, *110*, 7238-7248.

[6] Hvolbćk, B.; Janssens, T. V. W.; Clausen, B. S.; Falsig, H.; Christensen, C. H.; Nřrskov, J. K. *Nano Today* **2007**, *2*, 14-18.

[7] Liu, X.; Atwater, M.; Wang, J.; Huo, Q. *Colloid Surface B* **2007**, *58*, 3-7.

[8] Chen, J.; Saeki, F.; Wiley, B. J.; Cang, H.; Cobb, M. J.; Li, Z.-Y.; Au, L.; Zhang, H.; Kimmey, M. B.; Li; Xia, Y. *Nano Lett* **2005**, *5*, 473-477.

[9] Hu, M.; Chen, J.; Li, Z.-Y.; Au, L.; Hartland, G. V.; Li, X.; Marquez, M.; Xia, Y. *Chem Soc Rev* **2006**, *35*, 1084-1094.

[10] Nath, N.; Chilkoti, A. *J Fluoresc* **2004**, *14*, 377-389.

[11] Oldenburg, S. J.; Averitt, R. D.; Westcott, S. L.; Halas, N. J. *Chem Phys Lett* **1998**, *288*, 243-247.

[12] Kelly, K. L.; Coronado, E.; Zhao, L. L.; Schatz, G. C. *J Phys Chem B* **2002**, *107*, 668-677.

[13] Hao, E.; Li, S.; Bailey, R. C.; Zou, S.; Schatz, G. C.; Hupp, J. T. *J Phys Chem B* **2004**, *108*, 1224-1229.

[14] Halas, N. *Opt Photon News* **2002**, *13*, 26-30.

[15] Wang, H.; Brandl, D. W.; Nordlander, P.; Halas, N. J. *Acc Chem Res* **2006**, *40*, 53-62.

[16] Kooij, E. S.; Poelsema, B. *Phys Chem Chem Phys* **2006**, *8*, 3349-3357.

[17] Orendorff, C.; Sau, T.; Murphy, C. *Small* **2006**, *2*, 636-639.

[18] Mie, G. *Ann Phys* **1908**, *330*, 377-445.

[19] Kreibig, U.; Vollmer, M. *Optical Properties of Metal Clusters*; Springer: Berlin, **1995**; Vol. 25.

[20] Frens, G. *Nature-Phys Sci* **1973**, *241*, 20-22.

[21] Day, H. A.; Bartczak, D.; Fairbairn, N.; McGuire, E.; Ardakani, M.; Porter, A. E.; Kanaras, A. G. *CrystEngComm* **2010**, *12*, 4312-4316.

[22] Walther, A.; Muller, A. H. E. *Soft Matter* **2008**, *4*, 663-668.

[23] Duff, D. G.; Baiker, A.; Edwards, P. P. *Langmuir* **1993**, *9*, 2301-2309.

[24] Duff, D. G.; Baiker, A.; Gameson, I.; Edwards, P. P. *Langmuir* **1993**, *9*, 2310-2317.

[25] Halas, N. *MRS Bulletin* **2005**, *30*, 362-368.

[26] Nikoobakht, B.; El-Sayed, M. A. *Chem Mater* **2003**, *15*, 1957-1962.

[27] Sun, Y.; Xia, Y. *Science* **2002**, *298*, 2176-2179.

[28] Xia, Y.; Xiong, Y.; Lim, B.; Skrabalak, S. *Angew Chem, Int Ed* **2009**, *48*, 60-103.

[29] Ji, X.; Song, X.; Li, J.; Bai, Y.; Yang, W.; Peng, X. *J Am Chem Soc* **2007**, *129*, 13939-13948.

[30] Turkevich, J.; Stevenson, P. C.; Hillier, J. *Disc Faraday Soc* **1951**, *11*, 55-75.

[31] Yong, K.-T.; Sahoo, Y.; Swihart, M. T.; Prasad, P. N. *Colloids Surf, A* **2006**, *290*, 89-105.

[32] Zhang, Q.; Xie, J.; Lee, J. Y.; Zhang, J.; Boothroyd, C. *Small* **2008**, *4*, 1067-1071.

[33] Jana, N. R.; Gearheart, L.; Murphy, C. J. *J Phys Chem B* **2001**, *105*, 4065-4067.

[34] Pillai, Z. S.; Kamat, P. V. *J Phys Chem B* **2003**, *108*, 945-951.

[35] Bartczak, D.; Kanaras, A. G. *Langmuir* **2010**, *26*, 7072-7077.

[36] Pengo, P.; Pasquato, L. In *The supramolecular chemistry of organic - inorganic hybrid materials*; Rurak, K., Martinez-Manez, R., Eds.; John Wiley & Sons, Inc. : Hoboken, New Jersey, **2010**, p 113-154.

[37] Cortie, M. B.; McDonagh, A. In *Gold Chemistry: Applications and future directions in life sciences*; Mohr, F., Ed.; WILLEY-VCH Verlag GmbH & Co. KGaA Weinheim, **2009**, p 321-343.

[38] Wang, Z.; Levy, R.; Fernig, D. G.; Brust, M. *Bioconjug Chem* **2005**, *16*, 497-500.

[39] Coomber, D.; Bartczak, D.; Gerrard, S. R.; Tyas, S.; Kanaras, A. G.; Stulz, E. *Langmuir* **2010**, *26*, 13760-13762.

[40] Levy, R.; Thanh, N. T. K.; Doty, R. C.; Hussain, I.; Nichols, R. J.; Schiffrin, D. J.; Brust, M.; Fernig, D. G. *J Am Chem Soc* **2004**, *126*, 10076-10084.

[41] Kanaras, A. G.; Kamounah, F. S.; Schaumburg, K.; Kiely, C. J.; Brust, M. *Chem Commun* **2002**, 20, 2294-2295.

[42] Loweth, C. J.; Caldwell, W. B.; Peng, X.; Alivisatos, A. P.; Schultz, P. G. *Angew Chem, Int Ed* **1999**, *38*, 1808-1812.

[43] Wuelfing, W. P.; Gross, S. M.; Miles, D. T.; Murray, R. W. *J Am Chem Soc* **1998**, *120*, 12696-12697.

[44] Schmid, G.; Lehnert, A. *Angew Chem, Int Ed* **1989**, *28*, 780-781.

[45] Hermanson, G. T. *Bioconjugate Techniques*; 2nd ed.; Elsevier Inc. , **2008**.

[46] Cliff, W. J. *Blood vessels (Biological structure and function; 6)*; Cambridge University Press: Cambridge, **1976**.

[47] Sumpio, B. E.; Timothy Riley, J.; Dardik, A. *Int J Biochem Cell Biol* **2002**, *34*, 1508-1512.

[48] Michiels, C. *J Cell Physiol* **2003**, *196*, 430-443.

[49] Dejana, E.; Corada, M.; Lampugnani, M. G. *FASEB J* **1995**, *9*, 910-918.

[50] Clauss, M.; Breier, G. *Mechanisms of angiogenesis*; Brikhauser Verlag, Basel-Boston-Berlin, **2005**.

[51] Schnittler, H. J. *Basic Res Cardiol* **1998**, *93*, 30-39.

[52] Folkman, J. *Semin Cancer Biol* **2003**, *13*, 159-167.

[53] Carmeliet, P.; Jain, R. K. *Nature* **2000**, *407*, 249-257.

[54] Teicher, B. A. *Crit Rev Oncol/Hematol* **1995**, *20*, 9-39.

[55] Shanafelt, T. D.; Kay, N. E. *Semin Oncol* **2006**, *33*, 174-185.

[56] Vincent, L.; Kermani, P.; Young, L. M.; Cheng, J.; Zhang, F.; Shido, K.; Lam, G.; Bompais-Vincent, H.; Zhu, Z.; Hicklin, D. J.; Bohlen, P.; Chaplin, D. J.; May, C.; Rafii, S. *J Clin Invest* **2005**, *115*, 2992-3006.

[57] Segura, I.; Serrano, A.; De Buitrago, G. G.; Gonzalez, M. A.; Abad, J. L.; Claveria, C.; Gomez, L.; Bernad, A.; Martinez-A, C.; Riese, H. H. *FASEB J* **2002**, *16*, 833-841.

[58] Kim, K. J.; Li, B.; Winer, J.; Armanini, M.; Gillett, N.; Phillips, H. S.; Ferrara, N. *Nature* **1993**, *362*, 841-844.

[59] Hood, J. D.; Bednarski, M.; Frausto, R.; Guccione, S.; Reisfeld, R. A.; Xiang, R.; Cheresh, D. A. *Science* **2002**, *296*, 2404-2407.

[60] Chen, J.; Wang, D.; Xi, J.; Au, L.; Siekkinen, A.; Warsen, A.; Li, Z.-Y.; Zhang, H.; Xia, Y.; Li, X. *Nano Lett* **2007**, *7*, 1318-1322.

[61] Lowery, A. R.; Gobin, A. M.; Day, E. S.; Halas, N. J.; West, J. L. *Int J Nanomedicine* **2006**, *1*, 149-154.

[62] Loo, C.; Lowery, A.; Halas, N.; West, J.; Drezek, R. *Nano Lett* **2005**, *5*, 709-711.

[63] Lal, S.; Clare, S. E.; Halas, N. J. *Acc Chem Res* **2008**, *41*, 1842-1851.

[64] Cole, J. R.; Mirin, N. A.; Knight, M. W.; Goodrich, G. P.; Halas, N. J. *J Phys Chem C* **2009**, *113*, 12090-12094.

[65] O'Neal, D. P.; Hirsch, L. R.; Halas, N. J.; Payne, J. D.; West, J. L. *Cancer Lett* **2004**, *209*, 171-176.

[66] Huang, X.; Jain, P.; El-Sayed, I.; El-Sayed, M. *Lasers Med Sci* **2008**, *23*, 217-228.

[67] Link, S.; El-Sayed, M. A. *Int Rev Phys Chem* **2000**, *19*, 409-453.

[68] Govorov, A. O.; Richardson, H. H. *Nano Today* **2007**, *2*, 30-38.

[69] Dinh, H.-K. B.; Zhao, B.; Schuschereba, S. T.; Merrill, G.; Bowman, P. D. *Physiol Genomics* **2001**, *7*, 3-13.

[70] Kühl, N. M.; Rensing, L. *Cell Mol Life Sci* **2000**, *57*, 450-463.

[71] Creagh, E. M.; Sheehan, D.; Cotter, T. G. *Leukemia* **2000**, *14*, 1161-1173.

[72] Lindquist, S. *Annu Rev Biochem* **1986**, *55*, 1151-1191.

[73] You, C.-C.; Chompoosor, A.; Rotello, V. M. *Nano Today* **2007**, *2*, 34-43.

[74] Stöber, W.; Fink, A.; Bohn, E. *J Colloid Interface Sci* **1968**, *26*, 62-69.

[75] Skrabalak, S. E.; Au, L.; Li, X.; Xia, Y. *Nat Protocols* **2007**, *2*, 2182-2190.

[76] Turkevich, J.; Stevenson, P. C.; Hillier, J. *J Phys Chem* **1953**, *57*, 670-673.

[77] Busbee, B.; Obare, S.; Murphy, C. *Adv Mater* **2003**, *15*, 414-416.

[78] Sun, Y.; Xia, Y. *J Am Chem Soc* **2004**, *126*, 3892-3901.

[79] Kumar, S.; Gandhi, K. S.; Kumar, R. *Ind Eng Chem Res* **2006**, *46*, 3128-3136.

[80] Van Blaaderen, A.; Van Geest, J.; Vrij, A. *J Colloid Interface Sci* **1992**, *154*, 481-501.

[81] Lee, G.-J.; Shin, S.-I.; Kim, Y.-C.; Oh, S.-G. *Mater Chem Phys* **2004**, *84*, 197-204.

[82] Sau, T. K.; Murphy, C. J. *Philos Mag* **2007**, *87*, 2143-2158.

[83] Gole, A.; Murphy, C. J. *Chem Mater* **2004**, *16*, 3633-3640.

[84] Phonthammachai, N.; Kah, J. C. Y.; Jun, G.; Sheppard, C. J. R.; Olivo, M. C.; Mhaisalkar, S. G.; White, T. J. *Langmuir* **2008**, *24*, 5109-5112.

[85] Alam, M. R.; Maeda, M.; Sasaki, S. *Nucleic Acids Symp Ser (Oxf)* **1999**, *42*, 173-174.

[86] Alam, M. R.; Maeda, M.; Sasaki, S. *Bioorg Med Chem* **2000**, *8*, 465-473.

[87] Chan, W. C. W.; Nie, S. *Science* **1998**, *281*, 2016-2018.

[88] Eck, W.; Craig, G.; Sigdel, A.; Ritter, G.; Old, L. J.; Tang, L.; Brennan, M. F.; Allen, P. J.; Mason, M. D. *ACS Nano* **2008**, *2*, 2263-2272.

[89] Giordano, R. J.; Anobom, C. D.; Cardó-Vila, M.; Kalil, J.; Valente, A. P.; Pasqualini, R.; Almeida, F. C. L.; Arap, W. *Chem Biol* **2005**, *12*, 1075-1083.

[90] Starzec, A.; Ladam, P.; Vassy, R.; Badache, S.; Bouchemal, N.; Navaza, A.; du Penhoat, C. H.; Perret, G. Y. *Peptides* **2007**, *28*, 2397-2402.

[91] Kim, J. G.; Mengna, X.; Hanli, L. *IEEE Eng Med Biol* **2005**, *24*, 118-121.

[92] Prahl, S. Optical Absorption of Hemoglobin. **1999**, http://omlc.ogi.edu/spectra/hemoglobin/ Oregon Medical Laser Center Oregon (last accessed: 04-09-2010).

[93] Hale, G. M.; Querry, M. R. *Appl Opt* **1973**, *12*, 555-563.

[94] Huff, T. B.; Tong, L.; Zhao, Y.; Hansen, M. N.; Cheng, J.-X.; Wei, A. *Nanomedicine* **2007**, *2*, 125-132.

Appendix A – list of reagents suppliers

All reagents were purchased from the following suppliers and used without further purification:

A1. Sigma-Aldrich:

sodium tetrachloroaurete (III) dihydrate, trisodium citrate, sodium borohydride, silver nitrate, L-ascorbic acid, ammonia solution (30%), absolute ethanol, methanol, acetone, acetonitrile, chloroform, isopropanol, tetraethyl orthosilicate (TEOS), (3-aminopropyl)trimethoxysilane (APTMS), tetrakis(hydroxymethyl)phosphonium chloride (THPC), sodium hydroxide, potassium carbonate, formaldehyde, tris(hydroxymethyl)aminomethane (Tris), boric acid, piperazine-N,N'-bis(2-ethanesulfonic acid) (PIPES), sodium phosphate monobasic, sodium phosphate dibasic, ethylenediaminetetraacetic acid (EDTA), sodium hydroxide, sodium azide, agarose, mercaptoethanol, dithiothreitol, cysteamine, cysteine, α-lipoic acid, 11-amino-1-undecanethiol, Ellman's reagent – 5,5'-dithiobis(2-nitrobenzoic acid), FluoroProfile Protein Quantification Kit, porcine gelatin, Hank's Buffered Salt Solution (HBSS), fetal bovine serum (FBS), trypsin, trypan blue, TRIzol reagent, cobalt II chloride ($CoCl_2$);

A2. ProChimia Surfaces Sp. z o.o:.

α-thio-ω-carboxy polyethylene glycol (OEG) and 46-mercapto-22,43-dioxo-3,6,9,12,15,18-hexaoxa-21,44-diazahexatetraconta-31,33-diyn-1-oic acid (DA-PEG);

A3. Strem-Chemicals, Inc.:

bis(p-sulfonatophenyl)phenyl phosphine dehydrate dipotassium salt (BSPP);

A4. Alfa Aesar:

hexadecyltrimethylammonium bromide (CTAB);

A5. Pierce Biotechnology:

N-hydroxysulfosuccinimide (s-NHS) and 1-(3-(dimethylamino)propyl)-3-ethyl-carbodiimidemethiodide (EDC);

***A6. Agar Scientific Ltd.*:**

osmium tetroxide, uranyl acetate, lead nitrate, Spurr resin and glutaraldehyde;

A7. 3M:

perfluorohexane (FC-72);

A8. Anna Spec Inc.:

HiLyte Fluor 680 amine (HiLyte);

A9. Activotec SPP Ltd.:

P1 (KPQPRPLS), P2 (KATWLPPR) and P3 (KPRQPSLP) octa-peptides, as well as CALNN and CALNN-Ahex-FQGII;

A10. Link Technologies Ltd. and SAFC Supply Solutions:

Phosphoramidite monomers and reagents for OL synthesis;

A11. Worthington:

Type 1 collagenase solution;

A12. Invitrogen:

M199 growth media, Penicillin / Streptomycin, glycogen and TNF-α;

A13. Autogen Bioclear:

human serum;

A14. Gibco:

DNEM media growth and reduced growth factor membrane matrix (Geltrex);

A15. PeproTech, Inc.:

VEGF-B_{167};

A16. Applied Biosystems:

VEGF A, HIF1-α, V-MYC, GAPDH, ELAM-1 and ICAM-1 TaqMan primers, 10 x RT buffer, random primers, RNAsin, dNTPs, nuclease-free water and reverse transcriptase and 2 x PCR mix;

A17. Innova Biosciences, Ltd.:

LL-RPE fluorescent label.

Appendix B – supplementary information

B1. OEG and DA-PEG ligands quantification:

Average number of DA-PEG and OEG ligands, attached to each nanoparticle, was quantified with Ellman's method (see **chapter 3** for experimental details). In tables below, 5 ÷ 10 independent measurements from each set of quantification-experiments are shown.

Table B1.1. DA-PEG ligand quantification.

Estimated number of DA-PEGs			
15.5 ± 1.5 nm spherical NPs	**Average**	**3.25 ± 1.5 nm spherical NPs**	**Average**
2027	**2073 ± 250**	82	**67 ± 22**
2118		37	
1944		64	
1945		72	
2330		80	

Table B1.2. OEG ligand quantification – different types of NPs.

Estimated number of OEGs							
SP	Average	**NR**	Average	**HG**	Average	**CS**	Average
2187	**1876 ± 156**	6976	**6820 ± 877**	55898	**55871 ± 570**	21893	**21368 ± 830**
1738		6265		54996		21772	
1879		5662		55849		21533	
1787		5902		56273		20747	
2056		7798		54925		22382	
1782		7173		55626		20177	
1687		7554		55982		21156	
1798		7816		56716		21825	
1865		7432		56032		22217	
1987		5624		56413		19976	

B2. Octa-peptides quantification:

Average number of octa-peptides, attached to each nanoparticle, was estimated with FluoroProfile Protein Quantification Kit (see **chapter 3** for experimental details). In tables below, 5 ÷ 10 independent measurements from each set of quantification-experiments are shown.

Table B2.1. Octa-peptide quantification; spherical gold NPs.

Estimated number of octa-peptides			
P1	Average	**P3**	Average
384	**436 ± 44**	420	**417 ± 10**
398		441	
466		419	
452		402	
469		412	
442		414	
485		417	
358		421	
424		418	
486		412	

Table B2.2. P1 peptide quantification; anisotropic NPs.

Estimated number of P1 peptide					
NR	Average	**HG**	Average	**CS**	Average
1469		17193		6941	
1677		18909		7291	
1501	**1457 ± 149**	19845	**17514 ± 1904**	7125	**6931 ± 300**
1346		15028		6518	
1295		16596		6781	

B3. Calculations of the number of gold atoms per nanoparticle.

Each type of NPs (column 1, **Table B3.1.**) was imaged with transmission electron microscope. On images, the size of NPs was measured. Statistical analyses of the size distribution were drowned into histograms. From histograms, the average size of NPs in each sample was estimated (column 2, **Table B3.1.**).

Assuming that NPs possess fcc crystal structure [1,2], in each unit cell there are 8 atoms at the edges and 6 atoms at the faces, thus the single unit cell contains 4 atoms. Since, 1 mole of gold weights 197 g and contains $6.02 \cdot 10^{23}$ atoms, while the density of gold is 19.32 g/cm^3, there is $5.9 \cdot 10^{22}$ atoms/cm^3. Consequently, 4 atoms (the unit cell) will occupy the volume of $6.7 \cdot 10^{-2}$ nm^3. Taking the dimensions of NPs, their volumes can be easily calculated (column 3, **Table B3.1.**; Note: for hollow and core/shell NPs the volume of gold part of the NP equals to the volume of the whole NP minus the volume of hollow or silica interior). By dividing the volume of NP by the volume of the unit cell and multiplying by the number of gold atoms in the unit (4), the number of gold atoms per NP was calculated (column 4, **Table B3.1.**).

These numbers multiplied by the weight of a gold atom ($197 / 6.02 \cdot 10^{23}$) gave the weight of a single NP (column 5, **Table B3.1.**).

Table B3.1. Gold atoms per nanoparticle.

Type of NP	Average size [nm]	Volume of NP [nm^3]	No. of gold atoms per NP	Weight of NP [g]
spherical	15	1766	105448	$3.45 \cdot 10^{-17}$
nanorod	16 x 47	12032	718328	$2.35 \cdot 10^{-16}$
hollow	92 x 9	108278	6464370	$2.12 \cdot 10^{-15}$
core/shell	44 x 6	15863	947061	$3.10 \cdot 10^{-16}$

References:

[1] Xia, Y.; Xiong, Y.; Lim, B.; Skrabalak, S. *Angew Chem, Int Ed* **2009**, *48*, 60-103.

[2] Day, H. A.; Bartczak, D.; Fairbairn, N.; McGuire, E.; Ardakani, M.; Porter, A. E.; Kanaras, A. G. *CrystEngComm* **2010**, *12*, 4312-4316.

B4. Laser-hyperthermia with OEG NPs and P1-OEG NPs.

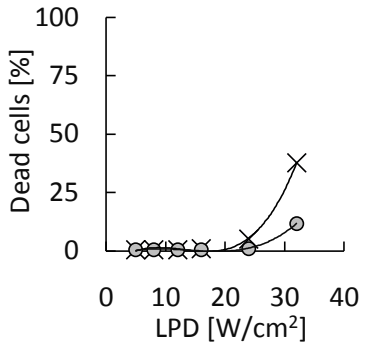

Figure B4. HUVECs number after the treatment with variable laser power density (LPD). Crosses represent laser-treated cells after 1 h post-treatment incubation, while dots after 24 h.